Photoelectric properties of ZnSe

Qidwai, A. A.

PHOTOELECTRIC PROPERTIES OF ZnSe

By

A.A. QIDWAI, B.Sc.(Hons.), M.Sc., M.Phil.

Presented in candidature for the degree of

Doctor of Philosophy

in the

University of Durham

July 1982

"How is it that you adopt the attitude of disbelief towards your Lord when the fact is that you were lifeless and He gave you life, and He will take away life from you and will again restore you to life : then you shall ultimately return to Him. He it is Who created for you all that there is on the Earth ; He then turned to the sky and ordered it into seven heavens. And He has full and perfect knowledge of everything".

: AL-QURAN :

ACKNOWLEDGEMENT

I would like to extend my thanks to all those who have helped me in any way during my doctoral research and especially to those mentioned below :-

Dr. J. Woods, my supervisor, for his constant help and encouragement.

Professor G.G. Roberts, chairman, for the use of departmental facilities and the workshop staff, headed by Mr. F.Spence, for their invaluable help and advice.

Dr. G.J. Russell and Mr.N.F. Thompson, for providing the single crystals.

Mr. A.E. Thomas for help during the experimental work.

Mrs.S. Mellanby for typing the thesis.

Mr. P.C. Pande for proof-reading.

The contributions of the Pakistan Government for the award of a scholarship and the University of Karachi for study leave are gratefully acknowledged.

Special thanks are due to my wife, Nasreen, and my sons, Asim and Raheel, for their support and contributions to a happy home and enjoyable family life.

ABSTRACT

Various photoelectric techniques have been exploited in an investigation of the ionization energies of donor and acceptor type defects, and the photoionization cross-sections for electrons and holes from the acceptors in single crystals of zinc selenide doped with indium, gallium or copper. Measurements of d.c. photoconductivity and infra-red quenching were made on high resistivity material, whereas low resistivity samples were fabricated into Schottky diodes for investigation using transient photocapacitance and photocurrent techniques. Interest was focussed on zinc selenide doped with indium or gallium where strong compensation effects occurred, i.e. the resistivity increased with increasing indium (gallium) content. Self-activated acceptor centres with hole ionization energies of 0.59 eV and 0.55 eV were clearly revealed by the above techniques in indium or gallium doped samples. With increasing indium concentration a new acceptor with an ionization energy of 0.41 eV appeared. This may have been responsible for the compensation effect. To ensure that the observations were not affected by the presence of unintentionally incorporated copper impurities, Schottky diodes on samples deliberately doped with copper have also been examined. The dominant copper acceptor level was clearly revealed. It lay $\sim$ 0.67 eV above the valence band.

CONTENTS

CHAPTER 1

INTRODUCTION

In the work to be described in this thesis, various photoelectric phenomena have been exploited in an attempt to reveal the energetic positions and photo-ionization cross-sections of the various donor and acceptor type defects which occur in zinc selenide doped with impurities such as indium, gallium and copper. In what follows a very brief account is given of the three major photoelectric effects, and then the technological importance of zinc selenide is described.

1.1 PHOTOELECTRIC EFFECT

(A) THE PHOTOEMISSIVE EFFECT

The photoemissive effect was first discovered by Hertz (1887), during his experiments on electrical resonance. Photoemission is a process in which electrons are ejected from the surface of matter as a result of interaction of electromagnetic radiation (light) with that matter. If $h\nu$ is the photon energy of the incident radiation, ϕ_{ph} is the photoelectric work function, and $\frac{1}{2} mv^2$ is the kinetic energy of the escaping electron, then the energy balance of action and reaction is given by Einstein's photoelectric equation

$$h\nu = \frac{1}{2} mv^2 + \phi_{ph}.$$

When the fastest photoexcited electron is just able to leave the surface, the kinetic energy ($\frac{1}{2} mv^2$) is equal to zero, and

$$h\nu_o = \phi_{ph}.$$

where $h\nu_o$ is the threshold energy at which photoemission starts. As the interacting photon energy is increased above the threshold the number of ejected electrons increases rapidly. Electron emission comprises a chain

of three processes :

(1) photon interaction exciting an electron to a high energy state ;

(2) scattering of the excited electron, which loses energy in the process ; and

(3) the escape of the excited electron.

In a Schottky diode photoelectrons can be excited from the metal of the blocking contact into the semiconductor. This leads to a short-circuit photocurrent which can be determined and thus provide information about the barrier height at the contact.

(B) PHOTOCONDUCTIVITY

Photoconductivity is a volume photoelectric phenomenon and was first observed by Smith in 1873. The pioneer work on the investigation of photoconductivity was done by Gudden and Pohl (1928) and their co-workers. In II-VI compounds the effect has attracted much attention during the last two decades because of the high photoconductive sensitivity of these materials. In addition, the range of bandgaps in these compounds allows maximum photosensitivity to be obtained at wavelengths ranging from the near infra-red to the near ultra-violet. Since much of the work to be described in this thesis is concerned with photoconductive effects, the whole of Chapter 2 is devoted to a review of this topic.

(C) THE PHOTOVOLTAIC EFFECT

The photovoltaic effect which is also a type of volume photoelectric effect, was discovered by Adams and Day in 1876. Historically, the photovoltaic effect was more frequently studied than photoconductivity ; and there were frequent references in the early literature, Hughes and Du Bridge (1932) and Moss (1952).

The photovoltaic effect (PVE) is one in which an electromotive force is generated when photons are absorbed in an inhomogeneous semiconductor. The inhomogeneity or internal potential barrier in the semiconductor is necessary to separate the electrons and holes generated by the absorption of light. The

inhomogeneity can be created by making a metal-semiconductor contact or a p-n junction.

Using this effect it is possible to convert sunlight directly into electrical power with solar batteries, made up of photovoltaic cells. The first solar cell of reasonable efficiency, using a diffused silicon p-n junction was prepared by Chapin et al (1954). Among the II-VI compounds CdS has the best prospect as a cheap and efficient solar cell material.

Our interest, as will become clear later, is in the effects of the electronic transitions which occur when incident photons are absorbed in those regions of a semiconductor (zinc selenide) where an internal electric field exists. An electronic transition involving a bound state and a band of states results in a change of the charge configuration of the defect state as the freed carrier is swept away by the internal electric field. If the consequences of the change of charge state can be measured in some way, for example by observing changes in the capacitance or conductance of a device, then the ionisation energy and photoionization cross-section of the defect can be determined.

1.2 TECHNOLOGICAL IMPORTANCE OF ZnSe

ZnSe is one of the members of the twelve binary compounds formed by the metals Zn, Cd, and Hg of column II of the periodic table and the chalcogens O, S, Se and Te of column VI. Relatively little is known about the Hg compounds ; HgSe and HgTe are semi-metals and are therefore very different from the other compounds. The compounds formed by Zn, Cd and S, Se, Te ; have the zincblende (cubic) or the wurtzite (hexagonal) structure, and possess direct energy band-gaps.

ZnSe has a bandgap of the order of 2.67 eV at room temperature, and has potential as a material for light emitting diodes (LED s), emitting in the visible region of the spectrum, particularly in the green and yellow. Schottky diodes (metal-semiconductor) and metal-insulator-semiconductor (MIS) devices prepared on low resistivity n-type ZnSe, are probably the brightest LED's yet

produced on II-VI compounds (see Allen et al (1972) and Özsan and Woods (1975)). The most efficient structure for an LED would be a p-n junction, giving injection luminescence in the range from blue to red,(see Kosai et al (1979)). The fabrication of such a device needs low resistivity n and p-type ZnSe. It is not difficult to prepare ZnSe with n-type conductivity of the order of 10^{-1} to 1.0 Ω^{-1} cm^{-1}. Unfortunately, however, because of the phenomenon of self-compensation, common to all II-VI compounds, low resistivity p-type ZnSe has not yet been prepared.

Many attempts in the past few years have been made to achieve p-type conductivity in ZnSe by (a) incorporating acceptors during bulk crystal growth or (b) using ion-implantation techniques. In principle, acceptors can be introduced into ZnSe either by replacing a Zn ion with a group I element (Li, Na) or by replacing Se with a group V element (N, P, As).

Merz et al (1973) introduced Li and Na in the presence of excess Zn into ZnSe grown from the vapour phase, but no p-type conductivity was claimed. They found binding energies of 114 $\pm$ 2 meV and 90-100 meV for Li_{Zn} and Na_{Zn} substitutional acceptors. Bhargava et al (1979) have produced p-type ZnSe with a resistivity of the order of $\lesssim 10^{9}$ Ω-cm by incorporating Li, Na, Cu and P into ZnSe grown by liquid phase epitaxy. Kosai et al (1979) reported that they produced p-type epilayers, using Li, Na, N and P as dopants, on ZnSe substrates. The resistivities of their layers were $\gtrsim 10^{5}$ ohm-cm. Fitzpatrick et al (1981) introduced group V elements into ZnSe and suggested that they form good shallow acceptors, but no p-type conductivity was reported. In an attempt to produce p-type ZnSe, Robinson and Kun (1975) used group III elements. They claimed to have prepared p-n junctions in heavily doped ZnSe and Zn (S, Se) by introducing gallium, indium or thallium in the presence of excess zinc during crystal growth.

Ion-implantation has also promised to be a powerful technique for forming p-n junctions in semiconductors. It is a process where controlled amounts of chosen foreign species can be introduced into the surface regions of a semiconductor.

The principal advantages of ion-implantation are (a) the total amount and purity of material implanted can be accurately controlled and monitored, (b) the concentration of impurities as a function of depth can be controlled by means of the ion energy, and thus it is possible to implant a buried layer of dopant, (c) implantation and subsequent annealing are comparatively brief low-temperature processes, and therefore the diffusion of unwanted materials from the surface is minimized, and (d) it is a non-equilibrium process, so that solubility limits can be exceeded and it is possible to introduce rapidly and deeply a material which does not readily diffuse. Arsenic and phosphorus implants in normal n-type CdS and ZnSe, created acceptors and produced p-n junctions, see Pollard and Hartke (1969). Chung and Tai (1976), and Yamaguchi et al (1977) have made electroluminescent p-n junction devices by implanting N-ions in ZnSe. Recently Stutius (1982) and Wu et al (1982) published the results of their studies of N-ion implanted layers of ZnSe, and Wu et al claimed to have achieved p-type conductivity.

The totality of the published work suggests that only high resistivity p-type ZnSe can be made. Werkhoven et al (1981) have renewed the hope of obtaining p-type conductivity in ZnSe by appropriate doping and avoiding extrinsic impurities rather than native defects responsible for n-type conductivity. This view was also shared by Dean et al (1978) and Kosai et al (1979) who felt that back-ground impurities play a much more important role in II-VI compounds. The main difficulty in producing low resistivity p-type ZnSe, as pointed out earlier, is the phenomenon of self-compensation. For example, when Li_{Zn} is introduced substitutionally to form acceptor levels it occupies interstitial sites as well and then forms shallow donors, Li_{Int}, which compensate the acceptors,see Henry et al (1971) and Neumark (1980). One difficulty involved in the incorporation of Ga and In as acceptors is that it is well known that they form shallow donors, see Merz et al (1972).

According to Stutius (1981), n-type ZnSe layers grown by organometallic chemical vapour deposition (OM-CVD) could become important for heterojunction

solar cells and optoelectronic devices, sincethe lower temperature of preparation may reduce the concentration of accidentally incorporated impurities.

II-VI compounds are also candidate materials for use as infra-red optical components, see Lewis and Hill (1980). In such applications, the limits of transmission are set by the bandgap of the solid at short wavelengths and by multiphonon absorption processes in the crystalline lattice at long wavelengths. With the exception of CdTe, the widths of the bandgaps allow useful transmission in the visible portion of the electromagnetic spectrum, while the infra-red transmission usually extends beyond 12 μm.

1.3 SUMMARY OF OUR RESEARCH

In recent years various attempts have been made in this laboratory to grow p-type ZnSe by introducing indium or gallium and to prepare p-n junction electroluminescent devices, following the claims of Robinson and Kun (1975). However, no p-type conductivity was obtained as the work of Jones and Woods (1976) and Vincent (1980) has shown, although unusual compensation effects were observed. The problem remained unresolved, but interest grew in discovering what types of defect centres indium or gallium create in ZnSe.

The work described in this thesis, therefore, was concentrated on

(a) a study of the defect centres which occur in undoped and doped ZnSe, with particular reference to material doped with indium and gallium;

(b) the reasons why increasing concentrations of indium and gallium result in increasing resistivities as compensation becomes more pronounced.

In the flow chart, shown overleaf, the research programme is outlined to show at a glance the framework of the work to be described here.

FLOW-CHART

PURPOSE: Investigation of deep and shallow defects.

MATERIAL:
1. ZnSe (undoped)
2. ZnSe : Cu
3. ZnSe : Cl
4. ZnSe : Cu, Cl
5. ZnSe : In
6. ZnSe : Ga
7. ZnS : (undoped)
8. ZnS : Ga

DEVICES:
(a) Photoconductors - Fabricated on high resistivity samples.
(b) Schottky diodes - Fabricated on low resistivity samples.

TECHNIQUES:
(1) Photoconductivity (Chapters 2 & 5).
(2) Infra-red quenching of photocurrent (Chapters 2 & 5).
(3) Photoionization cross-section (proportional to inverse of light intensity), (Chapters 2 & 5).
(4) Transient Photocurrent (Chapters 3 & 6).
(5) Transient photocapacitance (Chapters 3 & 6).
(6) Steady state photocapacitance (Chapters 3 & 7).
(7) Infra-red quenching of photocapacitance (Chapter 7).

RESULTS:
(a) Location of the positions of donor levels.
(b) Self-activated centres formed by chlorine, indium or gallium.
(c) Determination of the position of the copper level.
(d) Determination of the concentration of deep-acceptor centres (i.e. self-activated centres).
(e) Calculation of the absolute values of the photoionization cross-section of holes.

CHAPTER 2

PHOTOCONDUCTIVITY AND PROBLEMS RELATED TO DEFECTS

2.1 INTRODUCTION

This chapter deals with the problems associated with photoconductive spectroscopy. In the work to be described in this thesis, we have used photoconductivity measurements to study deep defects. The following sections therefore are concerned with an analytic approach to this subject.

2.2 PHOTOCONDUCTIVITY

2.2.1 Introduction

In the dark, under conditions of thermal equilibrium, the thermally generated carriers in a semiconductor or insulator are distributed among the available energy states according to Fermi statistics. The electrons (and holes) occupying the conduction states determine the dark electrical conductivity. Under constant illumination a steady state photocurrent is reached when the rate of photogeneration is balanced by the various recombination processes through which the carriers tend to relax to the normal thermal equilibrium distribution. This process which is called photoconductivity thus involves, (a) absorption of light and photogeneration of carriers, (b) transport of the carriers and, (c) recombination.

Photoconductivity is then defined as the increase in conductivity associated with the optical generation of excess carriers in a semiconductor or insulator.

Nix (1932) and Hughes (1936) in two review papers discussed the early investigations of photoconductivity by Gudden and Pohl. Gudden and Pohl divided all photoconducting materials into two classes, which they named (1) Idiochromatic and, (2) Allochromatic. Idiochromatic materials are in

fact intrinsic photoconductors and allochromatic materials are impurity photoconductors. Intrinsic photoconductors are those which show photoconductivity when in a pure form ; the photoconductivity being associated directly with the intrinsic properties of the material itself. Such materials exhibit photoconductivity under bandgap excitation. In impurity photoconductors the photoconductivity is associated mainly with the presence of defects.

Photoconductivity in II-VI compounds has attracted much attention during the last two decades. The first obvious reason for this is that these compounds have high photoconductive sensitivity. In addition the range of bandgaps in these compounds allows maximum photosensitivity to be obtained at wavelengths ranging from the near infra-red to the near ultraviolet.

For a material in which both kinds of charges (i.e. electrons and holes) are taken into considerations, the conductivity is defined as :

$$\sigma = nq\mu_n + pq\mu_p \qquad (2.1)$$

where

n = electron density,

p = hole density,

μ_n = electron mobility,

μ_p = hole mobility,

and, q = carrier charge.

But for a material in which the conductivity is dominated by carriers of one kind (e.g. n-type), the expression (2.1) may be written as,

$$\sigma = nq\mu_n \qquad (2.2)$$

Optical excitation of such a material will change its conductivity and eqn (2.2) then takes the form,

$$\Delta\sigma = \Delta n q \mu_n + n q \Delta \mu_n . \tag{2.3}$$

If the excitation rate (i.e. the intensity of light) is I_L, the change in carrier density, Δn, can be related to free carrier lifetime τ_n by

$$\Delta n = I_L \tau_n \tag{2.4}$$

Substitution of (2.4) in (2.3) will give,

$$\Delta\sigma = I_L q \mu_n \tau_n + n q \Delta \mu_n . \tag{2.5}$$

Equation (2.5) states that the change in conductivity (i.e. the photoconductivity) is related to (i) the excitation rate I_L, (ii) the lifetime τ_n and (iii) the mobility μ_n.

The free (majority) carrier lifetime, τ_n, is an important and key parameter in determining the photosensitivity of a photoconductor. The term photosensitivity is defined as the change in conductivity caused by the excitation divided by the excitation intensity, or the photoconductivity per unit excitation intensity. Photosensitivity may also be defined in another way using the photoconductive gain, G,

$$G = \tau_n \mu_n \frac{V}{L^2} , \tag{2.6}$$

where G is defined as the ratio of the number of charge carriers which pass between the electrodes per second for each photon absorbed. Here V is the voltage applied across a distance L in the photoconductor. In a photoconductor, very high values of gain can be obtained by increasing the electric field. The maximum gain corresponds to the maximum voltage that can be applied before

carrier injection from the ohmic cathode dominates the conductivity. Other processes that may limit the gain at high applied electric fields are impact ionization or dielectric breakdown.

2.2.2 Free Carrier Lifetime and Response Time

The free carrier lifetime and response time are identical in a trap (see § 2.2.3) free photoconductor, but differ in a material containing traps. They are both important in determining the photoconductive nature of the material.

The free carrier lifetime is the time an excited electron spends in the conduction band (or an excited hole spends in the valence band). The majority carrier lifetime is the free lifetime of the majority carrier, i.e. of electrons in n-type material and holes in p-type material.

If the majority carriers (e.g. electrons in n-type material) stay longer in the conduction band after optical excitation and have a large enough free carrier lifetime of the order of milli-seconds the crystal is a good photoconductor. Under certain conditions the majority carrier lifetime (τ_n) can change with temperature, illumination intensity, etc. If there are N recombination centres (see § 2.2.3) per unit volume which can capture a free carrier, the lifetime can be expressed as,

$$\tau_n = (v \ S \ N)^{-1},$$

where,

v = Thermal velocity of electrons,

S = Capture cross-section of the recombination centre.

In a trap free material, or at high light intensities, the free electron lifetime is equal to the response time. The response time is defined as the time for the photocurrent to decay to $\frac{1}{e}$ of its value under steady state conditions, after the termination of the excitation. In practice the free carrier lifetime is rarely equal to the response time and for this reason the measurement of photoconductive response does not give a measure of the lifetime.

However, if the photoconductive gain G for the material is measured, and the mobility of the carriers is known, then eqn. (2.6) may be used to determine τ_n.

2.2.3 Traps and Recombination Centres

A deep level impurity in a semiconductor may act either as a trap or as a recombination centre, depending on the temperature and other doping conditions, whereas a shallow impurity will act only as a trap. If the captured carrier has a greater probability of being thermally re-excited to the free-state than of recombining with a carrier of opposite sign at the imperfection, the centre is a trapping centre or trap. On the other hand, if the captured carrier has a greater probability of recombining, the imperfection is a recombination centre.

There is a qualitative difference between traps and recombination centres which depends on their relative cross-sections for minority and majority carrier capture, and also on the relative carrier concentrations. If the minority carriers are holes we expect defects X^- to be recombination centres ; they are attractive to holes, and the species X^o formed on capture may have a substantial electron capture cross-section. On the other hand, defects $X^=$ are attractive to holes but repulsive to electrons, so they may be less efficient in causing recombination.

The concept of demarcation levels is particularly helpful in determining the positions of traps and recombination centres in the forbidden gap of a photoconductor. The electron demarcation level D_n, see Fig 2.1, is defined by the following equation,

$$\nu_n^* \exp(-E/kT) = pv S_p. \qquad (2.7)$$

The left-hand side of this expression is the rate of thermal excitation of an electron into the conduction band and is the product of the number of chances per second that an electron has to jump and a transition probability factor ; E

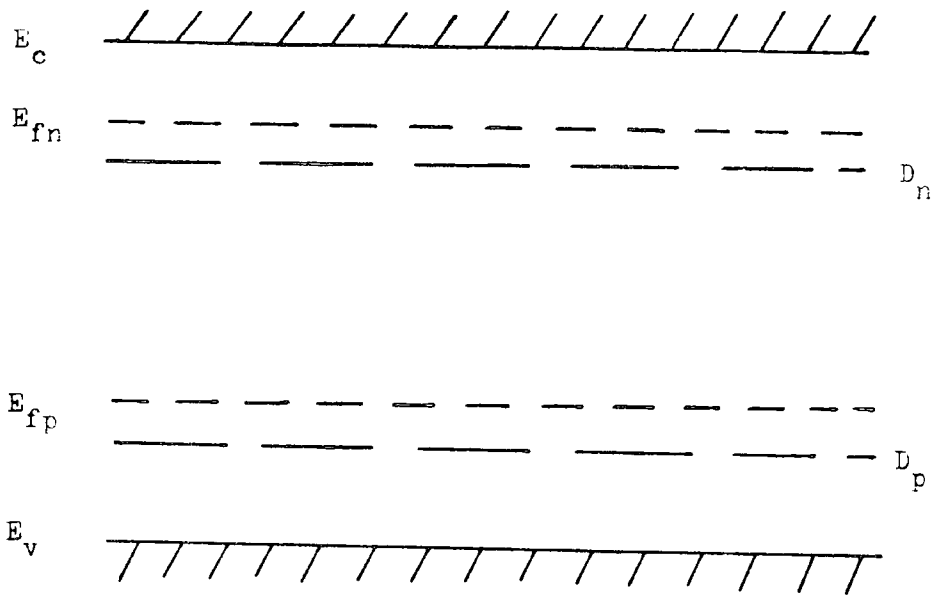

Fig 2.1 : DEMARCATION LEVELS

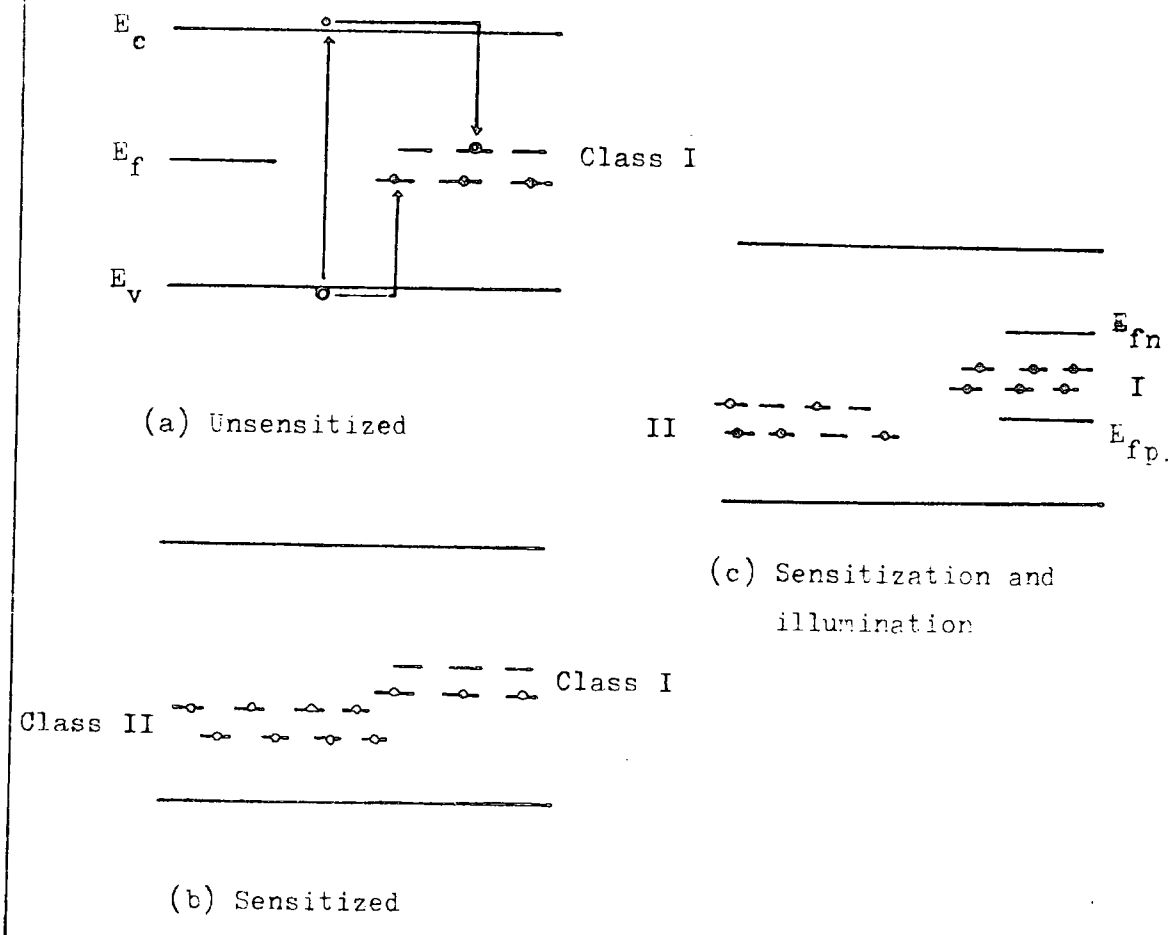

Fig 2.2 : SCHEMATIC OUTLINE OF SENSITIZATION

gives the energy difference between E_c and D_n ; v is the thermal velocity of carrier ; S_p is the capture cross-section of the electron for a free hole ; and lastly p is the density of free holes. The right-hand side of eqn. (2.7) is the reciprocal of the time required for a free hole to be captured by the centre.

At the demarcation level D_n, the states have equal roles as traps and recombination centres, since an electron in one of these states is equally likely to be thermally excited into the conduction band or to capture a free hole. States lying above D_n rapidly take on a predominantly trap character, since the rate of thermal exchange with the conduction band increases exponentially. It is obvious that states above D_n are in thermal contact with the conduction band and their occupancy is given by the Fermi-function centred on E_{fn}, so that,

$$E = E_{fn} + kT \ln \frac{n_g}{n_p} ,$$

where,

n_g = No.of ground states occupied by electrons,

n_p = No. of ground states occupied by holes,

when $n_g = n_p$, $E = E_{fn}$, the demarcation line coincides with the steady state Fermi-level of electrons.

By similar arguments, the states lying between the hole demarcation level D_p, and the valence band act predominantly as hole traps and their occupancy is given by the Fermi function centred on E_{fp}.

From this discussion we conclude that the occupancy of states lying between D_n and the conduction band, and between D_p and the valence band, is governed by their respective steady state Fermi-levels and that the character of these states is predominantly trap-like. The occupancy of states lying between D_n and D_p is governed by the kinetic processes of capturing free electrons and free holes and this occupancy is uniform, that is the same at

all energies between D_n and D_p. Further, the states lying between D_n and D_p are predominantly recombination centres.

2.2.4 Sensitization

In practice, a relatively pure n-type crystal has a fairly short life-time for electrons. Such a crystal is regarded as an insensitive photo-conductor. It can be converted into a sensitive photoconductor by the incorporation of appropriate impurities. The imperfections that give rise to photosensitivity have a large capture cross-section for holes and, a very small capture cross-section for electrons. These imperfections produce so called Class II centres. They are closer to the valence band and are normally compensated acceptor-type imperfections with negative charge in thermal equilibrium.

The other important centres are fast recombination centres known as Class I centres. They are present even in unsensitized material. The identity of these centres is still unknown, but they quickly capture free holes and then free electrons recombine rapidly, Fig 2.2 (a) . The effect of Class I centres is to reduce the free carrier life-time.

When there are both Class I and Class II centres in a crystal, the recombination process is modified. Fig 2.2(b) shows that Class II centres are filled with electrons and have very small capture cross section (10^{-20} cm^2) for electrons, and a somewhat normal cross-section for holes (10^{-15} cm^2). Under illumination a redistribution of electrons and holes takes place among these two types of centres. There is a strong tendency to shift electrons from Class II states to Class I states, since free holes tend to accumulate in the Class II states owing to the large capture cross-section of these states for holes, (see Fig 2.2(c)).

Photosensitivity will then be improved because:(1) the electrons have moved to Class I centres thus reducing the density of holes in these centres, which were responsible for the rapid recombination of free electrons; (2) the

holes that were in Class I centres have now shifted to Class II centres. The lifetime of the free carriers will therefore be increased, because they now, for the most part, meet centres with small capture cross-sections.

2.2.5 Capture and Ionization Cross-Sections

The capture cross-section of a centre reflects its ability to capture a free carrier. The cross-section is not only determined by the mechanisms by which a free carrier loses all the energy between the free state and its final bound state, but there is the possibility that the carrier may first be captured into an excited state of the centre with a small energy loss requiring the emission of only a few phonons. From the excited state the charge may then proceed to the ground state by further phonon cascade processes or by other mechanisms.

In considering capture processes of any centre the sign of the charge carriers relative to the charged state of the centres is important, since this determines whether the process is attractive, neutral or repulsive. It is convenient to consider the trapping centres with positive, neutral or negative charges (N_T^+, N_T^o or N_T^-) when empty. For electron capture by an N_T^+ trap, the process is $N_T^+ + q \rightarrow N_T^o$ and the action is attractive. The generation process for the same trap is $N_T^o \rightarrow N_T^+ + q$, and again is attractive. On the other hand, for a trap with intrinsic charge N_T^- when empty, the capture process is $N_T^- + q \rightarrow N_T^{2-}$, and is repulsive because of the Coulombic barrier around the N_T^- charged trap. Therefore one may expect the capture cross-section to be very small (10^{-21} cm^2 or less). The magnitude of the cross-sections reported in the literature (see Milnes, 1973) cover an enormous range, from 10^{-12} to 10^{-22} cm^2. The giant trapping cross-sections of 10^{-15} to 10^{-12} cm^2 are associated with attractive centres. Cross-sections from 10^{-17} to 10^{-15} cm^2 are usually associated with neutral centres, and tiny cross-sections of 10^{-22} cm^2, are associated with repulsive centres.

The opposite process of capture is ionization and this may be defined in terms of the probability of the centre emitting an electron or hole. Ionization may be achieved by thermal or optical processes. The optical ionization process is called photoionization and occurs at a rate,

$$e_n^o = \sigma_n^o \phi \ , \tag{2.8}$$

where, e_n^o = Optical electron emission rate,

σ_n^o = Photoionization cross-section of electron,

and, ϕ = Photon flux (No.of photons/cm^2-sec).

The corresponding expression for holes is

$$e_p^o = \sigma_p^o \phi \ , \tag{2.9}$$

where, e_p^o = Optical hole emission rate,

and, σ_p^o = Photoionization cross-section of hole.

Equation (2.9) may also be used to describe an electron capture process, where the electron is optically excited from the valence band to centre.

2.3 INFRA-RED QUENCHING

The technique of optical quenching can be used to obtain information about the sensitizing, Class II, centres. The optical frequency at which optical quenching effects are observed in the II-VI compounds is generally in the near or medium infra-red (IR).

The phenomenon of quenching is defined as the reduction in photocurrent following secondary irradiation (with infra-red). The electronic processes involved in quenching are illustrated in Fig (2.3);

(a) Near bandgap light (Primary excitation) generates a photocurrent in the photoconductor,

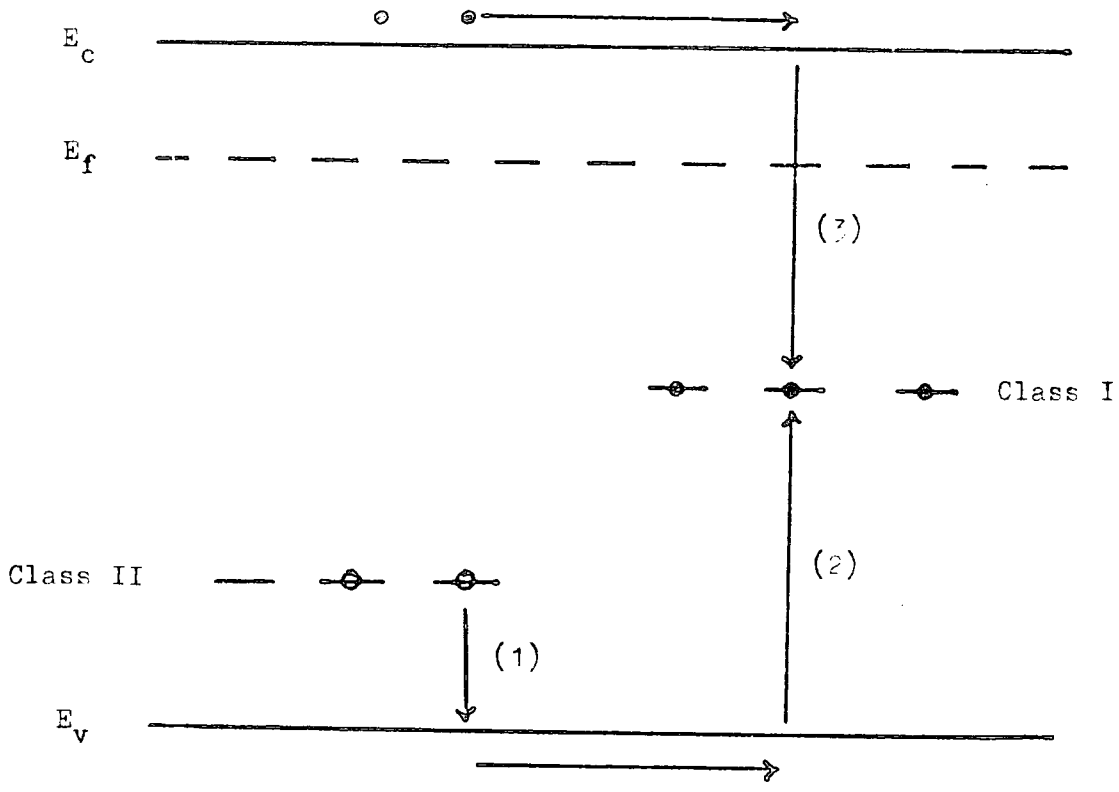

Fig 2.3 : THE TRANSITIONS INVOLVED IN THE INFRA-RED QUENCHING OF PHOTOCURRENT

(b) The infra-red radiation (Secondary excitation) excites electrons from the valence band to the Class II centres and holes are produced in the valence band, (Transition 1),

(c) These holes are quickly captured by Class I centres, (Transition 2),

(d) The conduction band electrons can then recombine with these holes, (Transition 3), and the free electron lifetime is consequently reduced. A quenching of photocurrent then results.

Optical quenching can therefore be used to obtain information about the Class II centres which are closer to valence band and are easily filled by infra-red excitations. In some compounds (e.g. ZnS:Cu) the infra-red radiation, which is used to quench the conductivity induced by primary excitations, can also separately create its own electron photocurrent, see Ullman and Dropkin (1961) and Blount et al (1967). This complicates the quenching behaviour and can lead to incorrect conclusions about the sensitizing centres.

2.4 METAL-SEMICONDUCTOR (OHMIC) CONTACTS

For photoconductivity measurements, it is usually necessary to make electrical contacts to the material. Such contacts would be considered ideal if they introduced no resistance to the flow of current, and if they were unaffected by illumination, temperature or applied electric field.

In order to obtain an ohmic contact between a metal and an n-type semiconductor, it is necessary that the metal work function (ϕ_m) be smaller than the semiconductor work function (ϕ_s). When the metal and semiconductor are apart, Fig 2.4(a), the Fermi-level in the metal (E_F^m) is higher than that in the semiconductor (E_F^s). But when contact is made electrons from the metal side are injected into the semiconductor in order to attain thermal equilibrium, and the two Fermi levels are forced into coincidence. The accumulation of electrons in the surface region of the semiconductor causes the energy bands

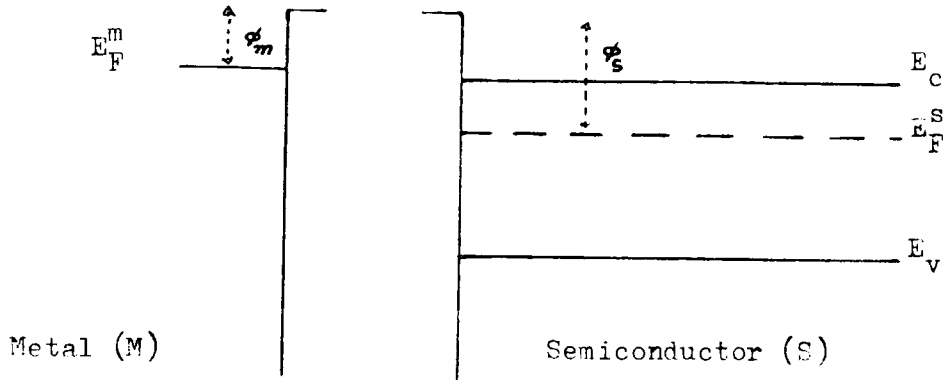

(a) Metal-Semiconductor At No Contact

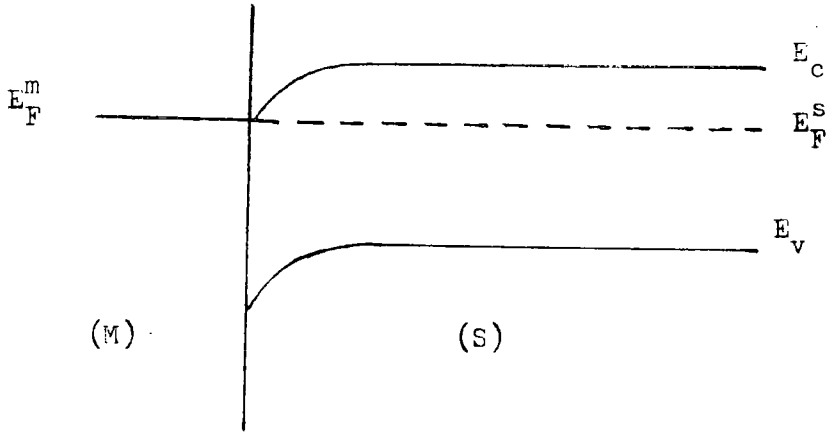

(b) Metal-Semiconductor (M-S) Ohmic Contact

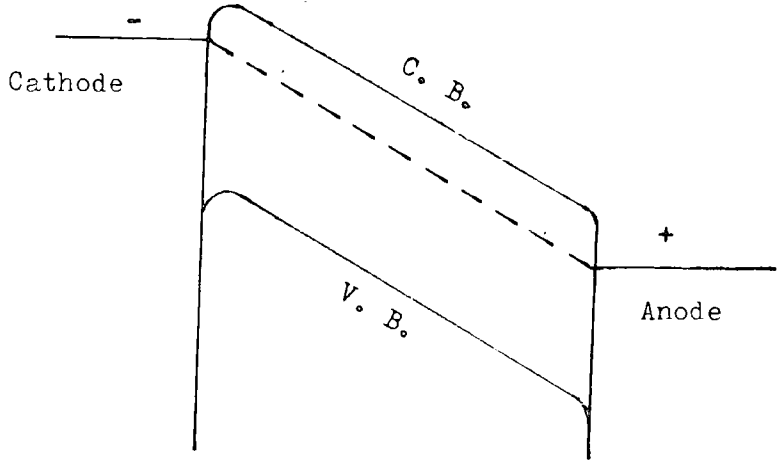

(c) M-S Ohmic Contacts With Applied Electric Field

Fig 2.4 : SCHEMATIC REPRESENTATION OF OHMIC CONTACTS

to bend upwards as shown in Fig 2.4 (b). This type of electrode obeys Ohm's law to a certain extent and provides Ohmic contact.

Ohmic contacts offer no barrier to the flow of current. When the contacts are formed the negative charges (electrons) accumulate at the semiconductor surface and provide a plentiful supply of carriers which take part in the conduction process. The equilibrium situation with zero electric field is changed when the field is applied. The cathode part of the system receives more electrons injected from the metal electrode and stays at higher potential, Fig 2.4(c). The cathode region can be considered as a charge reservoir that supplies charges to the anode region which is at a lower potential energy.

A simple photoconductive device may be formed by using two Ohmic contacts on a semiconductor or insulator. In Chapter 4 the methods of making Ohmic contacts on ZnSe and ZnS crystals are described.

2.5 SPECTRAL DISTRIBUTION OF PHOTOIONIZATION CROSS-SECTION

Photoconductivity measurements can also be used to analyse the variation of the photoionization cross-section of a deep impurity level as a function of photon energy. The absolute values of the cross-sections cannot be determined from this method.

The method makes use of the fact that the occupancy of an impurity level is not changed during illumination with photons of different energy if the photocurrent is kept constant. Thermal excitation from the centres can be neglected if the temperature is kept low enough. The steady state photocurrent can be kept constant at different photon energies ($h\nu$) by changing the intensity of light, $I_L(h\nu)$. Constant photocurrent means a constant density of free-electrons if we assume that the electron mobility is not changed. A constant free-electron density, then implies that the occupancy of the impurity level is constant.

Consider a deep centre with its level in the top half of the bandgap. The photoionization cross-section for exciting electrons from deep centres to

the conduction band is given (see Grimmeiss and Ledebo, 1975), by

$$\sigma_n^o (h\nu) \alpha \frac{1}{I_L (h\nu)} \qquad (2.10)$$

By plotting log $(1/I_L)$ against $h\nu$ (the photon energy of exciting light) the spectral distribution of the photoionization cross-section is obtained.

If there is more than one energy level present in the sample, eqn.(2.10) still holds as long as the rates of optical emission of the other levels can be neglected. The shallow impurity levels will not influence the measurements, if the temperature is low enough.

So far only excitations from the impurity levels to the conduction band have been considered. As soon as $h\nu > (E_T - E_V)$, where E_T and E_V refer to the impurity level and the top of the valence band, two step excitation process will occur, and holes will be created in the valence band. The situation becomes complicated when these holes are captured by impurity centres. The captured holes will accumulate in these levels resulting in a change of occupancy. Thus the method cannot be applied to levels which are in the lower part of the bandgap.

Infra-red quenching can be utilised to determine the spectral distribution of the photoionization cross-section, σ_p^o, for the excitation of holes from sensitizing centres to the valence band. If the quenching is kept constant by controlling the light intensity, and therefore the hole occupancy, a similar expression to (2.10) can be used and,

$$\sigma_p^o \alpha \frac{1}{I_L (h\nu)} \qquad (2.11)$$

Here I_L is the intensity of light needed to keep the quenching constant. Again a plot of log $(1/I_L)$ against $h\nu$ will give the spectral distribution of the photoionization cross-section of holes.

Such cross-section plots can be used to determine the positions of the deep levels in the bandgap region. If the measured photoionization cross-sections are fitted to the Lucovsky model (see § 2.7), a threshold can be found on the energy axis, which gives the position of the energy level.

2.6 SHALLOW AND DEEP CENTRES

A defect state may be defined as an electronic energy state introduced into the forbidden gap of a semiconductor as a result of a perturbation of the bonding structure of the host material by the presence of a lattice defect or impurity. The defects can be classified as either (a) shallow, or (b) deep centres.

(a) Shallow Centres - Shallow centres are located near their related band edges. For instance, shallow donors are very close to the conduction band and shallow acceptors very close to the valence band. These centres are typically substitutional impurities which possess an excess (donor) or deficient (acceptor) valence electron relative to the atom replaced in the host material. In standard nomenclature, donor centres are defined as those centres which become more positively charged when ionized, and acceptor centres as those which become more negatively charged when ionized.

A hydrogenic or Coulombic potential type of model is associated with shallow centres. Kohn (1957), Larson (1969),and Woodbury and Aven (1974) have all discussed shallow defects using this model. The criterion for the use of the hydrogenic model is largely a self-consistent one. It is based on the idea that the wave function describing the bound electron is spread out over many lattice atoms and hence can be described in terms of the single electron effective mass theory. Thus only the long range Coulombic interaction is effective as in the case of the hydrogen atom. The simple defect will bind an extra charge the same fashion as the point charge nucleus of a hydrogen atom

holds its single electron. The binding energy is given by

$$E_n = \frac{(m^*/m_o)}{n^2 \varepsilon^2} \times 13.5 \text{ eV} \qquad (2.12)$$

where,

m^* = Effective electron mass (in case of donor) in the conduction band,

m_o = Electron mass in free space,

ε = Permittivity of semiconductor,

n = Integer

Because of the relatively large dielectric constant of most semiconductors, the Coulombic field and the corresponding binding energy between the donor atom and the bound electron are reduced compared with that of the hydrogen atom. This, in turn, ensures that the electron is indeed in a large orbit.

(b) Deep Centres - Deep centres may be simply defined as those defects which are positioned deeper than the corresponding shallow centres in the bandgap. For deep centres the hydrogen model is known to be inadequate and significant deviations from a Coulombic potential are anticipated. The large ionization energies of these centres imply a strong potential which acts to localize the carrier wave function near the site of the defect. The localization is in contrast with the diffuse nature of shallow centres where the binding energy is diluted by the square of the dielectric constant (see eqn.2.12) of the semiconductor. As the ionicity of the semiconductor increases, the dielectric constant decreases, and defect states become deeper.

Several attempts have been made by Bebb and Chapman (1967), Lucovsky (1965) and Berezin and Kirii (1970) to describe the ground state wave function for a deep centre, using potentials which deviate from a pure Coulombic potential. For these defects there is no long range binding, and it is

reasonable to expect only the one S-like bound state as for a delta-function potential. The Lucovsky model is described in the following section, which is based on a delta-function potential.

The elements copper (Cu), silver (Ag) and gold (Au), well known as luminescence activators, from group I of the periodic table, occupy (substitutionally) group II (Zn,Cd) lattice sites in II-VI compounds and form deep acceptors. The group VII elements, namely Chlorine (Cl), Bromine (Br) and Iodine (I) occupy anion sites (i.e. S, Se) ; and group III elements, namely Aluminium (Al), Indium (In) and Gallium (Ga) occupy cation sites (i.e. Zn,Cd) and form deep donors.

In addition to defects created by deliberately added impurities, natural defects always exist. In II-VI compounds, group II interstitials and group VI vacancies are expected to produce donor states. Similarly, group II vacancies and group VI interstitials form acceptor states.

An association of either a group III or a group VII element with a group II vacancy forms the so-called A-centre, responsible for the self-activated (SA) emission. The mechanism of this acceptor centre was explained by Prener and Williams (1956a, 1956b), and Prener and Weil (1959) in connection with ZnS. They suggested the centre consisted of an association at nearest neighbour sites of the doubly ionized zinc acceptor vacancy defect (V_{Zn}^{2-}) and the ionized impurity donors (Cl_{s}^{1+}, Al_{Zn}^{1+} etc). Such a complex is written as,

$$(V_{Zn}^{2-} - Cl_{s}^{1+})' \quad \text{and} \quad (V_{Zn}^{2-} - Al_{Zn}^{1+})' \quad \text{etc.}$$

Each has an effective negative charge and can be considered to behave like a compensated singly ionized acceptor, introducing a filled localized level above the valence band.

2.7 LUCOVSKY MODEL

Systematic investigations on deep level impurities can only be carried out if the experimental results can be compared with theoretical calculations. In one of his papers, Lucovsky (1965) calculated the magnitude of photo-ionization cross-sections, $\sigma^{o}(h\nu)$, associated with deep levels by studying the transition from the impurity level to a parabolic band with the assumption of a delta-function potential for the impurity centre. The calculation assumes a short range ion core potential rather than long range Coulomb potential. To simplify the algebra, the core potential was taken to be a delta-function. The wave-function for the delta-function potential is

$$\psi(r) = \left(\frac{\alpha}{2\pi}\right)^{\frac{1}{2}} \frac{1}{r} \exp(-\alpha r) \; ; \quad r > 0$$

where α is related to the ionization energy of the impurity level, ΔE_i^o, and the effective mass m* by the relation

$$\alpha = \left(\frac{2\, m^*\, \Delta E_i^o}{\hbar^2}\right)^{\frac{1}{2}} .$$

The expression for the photoionization cross-section, σ^o, is then given as

$$\sigma^o(h\nu) = \frac{1}{n}\left(\frac{E_{eff}}{E_o}\right)^2 \frac{16\,\pi\, e^2\, \hbar\, (\Delta E_i^o)^{\frac{1}{2}}\, (h\nu - \Delta E_i^o)^{3/2}}{3\, m^*\, c\, (h\nu)^3} \qquad (2.13)$$

where n is index of refraction for the material and E_{ef}/E_o is the effective field ratio for the radiation inducing the transition. The expression (2.13) in a

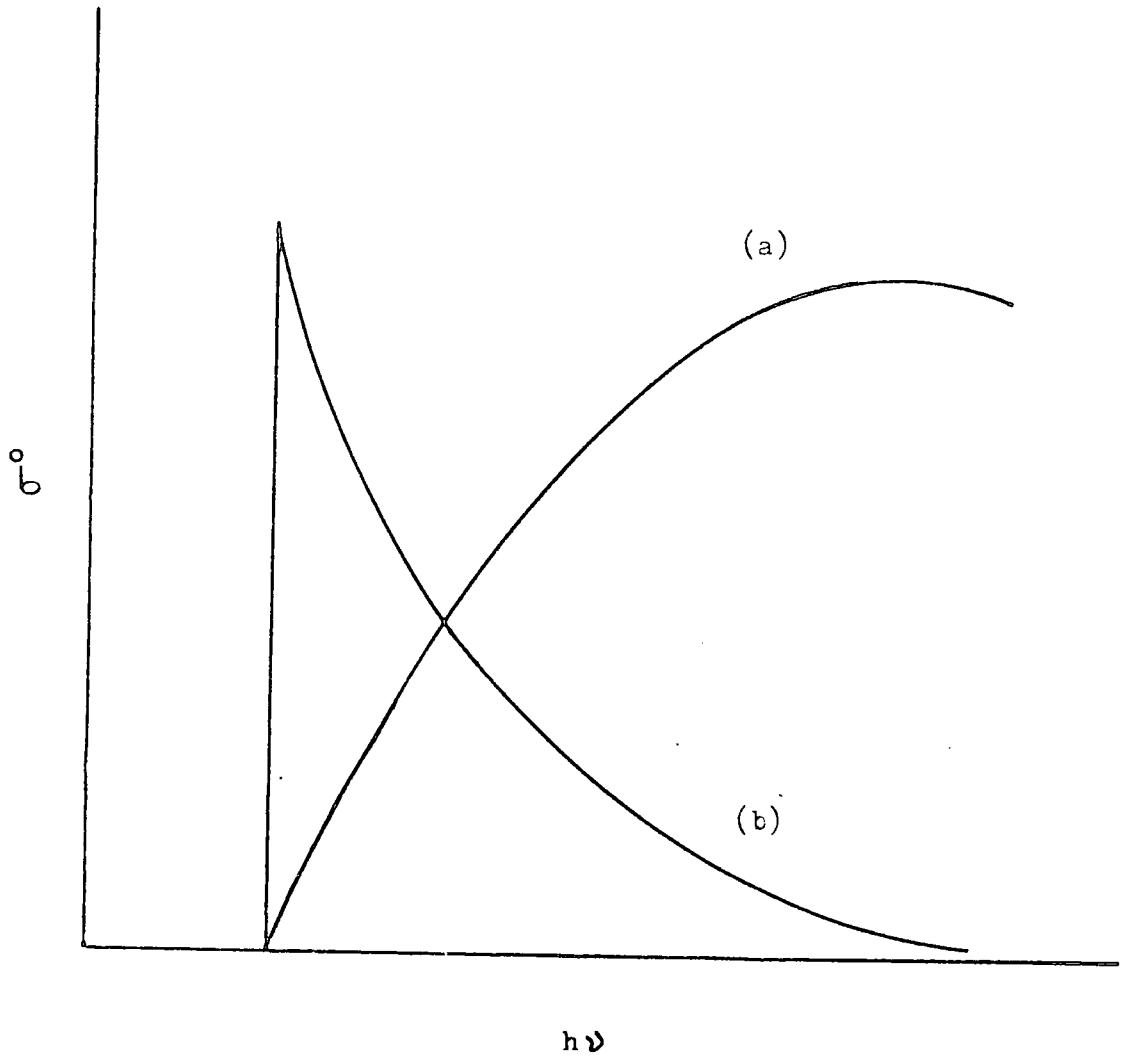

Fig 2.5 : SPECTRAL DISTRIBUTION OF PHOTOIONIZATION CROSS-SECTIONS

(a) DELTA FUNCTION

(b) COULOMBIC MODEL

modified form was used by Grimmeiss et al (1976), i.e.

$$\sigma^{o} \quad \alpha \quad (h\nu - \Delta E_i^{o})^{3/2} \left\{ h\nu \left[h\nu + \Delta E_i^{o} \left(\frac{m_o}{m^*} - 1 \right) \right]^2 \right\}^{-1} \qquad (2.14)$$

where $\frac{m_o}{m^*}$ is effective mass ratio. The cross-section described by eqn. (2.14) has been used in our curve fitting procedure, to determine the values of threshold.

The function σ^{o}, given in eqns. (2.13) and (2.14) rises from zero at $h\nu = \Delta E_i^{o}$, has a maximum at $h\nu = 2\,\Delta E_i^{o}$, and falls off approximately as $h\nu^{-3/2}$ for $h\nu \gg \Delta E_i^{o}$, see Fig 2.5 (a). This is to be contrasted with the Coulombic model for shallow centres, where the cross-section has a maximum at $h\nu = \Delta E_i^{o}$ and falls off approximately as $h\nu^{-3}$ for $h\nu > \Delta E_i^{o}$, (see Fig 2.5(b)).

CHAPTER 3

STEADY STATE AND TRANSIENT PHOTOCAPACITANCE AND TRANSIENT PHOTOCURRENT EFFECTS

3.1 METAL-SEMICONDUCTOR RECTIFYING CONTACTS

3.1.1 Introduction

Investigations of metal-semiconductor contacts go back more than a hundred years to the early work of Braun (1874) who discovered the asymmetric nature of electrical conduction between metal contacts and semiconductors, such as copper and iron sulphide. Although the rectification mechanism was not understood, contacts between metals and semiconductors were used extensively as detectors in early experiments on radio. The first step towards understanding the rectification action of metal-semiconductor contacts was taken by Schottky, Störmer, and Waibal in 1931. In 1938 Schottky and, independently, Mott, pointed out that the observed direction of rectification could be explained by supposing that electrons passed over a barrier through the normal processes of drift and diffusion. In the model first put forward by Schottky (1938) and elaborated by Schottky and Spenke (1939), the semiconductor is assumed to be homogeneous right up to the boundary with the metal, so that the uncompensated donors give rise to a uniform space-charge in the depletion region. The electric field strength therefore decreases linearly with distance from the interface in accordance with Gauss's theorem, and the electrostatic potential decreases quadratically. The resulting parabolic barrier is known as a Schottky Barrier (see Fig 3.1a). A somewhat different model was given by Mott (1938), but it is rarely encountered in practice.

3.1.2 The Schottky-Mott Theory

Schottky barriers are formed by making contact between a metal of work function (ϕ_m) and a semiconductor of lower work function (ϕ_s). Such barriers usually demonstrate their presence by giving rise to rectification effects, i.e. the resistance to current flow is much less for one direction of the applied field than for the reverse direction.

The energy band diagram between a metal and an n-type semiconductor for a Schottky barrier is illustrated in Fig 3.1(a). Because of the mismatch of the work functions, electrons transfer from the semiconductor to the metal and the two Fermi-levels move into coincidence. An electric field, due to the contact potential is then set up and exists largely within the semiconductor. It opposes further flow of electrons from the semiconductor to the metal and allows equilibrium to be established. Since the semiconductor is n-type, the positive charge will be provided by conduction electrons moving to the metal, leaving uncompensated positive donor ions in a region depleted of electrons. Because the donor concentration is many orders of magnitude less than the concentration of electrons in the metal, the uncompensated donors occupy a layer of appreciable thickness W, known as the depletion width, and the bands in the semiconductor are bent as shown in Fig 3.1(a). A barrier is formed by the negative charges located at the metal contact and positive charges, in the form of uncompensated donors, distributed in a volume of the semiconductor extending a distance W from the contact. This type of parabolic barrier is known as a Schottky barrier. In an ideal situation, the barrier height is,

$$\phi_{bo} = \phi_m - \chi_s, \tag{3.1}$$

but due to the reduction of ϕ_m as a result of the image force and the electric field, the actual barrier height ϕ_{bn} is smaller than ϕ_{bo}, see Fig 3.1(a). Here χ_s is the electron affinity of the semiconductor. Although, eqn.(3.1) is usually

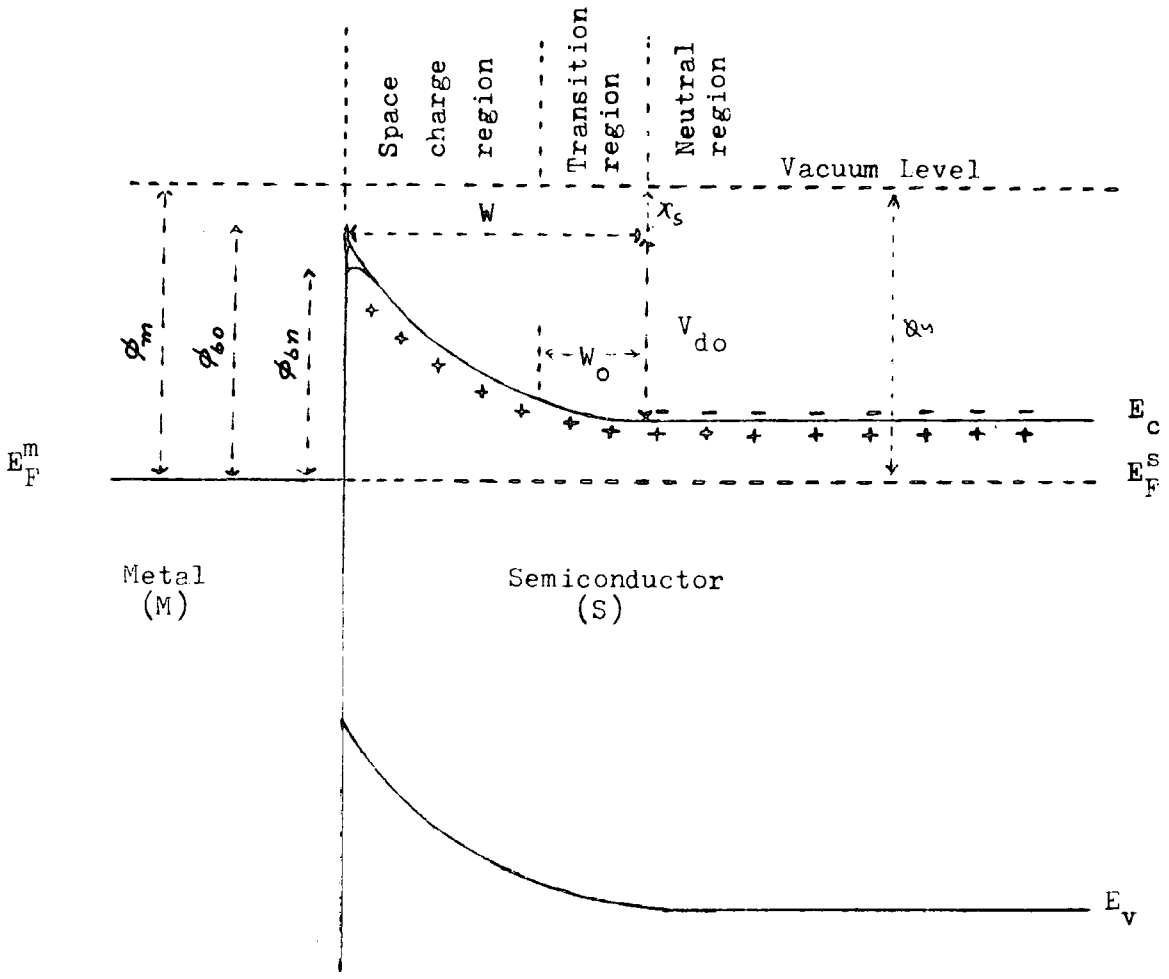

Fig 3.1(a) : DETAILED ENERGY BAND DIAGRAM OF A SCHOTTKY CONTACT

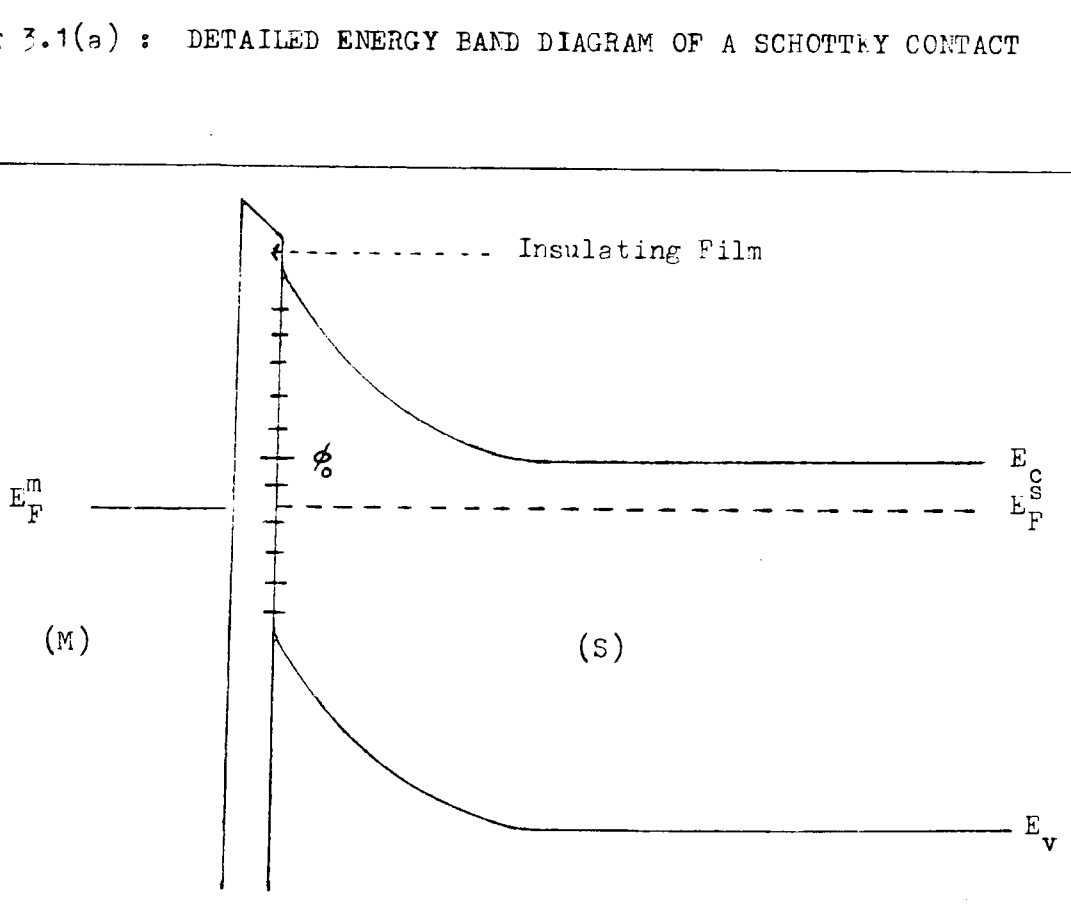

Fig 3.1(b) : SCHOTTKY CONTACT WITH SURFACE STATES

attributed to Schottky, in fact it was first stated by Mott (1938). Also, according to Mott (1938), the band bending or "diffusion potential", V_{do}, should be equal to the difference between the metal and semiconductor work functions,

$$V_{do} = \phi_m - \phi_s.$$

The region beyond W is"the neutral region" where the space charge of the ionized dopant is exactly cancelled by the mobile carriers. The second region W_o, close to the neutral region is known as the "transition region". In this part both thermal generation and recombination processes are active, and it is inoperative as far as optical processes are concerned, see Braun and Grimmeiss (1973). It is independent of bias. The most important region is $(W-W_o)$ which is totally depleted of mobile carriers, and is called the space charge region. The width of this region increases with reverse bias and decreases with forward bias.

3.1.3 Surface States

Surface states arise because the surface of the semiconductor interrupts the perfect periodicity of the crystal lattice. A very high density of surface states might be expected on theoretical grounds, because the lattice discontinuity at the surface would constitute one unpaired electron per atom perbond which is directed away from the surface. This unsatisfied bond is called a "dangling bond", and can either give up its electron and act as a donor or accept another electron and act as an acceptor. The number of detectable surface states depends on how the surface atoms are arranged. The perturbation introduced by the discontinuity in the lattice where the surface is formed may result in a rearrangement of surface atoms compared to their disposition along the same plane within the crystal, with possibly a resulting stretching and twisting of bonds. The atoms on the surface form a two-dimensional lattice, Heine (1972), with a continuous range of energies which may overlap the valence and conduction bands, though only those within the forbidden gap play a role in contact phenomena. The

existence of surface states means that the energy bands are usually bent near a free surface.

Surface states have a profound effect on the barrier height at a metal semiconductor contact. Suppose that the metal and semiconductor remain separated by a thin insulating layer (10 - 20 Å) as shown in Fig 3.1(b), and that there is a continuous distribution of surface states at the semiconductor surface characterized by a neutral level ϕ_o. The neutral level is a demarcation level to which surface states are filled when the surface is electrically neutral. If states below ϕ_o are empty, the surface has a net positive charge (donor-like) while, if states above ϕ_o are filled, the surface has a net negative charge (acceptor-like). In the absence of surface states, the negative charge Q_m on the surface of the metal must be equal and opposite to the positive charge Q_d of the uncompensated donors. In the presence of surface states, the neutrality condition becomes $Q_m + Q_d + Q_{ss} = 0$, where Q_{ss} is the charge in the surface states. The occupancy of the surface states is determined by the Fermi level, E_F^s, and the states are supposed to be filled up to the Fermi level and emptied above it. If the neutral level ϕ_o happens to be above E_F^s as shown in Fig 3.1(b), the surface states contain a net positive charge and Q_d must therefore be smaller than if surface states were absent. This means that the width W of the depletion region will be correspondingly reduced, and the amount of band bending (proportional to W^2) will also be decreased. As a result the barrier height is reduced because it is proportional to the band bending. The reduction in the barrier height has the effect of pushing ϕ_o towards E_F^s ; i.e. it tends to reduce the positive charge in the surface states. On the other hand, if ϕ_o happens to be below E_F^s, Q_{ss} is negative and Q_d must be greater than if surface states were absent. This means that the depletion width and the barrier height will both be increased and ϕ_o will be pulled up towards E_F^s.

The Schottky barrier shown in Fig 3.1(b) is supposed to be the actual barrier formed in practice, because it is difficult to avoid the formation of

an insulating layer (oxide) and accompanying surface states. In the presence of surface states : (1) the barrier height will be changed, (2) the barrier will be independent of metal work function, Bardeen (1947) and, (3) the bands will bend upwards towards the surface if the surface charge is negative, and downwards if the charge is positive.

3.1.4 The Capacitance of the Schottky Barrier

The capacitance of the Schottky barrier is associated with the depletion region and its charge state. The capacitance is usually measured by superimposing a small alternating voltage on a reverse D.C. bias, which yields the differential capacitance C $\left(= \frac{dQ}{dV} \right)$. The differential capacitance is therefore not constant but decreases as the reverse bias V_r is increased. When reverse bias is applied, electrons in the conduction band of the semiconductor recede further from the metal and increase the width of the depletion region W, so that the capacitance decreases. In addition, there is a parallel conductance due to the reverse current of the diode, so the equivalent circuit, consists of a capacitance in parallel with a resistance.

The charge state of the barrier region is quite complex and at first sight it is difficult to realize which charge is responsible for the capacitance. There are three sources of charge in the barrier region : (1) the positive charge Q_d due to the uncompensated donors in the depletion region, (2) the positive charge Q_h due to extra holes in the valence band and, (3) the negative charge Q_m due to electrons on the surface of the metal. An increase in reverse bias increases the magnitude of Q_d and decreases Q_h. The variation of the bias varies the total current through the depletion region which consists of the conduction current plus a displacement current. The displacement current (J_d) arises because the electric field in the depletion region increases with time as the bias increases. The conduction current has two parts, (1) a component J_{C1} due to drift and diffusion of electrons injected over the barrier from the metal and, (2) a component J_{C2} which arises because there is a flow of electrons and

holes out of the depletion region as the negative bias increases. The component J_{C1} exists even if the bias is constant in time and constitute the reverse current of the diode and J_{C2} exists only if the bias is changing. The reverse current (J_{C1}) gives rise to the parallel conductance, while the displacement current (J_d) and the component J_{C2} of conduction current give rise to the capacitance.

The bias changes the depletion width, and this in turn changes the total charge per unit area Q_d due to the uncompensated donors, and also the electric field E in the depletion region. From Gauss's theorem,

$$\varepsilon_s \Delta E = \Delta Q_d ,$$

where ε_s is the permittivity of the semiconductor. From the concept of the displacement current,

$$C = \varepsilon_s \frac{\partial E}{\partial V_r} ,$$

and using the above expression, C can be rewritten as,

$$C = \frac{\partial Q_d}{\partial V_r} . \qquad (3.2)$$

The expression (3.2) shows that the capacitance can be calculated by considering only the charge due to the uncompensated donors and ignoring the charge due to the holes. The capacitance defined in this way is a differential capacitance per unit area ; i.e. it represents the response of the depletion region to a change ΔV_r in the reverse bias.

The differential capacitance, C, can be expressed in terms of the donor density, N_d, and the diffusion voltage, V_d, if the effect of the holes can be neglected. If we take the electric field in the depletion region at the

interface to be due to uncompensated donors only, then the simplified expression for the maximum electric field, see Rhoderick (1980), is

$$(E_{max})^2 = \frac{2q N_d}{\varepsilon_s} \left(V_d - \frac{kT}{q}\right) \tag{3.3}$$

From Gauss's theorem the charge due to the uncompensated donors is given by

$$Q_d = \varepsilon_s E_{max} = (2q \varepsilon_s N_d)^{\frac{1}{2}} \left(V_d - \frac{kT}{q}\right)^{\frac{1}{2}}.$$

So that

$$C = \frac{\partial Q_d}{\partial V_r} = \frac{\partial Q_d}{\partial V_d}$$

$$C = \left(\frac{q \varepsilon_s N_d}{2}\right)^{\frac{1}{2}} \left(V_d - \frac{kT}{q}\right)^{-\frac{1}{2}} \tag{3.4a}$$

Since, $V_d = V_{do} + V_r$, where V_{do} is the diffusion voltage at zero bias and V_r is the reverse bias, eqn. (3.4a) may be written as

$$C = \left(\frac{q \varepsilon_s N_d}{2}\right)^{\frac{1}{2}} \left(V_{do} + V_r - \frac{kT}{q}\right)^{-\frac{1}{2}} \tag{3.4b}$$

Or, $$\frac{1}{C^2} = \frac{2(V_{do} + V_r - kT/q)}{q \varepsilon_s N_d}$$

Or, $$d\left\{\frac{1}{C^2}\right\} = \frac{2}{q \varepsilon_s N_d} d(V_r) \tag{3.5}$$

$$\therefore \quad N_d = \frac{2 d(V_r)}{q \varepsilon_s d(C^{-2})} \tag{3.6}$$

The plot of C^{-2} against V_r, according to eqn.(3.5), will give a straight line if N_d is constant throughout the depletion region, with a

slope = $(2/q\varepsilon_s N_d)$ and the intercept (at $C^{-2} = 0$) $V_i = V_{do} - \frac{kT}{q}$. Equation (3.6) will give the magnitude of $N_d = N_D^+ - N_A^-$, the uncompensated donors in the depletion region of the Schottky barrier. If the term $\frac{kT}{q}$ is omitted from eqn. (3.4b), the result is equivalent to using the depletion approximation. In this case the capacitance per unit area is

$$C = \sqrt{\frac{q\,\varepsilon_s\,N_d}{2(V_{do}+V_r)}} = \frac{\varepsilon_s}{W} \qquad (3.7a)$$

where,

$$W = \sqrt{\frac{2(V_{do}+V_r)\varepsilon_s}{q\,N_d}} \qquad (3.7b)$$

The depletion region W as shown in Fig 3.1(a) and according to eqn. (3.7b) is dependent on bias, conductivity and temperature as follows :

(a) W is directly proportional to $V_r^{1/2}$, or the depletion width increases when the reverse bias increases, due to the electrons in the conduction band receding further from the metal contact ;

(b) W is inversely proportional to $N_d^{1/2}$, i.e. it is narrow for a high density of uncompensated donors and wider for samples containing lower values of donors. This shows that samples with high conductivity have very sharp band bending ; and,

(c) At higher temperature more donors are ionized and $N_d = N_D^+ - N_A^-$, is large, so that the depletion region has a smaller width. At lower temperatures N_d decreases and W increases.

3.1.5 Influence of Traps on the Schottky Barrier Capacitance

The energy diagram of the Schottky barrier (without interface states), containing donor-like traps is shown for n-type material in Fig 3.2(a), under reverse bias conditions.

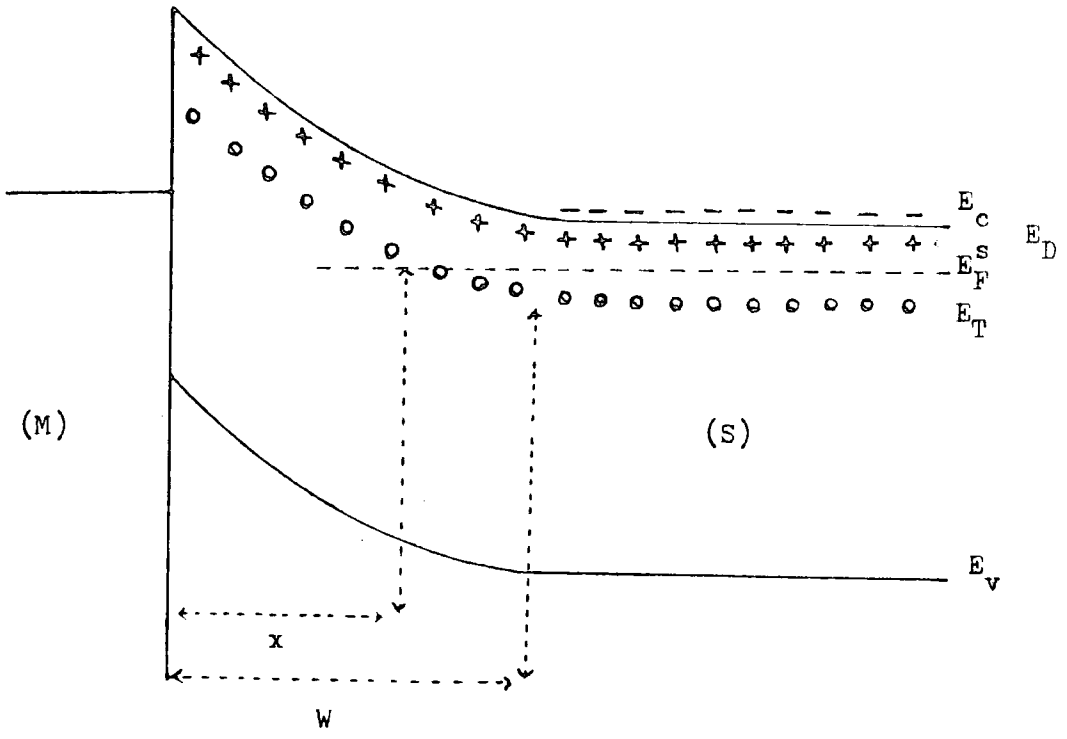

Fig 3.2(a) : ENERGY DIAGRAM OF A SCHOTTKY BARRIER (n-type material) WITH TRAPS (donor like)

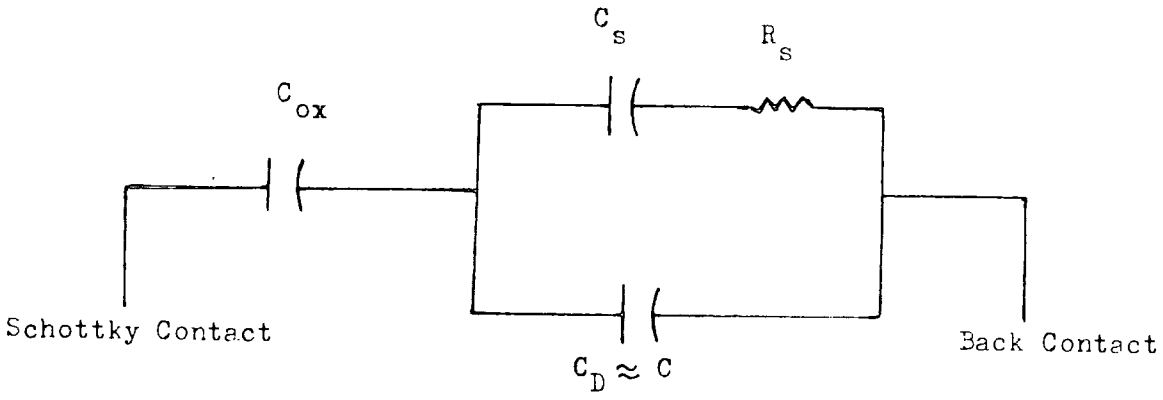

Fig 3.2(b) : EQUIVALENT CIRCUIT OF THE ACTUAL SCHOTTKY DIODE

If the applied voltage is changed from V_r to $V_r + \delta V_r$, the crossing point between E_F^s and E_T moves from x to x + δx. The traps which are then above the Fermi-level emit their electrons into the conduction band with an emission rate e_n. When the voltage is decreased again the opposite occurs, thus leading to an additional current in the external circuit of the diode.

At low temperature , the total charge emitted (after an infinite time) is

$$\delta Q = q N_T A \delta x.$$

where q is the electron charge, A is the diode area and N_T is the concentration of traps. It can be shown (see Vincent et al, 1975) that at higher temperature the total charge emitted is,

$$\delta Q = \frac{q N_T A}{n} \left(\frac{\epsilon_s N_D^+}{2 q V} \right)^{\frac{1}{2}} \delta V \qquad (3.8)$$

where n is the number of free carriers in the bulk, ϵ_s dielectric constant of the semiconductor; N_D^+ is the concentration of fixed positive charge (in the case of an n-type semiconductor) in the depletion region, without compensation.

If an AC-signal, $\delta V = \delta V_o \exp(j\omega t)$, is applied to the diode the current in the circuit is given by

$$i(t) = - \frac{d Q(t)}{t} = e_n Q(t)$$

or, $$Q(t) = \delta Q(t) - \int_o^t i \, dt$$

i.e., $$i(t) = e_n (x \delta V - \int_o^t i \, dt)$$

where $$x = \frac{N_T A}{n} \left\{ \frac{\epsilon_s q N_D^+}{2V} \right\}^{\frac{1}{2}}$$

The solution may be written (as given by Vincent et al, 1975).

$$i = x\, e_n \cos(\psi)\, \delta V_o \exp\left[j(\omega t + \psi) \right]$$

with

$$\tan\psi = e_n / \omega$$

This current has two components, one in phase and the other in quadrature with δV :

$$i_{phase} = \frac{e_n^2}{e_n^2 + \omega^2} \cdot \frac{\omega}{e_n} \times \delta V_o \exp(j\omega t)$$

and

$$i_{quad} = \frac{e_n^2}{e_n^2 + \omega^2} \times \delta V_o \exp\, j\left(\omega t + \frac{1}{2}\pi\right)$$

Thus, the traps introduce a conductance G_T given by

$$G_T = \frac{i_{phase}}{\delta V_o} = \frac{e_n\, \omega^2}{e_n^2 + \omega^2} \cdot \frac{N_T A}{n} \left(\frac{\varepsilon_s q N_D^+}{2V} \right) \qquad (3.9)$$

The exchange of electrons between the traps and the conduction band also leads to an additional capacitance :

$$C_T = \frac{1}{\omega} \frac{i_{quad}}{\delta V_o} = \frac{e_n^2}{e_n^2 + \omega^2} \cdot \frac{N_T A}{n} \left(\frac{\varepsilon_s q N_D^+}{2V} \right)^{\frac{1}{2}} \qquad (3.10)$$

In expressions (3.9) and (3.10), the terms n, N_T, N_D^+ and e_n are expected to vary with temperature. However, e_n is related to the temperature through,

$$e_n = e_{no} \exp\left[(E_T - E_c)/kT \right] \qquad (3.11)$$

and its variation with T can generally be considered as preponderant.

At high frequency, the additional capacitance C_T disappears while the conductance remains constant. The quantity $C_T \omega$ has a maximum for $\omega = e_n$. The conductive to capacitive current ratio in the diode is $G_T/C_T\omega = \omega/e_n$. So, the effect of the additional conductance increases with frequency. However, if the total capacitance of the barrier is $C = C_D + C_T$, with C_D (depletion region capacitance) independent of the frequency, the ratio $G_T/C_D\omega$ vanishes at high frequency. Thus the study of G_T and C_T can be made at moderate frequencies.

The general expression for the capacitance of a Schottky barrier is

$$C_D = A\left(\frac{\varepsilon_s q N_D^+}{2V}\right)^{\frac{1}{2}}$$

Then the measured capacitance in the presence of traps is

$$C = C_D + C_T = A\left(\frac{\varepsilon_s q N_D^+}{2V}\right)^{\frac{1}{2}}\left(1 + \frac{N_T}{n}\,\frac{e_n^2}{e_n^2 + \omega^2}\right) \qquad (3.12)$$

The expression (3.12) shows that there is an inverse relation between C and ω, the frequency. The situation becomes complicated when acceptors are also present.

The energy band diagram of the Schottky barrier as shown in Fig 3.2(a) is a simplified version of the more complicated Schottky barrier formed in practice. The actual Schottky barrier when made on an etched crystal usually contains an insulating oxide layer of etch compounds and gives rise to another additional capacitance, C_{ox}. The equivalent circuit of an etched Schottky barrier is then, as shown in Fig 3.2(b), where C_D, C_s & R_s are depletion layer capacitance, interface states capacitance and resistance representing the loss mechanism due to the surface states at the interface, respectively.

The parallel branch of this circuit can be regarded as a frequency dependent capacitance, C_p, with an equivalent parallel conductance G_p, see Özsan and Woods (1977), where

$$C_p = C_D + \frac{C_s}{1 + \omega^2 \tau^2} \qquad (3.13a)$$

and

$$G_p/\omega = \frac{C_s \omega \tau}{1 + \omega^2 \tau^2} \qquad (3.13b)$$

$\tau = R_s C_s$, is the time constant associated with interface states. The equivalent parallel conductance G_p of the network depends only on the surface state branch.

The effect of an interfacial layer on the capacitance has been analysed in some detail by Cowley (1966) and by Crowell and Roberts (1969). In the case of a thin interfacial layer ($\sim$ 30 Å), the occupation of any interface states will be determined by the Fermi-level in the metal. The interface states are then emptied or filled by the tunnelling of electrons from the metal and make no direct contribution to the capacitance. If the layer is thick enough, then the interface states may be partially in equilibrium with the semiconductor. This is a much more complicated situation because the interface states are now filled from the semiconductor. According to Cowley, the surface states have short time constants and can follow low frequency signals.

3.1.6 Measurement of the Schottky Barrier Height

(a) Photoelectric Method

The measurement of the barrier height by the photoelectric method is the most direct and accurate technique, Crowell et al (1962). When monochromatic light is incident upon the metal-semiconductor junction, a photocurrent may be

generated. With front wall (rectifying contact side) illumination the light can generate excited electrons in the metal, as well as electron-hole pairs in the semiconductor. Electrons emitted from the metal can surmount the barrier and are then accelerated in the high electric field of the depletion region and contribute to the short circuit photocurrent. According to Fowler (1931) the photocurrent per absorbed photon R, as a function of the photon energy, $h\nu$, can be approximated to

$$R \sim (h\nu - h\nu_o)^2$$

For $q\phi_{bn} \lesssim h\nu - E_g$

$$(R)^{\frac{1}{2}} \sim (h\nu - q\phi_{bn}) \qquad (3.14)$$

where, $h\nu_o$ = Barrier height ($\approx \phi_{bn}$)

E_g = Bandgap energy

When the square root of the photocurrent per incident photon ($\sqrt{R}$) is plotted against the incident photon energy, a straight line should be obtained, and the extrapolated value on the energy axis should give directly the barrier height reduced by the image force lowering factor.

(b) The Capacitance-Voltage Method

The relationship between the capacitance (C) of the depletion region and the applied bias (V) is given in many places in this chapter and it is obvious that the barrier height can also be determined from C-V measurements. If ϕ_{bn} is independent of the bias a plot of C^{-2} against V_r (reverse bias) should give a straight line with an intercept, $V_i = V_{do} - \frac{kT}{q}$, on the voltage axis.

The barrier height ϕ_{bn} is given by

$$\phi_{bn} = V_{do} + E_F \qquad (3.15)$$

Here E_F is the depth of the Fermi-level below the conduction band and is given by,

$$E_F = \frac{kT}{q} \ln \frac{N_c}{N_d} \quad (eV) \qquad (3.16)$$

which is easily computed if the doping concentration is known.

Expression (3.15) can be approximated to $\phi_{bn} \sim V_i$ to obtain a rough estimate of the barrier height.

3.2 STEADY-STATE PHOTOCAPACITANCE

3.2.1 Introduction

The change in the charge state and the subsequent effect of this change on the capacitance of the depletion region, brought about by exposure to light is called photocapacitance. In the past few years the study of photocapacitance effects in potential barriers (p-n junctions or Schottky diodes) has proved to be a powerful tool for investigating localized energy levels and associated centres in semiconductors. Photocapacitance techniques have been used by Grimmeiss and Olofson (1969) for Cu in GaP, Kukimoto et al (1973) for O in GaP, Marfaing et al (1974) for CdTe, Kosai et al (1979) for p-type ZnSe and many others.

In steady state measurements the photocapacitance spectrum is obtained by scanning the wavelength at a slow speed. For the study of shallow centres this type of measurement has been successfully applied by Marfaing et al to CdTe, because the relevant centres have short time constants and respond immediately. But for deep centres because of the large associated time constants this type of measurement introduces problems.

3.2.2 Study of Deep and Shallow Centres

Deep centres can be detected using the steady state photocapacitance technique, in which monochromatic light of different photon energies is scanned with a very slow speed or alternatively point by point plotting is employed. In the point by point method the sample is irradiated for a time long enough for a steady state value of photocapacitance to be obtained. This equilibrium value is recorded which is the actual magnitude for that particular wavelength of excitation. Before moving to the next wavelength, the initial value of the capacitance is restored by removing the first irradiation or by using another.

The capacitance of the depletion region is a function of $N_d = N_D^+ - N_A^-$, and is, see eqn. (3.7a),

$$C = \sqrt{\frac{q\,\varepsilon_s (N_D^+ - N_A^-)}{2\,(V_{do} + V_r)}} \qquad (3.17)$$

where,

N_D^+ = ionized donor concentration,

N_A^- = ionized acceptor concentration.

Let us consider that only one acceptor, E_T, is present, as shown in Fig 3.3(a), in the lower half of the bandgap. Light with photon-energy $h\nu > \Delta E_n^o$, will excite electrons from the level, i.e. N_A^- decreases, and so the photocapacitance will increase, according to eqn. (3.17). In the second case if $\Delta E_n^o > h\nu > \Delta E_p^o$, the centres are filled and N_A^- increases and the photocapacitance will decrease. The sign of the change in the photocapacitance indicates uniquely whether the centres involved are donors or acceptors. The wavelength of the light fixes the position of the levels from the band edges. The obvious thresholds in the photocapacitance spectrum are usually selected to calculate the appropriate

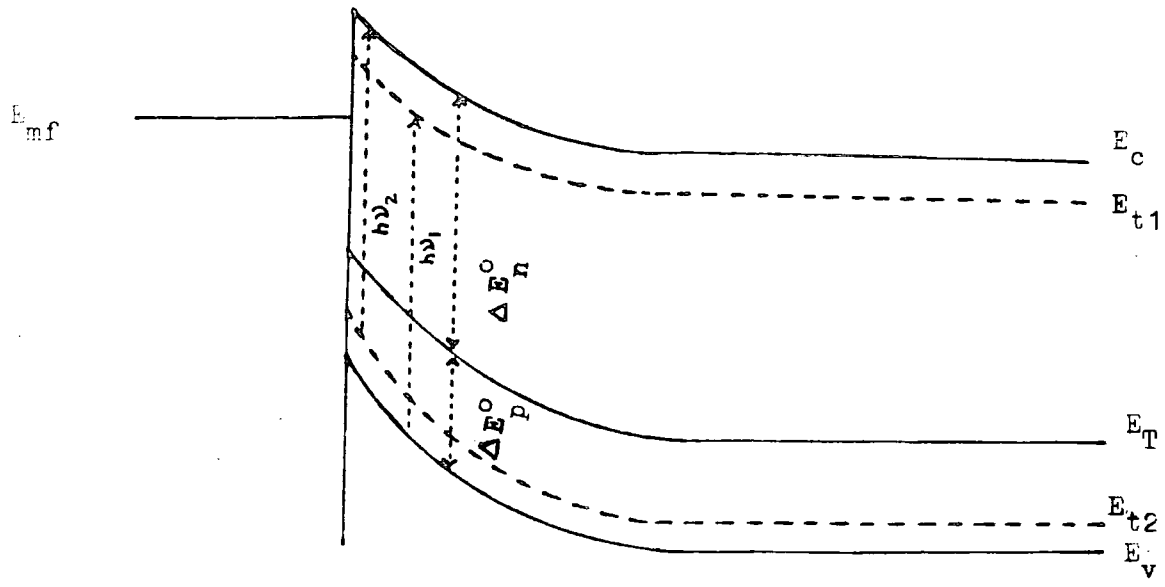

Fig 3.3(a) : PHOTOEMISSION FROM SHALLOW DONOR AND ACCEPTOR

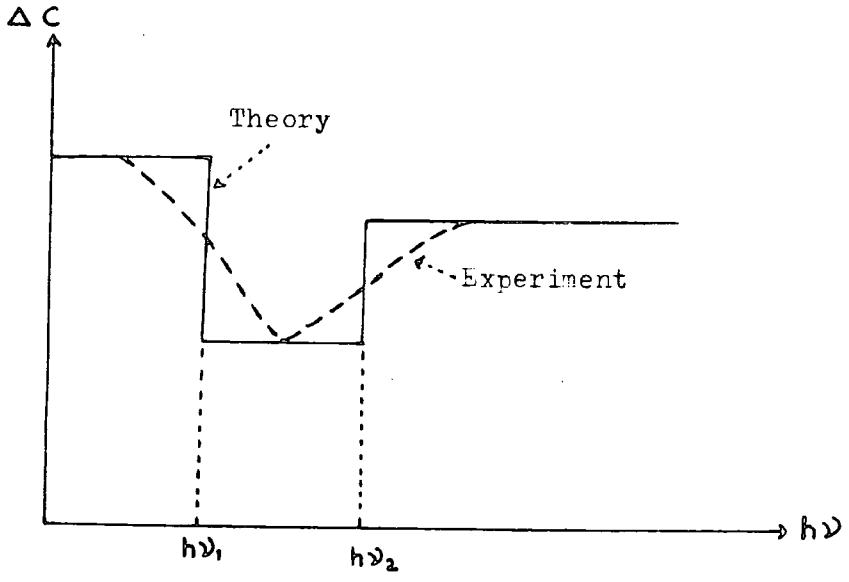

Fig 3.3(b) : PHOTOCAPACITANCE TECHNIQUE APPLIED TO THE STUDY OF SHALLOW LEVELS

energy levels. Sometimes, the choice of threshold is quite difficult.

With less deep centres or shallow centres, the time constant for establishing the steady state is short (of the order of a few seconds), owing to the large thermal emission rate, Herman and Sah (1973). The spectral variation of the photocapacitance will then give a satisfactory result even if the response is recorded directly by scanning the wavelength at a slow speed. Assume that a sample contains a shallow donor, E_{t1} ; and a shallow acceptor, E_{t2} , see Fig 3.3(a). To avoid complexity, the deep acceptor E_T is excluded in the present discussion. Suppose $h\nu_1$ and $h\nu_2$ are the threshold energies for the filling of the shallow donors and the emptying of the shallow acceptors respectively, then since the centres are hydrogenic there should be a sharp change in capacitance at $h\nu_1$ and $h\nu_2$, see Fig 3.3(b). However, because of photothermal ionization effects (see Sah, et al, 1971) the thresholds will not be very sharp. On average the variation of photocapacitance extends to both sides of the threshold ($h\nu_1$ or $h\nu_2$, etc) and for this reason the value of $h\nu_1$, for example, is taken as the photon energy at which the capacitance is reduced by half. Similarly $h\nu_2$ is found by determining the photon energy at which the capacitance is increased by half.

3.3 TRANSIENT TECHNIQUES

This is an important class of techniques in which the change of capacitance or current flowing in a p-n junction or a Schottky barrier is measured as a function of time.

For a proper description of deep level impurities, it is necessary to know which parameters characterize their physical properties. It is quite obvious that the energy of an impurity level within the bandgap is an important parameter. Furthermore, to describe recombination and excitation kinetics, the probabilities for capture and emission processes have to be known. However, the rate of recombination and excitation is proportional to the number of impurity levels. A knowledge of the density N_T of the centres is

also desirable. Hence, to characterize the electrical and optical properties of deep level impurities, at least ten quantities have to be known ; namely the thermal and optical capture constants of electrons and holes, the thermal and optical emission constants of electrons and holes, the ionization energy and the density.

In recent years, several techniques have been developed to characterize such centres. Sah, et al (1970), Björklund and Grimmeiss (1971), Henry (1973), Braun and Grimmeiss (1974) and several others have developed and applied different transient techniques to p-n junctions, and these methods can be applied equally well to Schottky diodes. A comprehensive review of these techniques has been given by Grimmeiss (1974).

Transient measurements are sometimes more advantageous and informative than steady state techniques. With photocurrent, one resorts to transient techniques, because above the photoemission threshold the photoemission current is usually much greater than the impurity photocurrent and it is difficult to separate the two contributions (i.e. photoemission plus impurity currents) in the steady state. The transient method exploits the fact that the photoemission response is effectively instantaneous, whereas the impurity effect can have a long time constant. Since deep centres have long time constants (i.e. small emission rates), they do not respond well in steady-state conditions.

3.4 THE TRANSIENT PHOTOCURRENT TECHNIQUE

3.4.1 Introduction

Consider the depletion region of a Schottky barrier, Fig 3.3(a), with a single deep level centre in the lower half of the bandgap, with an energy ΔE_p^o above the valence band and ΔE_n^o below the conduction band. When the barrier is illuminated with photons with energies somewhat smaller than the bandgap, Braun and Grimmeiss (1973) have shown that the net excitation rate can be neglected in the region W_o and in the neutral region, because of the competing recombination processes associated with free carriers and the tail

of their distribution extending from the neutral region into the space charge region. The only region that is active is the effective generation region $(W-W_o)$. Assuming that the photoexcitation via deep impurities simply adds to the photocurrent due to the photoemission of electrons from the metal into the semiconductor the total photocurrent is given by

$$J_R^o = J_B^o + J_T^o$$

$$= B\,(h\nu - q\phi_{bn})^2 + Aq(W-W_o)U$$

where, J_B^o = Photoemission Current

J_T^o = Impurity Current

B = A Constant

A = Contact area (Gold Contact)

W = Depletion layer width

W_o = Part of the depletion layer which is inoperative in optical process.

U = Total emission rate via the impurity level.

3.4.2 Photoionization Cross-Section of Holes

Assume initially that the diode is reverse biased and irradiated with a primary light with photon energy $h\nu_p$ greater than ΔE_n^o and less than the bandgap, Fig 3.3(a). When this radiation is removed, some of the centres are empty. Below freezeout temperature thermal processes can be neglected and the occupancy of the centres is not changed when the light is removed. The concentration of the empty centres is given by

$$p_T(o) = \frac{e_n^o}{e_n^o + e_p^o} N_T \qquad (3.18)$$

where,

e_n^o = optical emission rate of electrons

e_p^o = optical emission rate of holes

N_T = Concentration of deep centres.

Now when the sample is irradiated from a secondary source with photon energy $h\nu_s$ greater than ΔE_p^o but less than ΔE_n^o, the centres are again filled. The rate of decrease of empty centres is given by

$$p_T(t) = p_T(o) \exp(-e_p^o t)$$

and this leads to a transient photocurrent given by (Grimmeiss 1974, Grimmeiss et al, 1976),

$$J_T^o(t) = \frac{1}{2} q A(\nu - W_o) e_p^o p_T(o) \exp(-e_p^o t) \quad (3.19)$$

The natural logarithm of eqn. (3.19) gives

$$\text{Ln } J_T^o(t) = \text{Constant} - e_p^o t \quad (3.20)$$

A plot of Ln J_T^o against time (t) should yield a straight line with slope e_p^o. But,

$$e_p^o = \frac{1}{\tau} = \sigma_p^o \phi \quad (3.21)$$

where,

τ = Time constant

σ_p^o = Photoionization cross-section for hole emission

ϕ = Photon flux

With photon energies smaller than the Schottky barrier height, photoemission from the gold does not contribute to the transient photocurrent, the time constant of which is $(\sigma_p^o \phi)^{-1}$. So the time constant and relative photon flux are determined as a function of photon energy then a spectrum of σ_p^o versus $h\nu$ is obtained.

3.4.3 Integrated Charge

The integrated charge, Q, is the charge in the photocurrent transient required to fill the deep centres by optical transitions from the valence band. Not all of the depletion layer region is involved in the optical emptying and filling processes, because near the edge of the depletion layer electrons from the bulk material help to keep the deep centres filled. The charge Q is therefore given by (see Grimmeiss, et al, 1976)

$$Q = \int_0^\infty J_T^o(t)\, dt = \frac{1}{2} Aq (W - W_o) p_T(o) \qquad (3.22)$$

Hence, if only one type of deep centre is present, Q should be constant for all photons of energy $h\nu_s$ used to refill the centres as long as $h\nu_s < \Delta E_n^o$ and as long as $h\nu_p$ has a constant value greater than ΔE_n^o.

By integrating the photocurrent transient with respect to time, the charge flowing in the external circuit can be determined. If the transient photocurrent response is plotted on a linear graph, then Q is given by

$$Q = \text{Photocurrent transient}/_{\text{division}} \times \text{Time}/_{\text{division}} \times \text{Total Number of divisions} \qquad (3.23)$$

The integrated charge Q provides a measure of the number of unoccupied impurities, i.e.

$$\text{No. of unoccupied impurities} = \frac{Q}{q} \qquad (3.24)$$

3.4.4 Concentration of Deep Centres

The concentration, N_T, of deep centres can easily be found using the transient photocurrent technique. This requires the following steps :

(a) Measurement of Q at different bias :-

Once the values of $h\nu_p > \Delta E_n^o$ and $\Delta E_n^o > h\nu_s > \Delta E_p^o$ are fixed, the integrated charge Q is measured at different reverse biases.

(b) Depletion width W at different bias :- The width of the depletion region W can be calculated from C-V measurements using eqn.(3.7a), so that values of W are also known at different biases.

(c) A plot of Q against W may then be made, according to eqn.(3.22). The straight line implies that the deep centres are homogeneously distributed in the sample. The slope of the straight line will give the density of empty centres, p_T (o). If $e_n^o = e_p^o$, it follows from eqn. (3.18) that the total concentration of deep centres is

$$N_T = 2\, p_T\,(o) \qquad (3.25)$$

But when $e_n^o \neq e_p^o$, then eqn (3.18) must be used to find N_T. Finally, the intersection of the straight line on the W-axis will give the value of W_o, the width of the transition region.

3.5 TRANSIENT PHOTOCAPACITANCE

3.5.1 Introduction

With the steady state photocapacitance technique, the photoionization threshold energy is not easy to determine, because the photocapacitance curve depends on the incident photon flux and on the scanning rate of the wavelengths of the incident light. In principle, the emission time constant becomes very large at the threshold energy and hence the measurement of the true steady state photocapacitance is impracticable for deep centres.

The techniques discussed below exploit the phenomenon of photoionization and allow adequate time for centres to empty (or fill). Because of the long time constants involved with deep levels, the spectral variation of the photocapacitance is then recorded step by step.

3.5.2 Photoionization Cross-Section of Holes

Measurements of the spectral sensitivity for exciting electrons from the valence band to the deep centres can also be made using photocapacitance transient techniques. Changing the occupancy of the deep centres by irradiating with light of photon energy $h\nu_s$ results, not only in a photocurrent transient, but also in a transient change in capacitance with the same time constant $(\sigma_p^o \quad \phi)^{-1}$.

The technique described in section (3.4.2) may be repeated in this case to reveal the spectrum for the photoionization cross-section of holes, σ_p^o. From the sign of the capacitance change during the transient one can deduce whether the deep centres lie near the valence or conduction bands.

3.5.3 Photoionization Cross-Section of Electrons

The spectral dependence of the cross-section, σ_n^o, for photoionization of electrons from the deep centres to the conduction band can also be determined by the transient photocapacitance technique. This exploits the situation in which the centres are being emptied optically.

Consider a Schottky barrier as in Fig 3.3(a). The barrier region is illuminated with primary light of photon energy $h\nu_p > \Delta E_n^o$. The occupancy of all deep centres is determined by the corresponding photoionization cross-sections of holes and electrons. If the temperature is low enough the occupancy is not changed when the light source is removed. If the deep centres are in the lower half of the bandgap, the change in capacitance is given by,(see Grimmeiss, et al (1976)),

$$\Delta C = BN_T \frac{e_n^o}{e_n^o + e_p^o} \qquad (3.26)$$

where B is a constant.

In this situation the change in capacitance ΔC originally produced by the known primary source ($h\nu_p$) can be removed completely using a constant secondary irradiation with photon energy $h\nu_s$ less than ΔE_n^o but greater than ΔE_p^o. In obtaining the spectral variation one now proceeds to the next higher photon energy $h\nu_p > \Delta E_n^o$. Now when the barrier is illuminated again with light of the higher photon energy $h\nu_p$, the deep centres are emptied again, giving a transient change in capacitance, eqn. (3.26). The time constant τ for the optical emission from the deep centres is

$$\tau = \left[(\sigma_n^o + \sigma_p^o) \phi \right]^{-1} \tag{3.27}$$

By combining eqns. (3.26) and (3.27), the photoionization cross-section of electrons is obtained as

$$\sigma_n^o = \frac{\Delta C}{B N_T \phi \tau} \tag{3.28}$$

The time constant τ in eqn. (3.27) is determined as follows.

The reverse biased capacitance of a p^+n junction (or Schottky barrier) can be expressed as (see Grimmeiss, 1977),

$$C = \left[\frac{A^2 q \epsilon_s N_I}{2(V_d + V_r)} \right]^{\frac{1}{2}} \tag{3.29}$$

and $N_I = N_d - n_T(\infty) - [n_T(o) - n_T(\infty)] \; e^{-t/\tau}$.

Where, N_I = Total concentration of ionized impurity levels.

n_T = concentration of occupied impurity centres. After substituting

for N_I the expression (3.29) may be written,

$$C^2(t) = \frac{A^2 q\, \varepsilon_s}{2(V_d + V_r)} \left\{ N_d - n_T(\infty) - [n_T(0) - n_T(\infty)]\, e^{-t/\tau} \right\}$$

When $t \to \infty$; $e^{-\infty/\tau} \to 0$, therefore,

$$C^2(\infty) = \frac{A^2 q\, \varepsilon_s}{2(V_d + V_r)} \left\{ N_d - n_T(\infty) \right\} .$$

Hence,

$$C^2(\infty) - C^2(t) = \frac{A^2 q\, \varepsilon_s}{2(V_d + V_r)} \left[n_T(o) - n_T(\infty) \right] e^{-t/\tau}$$

Taking the natural logarithms,

$$\text{Ln} \left[C^2(\infty) - C^2(t) \right] = \text{Ln } K - t/\tau \qquad (3.30)$$

Where K belongs to all constant factors in the above equation.

A plot of Ln $[C^2(\infty) - C^2(t)]$ against t should give therefore a straight line with a slope of $\frac{1}{\tau}$.

3.5.4 Absolute Values of σ_n^o

It is difficult to calculate the absolute values of the photoionization cross-section of electrons from the deep centres to the conduction band using eqn. (3.28). However, an estimate can be made from the experimental results.

(a). Equation (3.27) can be used to find $(\sigma_n^o + \sigma_p^o)$, when τ and ϕ are known.

(b). From transient photocurrent measurements, the values of σ_p^o are known. For $h\nu < Eg/2$ σ_n^o is equal to zero and hence,

$$\sigma_p^o \approx \sigma_p^o + \sigma_n^o .$$

(c). A plot of $(\sigma_n^o + \sigma_p^o)$ against $h\nu$ from (a) and (b) will provide a broad spectrum.

For $h\nu > \frac{Eg}{2}$, $\sigma_p^o = 0$ and $(\sigma_n^o + \sigma_p^o) \equiv \sigma_n^o$ will give the absolute values of the photoionization cross-section of electrons.

3.5.5. Concentration of Photoionized Deep Centres

The concentration of photoionized deep centres, Δn, is given by

$$\Delta n = N_d \frac{\Delta C}{C_o} \tag{3.31}$$

where, ΔC = Photocapacitance at $h\nu$,

C_o = Capacitance in the dark at zero bias,

N_d = Uncompensated donor density.

Experimentally, the determination of Δn will require data from two different types of experiment. The first is C-V, see section (3.1.4) which provides the values of N_d and C_o. The second is described in section (3.5.3) and gives the values of ΔC at particular photon energies $h\nu$.

The Δn described here is similar to $p_T(o)$, the concentration of empty centres.

CHAPTER 4

CRYSTAL GROWTH AND EXPERIMENTAL PROCEDURE

4.1 CRYSTAL GROWTH

4.1.1 Preparation of the Charge

The charge or starting material for crystal growth was sometimes prepared by direct combination of 6N purity zinc and selenium, supplied by Metals Research Limited. The system used for the synthesis is shown in Fig 4.1(a). Elemental selenium and zinc were heated in a silica tube housed in a three zone furnace, with selenium in zone I and zinc in zone II. High purity argon was passed over the elements continuously. The non-metallic and metallic vapours from the first and second zones were mixed and passed to zone III, where supersaturation developed at the cooler part of the zone and yellow ZnSe powder condensed. This powder was subsequently sublimed and purified in the system shown in Fig 4.1(b).

Merck high purity grade zinc selenide, was also often used as the charge for crystal growth and this was subjected to the same purification process as the synthesised powder. The powder was contained in a boat which was placed in an open ended silica tube inside a simple, single zone furnace as shown in Fig 4.1(b). The powder was heated to 600^{o}C for ten hours in a stream of argon then the temperature was raised to 1150^{o}C. After a week, large platelet crystals formed downstream of the charge on the liner provided for the purpose. These were removed and used as the charge for the growth of boule type crystals.

ZnS crystals were grown from B.D.H. optran grade powder purified by distillation in vacuum ($\sim 10^{-5}$ torr). For this purpose the powder was put in a continuously pumped silica tube in a steep temperature gradient with the charge at 1150^{o}C. The ZnS then sublimed to the cooler end of the tube.

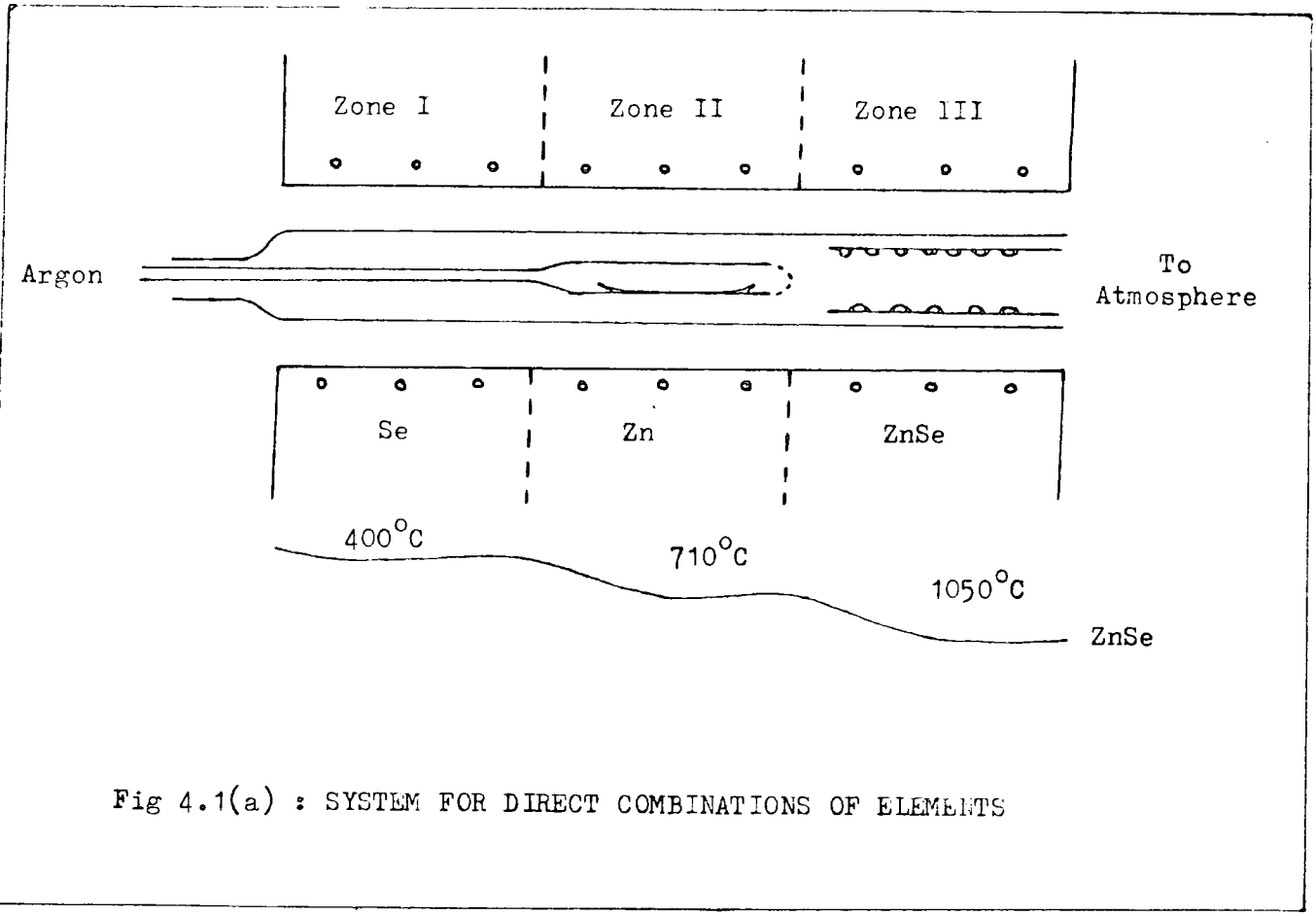

Fig 4.1(a) : SYSTEM FOR DIRECT COMBINATIONS OF ELEMENTS

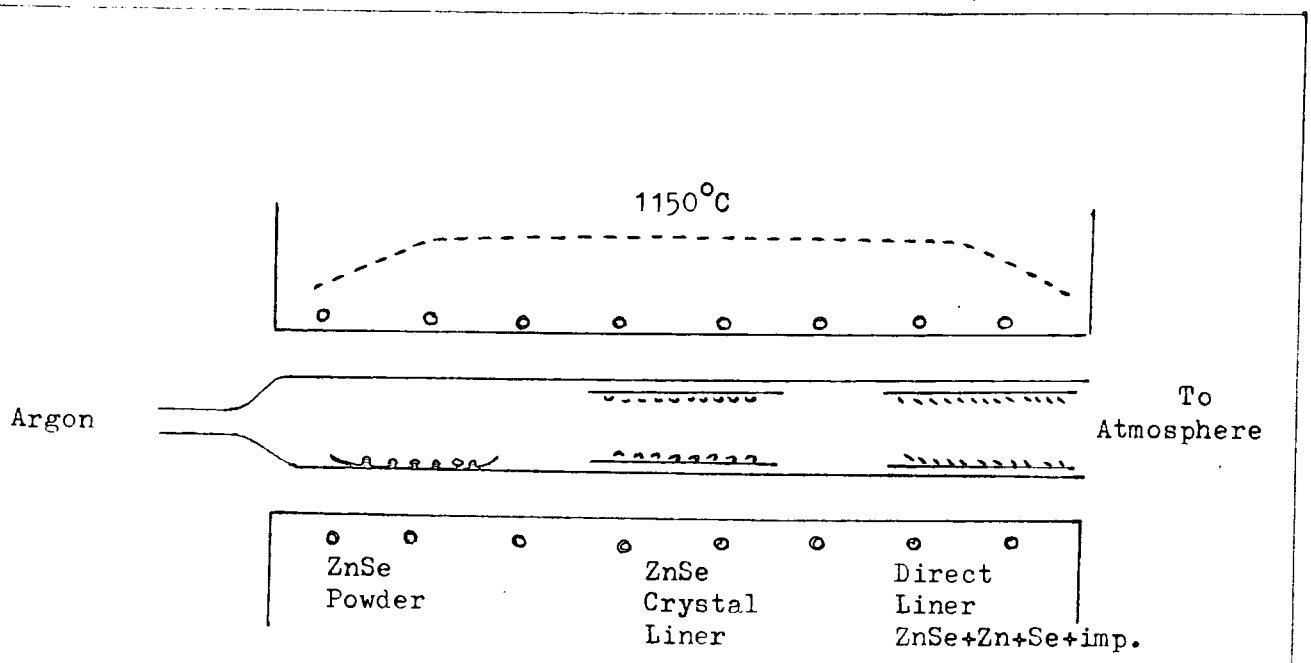

Fig 4.1(b) : THE ARGON FLOW CRYSTAL GROWTH SYSTEM

The colourless (white) part of the condensate was selected to use as the charge for the growth of large crystals.

4.1.2 Vapour Phase Growth

The growth of large crystals of ZnSe from the vapour phase has been described by Burr and Woods (1971) and Cutter and Woods (1979). Their method, illustrated in Fig 4.2(a), has been used to grow the ZnSe crystals used in the present work. About 20 gm. of purified (crystalline) charge was placed in the silica capsule with 0.20 gm. of zinc or selenium in the tail reservoir. The zinc or selenium in the tail was to be held at a temperature which would provide a vapour pressure to satisfy P_{min} conditions in the capsule, which Cutter and Woods have shown achieves a near stoichiometric composition of the growing crystal, and maintains a proper growth rate. After evacuating the capsule to 10^{-6} torr. and sealing, it was placed in a two zone vertical furnace with the charge at 1150°C and the zinc or selenium in the reservoir at 570°C or 320°C respectively. The growth tip, where condensation and nucleation of the sublimed ZnSe occurred, was first held at a higher temperature than the charge, so that any stray solid matter would evaporate. During the actual crystal growth the temperature difference along the tube was about 50°C. The temperature gradient was increased simply by pulling the silica tube upwards automatically at a rate of about 3 mm. per day through the temperature profile shown in Fig 4.2(a). In one week a boule 3 to 4 cm.long and 1.2 cm in diameter was usually grown. The crystal structure was cubic and a boule usually contained 4 to 5 large grains with dimensions of a few mm.

The crystals of ZnS were grown in a slightly different way. The method was based on that described by Piper and Polich (1961) and later modified by Russell and Woods (1979) in this department. The system is illustrated in Fig 4.2(b). An open silica tube was loaded into a tubular furnace so that the charge was near the flat region of the temperature profile. With ZnS the temperature at the centre of the furnace was controlled at 1600°C.

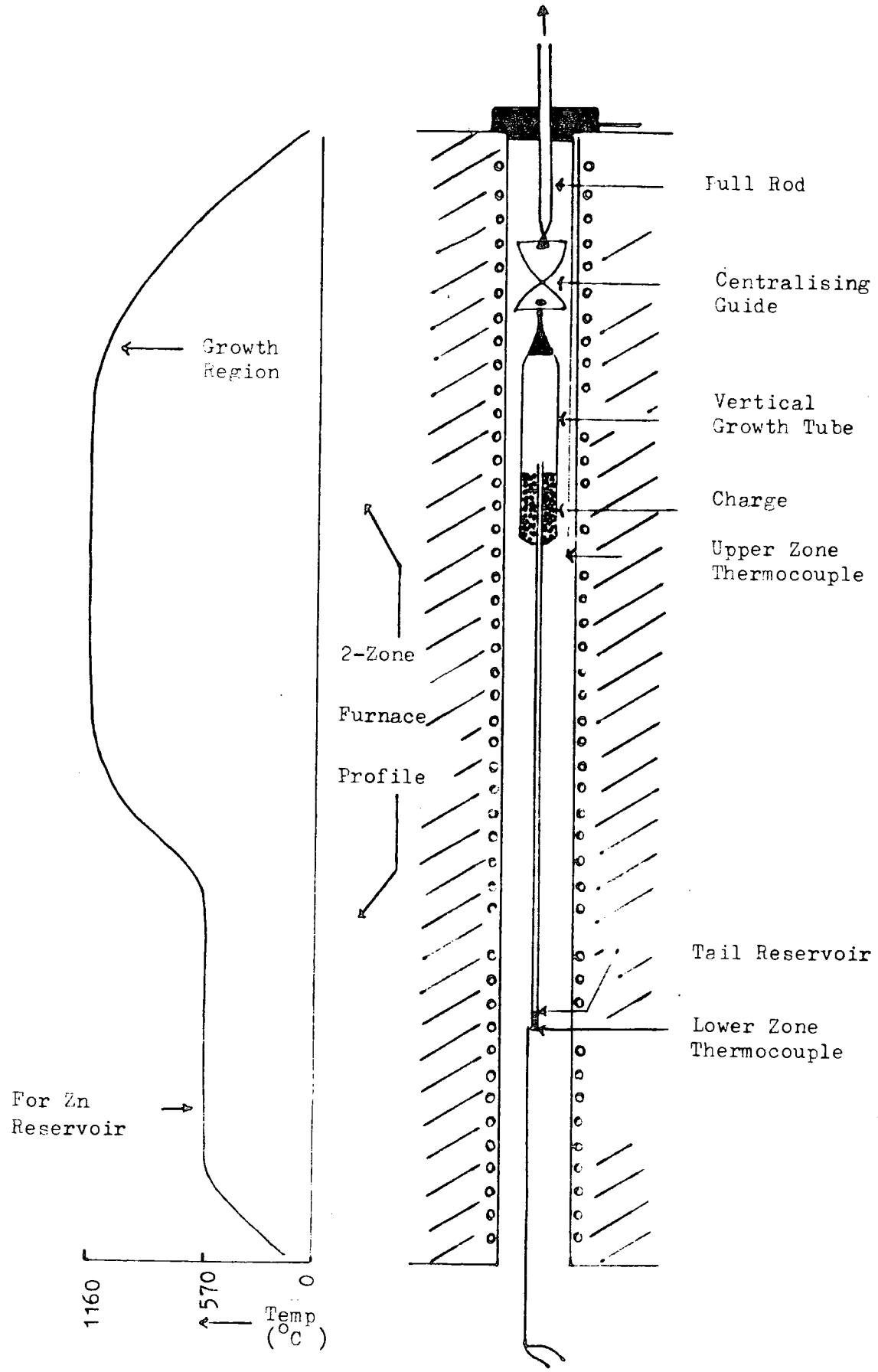

Fig 4.2(a) : VERTICAL GROWTH OF ZnSe

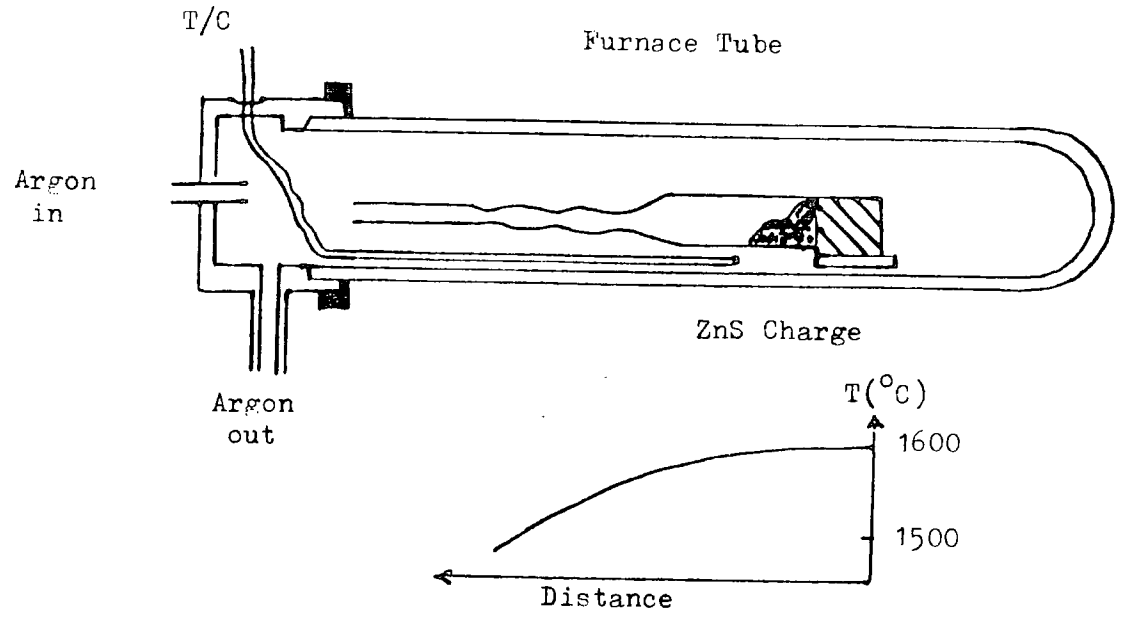

Fig 4.2(b) : VAPOUR PHASE GROWTH OF ZnS BY A MODIFIED PIPER-POLICH TECHNIQUE

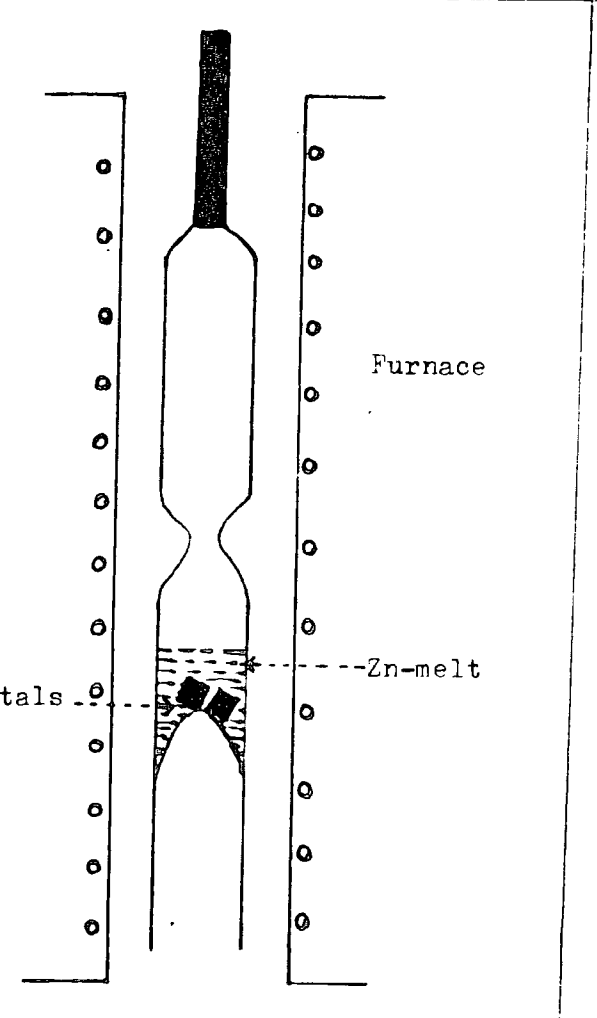

4.3 : HEAT-TREATMENT METHOD

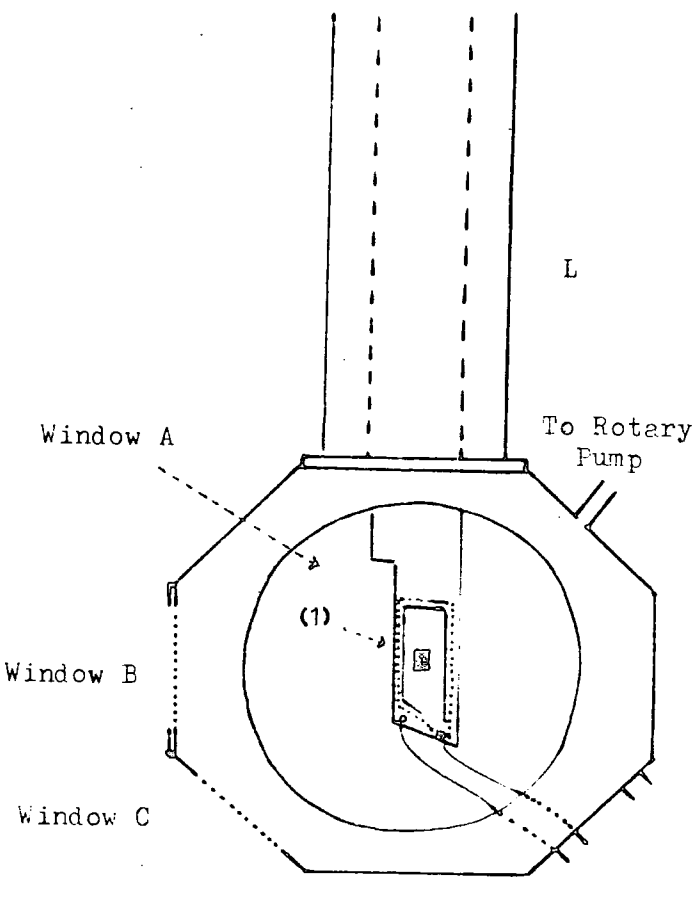

Fig 4.4 : CRYOSTAT

Argon was admitted via a needle valve, and was allowed to pass through the system at a rate of 100 ml per minute. As the ZnS was transported to the colder end of the growth capsule, condensation occurred at progressively hotter constrictions, with the result that the growth chamber was eventually sealed-off while it contained a pressure of approximately one atmosphere of argon. This procedure allowed unwanted volatile impurities to escape before the bulk of the crystal growth occurred. During the growth run which lasted 2-3 days, the silica became devitrified and subsequently was easily fractured to allow the grown boules to be removed. These boules were usually 3 to 4 cm long, 1 cm in diameter and optically clear.

4.1.3 Doping

In general the impurities investigated, namely chlorine, copper, indium or gallium were added during crystal growth. Chlorine doped ZnSe crystals were obtained by adding zinc chloride to the reservoir, while copper was introduced to the charge usually as the metal but sometimes as copper selenide. In some samples copper was diffused into ZnSe dice by heating them in molten zinc containing the required quantity of copper wire.

With indium or gallium, when doping concentrations in excess of 50 ppm were required, metallic indium or gallium was added to the charge. However, for lower concentrations, weighed pieces of the more heavily doped ZnSe were mixed with the charge.

4.2 HEAT TREATMENT

Aven and Woodbury (1962) and many others have shown that the resistivity of ZnSe crystals can be reduced by heating them in molten zinc. To carry out such heat treatment a silica tube some 6 mm in diameter and 12 cm long was used. A constriction in the central part of the tube was provided to help with the separation of the dice from the molten zinc at the end of the procedure.

After polishing and etching (see § 4.4), the dice were placed in the tube with 6N purity zinc shot and the whole tube was then evacuated to 10^{-3} torr and sealed off. The tube was placed vertically in the furnace, as shown in Fig 4.3, with the limb containing the crystals downwards. Many samples were heated in this way in molten zinc at 850°C for periods ranging from 1 hour to 6 days. At the end of the treatment, the tube was removed from the furnace, inverted and reinserted into the furnace from the lower end. Then by slowly tapping and shaking, the molten zinc was separated from the dice. When this treatment was carried out on indium and gallium doped ZnSe crystals, heavy dark precipitates were observed. Similar precipitation effects have also been reported by Ray and Kröger (1978) and Russell et al (1981). These phenomena are discussed in detail in the Appendix.

Some samples were also heated in selenium vapour. This treatment increases the resistivity of ZnSe, by decreasing the concentration of selenium vacancies which act as donors, and increasing the concentration of zinc vacancies which act as acceptors. For the selenium treatment, the crystals and 6N purity selenium shot were placed at opposite ends of the same sort of tube as described above. This was then placed in the furnace, with the selenium limb in the lower part of the furnace.

4.3 ATOMIC ABSORPTION ANALYSIS

Atomic absorption analysis was carried out on many indium and gallium doped ZnSe crystals to determine the concentration of dopant incorporated. The results are shown in Table 4.1.

The crystals were etched as described in section 4.4, then washed with distilled water and dissolved in 2 ml of nitric acid (HNO_3). Distilled water was added to make a total solution of 6 ml. Reference solutions containing 1.25 ppm, 5.0 ppm and 20.0 ppm of indium or gallium were also prepared. The analysis was carried out using a Perkin Elmer 403 atomic absorption spectro-

TABLE 4.1 : Atomic Absorption Analysis for ZnSe: In and ZnSe:Ga

Boule No.	Dopant and Nominal Content in ppm	Amount Dissolved in mg	Measured Content in ppm	Copper Content in ppm
386	In : 5	78	34.3	-
407	In : 5	98.5	13.9	-
407	In : 5	106.5	12.8	-
405	In : 50	95	55.9	-
410T	In : 100	104.5	106	-
410T	In : 100	108	108	-
410T	In : 100	47.5	114	5.3
410E	In : 100	108	108	-
410E	In : 100	101	105	-
410E	In : 100	94	110	5.2
408T	In : 250	109	275	-
408T	In : 250	107	261	-
408E	In : 250	87	210	-
349	In : 1000	111	800	-
387	Ga : 5	102	6.3	-
381	Ga : 50	159	50.6	-
382	Ga : 100	101	112	-
383	Ga : 250	110	373	-

T = Tip of Crystal Boule

E = End of Crystal Boule

photometer with Activion reference lamps. The sample solution was converted into atomic vapour and then its absorbance was measured at a selected wavelength which is characteristic for each individual element. The absorbance is proportional to the concentration of the element so that comparison with the reference solutions gives a measure of this quantity.

4.4 DEVICE PREPARATION

(a) Crystal Cutting and Polishing

The large crystal boules were cut into 1 mm thick slices and then into the dice of required dimensions, using a diamond saw. The rough surfaces of the dice were smoothed by mechanical polishing the ZnSe dice with 3 micron alumina and the ZnS dice with 1200 grade carborundum powder.

(b) Etching

The dice then were chemically etched to remove surface damage. ZnSe crystals were etched in a solution of 1% bromine in methanol. The dice were immersed and stirred in the solution for 4 minutes, then washed in methanol and finally immersed in carbon disulphide for 10 minutes. The carbon disulphide solution removed any possible compounds of selenium with bromine (i.e. Br_2Se or $Br_4\ Se_2$). The ZnS crystals were etched in bromine for 20 seconds and then washed with methanol. Finally, they were immersed in carbon disulphide for 10 minutes.

(c) Ohmic Contacts

Metallic indium was used to make ohmic contact to n-type ZnSe. Pure indium wire 1 mm in diameter, purchased from Johnson Matthey Chemicals Limited, was cleaned with nitric acid and then washed with water. When contacts were required, the wire was cut into tiny pieces and the fresh cut surfaces were pressed on the etched surfaces of the dice. Thereafter, the dice were heated in an argon atmosphere at 240^{o}C for 5 minutes, and then cooled to room temperature.

The alloy (In + 10% Cd) was used to make ohmic contacts to ZnS crystals.

(d) Schottky Contacts

Gold which has a high work function forms rectifying or Schottky contacts on n-type ZnSe. To make a Schottky diode the gold was deposited by vacuum evaporation. Before this was done an indium ohmic contact was prepared on one large area face of a die. It was then covered by a protective layer of lacomit. Afterwards, the opposite face of the die was polished and etched. The lacomit protected the indium contact from etchants, and could be removed easily when required. The freshly etched die was put on top of a copper mask in the evaporator and gold was deposited on to a circular area of 1-2 mm^2.

4.5 EXPERIMENTAL ARRANGEMENTS FOR ELECTRICAL AND OPTICAL MEASUREMENTS

4.5.1 Introduction

For all the electrical and optical measurements the devices were mounted on the copper cold finger (1) of a vacuum cryostat as shown in Fig 4.4. The cryostat had three polished silica windows (A, B & C) for optical transmission measurements, or for irradiation with more than one source. All electrical connections were made via a 4-way glass-to-metal seal. The sample was directly cooled by liquid nitrogen contained in limb 'L' of the cryostat.

4.5.2 Photoconductivity Measurements

The experimental arrangement for measurements of photoconductivity, infra-red quenching and photoionization cross-section is shown in Fig 4.5. The device with its contacts was mounted in the cryostat. A 250 W Quartz Halogen lamp (source A) with variable power supply, was used as the source in conjunction with a Barr and Stroud monochromator type VL2 with spectrosil A quality prisms.

For photoconductivity measurements the monochromator light source was used via large window A, but when IR quenching was investigated a second halogen lamp (source B) with appropriate filters was employed and irradiation occurred via windows B or C.

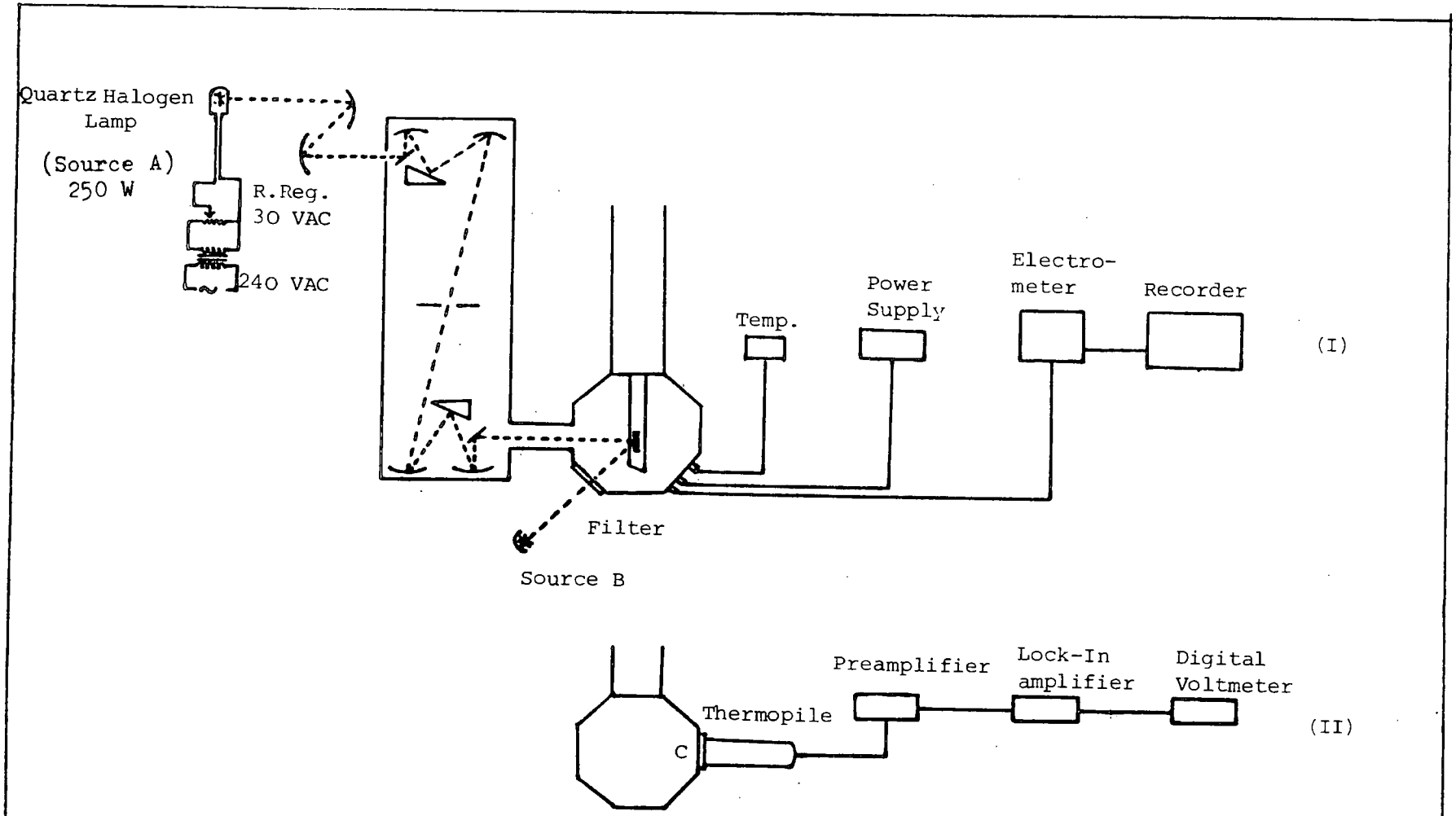

Figure 4.5 : Arrangement for measuring (I) Photoconductivity and Quenching

(II) Photoionization Cross-Section (αI_L^{-1})

The voltage applied to the sample was derived from a Farnell LT30-1 power supply, and the photocurrent was measured with a Keithley 602 Electrometer and recorded on a Honeywell Electronik 196 Chart Recorder.

In a series of measurements of photoionization cross-section a record of the light intensity was required, see Chapter 2. In that case the photocurrent was controlled by adjusting the voltage supply to the source A and the light intensity was measured with a Hilger & Watts Thermopile FT 16.301/602971. Since the output of the thermopile was very low, a phase sensitive detection system was used. For this the light was chopped and the thermopile output was fed to a lock-in amplifier, type 401, via a Nanovolt preamplifier, type 431, (see Part II in Fig 4.5).

The temperature of the sample was measured with a copper-constantan thermocouple.

4.5.3 Capacitance and Photocapacitance Measurements

The experimental arrangement for capacitance and photocapacitance measurements is illustrated in Fig 4.6. Both the capacitance and photocapacitance were measured over the frequency range 10-200 kHz using an Ortec Brookdeal Ortholoc Model 9502 in the two-phase mode. The reference signal was monitored with a digital frequency meter TF 2430.

The amplitude of the small A.C. voltage was reduced by means of an attenuator to $\sim$ 20-40 mV p-p (as read on an Oscilloscope type D1010) and the reduced A.C. signal was fed in turn to a mixer box. Contained in the latter was a D.C. voltage supply, the output of which could either be set to a constant biasing level or else could be ramped (with a variable time base facility). In the mixer box this D.C. bias voltage was superimposed upon the A.C. signal from the attenuator, and the combined waveform fed to the sample in the cryostat. The current passed through the sample and a resistor in the mixer box in series and the resultant voltage across the resistor was taken back as the input signal to the Ortholoc. The absolute value of the sample capacitance was determined

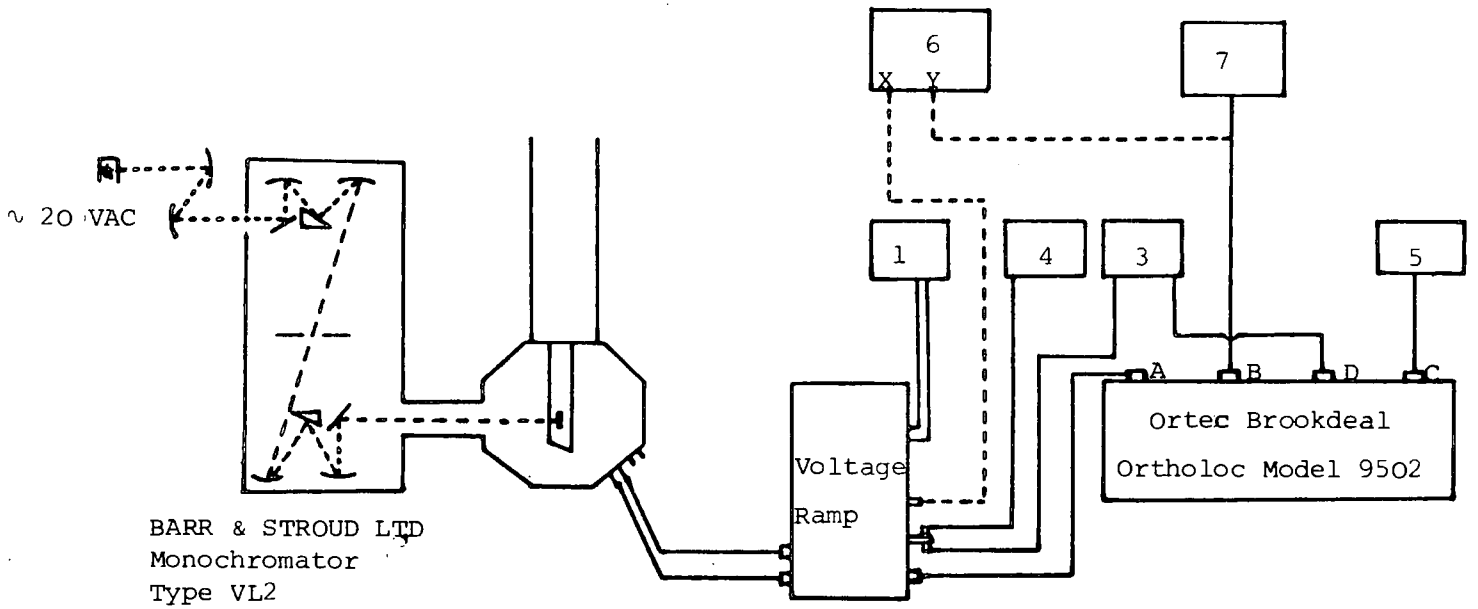

(A) Signal Input

(B) Output

(C) Reference Monitor

(D) Oscillator 5012F

(1) Digital Voltmeter 173B (Bradley)

(2) Recorder (Honeywell)

(3) MF Attenuator (Marconi)

(4) Oscilloscope Type D1010

(5) Digital Frequency Meter (TF 2430)

(6) Farnell XY Plotter

(7) Chart Recorder (Honeywell)

Figure 4.6 : Arrangement for measuring the photocapacitance and C-V.

by employing close tolerance silver mica capacitors as calibration standards.

A Farnell X-Y plotter was used to record the C-V curves in the dark at room and liquid nitrogen temperatures. During the photocapacitance measurements a Honeywell chart recorder was used.

CHAPTER 5

PHOTOCONDUCTIVE SPECTROSCOPY FOR DEEP CENTRE ANALYSIS

5.1 INTRODUCTION

The discussion in this chapter is concerned with the investigation of deep defect centres in undoped and doped ZnSe, and in some ZnS crystals. All crystals examined were grown in this department using vapour phase growth techniques,(see Cutter and Woods (1979),and Russell and Woods (1979).

Photoconductivity and infra-red (IR) quenching techniques, described in Chapter 2, have been employed. In addition, attempts have been made to find the defect parameters using a technique developed by Grimmeiss and Ledebo (1975), but these were not particularly successful.

It was generally assumed that all crystals were n-type, on the basis of the work by Jones and Woods (1976), and Vincent (1980). The photoconductive samples were prepared according to the method described in Chapter 4 and their measured dark resistivities ranged from 10^4-10^{13} Ohm-cm.

The experimental arrangement and the procedures for measuring the photoconductivity, IR quenching, etc., have already been described in Chapter 4. With the photoconductivity measurements, the spectrum was scanned from 0.54 eV (2.28 μm) to 3.00 eV (0.41 μm) for ZnSe and from 0.54 eV(2.28 μm) to 3.86 eV (0.32 μm) for the ZnS crystals, with drum speed $\approx$ 0.04 μm/min and slit width $\approx \frac{1}{2}$ mm. The quenching measurements were recorded step by step for each drum reading, in order to allow equilibrium to be established in 2 to 5 minutes. The measurements were made at room temperature ($\approx$ 295 K) as well as at liquid nitrogen temperature ($\approx$ 84 K).

In indium or gallium doped ZnSe, the actual concentrations (in ppm) of dopants were measured using atomic absorption spectroscopy, (see § 4.3,

Chapter 4. In the following chapters, we have recorded the nominal content (in ppm) of the dopants in individual samples.

5.2 ZnSe (UNDOPED) CRYSTALS

5.2.1 Photoconductive Spectral Analysis

This section is concerned with the measurements of the photoconductivity of ZnSe crystals with no intentionally added impurities. Two types of sample, cut from boules grown under two different growth conditions, were used. The samples, Nos. 172-1 and 370-C, were undoped and were grown with excess selenium and excess zinc in the reservoir respectively. The resistivity of No.172-1 was 7.6×10^{10} Ohm-cm and of No.370-C was 3.9×10^{11} Ohm-cm in the dark, at room temperature.

The variation of the photocurrent with photon energy ($h\nu$) is shown in Fig 5.1 for both types of sample. The room temperature response for sample No.172-1 is given in curve (a), which shows two thresholds one at 0.70 and the other at 1.60 eV. There is also a small dip at 0.88 eV that may indicate the presence of an additional threshold. The response at liquid nitrogen temperature for this sample is shown in curve (b), which has thresholds at 0.62, 0.94, 1.54 and 2.10 eV. The threshold at 2.10 eV is followed by a large exponential rise in photocurrent up to 2.40 eV and then by a slower increase to 2.66 eV as the photon energy increases. This part of the spectrum is associated with localized levels close to the valence and conduction bands. The photocurrent response at room temperature for sample No.370-C, is shown in Fig 5.1(c), which exhibited thresholds at 0.60 eV and 1.58 eV. This sample has a dip at 0.90 eV and a shoulder at 1.90 eV. The corresponding response at liquid nitrogen temperature curve (d),has thresholds at 0.62, 1.60, 2.10 and 2.50 eV. The threshold at 0.94 eV was absent in sample 370-C, instead a new threshold at 2.50 eV was observed ; in comparison with sample 172-1.

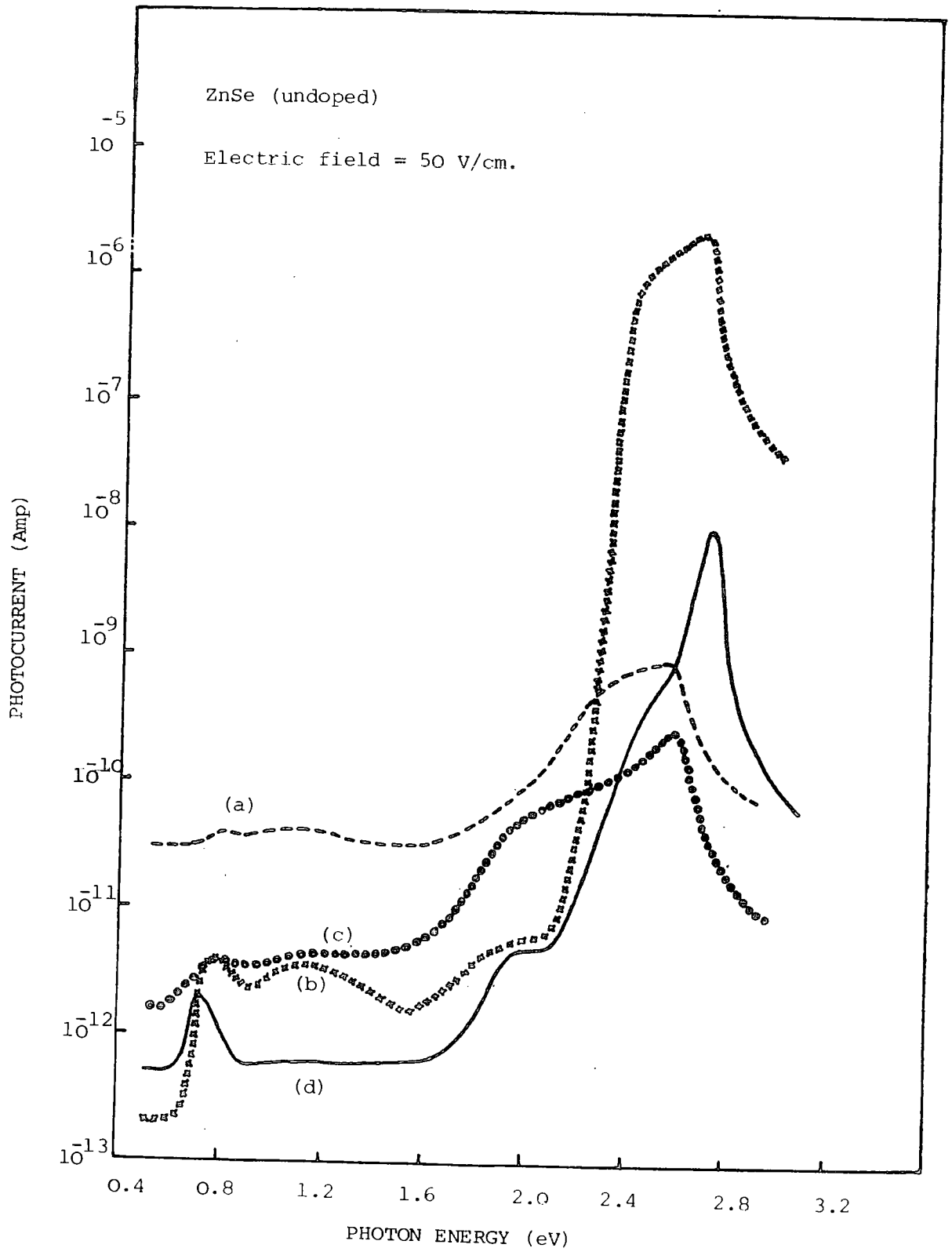

Figure 5.1 : Spectral response of photocurrent for undoped ZnSe with excess selenium recorded at 294 K (a), and at 84K (b), and for undoped ZnSe with excess zinc recorded at 294 K, (c) and at 84 K (d).

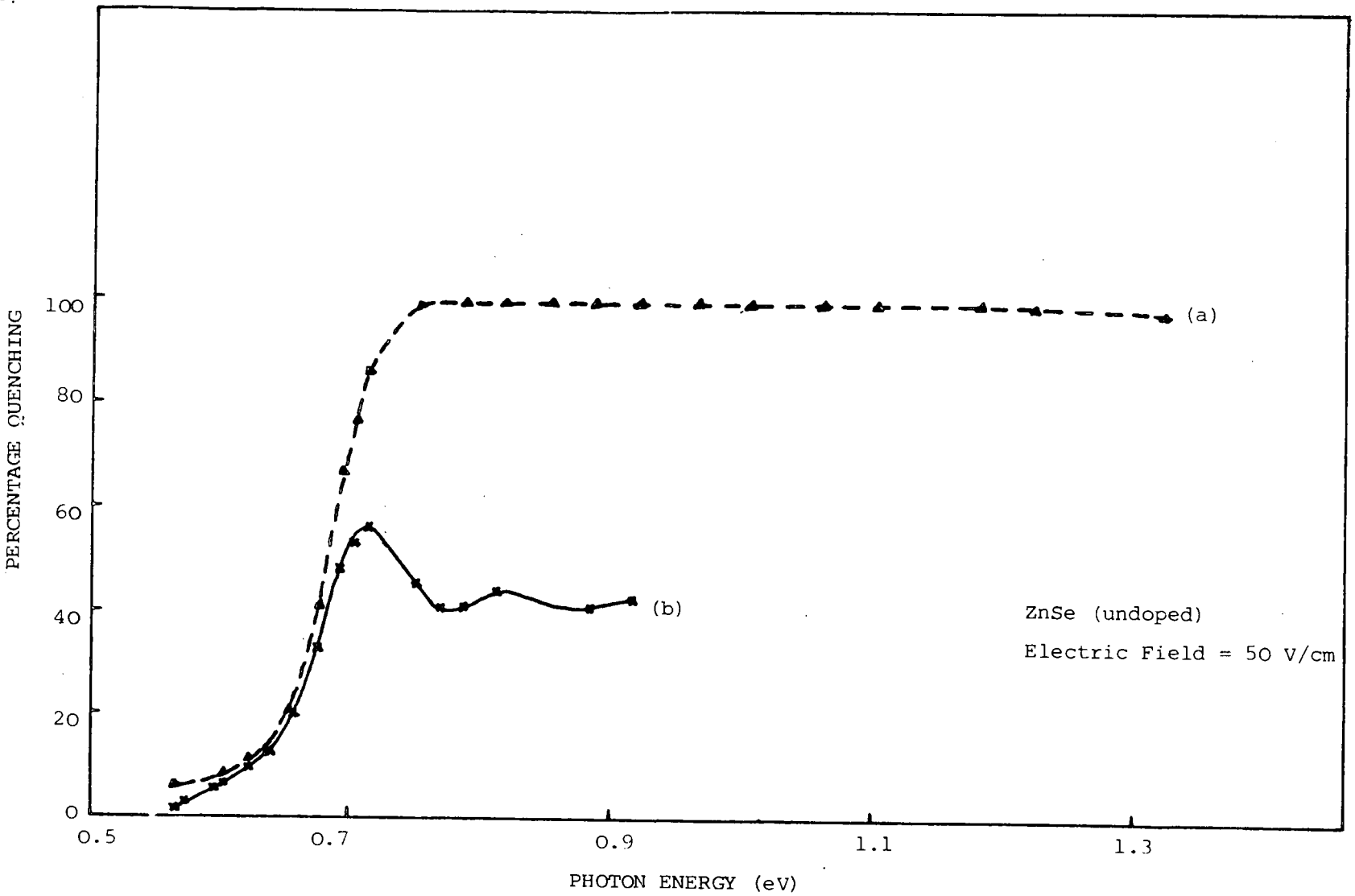

Figure 5.2 : Infra-red quenching of photocurrent (at 84 K) for (a) undoped ZnSe grown with excess selenium and (b) undoped ZnSe grown with excess zinc.

5.2.2 Infra-Red Quenching

The infra-red quenching spectra obtained from the two different types of undoped samples at liquid nitrogen temperature are shown in Fig 5.2. The room temperature response was negligibly small. The primary photocurrent was excited with tungsten light passing through a 0.44 μm filter and an infra-red absorbing filter.

The response for sample 172-1 is shown in Fig 5.2(a), which reveals one pronounced threshold at 0.65 eV. The other sample 370-C, had a practically identical threshold. With these results the threshold was taken as the point on the energy axis, from which the dominant quenching begins. The small tail at lower energies may be caused by a thermal effect or by the influence of nearby localized centres.

The interesting feature in the response of these undoped samples is that the selenium rich sample had a large quenching effect, nearly double that of the zinc rich sample. When there is an excess of selenium in the tail during growth as with sample 172-1, conditions are favourable for the production of zinc vacancies due to charge compensation effects. Copper which has a high diffusion coefficient and is a common contaminant in ZnSe,(see Yamaguchi and Shigematsu (1978), is readily soluble and can occupy zinc vacancies under these conditions. There have been numerous suggestions, (Woods and Russell (1981), that copper may have been introduced into our crystals during growth from or via the silica tube, even if copper is not introduced intentionally. When copper as an unavoidable impurity is present, it has a higher probability of being introduced into samples grown with excess selenium. A higher concentration of copper in sample 172-1, may be the cause of the larger quenching effect.

5.3 ZnSe: Cu, ZnSe : Cl AND ZnSe : Cu,Cl DOPED CRYSTALS

5.3.1 Photoconductive Spectral Analysis

The photoconductive responses of ZnSe samples doped with copper, chlorine or copper and chlorine are shown in Figs 5.3 and 5.4. The impurities were added during crystal growth. The dark resistivities of the ZnSe:Cu,

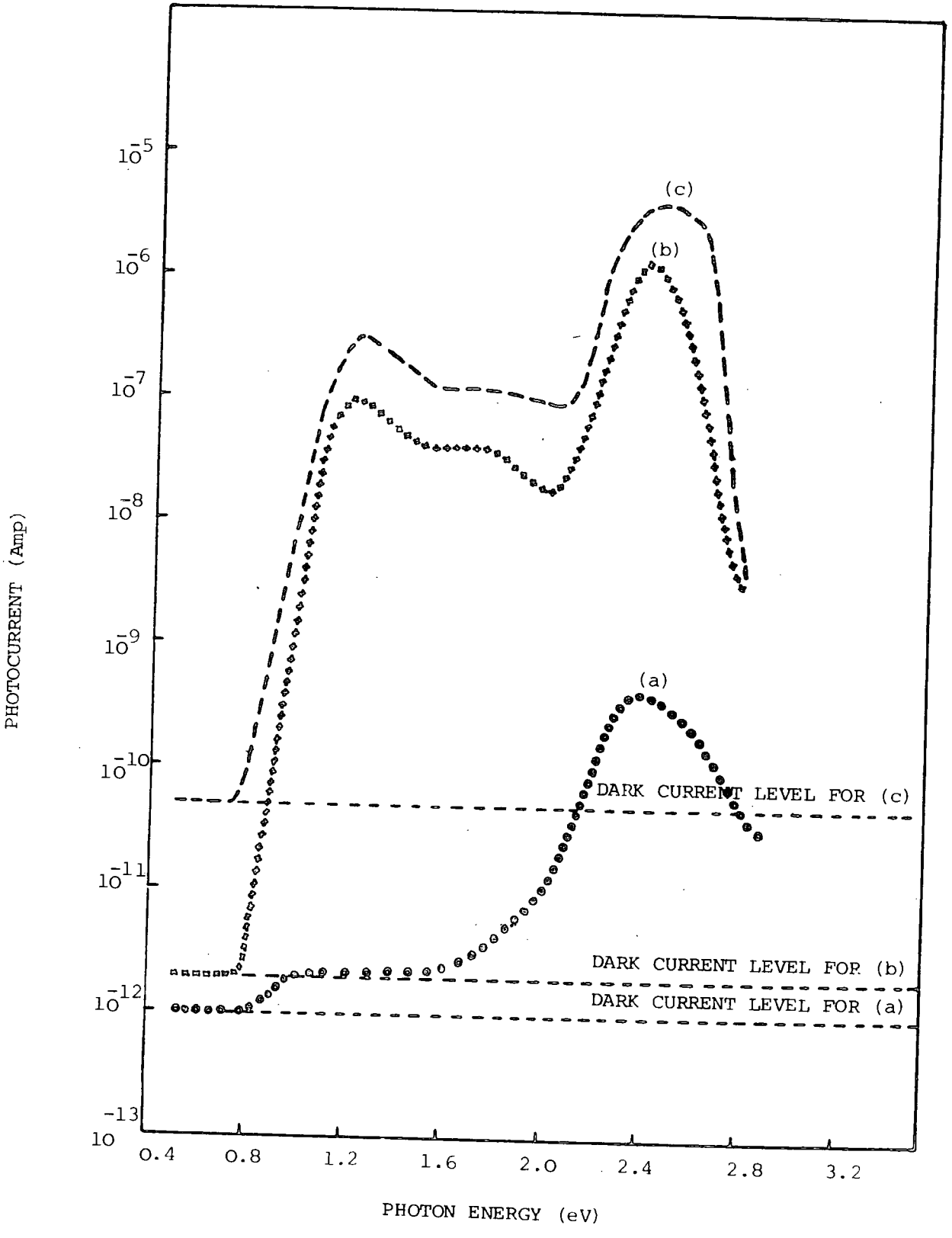

Figure 5.3 : Spectral response of photocurrent (at 294 K) for (a) ZnSe:Cu, (b) ZnSe:Cl and (c) ZnSe:Cu,Cl.

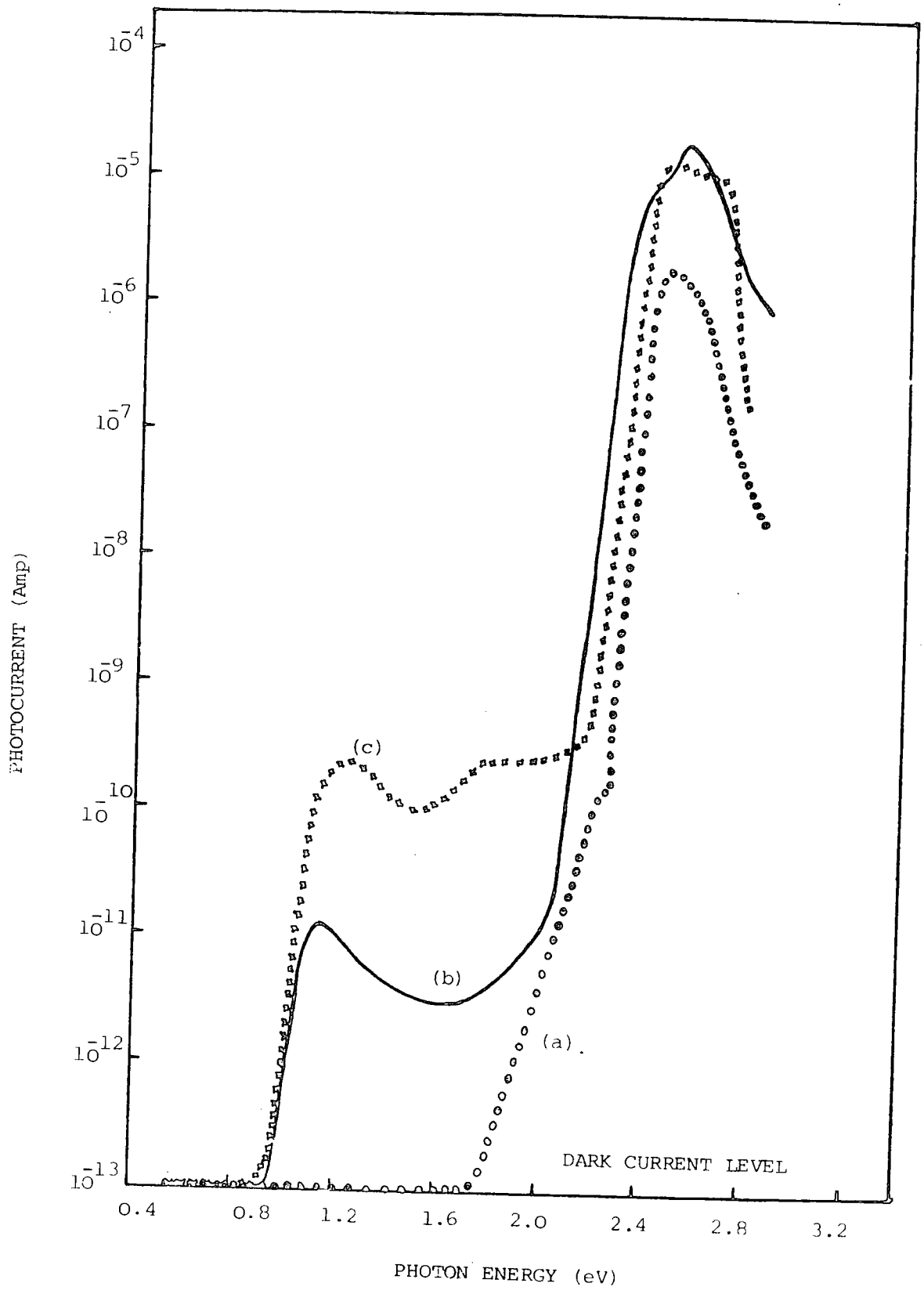

Figure 5.4 : Spectral response of photocurrent (at 84K) for (a) ZnSe:Cu, (b) ZnSe:Cl and (c) ZnSe: Cu,Cl.

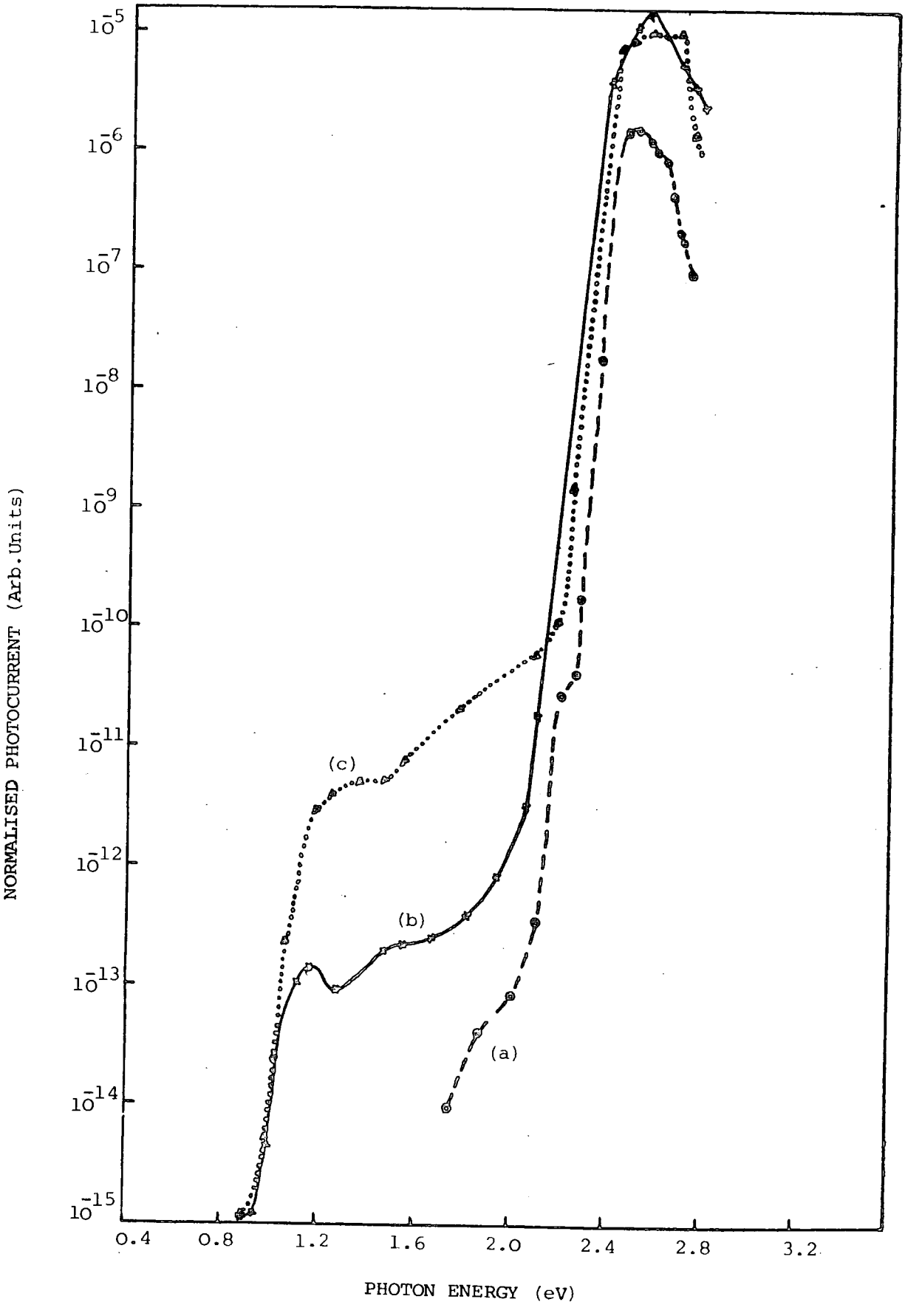

Figure 5.5 : Spectral responses of Figure 5.4 normalised for constant incident photon energy.

ZnSe:Cl and ZnSe:Cu,Cl samples were 4.5×10^{12}, 3×10^{11} and 9×10^{10} Ohm-cm, respectively. The curves in Fig 5.4 are plots of raw data. The curves have been corrected to constant energy of excitation and the resultant curves are shown in Fig 5.5.

Sample 158-1 was the copper doped ZnSe sample and its room temperature response is shown in Fig 5.3(a). It had two thresholds, one at 0.80 eV and the other at 1.60 eV. The sample had maximum photocurrent (4.4×10^{-10} A) at 2.38 eV which was $\sim 10^2$ times larger than the dark current level (10^{-12} A). The liquid nitrogen temperature response is shown in Fig 5.4(a). The first threshold was near 1.70 eV and the second (not very clear) near 2.26 eV. The low energy response at 0.80 eV was absent at liquid nitrogen temperature. The maximum photocurrent (2×10^{-6} A) occurred at 2.48 eV at nitrogen temperature and was $\sim 10^7$ times larger than the dark current. The responses measured at liquid nitrogen temperature were corrected to allow comparison of corrected and uncorrected curves to determine whether any shifts in the thresholds were apparent. The corrected response is shown in Fig 5.5(a) and shows no shift in the 1.70 and 2.26 eV thresholds, but a new threshold at 2.02 appeared.

The photocurrent spectrum for the chlorine doped sample 358E, measured at room temperature, is shown in Fig 5.3(b). A large photoconductive response was observed, even at room temperature. The first threshold was at 0.76 eV and the second at 2.02 eV. A plateau between 1.50-2.00 eV was also fairly prominent. The peak was at 2.38 eV and the magnitude of the current there was 10^6 times larger than the dark current (2×10^{-12} A). The response at liquid nitrogen for this sample is shown in Fig 5.4(b). Significant response in the infra-red region in contrast with the copper doped sample was very evident, the first sharp increase in photocurrent began at 0.94 eV and the second at 2.06 eV. In the region between 1.70 eV and 2.06 eV there may have been another threshold but it was not clearly resolved. The peak photocurrent was at 2.54 eV, which represents a shift to higher energy compared with room temperature, which

is the normal situation due to the larger bandgap at low temperature. The maximum photocurrent (2×10^{-5} A) at 2.54 eV was $\approx 10^{8}$ times larger than the dark current (1×10^{-13} A). The corrected spectral response curve is shown in Fig 5.5(b). It shows the emergence of a new threshold at 1.30 eV while the other thresholds remained unchanged.

Sample No. 135-2, doped simultaneously with chlorine and copper during growth, also showed good sensitivity at both temperatures. The room temperature response, Fig 5.3(c), had a low energy threshold at 0.73 eV with a band showing some slight structure stretching from 1.53 to the second threshold near 2.02 eV. The maximum photocurrent (4×10^{-6} A) at 2.46 eV was $\approx 10^{5}$ times larger than the dark current (5×10^{-11} A). The low temperature response is shown in Fig 5.4 (c). Three clear thresholds are apparent at 0.88, 1.50 and 2.20 eV respectively. The maximum photocurrent (1.5×10^{-5} A) lay in a band ranging from 2.44 eV-2.68 eV and, was $\approx 10^{8}$ times larger than the dark current (1×10^{-13} A). The corrected response is shown in Fig 5.5(c) from which it can be seen that there is no shift in the positions of the thresholds in the corrected or uncorrected responses.

5.3.2 Infra-Red Quenching

Detailed quenching measurements were made on the copper and chlorine doped ZnSe samples in an attempt to understand the positions occupied by copper and self-activated centres in the bandgap region. The quenching spectra plotted as quenching percentages of the primary photocurrent are shown in Figs 5.6-5.8. Measurements were carried out with different intensities and photon energies of primary (near bandgap) and secondary (infra-red) light.

The results plotted in Fig 5.6 are for the copper doped ZnSe, sample No.158-1. The quenching spectrum (a)was measured at room temperature and shows the threshold near 0.62 eV. Except for this curve all the rest of the responses were measured at liquid nitrogen temperature. The primary excitation for curves (a), (b) and (c) was made using a 0.52 μm filter and

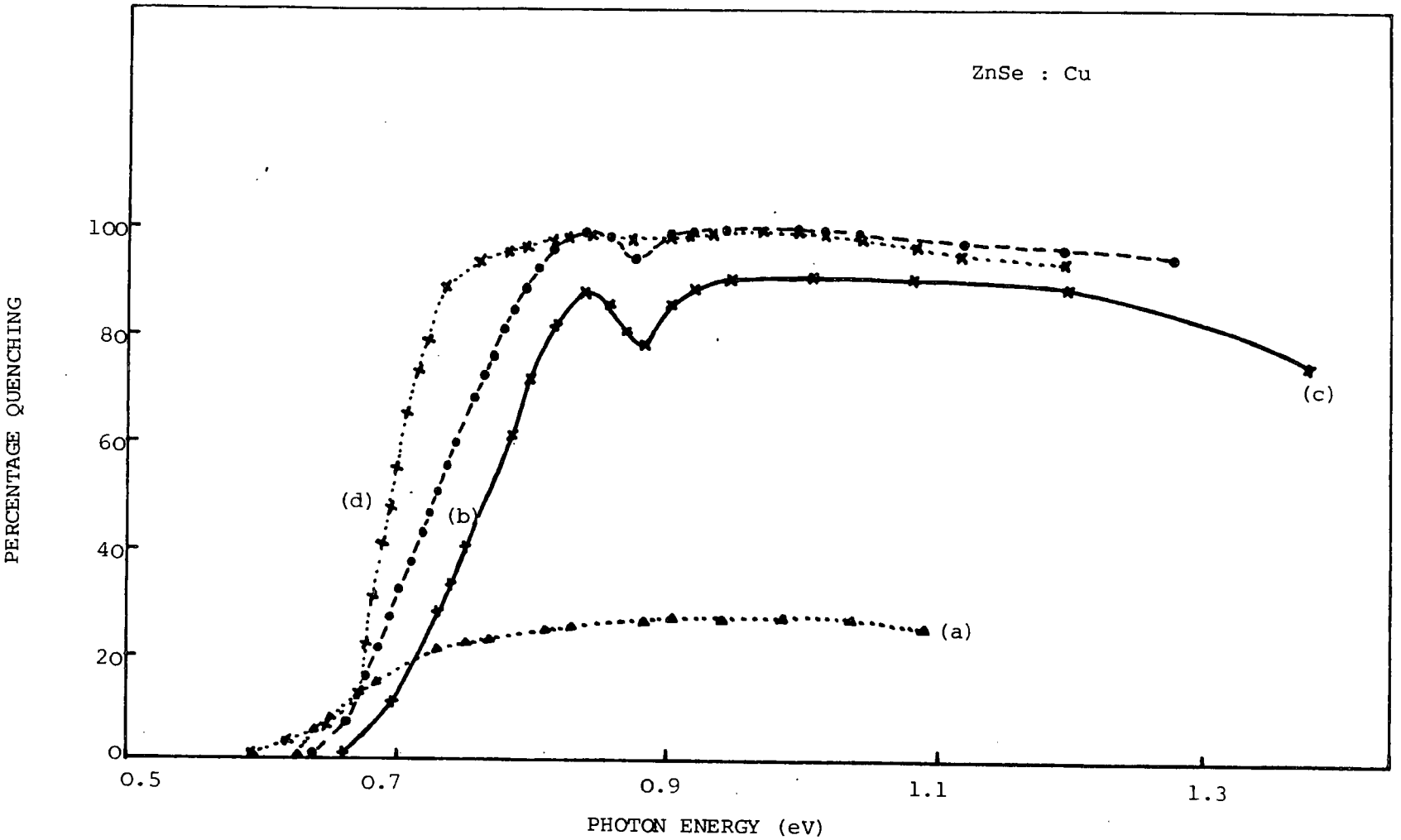

Figure 5.6 : Infra-red quenching of photocurrent in ZnSe:Cu (a) at 295 K, primary excitation using 0.52 μm + IR Abs.Filters, (b) at 84K, primary excitation using 0.52 μm + IR Abs.Filters, (c) at 84 K, primary excitation as in (b) but secondary excitation reduced to 50% of intensity of (b) and (d) at 84 K, primary excitation through 0.44 μm + IR Abs.Filters.

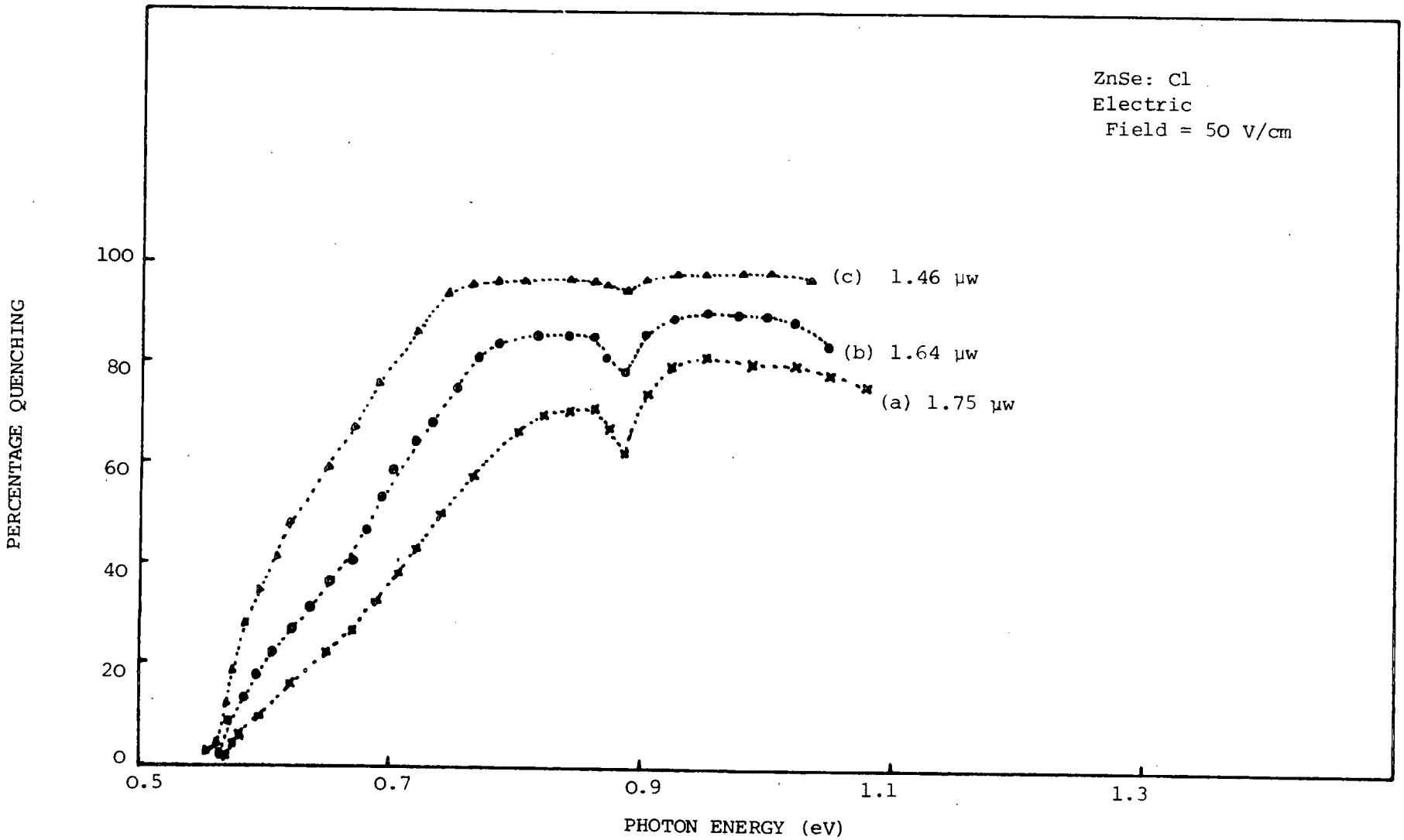

Figure 5.7 : Infra-red quenching of photocurrent in ZnSe:Cl at 86 K, using different intensities of primary light (0.52 µm + IR Abs.Filters)

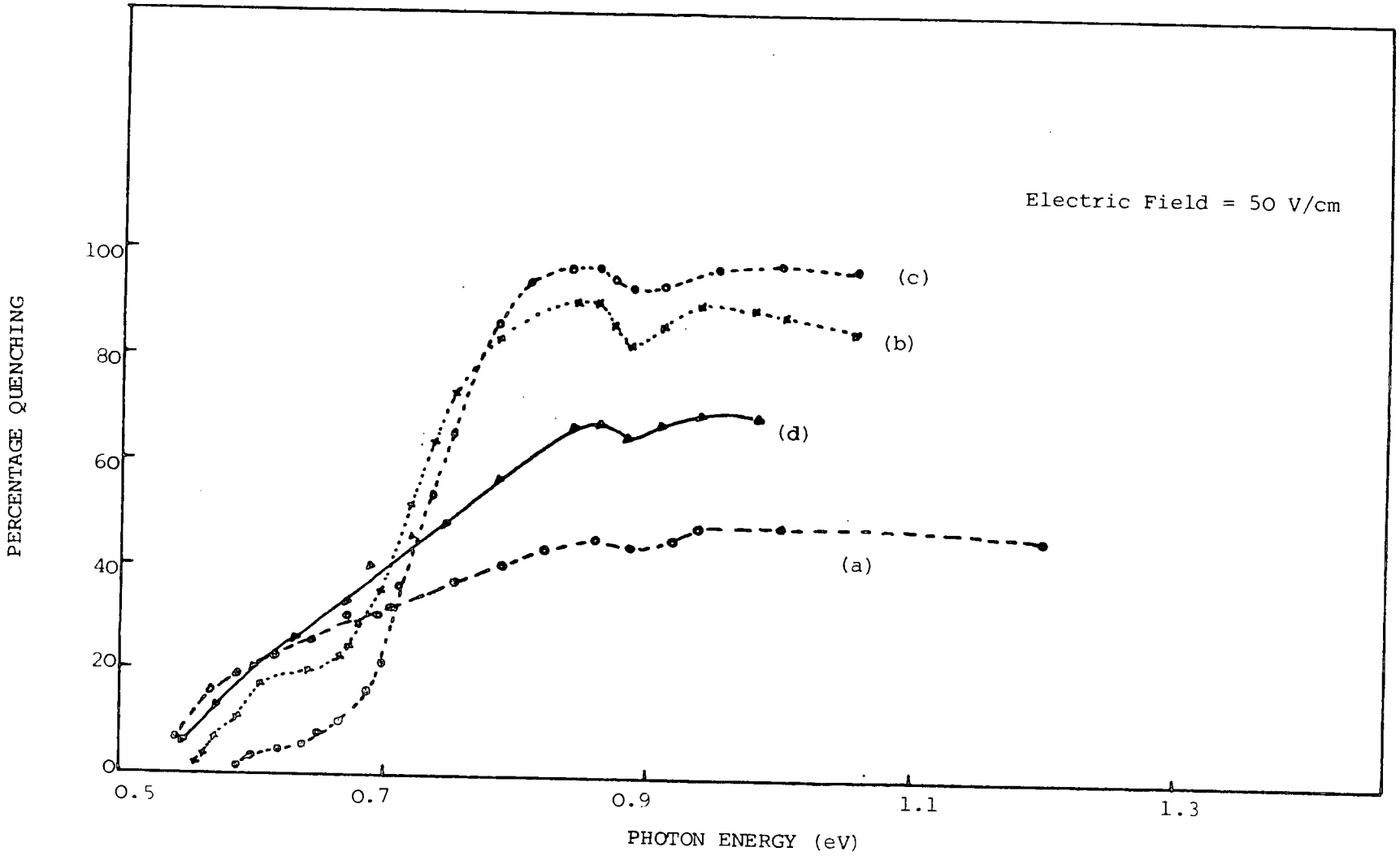

Figure 5.8 : Infra-red quenching of photocurrent in (a) ZnSe:Cu,Cl at 294 K, (b) ZnSe:Cu, Cl at 84 K, (c) ZnSe:Cu at 84 K, and (d) ZnSe:Cl at 84 K.

for (d) a 0.44 μm filter, together with an IR absorber filter. The spectrum (b) shows the threshold near 0.64 eV. When the intensity of the infra-red light was reduced to 50% of that used to obtain curve (b), using a 50% neutral filter, the quenching threshold shifted to 0.66 eV and the percentage quenching was reduced,(see curve(c)). When the primary excitation was made via the 0.44 μm filter, the quenching as shown in Fig 5.6(d) developed a tail extending from 0.60 eV, with strong quenching starting at 0.66 eV. It may be argued that this is the actual threshold indicating the position of a level 0.66 eV above the valence band.

In Fig 5.7, the quenching responses are for ZnSe:Cl, sample No. 358-1, at 86 K and with different primary light intensities. The maximum primary excitation intensity was used to obtain curve (a) and then this intensity was decreased for (b) and for (c). The intensity of the secondary light (IR) was the same for each. As the intensity of the primary light decreased the percentage quenching increased. This behaviour is the reverse of the case described in Fig 5.6 (b) and (c). Thus for effective quenching, the intensities of the primary and secondary radiation should be comparable. If the primary radiation is too intense or the secondary is too weak the quenching will be small. The threshold in Fig 5.7 for ZnSe:Cl is near (0.55-0.57) eV and is substantially unaffected by the variation in the intensity of the primary light.

The room temperature response was negligibly small for the ZnSe:Cl sample. Quenching spectra for ZnSe:Cu, ZnSe:Cl and ZnSe:Cu,Cl samples measured under comparable conditions are shown in Fig 5.8.

The crystal doped with copper and chlorine, sample No.135-2, showed quenching at room temperature as illustrated in Fig 5.8(a), with a threshold at 0.54 eV. The low temperature response for this sample clearly exhibited two thresholds, at 0.56 eV and 0.67 eV,(see Fig 5.8(b)). The quenching spectra for ZnSe:Cu, sample No.158-3, curve (c), and ZnSe:Cl, Sample No.358-2, curve (d), had different shapes and only one well-defined threshold,which was

at 0.55 eV for ZnSe:Cl and 0.67 eV for ZnSe:Cu.

These quenching measurements show quite conclusively that the threshold at 0.64-0.67 eV occurs in ZnSe:Cu samples, while that at 0.55-0.57 eV appears in the ZnSe:Cl crystals. The ZnSe:Cu,Cl samples exhibit both quenching thresholds. The obvious explanation of the results is that the copper centres lie some 0.64-0.67 eV above the top edge of the valence band while the self-activated centres lead to levels 0.55-0.57 eV above the valence band.

5.4 ZnSe: In AND ZnSe: Ga CRYSTALS

5.4.1 Photoconductive Spectral Analysis

(A) ZnSe: In Doped

The photoconductive spectral response curves for ZnSe samples doped with different concentrations of indium are shown in Figs 5.9 - 5.11. The sample from boule No.407, doped with 5 ppm In, had a low resistivity (7×10^2 Ohm-cm) and showed no detectable photoconductive effect at any temperature. The responses shown in Fig 5.9 are those obtained at room temperature from samples doped with 50 ppm, 100 ppm and 1000 ppm indium. Samples with 50 ppm indium were cut from two different boules, No.375 and No.405. The sample 375-1, grown from Durham Grade material, had a resistivity $\rho = 7 \times 10^5$ Ohm-cm, and was photoconductive at room temperature as well as at liquid nitrogen temperature. In contrast, the sample 405-1, grown from Mixed (Durham-Merck grades) grade material, had a resistivity of 5.1×10^4 Ohm-cm, and a negligible photoconductive response at room temperature.

The room temperature response of sample 375-1 is shown in Fig 5.9(a). It has one peak ($h\nu$ = 2.30 eV) with a clear threshold at 1.88 eV. It also shows a small feature at lower energies with its maximum at 1.20 eV. The response of sample 410-1, doped with 100 ppm In, which had a resistivity of 2.9×10^{12} Ohm-cm ; is shown in Fig 5.9(b). This sample has a more structured spectrum with two decisive thresholds at 0.70 and 2.02 eV. Two peaks at

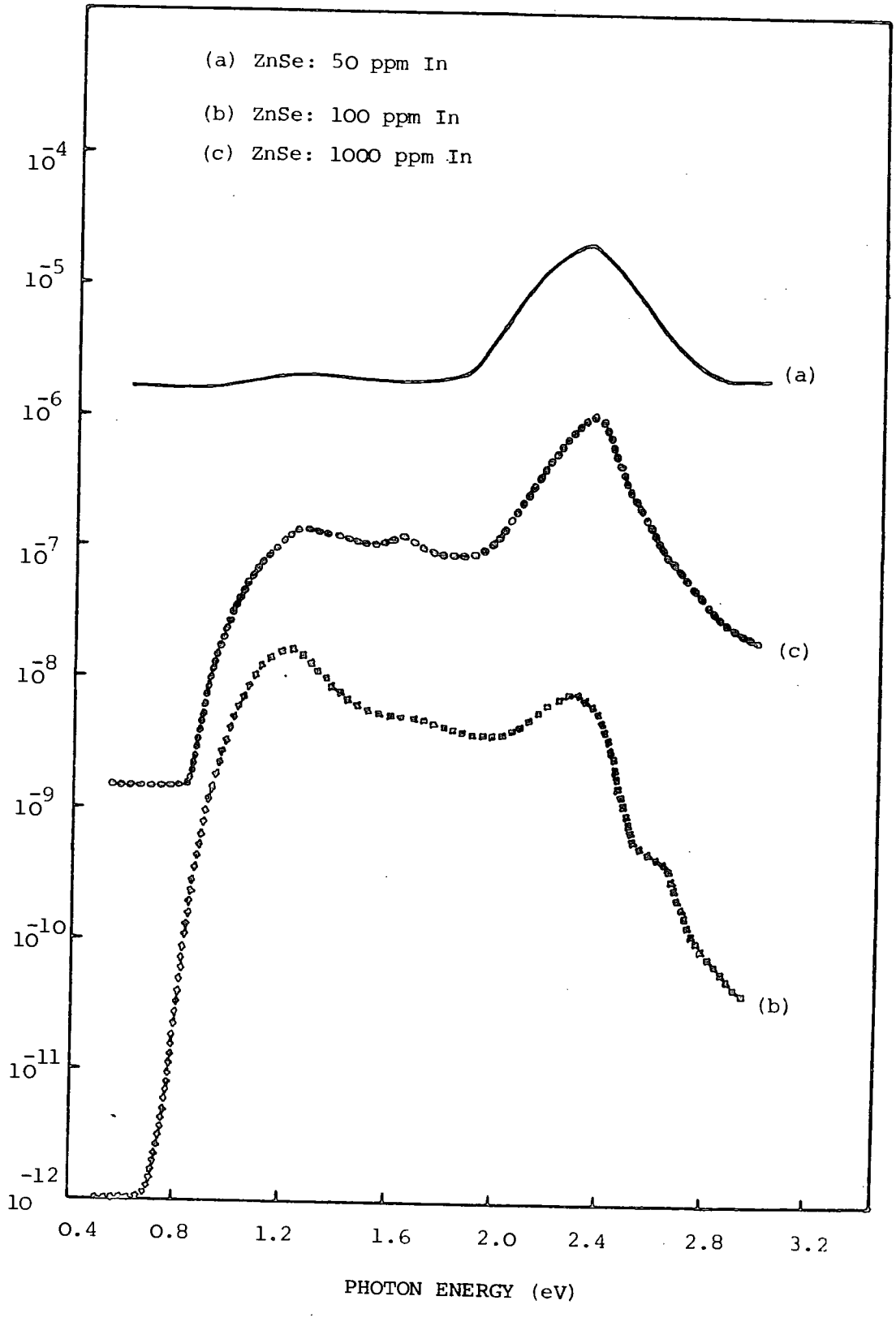

Figure 5.9 : Spectral response of photocurrent (at 294 K) for ZnSe containing different concentrations of Indium.

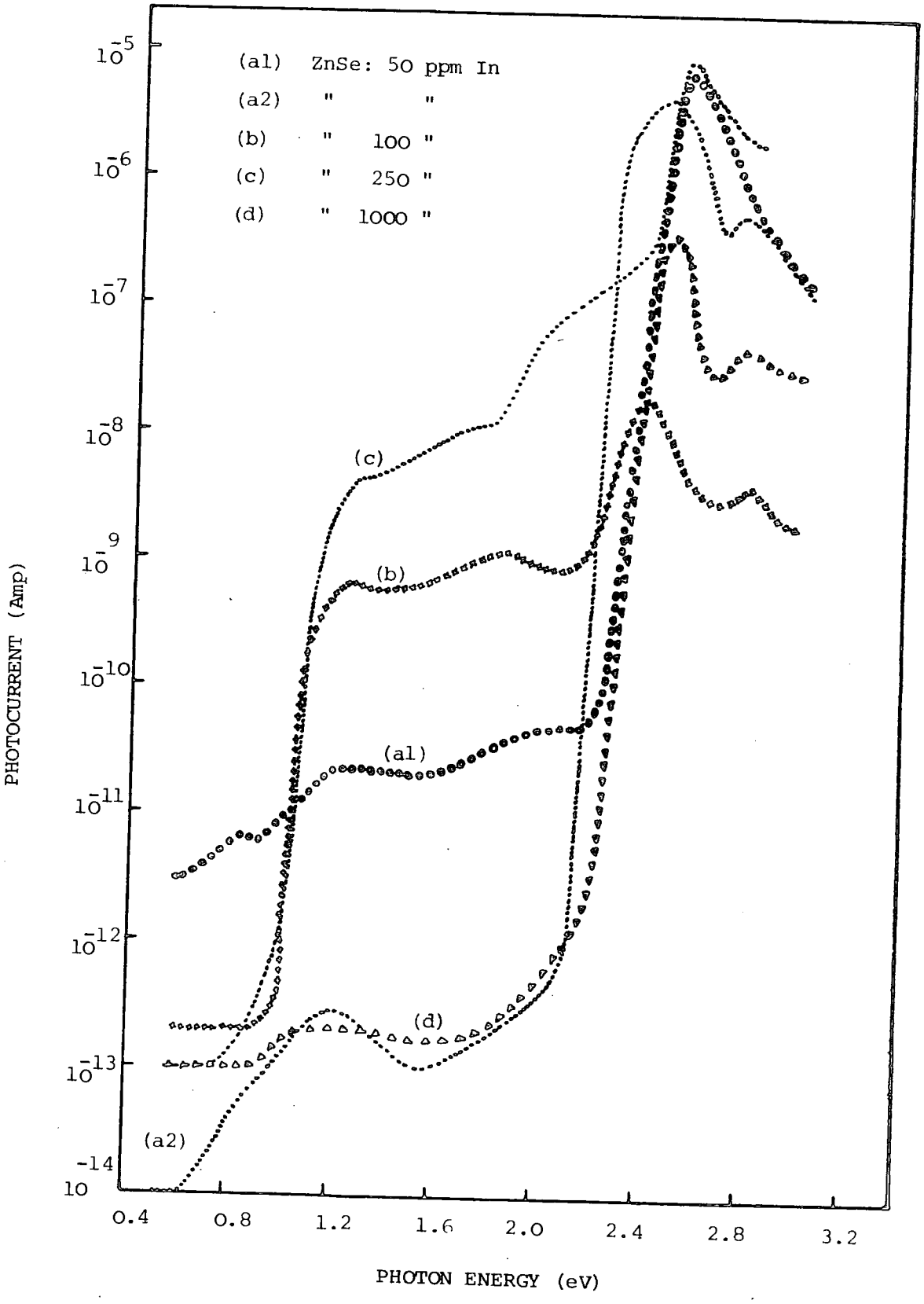

Figure 5.10 : Spectral response of photocurrent (at 85 K) for ZnSe containing different concentrations of indium.

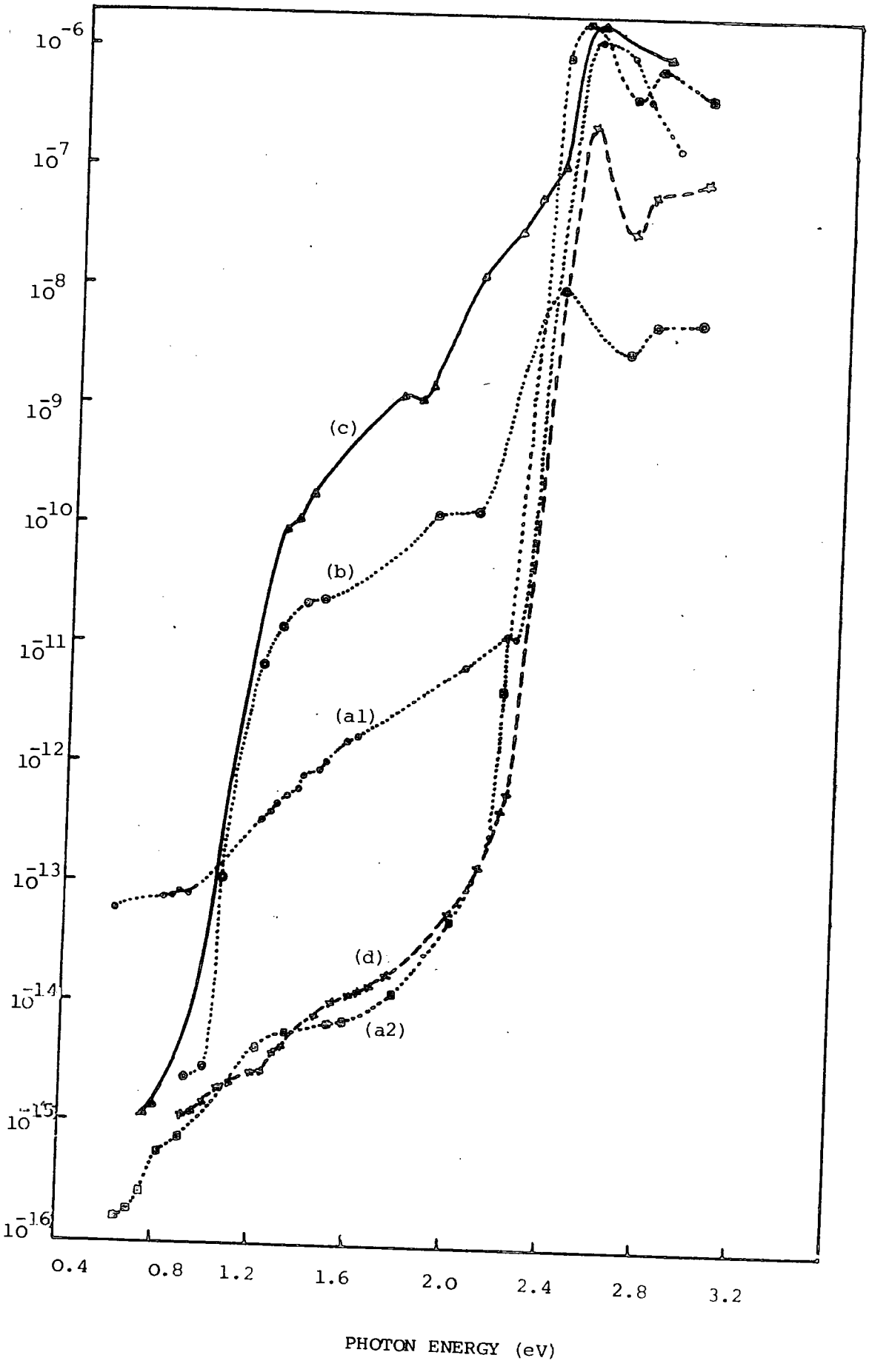

Figure 5.11 : Spectral responses of Fig 5.10 normalised for constant incident photon energy.

$h\nu$ = 1.2 eV, and $h\nu$ = 2.38 eV and two shoulders near 1.70 and 2.66 eV were also apparent. The other sample which also gave a reasonable response at room temperature was 349-1, containing 1000 ppm In, which had a resistivity of 2 x 10^{10} Ohm-cm ; its spectrum is shown in Fig 5.9(c). The clear thresholds here were at 0.82 and 1.90 eV. The spectrum also shows a structure with its maxima at 1.64 eV.

The photoconductive responses of ZnSe samples doped with 50, 100, 250 and 1000 ppm indium were also measured at liquid nitrogen temperature and are shown in Fig 5.10. Later, these responses were corrected at each wavelength for constant energy of the exciting source,and the resultant curves are shown in Fig 5.11. There was not much difference between the corrected and uncorrected responses. The positions of the important thresholds remained virtually unchanged. The two sets of curves in Figs 5.10 and 5.11 are shown to illustrate that the correction for the spectral distribution of the source and the dispersion of the monochromator made little difference to the measured threshold energies.

The two samples with 50 ppm of indium led to the curves shown in Figs 5.10 (a1) and (a2). The sample (405-1) illustrated in (a1) gave thresholds at 0.61 , 0.88, 1.54 and 2.20 eV. The threshold at 2.20 eV was associated with a large peak ($h\nu$ = 2.55 eV). With the sample (375-1) from which curve (a2) was obtained, the first threshold on the low energy side occurred at 0.66 eV, but the second at 0.88 eV was not clearly observed, but there was a change of slope in the photocurrent response near 0.86 eV which reveals the presence of a similar centre to that involved in (a1) near 0.88 eV. The third and fourth thresholds were at 1.54 eV and 2.12 eV respectively. The overall photoconductive response in (a2) clearly showed three peaks, at 1.20, 2.48 and 2.78 eV, the third of which is very near to the bandgap. The corrected results for both samples are shown in Figs 5.11 (a1) and (a2). The photocurrent plotted as ordinate is now in arbitrary units, because the plots are of photocurrent at

constant energy flux against hν , where the energy flux is a relative measurement. After correction, the sample 405-1, Fig 5.11 (a1), showed thresholds at 0.61 , 0.91 and 2.23 eV, that at 1.54 eV was not clearly resolved. With sample 375-1, Fig 5.11 (a2), the thresholds were at 0.64, 0.88, 1.60 and 2.14 eV. Obviously the thresholds did not shift very much after correction.

With sample 410-1, the photoconductive response revealed thresholds at 0.90, 1.50, 2.10 and 2.69 eV as shown in Fig 5.10 (b). The corrected form of this spectrum is given in Fig 5.11 (b) with thresholds now at 0.90, 1.44, 2.08 and 2.69 eV. The peak positions in the uncorrected response were 2.41 and 2.80 eV, and after correction the peak near 2.41 remained unchanged and that at 2.80 eV assumed the shape shown in the Fig 5.11 (b).

The response in Fig 5.10 (c) is for the sample 408-1, containing 250 ppm In. The various features were not so well defined, but changes of slopes and shoulders help to fix the positions of the thresholds at 0.75,1.36,1.82 and 2.38 eV. The maximum photocurrent (9×10^{-6} A) showed that the peak position occurred at 2.53 eV. The corrected response is plotted in Fig 5.11(C) with thresholds at 0.75, 1.32, 1.82 and 2.38 eV.

The last sample 349-1, in this indium doped family, contained 1000 ppm indium, and its response revealed thresholds at 0.91, 1.75, 2.20 and 2.68 eV, Fig 5.10 (d). The thresholds at 1.75 and 2.20 eV were not well defined. The higher energy side of the spectrum again revealed two peaks at 2.50 eV and 2.77 eV. When corrected the thresholds were 0.91, 1.24, 1.75, 2.20 and 2.68 eV, (see Fig 5.11 (d)).

(B) ZnSe:Ga

Since gallium belongs to the same group III column of the periodic table as indium, some crystals of ZnSe were doped with gallium during growth and their photoconductivity was investigated. The samples contained 5ppm, (ρ = 92.0 Ohm-cm) ; 50 ppm, ($\rho = 2.9 \times 10^{3}$ Ohm-cm) ; 100 ppm, ($\rho = 2.6 \times 10^{5}$ Ohm-cm); and 250 ppm, ($\rho = 2 \times 10^{7}$ Ohm-cm) ; gallium.

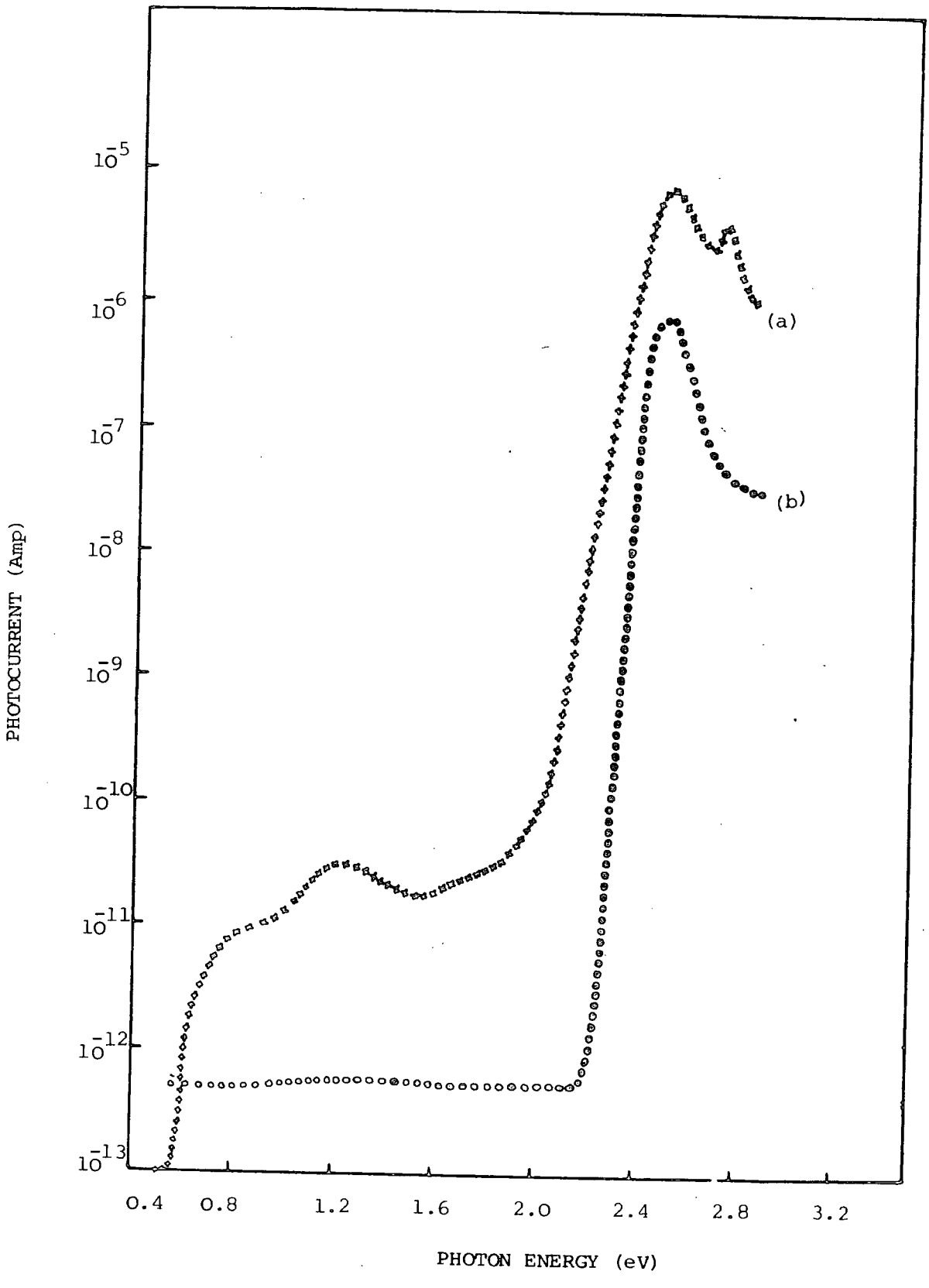

Figure 5.12 : Spectral response of photocurrent (at 83 K) for

(a) ZnSe: 100 ppm Ga

(b) ZnSe: 250 ppm Ga

The samples with 5 and 50 ppm gallium were not photoconductive at any temperature. The spectra of the samples doped with 100 ppm and 250 ppm gallium, measured at liquid nitrogen temperature are given in Fig 5.12. Curve (a) is for sample 382-1, with 100 ppm Ga, which showed a low energy threshold at 0.58 eV. This threshold was also observed in our undoped and 50 ppm indium doped samples, (see Fig 5.1 and 5.10 (a)). All the other thresholds were not so clearly defined, but could be resolved near 0.94, 1.52, 1.84 and 2.06 eV. This sample also showed two peaks near the bandgap, one at 2.50 eV and the other at 2.73 eV. The second sample containing 250 ppm gallium, sample No.383-1, had a negligibly small photoconductive response on the low energy side, $h\nu < 2.16$ eV, Fig 5.12 (b), but there was a sharp rise with a pronounced threshold at 2.16 eV. In contrast with the 100 ppm sample, only one peak at 2.50 eV was apparent.

5.4.2 Selenium Treatment and Selenium Vacancies

The photoconductive response curves shown in Figs 5.1 (b) and (d), Figs 5.10 (a1) and (a2) and Fig 5.12 (a), all have a low energy threshold at $\sim$ 0.60 eV. An attempt was made to investigate the nature of this level, by heating two different 50 ppm indium doped samples in selenium vapour. Sample No.405-3 Se, was heated in selenium vapour at 440^{o}C (Vapour pressure 10 Torr) for three days and, sample No.405-4 Se at 540^{o}C (Vapour pressure 100 Torr) for the same period. The treatment increased the resistivities of the samples from 5.1×10^{4} Ohm-cm to 2×10^{8} Ohm-cm for 405-3 Se and 1×10^{12} Ohm-cm for 405-4 Se. The resistivity of that sample was larger having been treated in a higher Se-pressure. The increase in resistivity is due to the diffusion of selenium atoms into the crystals thereby increasing the concentration of zinc vacancies (acceptor centres) and filling the selenium vacancies (donors), (see Stringfellow and Bube (1968)). The selenium treated samples (doped with 50 ppm In) have the room temperature photoconductive responses shown in Fig 5.13. Before Se-treatment there was negligible response

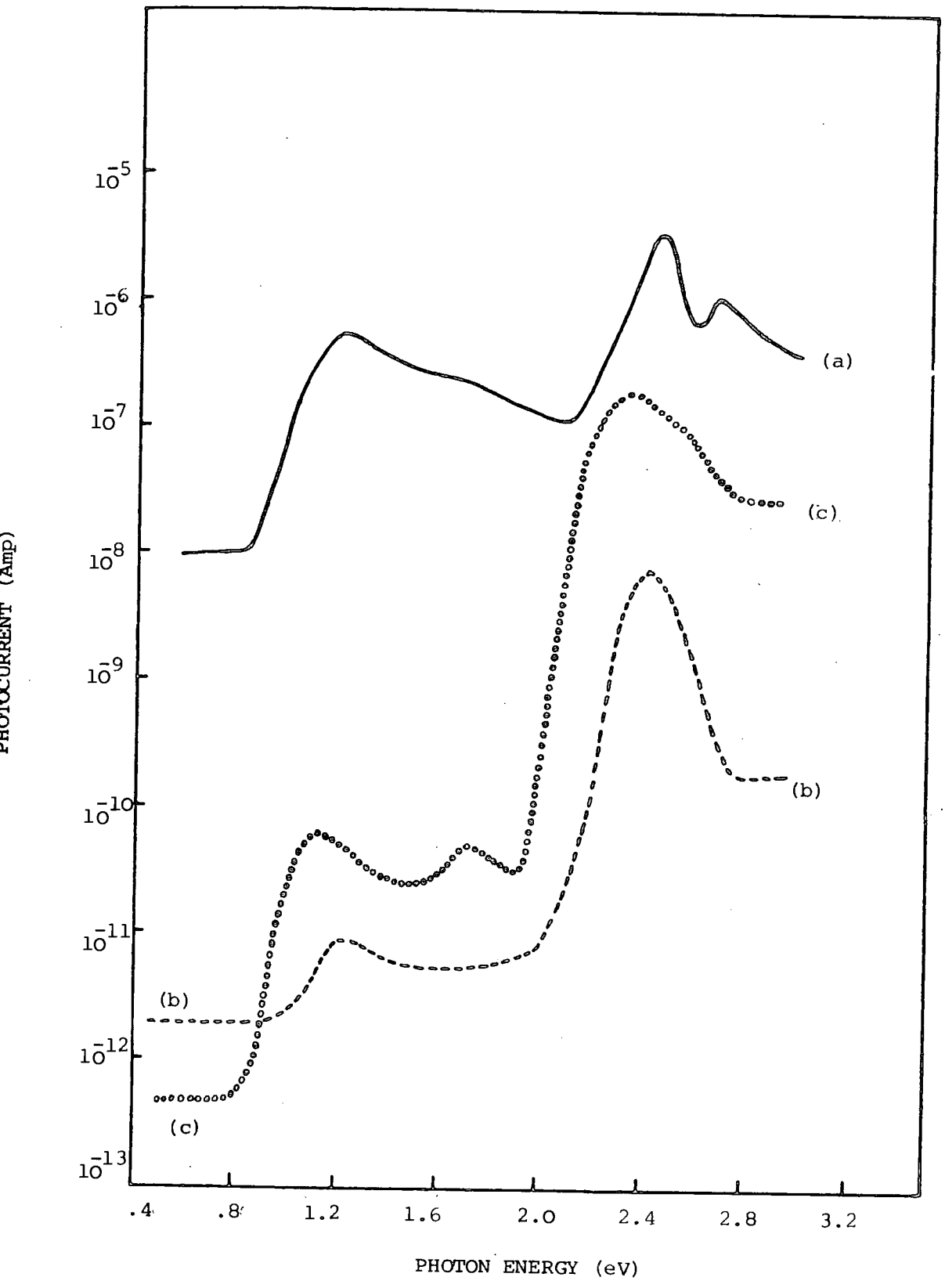

Figure 5.13 : Spectral response of photocurrent (at 295 K) for selenium treated ZnSe:In Samples

(a) ZnSe:50 ppm In-3 days in Se-vap.at 440^{o} C,

(b) ZnSe: 50 ppm In-3 days in Se-vap.at 540^{o}C and

(c) ZnSe: 5 ppm In-3 days in Se-vap.at 500^{o}C.

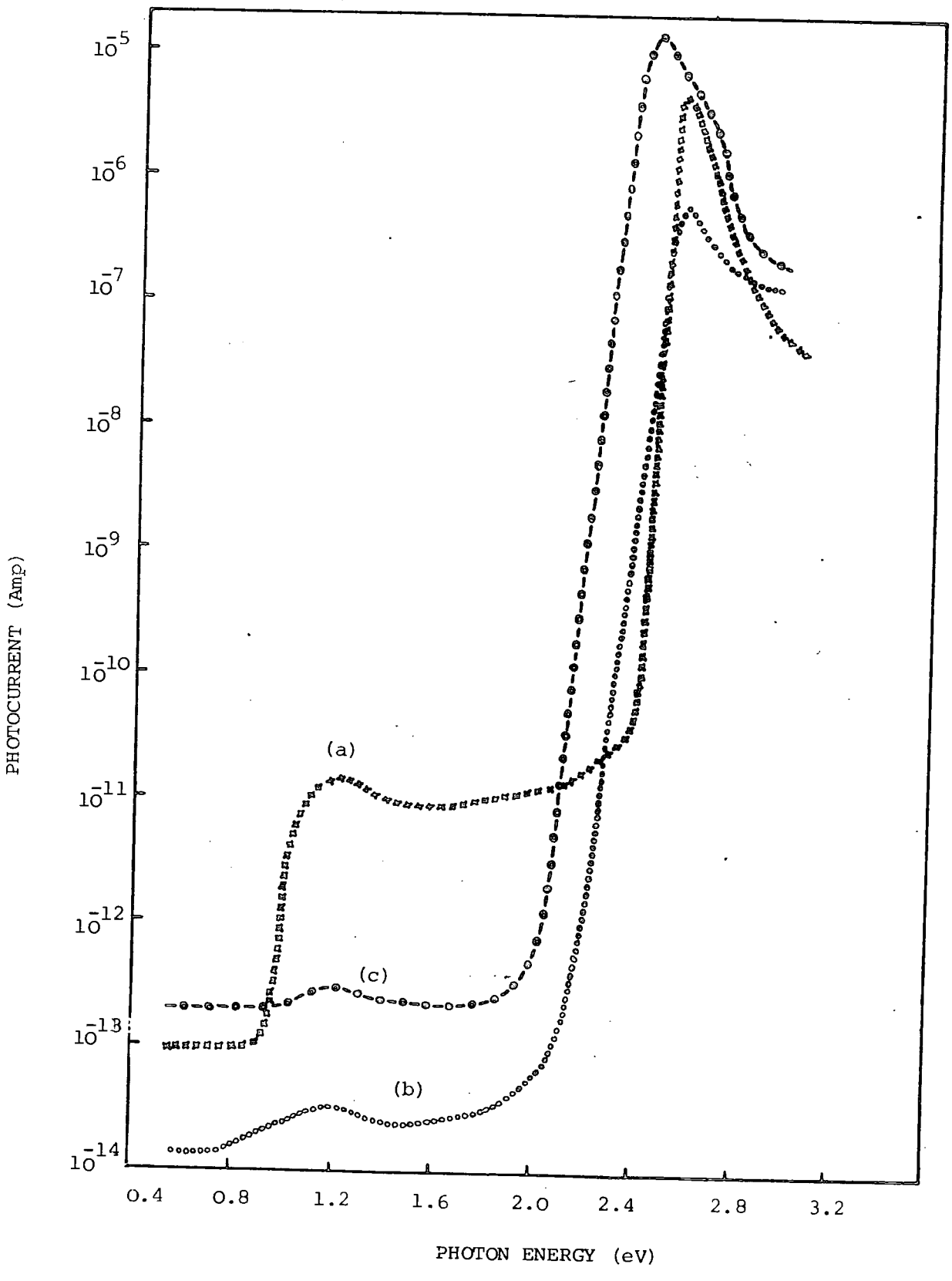

Figure 5.14 : Spectral response of photocurrent (at 85 K) for selenium treated ZnSe:In (see in Figure 5.13 for (a), (b) and (c)).

at room temperature. Sample 405-3 Se had a large dark current in comparison with sample 405-4 Se, due to the difference in resistivities. The thresholds in 405-3 Se were at 0.82, 2.10 and 2.60 eV, Fig 5.13 (a) ; and in 405-4 Se were near 0.92 and 2.00 eV,(see Fig 5.13 (b)). The photoconductive responses at nitrogen temperatures are shown in Fig 5.14. The interesting aspects of all these curves is that there is no threshold near 0.60 eV. The first thresholds are at 0.90 eV and 0.80 eV in 405-3 Se and 405-4 Se samples, respectively. The peak position in both samples occurred at 2.57 eV, which is nearly the same position as before Se-treatment, (see Fig 5.10 (a1)).

As stated in section 5.4.1, the sample doped with 5 ppm indium had a low resistivity and was not photoconductive. This sample was also heated in selenium vapour (pressure 40 Torr) for 3 days at 500^{o}C. Its resistivity then increased to 6 x 10^{13} Ohm-cm and its room temperature photoconductive response is shown in Fig 5.13 (c). Thresholds were then apparent at 0.80, 1.50 and 1.90 eV. The higher energy side shows a pronounced band peaking at 2.37 eV with a change of slope near 2.57 eV. The low temperature response for this sample No.407-2, is illustrated in Fig 5.14 (c). There is no response near 0.60 eV, the first threshold is at 1.00 eV, and the peak position occurs at 2.46 eV.

5.4.3 Infra-Red Quenching

The spectral response of infra-red (IR) quenching was measured for the indium doped samples and also for the sample doped with 100 ppm gallium, see Figs 5.15 and 5.16. The primary excitation was via a 0.44 μm band pass filter together with Infra-red absorbing filter.

The room temperature responses were negligibly small and quenching measurements were only possible at 85 K. The smallest quenching effect ($\sim$ 50%) was found with the sample 408-1, doped with 250 ppm In ; and the maximum (90%) for the samples containing 50 and 1000 ppm In, Fig 5.15. None of the quenching thresholds was sharp as with the ZnSe:Cl and ZnSe:Cu samples

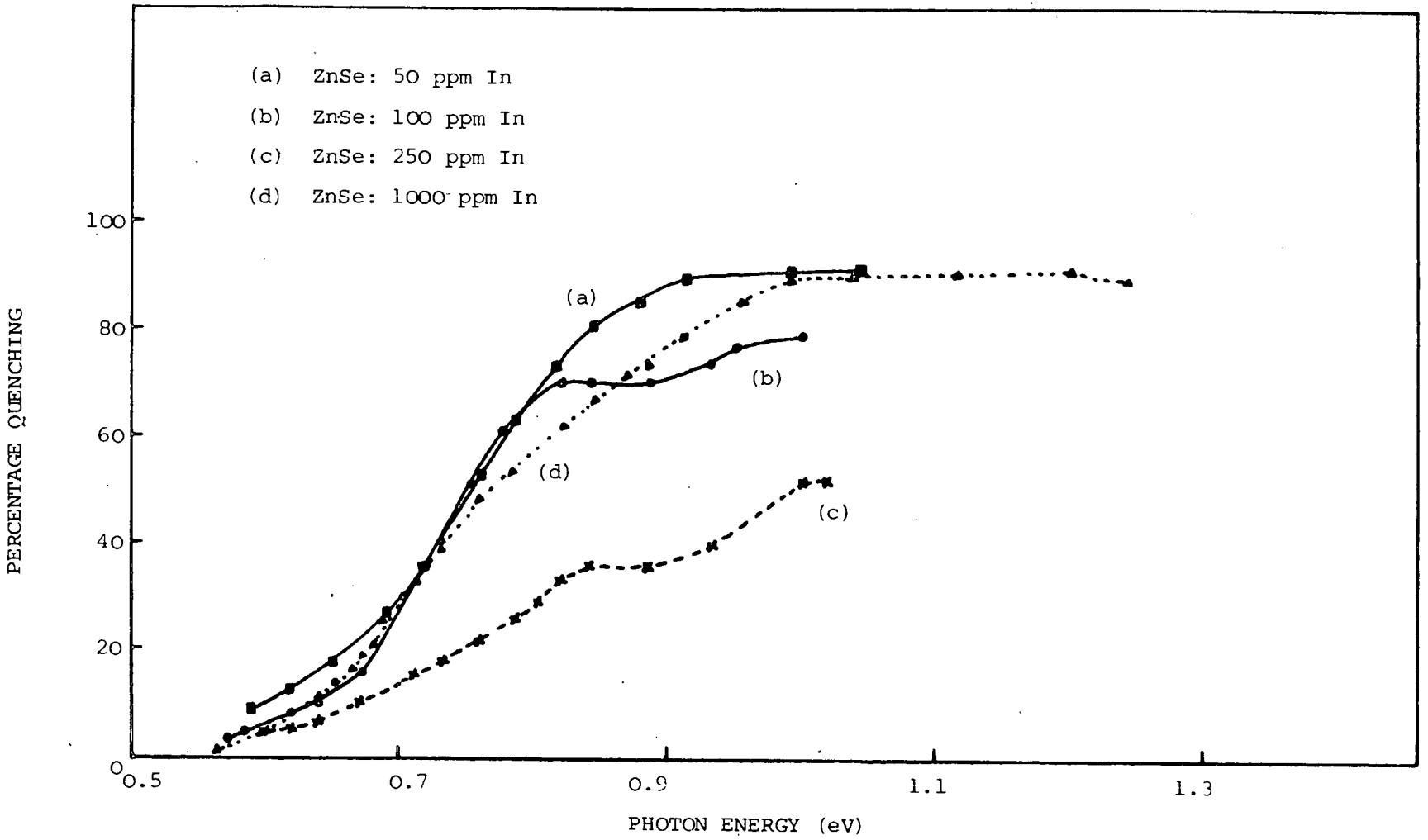

Figure 5.15 : Infra-red quenching of photocurrent (at 85 K) for ZnSe containing different indium concentrations

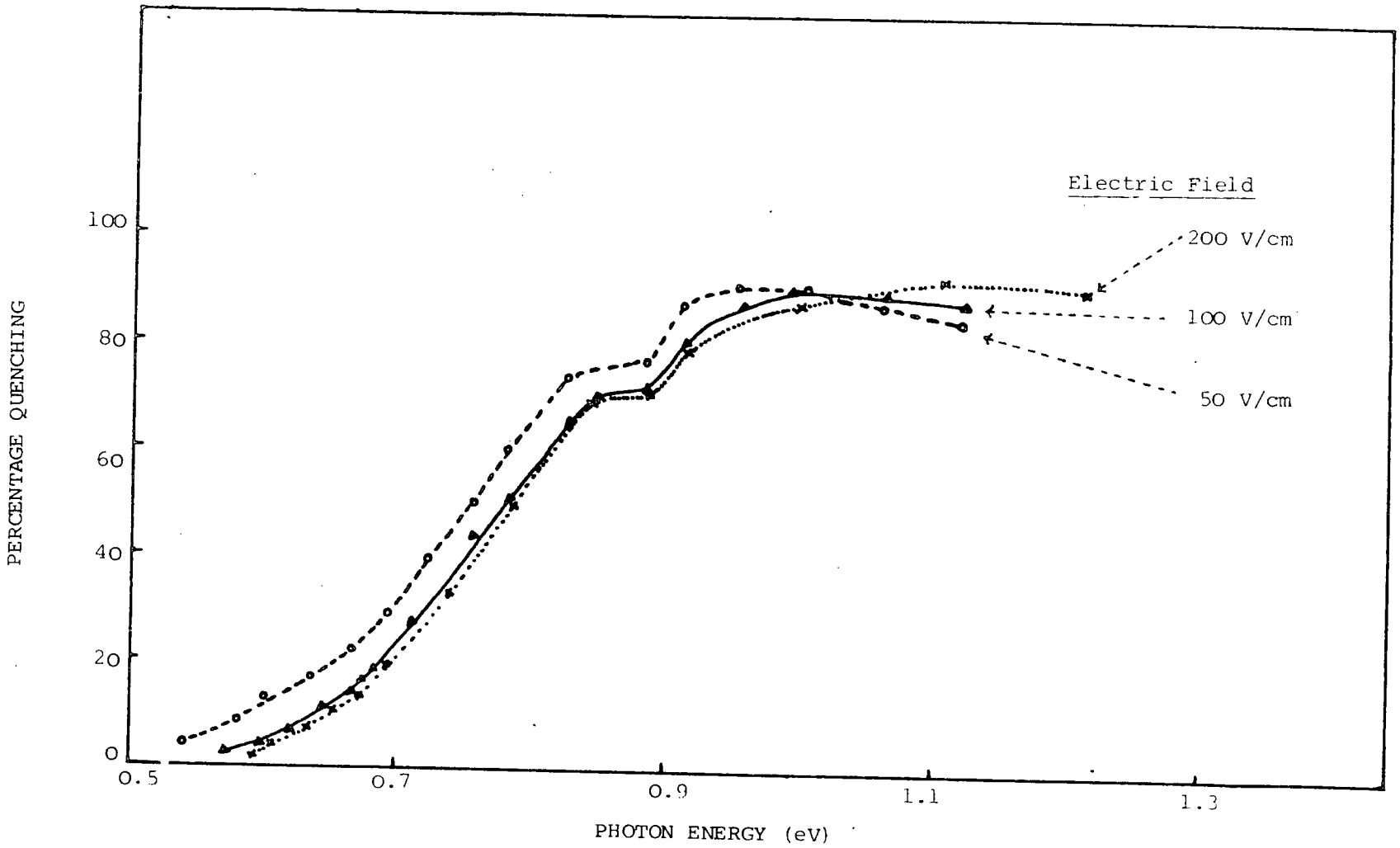

Figure 5.16 : Infra-red quenching of photocurrent (at 84 K) for ZnSe: 100 ppm Ga at different electric fields.

shown in Figs 5.6-5.8. The long wavelength limit from which the quenching began in ZnSe: 50 ppm In, corresponds to $h\nu$ = 0.59 eV but the major quenching seemed to begin near 0.64 eV, see Fig 5.15 (a). In ZnSe: 100 ppm In, the quenching curve also had two curvatures, one starting at 0.57 eV and another at 0.65 eV, Fig 5.15 (b). With the 250 ppm In sample, the quenching threshold was at 0.60 eV and there was no indication of any other threshold, Fig 5.15(c). The last sample with the highest concentration of indium, i.e. 1000 ppm ; also showed two curvatures in the quenching behaviour, Fig 5.15 (d). The first threshold was about 0.56 eV and the second 0.63 eV.

These observations suggest that there are two deep centres with levels some 0.58 eV and 0.64 eV above the valence band.

The same quenching technique was adopted with the ZnSe : 100 ppm Ga samples. The responses at 84 K with different applied electric fields are shown in Fig 5.16. The quenching thresholds shifted from lower to higher energy as the electric field increased, but the percentage quenching was unaffected. The thresholds shifted from 0.54 eV through 0.57 eV to 0.60 eV, as the electric field was increased from 50 V/cm to 100 v/cm and 200 V/cm.

The irregularity in the responses near 0.90 eV is attributed to a decrease in the secondary source intensity at that energy.

5.5 PHOTOIONIZATION CROSS-SECTION OF ELECTRONS AND HOLES

The technique involved in measuring the spectrum of the photoionization cross-section has been reviewed in Chapter 2. Since many of the parameters in eqns. (2.10 and 2.11), such as the density of impurity levels, capture cross-section and the free-electron concentration were not known, absolute measurements were not possible.

Some of the experimental difficulties which were encountered were overcome in the following ways :

(a) Constant photo-current was achieved by controlling the voltage supplied to the lamp using a rotary Regavolt. The method was manual and not precise.

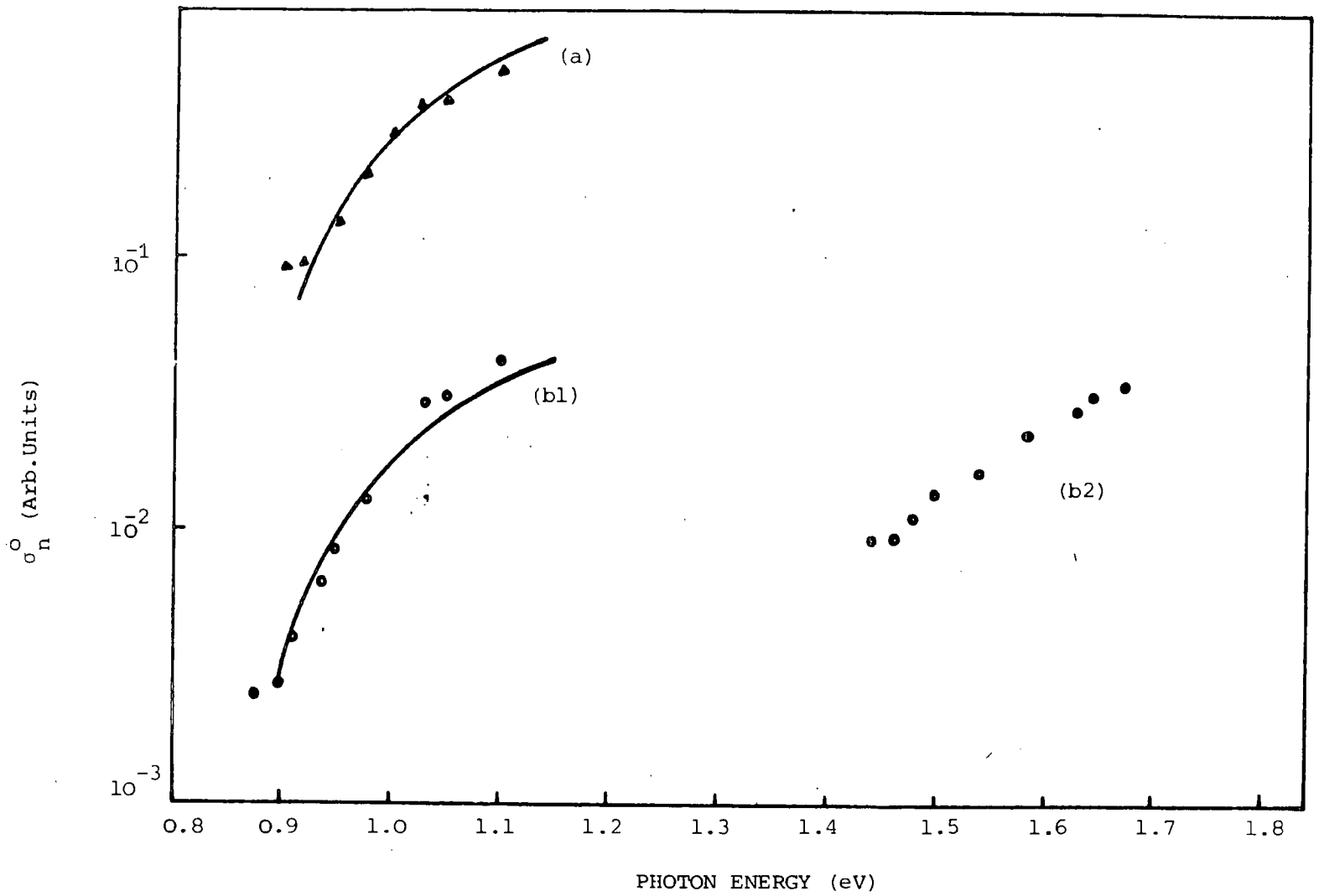

Figure 5.17 : Spectral dependence of the photoionization cross-section of electrons for (a) ZnSe:Cl and for (b1 & b2) ZnSe:Cu, Cl. Solid lines are the Lucovsky plots.

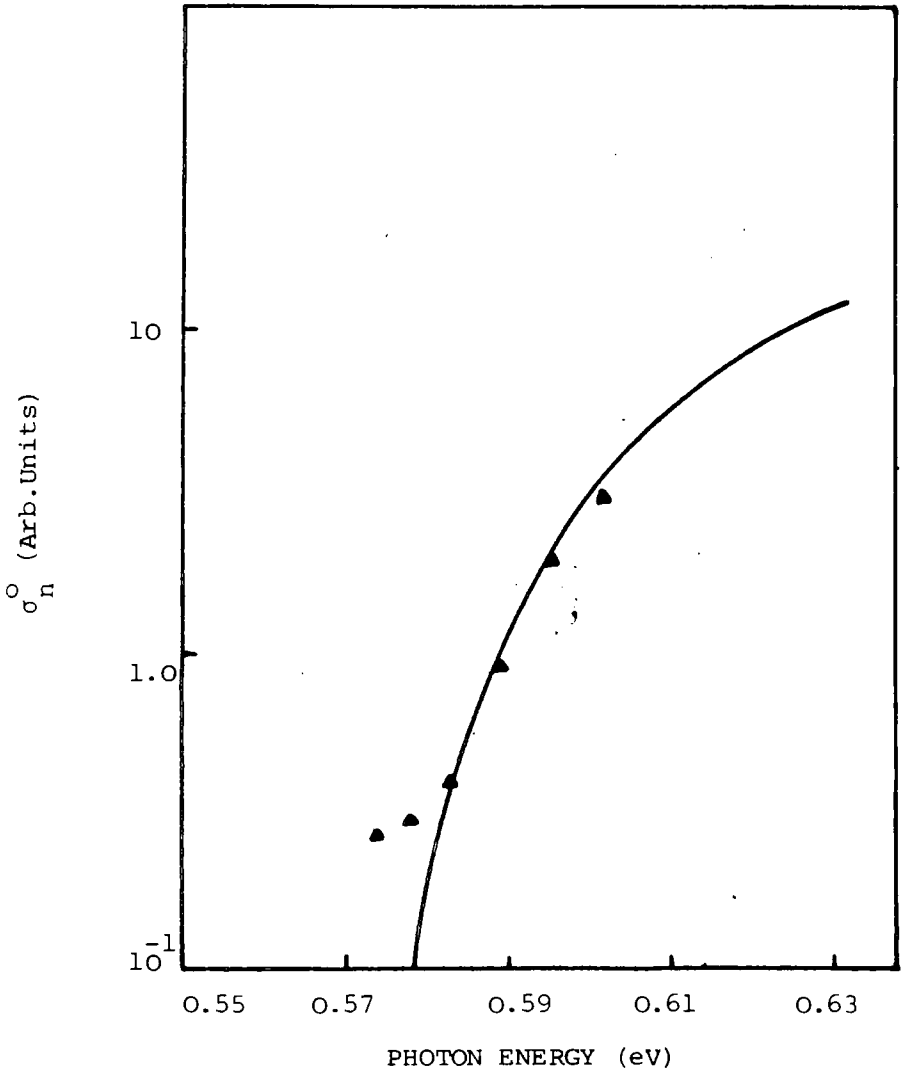

Figure 5.18 : Spectral dependence of the photoionization cross-section of electrons for ZnSe: 50 ppm In (▲). Solid line is the Lucovsky plot.

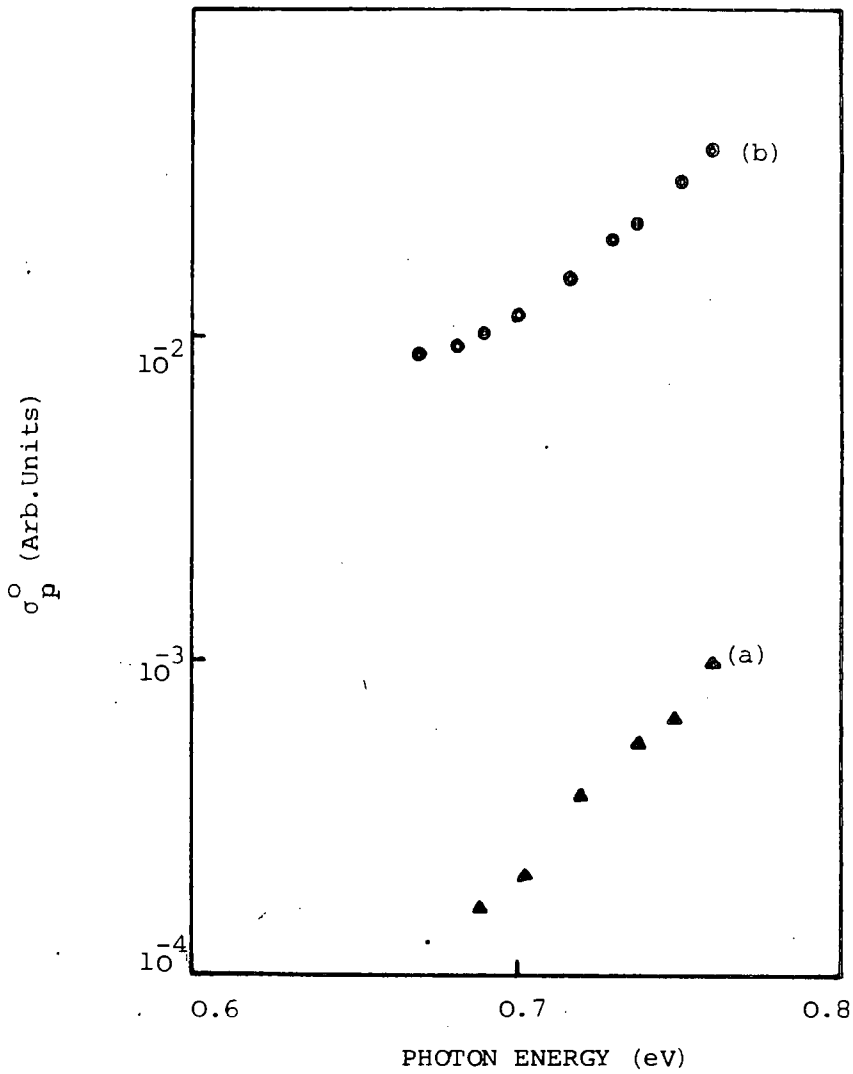

Figure 5.19 : Spectral dependence of the photoionization cross-section of holes for (a) ZnSe:Cu and (b) ZnSe:Cl.

(b) The light intensity was monitored after reflection from the sample stage, which was set at an angle of 45° to the incident illumination. This decreased the measurable light intensity.

(c) Thermal gradients introduced difficulties with the thermopile, when measurements were made at liquid nitrogen temperature , and heavy thermal insulation was needed.

However, some satisfactory measurements were made and the results are plotted in Figs 5.17-5.19. The plots are of the logarithm of [excitation intensity $]^{-1}$ which is proportional to the cross-section against the photon energy $h\nu$ of the excitation. The variation of the photoionization cross-section of electrons, σ_n^o , for ZnSe : Cl, sample No. 358-L, is shown in Fig 5.17 (a). The position of the threshold was found using Lucovsky's theoretical (see eqn. 2.14) plot which is shown here as the solid line. This revealed a level 0.91 eV below the conduction band. The spectra (b1) and (b2) in the same figure are for the ZnSe: Cu, Cl, No. 135-L, in which only (b1) gave a definite threshold at 0.90 eV, following Lucovsky's method. An indium doped sample No.405-L, ZnSe : 50 ppm In, had a photoionization cross-section for electrons, σ_n^o , as shown in Fig 5.18, which revealed a threshold at 0.58 eV.

The variation of the photoionization cross-section for holes, σ_p^o ; which involves the transfer of holes from deep impurity centres to the valence band was investigated using infrared quenching. As described earlier in Chapter 2, the idea is to keep the quenching photocurrent constant by controlling the light intensity I_L ; σ_p^o is then proportional to $(I_L)^{-1}$. The spectrum of σ_p^o against $h\nu$ is shown in Fig 5.19 for ZnSe: Cu and ZnSe: Cl. Lucovsky's method was not successful in fixing the position of the thresholds, but the spectra suggest approximate positions of the levels at 0.69 eV for ZnSe : Cu, Fig 5.19 (a) and; 0.67 eV for ZnSe:Cl, Fig 5.19 (b). These values relate to the positions of the levels above the valence band.

5.6 DISCUSSION OF THE ZnSe RESULTS

A summary of the measured thresholds for photoconductivity and IR-quenching in undoped ZnSe and samples doped with copper, chlorine, indium or gallium at T $\sim$ 85 K, is given in Tables 5.1 and 5.2. The levels recorded in the tables are those for which the thresholds were clearly defined. Comparison with the literature can be confusing, because for example, Stringfellow and Bube (1968) and many others discuss photoconductivity and quenching in terms of thresholds, but Adachi and Machi (1975) and many others make use of the peak positions in their explanations. This may be one of the reasons for the discrepancies in the results of different workers.

The photoconductive responses of all the undoped and doped crystals show an exponential increase with $h\nu$ for $h\nu$ > 2.20 eV. This part of the spectrum is important, because all the sensitizing centres (e.g. Cu and SA centres) lie closer to the valence band and photons with these energies are able to excite electrons to the conduction band from them. Chlorine is a shallow donor in ZnSe, and gives rise to a level 0.027 eV below the conduction band, (see Merz, et al (1972). When chlorine is present charge compensation effects, lead to the production of SA-centres (i.e. $(V_{zn}\text{-}Cl_{se})'$), giving high photosensitivity, see Lorenz et al (1963) and Woodbury and Aven (1964). Self-activated centres involving group III elements, such as indium and gallium have also been described previously, (see Jones and Woods (1974)).

Since the photoconductive sensitivity at room temperature was very small, due to high dark current levels in different samples, reliable discussion is only possible for the results obtained at liquid nitrogen temperatures. At low temperature, the photocurrent was enhanced by several orders of magnitude, giving better resolution where thermal effects are minimized.

The chlorine, indium or gallium doped crystals, had the largest photoconductive sensitivity with a sharp threshold at 2.10 - 2.20 eV ; which puts the corresponding levels between 0.60 and 0.70 eV above the top edge of the

Sample	Threshold (a) (eV)	Threshold (b) (eV)	Threshold (c) (eV)	Threshold (d) (eV)	Threshold (e) (eV)	Peak 1 (eV)	Peak 2 (eV)	Peak 3 (eV)
ZnSe (Se-tail)	0.62	0.94	1.54	2.10		2.40-2.66		
ZnSe (Zn-tail)	0.62		1.60	2.10	2.50		2.71	
ZnSe:Cu			1.70	2.26		2.48		
ZnSe:Cl		0.94		2.06		2.54		
ZnSe:Cu,Cl		0.88	1.50	2.20		2.44-2.68		
ZnSe:50 ppm In	0.61 , 0.66	0.88,	1.54	2.20, 2.12		0.84, 1.20	2.55, 2.48	2.78
ZnSe:100 ppm In		0.90	1.50	2.10	2.69	2.41		2.80
ZnSe:250 ppm In		0.75	1.36	1.82	2.38	2.53		
ZnSe:1000 ppm In		0.91	1.75	2.20	2.68	2.50		2.77
ZnSe:100 ppm Ga	0.58	0.94	1.52	1.84-2.06		2.50		2.73
ZnSe:250 ppm Ga				2.16		2.50		

TABLE 5.1 : Summary of Photoconductivity Results from ZnSe Crystals at L.N.Temp.

TABLE 5.2 : Summary of IR quenching results from ZnSe crystals at L.N.Temp.

SAMPLE	THRESHOLD (a) eV	THRESHOLD (b) eV
ZnSe	-	0.65
ZnSe:Cu	-	0.64,0.66, 0.67
ZnSe:Cl	0.55-0.57	-
ZnSe:Cu,Cl	0.56	0.67
ZnSe:50 ppm In	0.59	0.64
ZnSe:100 ppm In	0.57	0.65
ZnSe:250 ppm In	0.60	-
ZnSe: 1000 ppm In	0.56	0.63
ZnSe: 100 ppm Ga	0.54-0.60	-

valence band. In undoped ZnSe, this threshold is at 2.10 eV, which places the level 0.70 eV above the valence band. The copper doped sample has thresholds at 1.70 and 2.28 eV, which suggests centres 1.10 and 0.52 eV above the valence band.

The photoconductive thresholds observed at 0.90 and $\sim$ 1.50 eV in many undoped and doped ZnSe crystals may belong to donor levels below the edge of the conduction band. The level in the mid-gap energy region may be associated with Class I centres.

The photoconductive results are not decisive in fixing the positions of the copper and SA-centres. On the other hand, the results of the IR quenching are more uniquely interpretable.

In undoped and copper doped crystals the position of the level calculated from the quenching threshold is (0.65 $\pm$ 0.02) eV, and this is certainly due to copper. With the chlorine doped material quenching puts the level at (0.56 $\pm$ 0.01) eV, which is probably the position of the self-activated centre above the valence band. These conclusions are supported by the measurements on ZnSe doped with copper and chlorine, which clearly showed the presence of both levels. Incidentally our results agree with those of Stringfellow and Bube (1968) who found the levels of the SA-centres to be closer to the valence band than those of copper.

In the indium doped samples two quenching thresholds were detected and it is suggested that the first threshold at (0.58 $\pm$ 0.02) eV belongs to the SA-centres while the other near (0.65 $\pm$ 0.02)eV is associated with copper impurity. The unintentionally incorporated copper might be picked up during crystal growth.

In the gallium doped sample one threshold only at (0.54 - 0.60)eV was found, and this is due to SA-centres.

The infra-red quenching results suggest that there is a slight difference in the positions of the SA-centres involving Cl or In. Prener and

Weil (1959) in studying luminescence in ZnS discussed SA-centres formed with group III or group VII elements. A halide ion (such as Cl) occupies a site adjacent to the zinc vacancy by replacing an S atom, whereas a trivalent metal (e.g. Al, In, Ga) must occupy a zinc site further from the vacancy. The binding energy of a hole to this defect would then be expected to be smaller the closer the effectively positive charged co-activator is to the Zn-vacancy. The level of the $(V_{Zn}-Cl_S)'$ defect would lie closer to the valence band than that of $(V_{Zn}-Al_{Zn})'$. The same argument would apply to ZnSe and support the suggestion that SA-centres due to chlorine are nearer to the valence band than the SA-centres formed by indium. This is supported by the results from luminescence studies, (see Jones and Woods (1974)).

Copper is a group I_a element and, in ZnSe, or other II-VI's, can give rise to two levels associated with Cu^{1+} and Cu^{2+} ions. In the chemically neutral state, copper has an electronic structure of (Ar) $3d^{10}4s'$ so that copper substituted for zinc, Cu^x_{Zn}, has the (Ar) $3d^9$ configuration. The Cu^x_{Zn} centre is due to Cu^{2+} ions, and is a deep neutral acceptor and is a sensitizing centre for n-type photo-conductivity and p-type dark conductivity. On the other hand Cu^{1+} has an electronic structure (Ar)$3d^{10}$ and gives Cu'_{Zn} centres. The presence of Cu^{1+} and Cu^{2+} ions gives broad "red" and "green" luminescence bands centres around 1.97 and 2.34 eV in ZnSe, respectively, (see Stringfellow and Bube (1968)). Copper may therefore form two deep centres, as many workers have suggested.

Bube and Lind (1958) found photoconductivity thresholds near 2.136 and 2.625 eV in ZnSe:Br, Cu ; and IR quenching thresholds near 0.60 eV. The level associated with the sensitizing centres was therefore 0.60 eV above the top of the valence band. Stringfellow and Bube (1968) placed the Cu'_{Zn} centres at 0.72 eV and the Cu^x_{Zn} centres at 0.35 eV above the valence band, from various photoelectric measurements. The SA-centres were located between 0.50 and 0.60eV above the valence band. Yu and Park (1973) in attempting to achieve p-type conduction in undoped ZnSe crystals, by heating in Se-vapour, found levels

0.65 ∿ 0.75 eV above the valence band, which they attributed to zinc vacancies and complexes containing zinc vacancies. Jones and Woods (1974) studied luminescence and placed Cu'_{Zn} 0.86 eV and Cu^{x}_{Zn} 0.35 eV above the valence band. The SA emission peaks were observed at 6150 Å (∿ 1.99 eV) for ZnSe:Cl and 6350 Å (∿ 1.94 eV) for ZnSe:In. This suggests that in ZnSe:Cl the SA-centre is 0.78 eV and in ZnSe:In is 0.83 eV above the valence band. Adachi and Machi (1975) from photoconductivity on phosphorus-ion-implanted ZnSe crystals, put the copper level 0.37 eV above the valence band. This value was derived from a measurement of the position of the maximum photocurrent. If this principle is applied to our photoconductivity results we also found levels (0.33-0.40) eV above the valence band and they might be due to Cu^{x}_{Zn} or indium on selenium sites in indium doped samples. Birchak et al (1976) from their optical and temperature quenching studies on ZnSe found two sensitizing centres with levels 0.68 and 1.40 eV above the valence band. They associated the first level with copper and the second level with cation (Zn) vacancies.

Many of the previous investigators have centred their efforts on the study of the deep centres which lie closer to the valence band, and have tended to ignore other deep centres which are farther from the valence band and nearer to the conduction band. These can act as electron traps as well as recombination centres. Kovalenko et al (1979) working on photoluminescence and photoconductivity found donor levels in ZnS and in ZnSe some 0.60 eV below the conduction band, whereas the sensitizing centres were located at 0.80 eV in ZnS and 0.85 eV in ZnSe above the valence band.

Our photoconductivity measurements suggest that the level 0.60 eV below the conduction band might be associated with the selenium vacancy. Yu and Park (1973) attributed a level at 0.92 eV to the selenium vacancy, although Shirakawa and Kukimoto (1980) found a Se-vacancy level 0.30 eV below the conduction band from DLTS measurements and 0.70 eV determined from optical

measurements. The identity of other deep centres is still unresolved and a whole range of native defects and their complexes are probably involved.

In conclusion, however, we can state that the results obtained from IR-quenching for identifications of SA and Cu centres agreed well with other published work.

5.7 ZnS AND ZnS: Ga CRYSTALS

5.7.1 Photoconductive Spectral Analysis

ZnS is potentially a good material for blue light emitting electroluminescent devices, see Lawther and Woods (1978) and Woods (1981), and although the material has been used as a Cathodoluminescence phosphor for many years much remains to be learnt about its defect levels. As grown crystals of ZnS in general have very high resistivity. Their low dark current indicates that the Fermi-level lies well below the bottom of the conduction band.

In this part of the Chapter, some photoconductivity measurements on undoped and gallium doped ZnS crystals are reported. The main experimental difficulty was to obtain a suitable source for excitation. The intensity of the excitation in the available Quartz Halogen source near the band gap was very weak, however despite this problem some results were obtained.

The samples for photoconductivity measurements were either cut into bars ($6 \times 3 \times 1$ mm^3) or squares ($4 \times 4 \times 1$ mm^3) using a diamond saw. They were then prepared for use as described in Chapter 4. The resistivities of all undoped ZnS samples ranged from 5×10^{12} to 3×10^{13} ohm-cm, and that of gallium doped ZnS was about 7×10^{12} ohm-cm, in the dark at room temperature.

The spectral responses of some undoped samples measured at room temperature are shown in Fig 5.20. Curve (a) is for the sample No.1HT65, cut from boule No.HT65. It shows two definite thresholds near 1.14 eV and 2.40 eV. The sample No. 6HT60 from boule No.HT60 shows the spectral dependence illustrated by curve (b) and has no definite threshold, but a rise in the photocurrent near

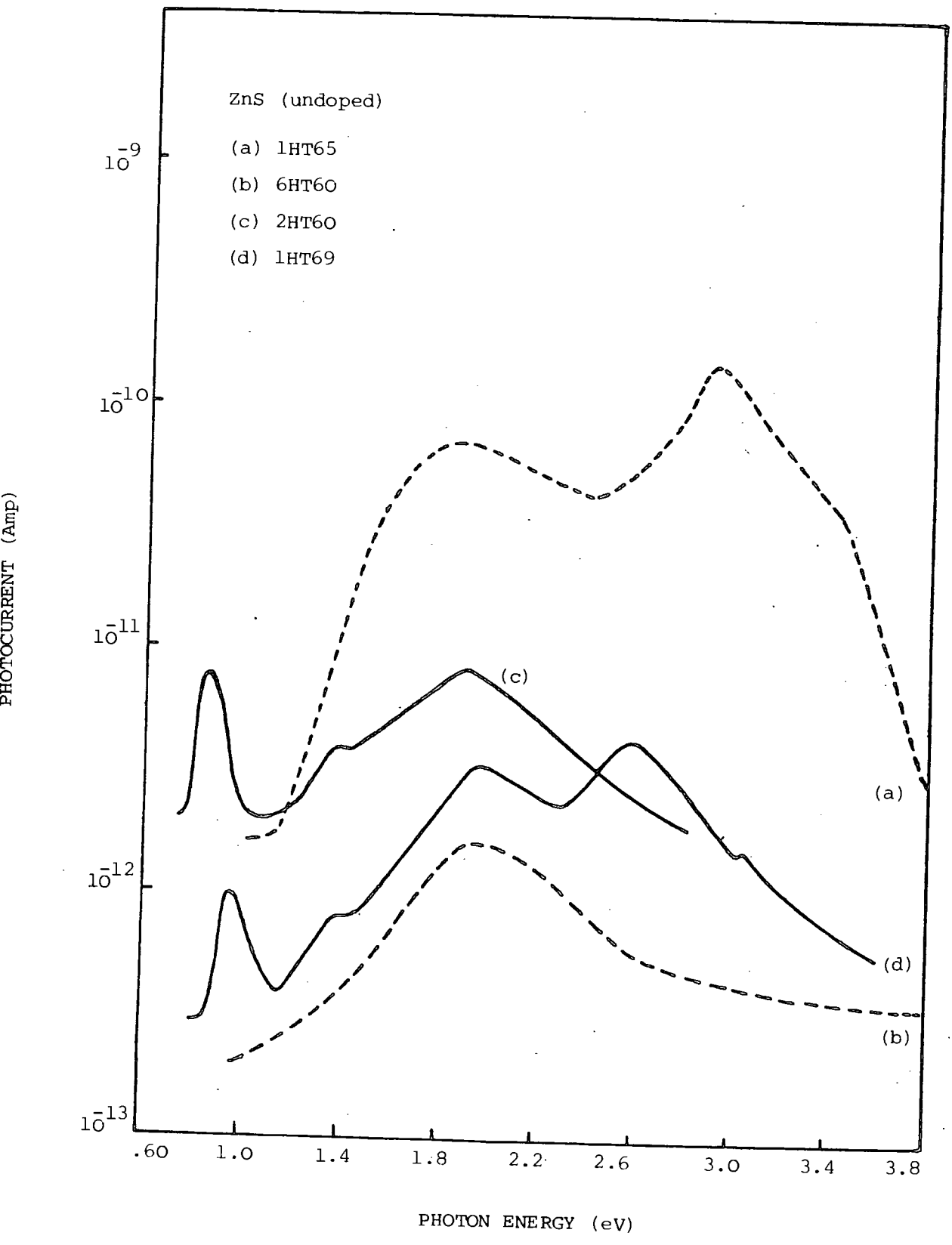

Figure 5.20: Photocurrent spectra for ZnS (undoped) samples (obtained from different crystal boules) at room temperature.

1.00 eV is obvious. The response shown in curve (c) is for sample No.2HT60, obtained from the same boule No.HT60 from which the sample 6HT60 was cut. The only deliberate difference between samples 2HT60 and 6HT60 was that different materials were used for contacts. Sample 2HT60 had indium contacts but 6HT60 and the other samples had indium-cadmium alloy contacts. Curve (c) shows two more thresholds,one at 0.76 eV and another at 1.10 eV which were absent in curve (b) for the same material with (In + Cd) alloy contacts. The thresholds observed in curve (c) may be associated with poor contacts rather than with bulk properties, because In-contacts on ZnS are not ohmic,(see Alfrey and Cooke (1957)). An unusual effect was also observed in the samples with In-contacts. Following the first run at liquid nitrogen temperature, scanning from long to short wavelengths, a second run showed a persistent increased current near 0.60 μm (2.07 eV), which was not observed in the samples with (In + Cd) alloy contacts. With the next sample No.1HT69 from boule No.HT69, the photoconductive spectrum, curve (d), shows thresholds near 0.86, 1.16, 1.46, 2.30 and 3.04 eV.

Some photoconductive spectra for sample No.6HT60 measured at liquid nitrogen temperature are shown in Fig 5.21. Four curves were obtained under rather different conditions. For example curve (a) was the first response for this sample at nitrogen temperature, and immediately after this second run led to curve (b). The sample was then heated to 400 K in the dark and cooled to liquid nitrogen temperature. When the response was measured again curve (c) was obtained. An immediate repeat produced a result similar to curve (b). After a second heating to 400 K and cooling to liquid nitrogen temperature as before, curve (d) was produced. These effects complicated the task of finding the thresholds associated with the positions of the defect levels. This behaviour which was also observed in other ZnS samples examined is obviously associated with complex trapping phenomena. In curve (b) the higher level of dark current after the removal of the first irradiation

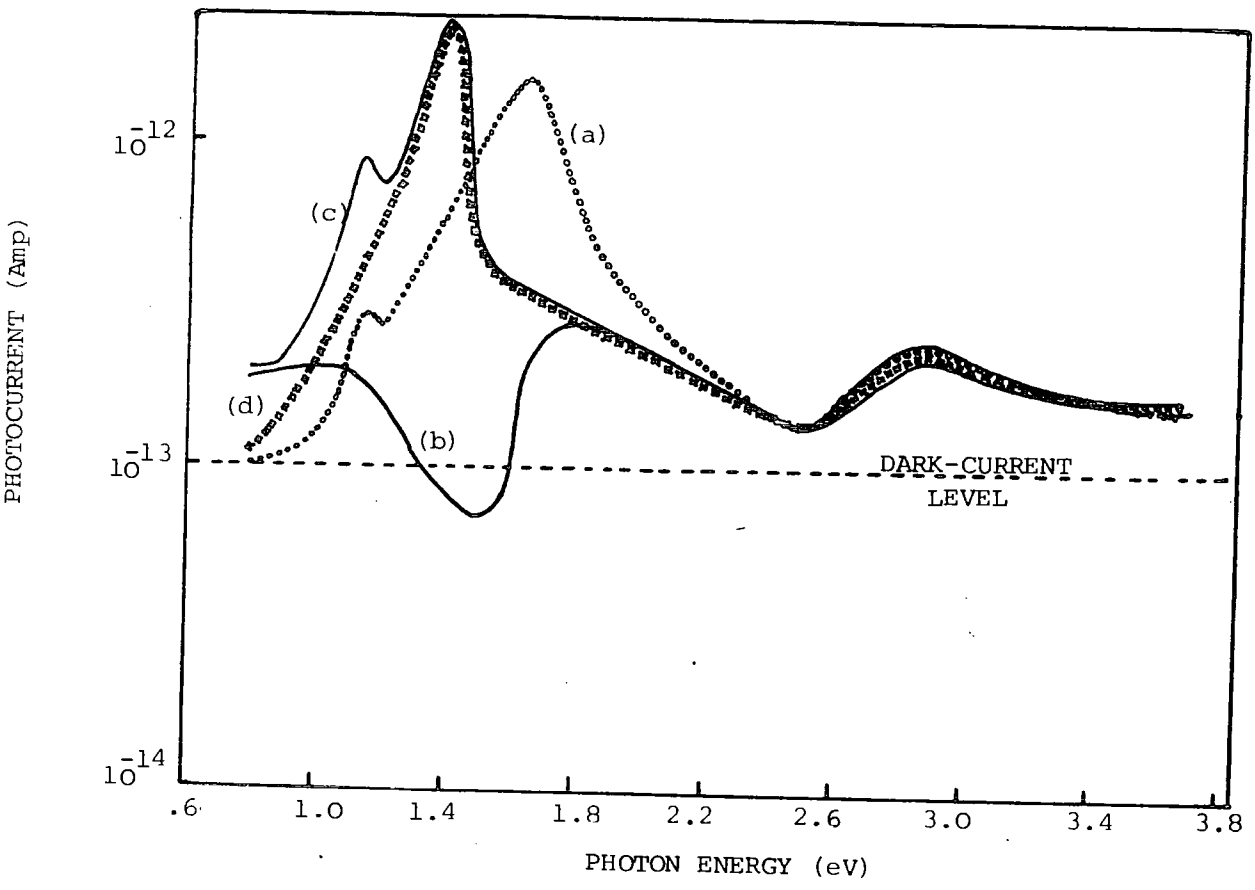

Figure 5.21 : Photocurrent spectra of ZnS (6HT60) at 84 K, (a) first scan, (b) second scan, (c) scan after heating and cooling and (d) scan after second cycle of heating and cooling.

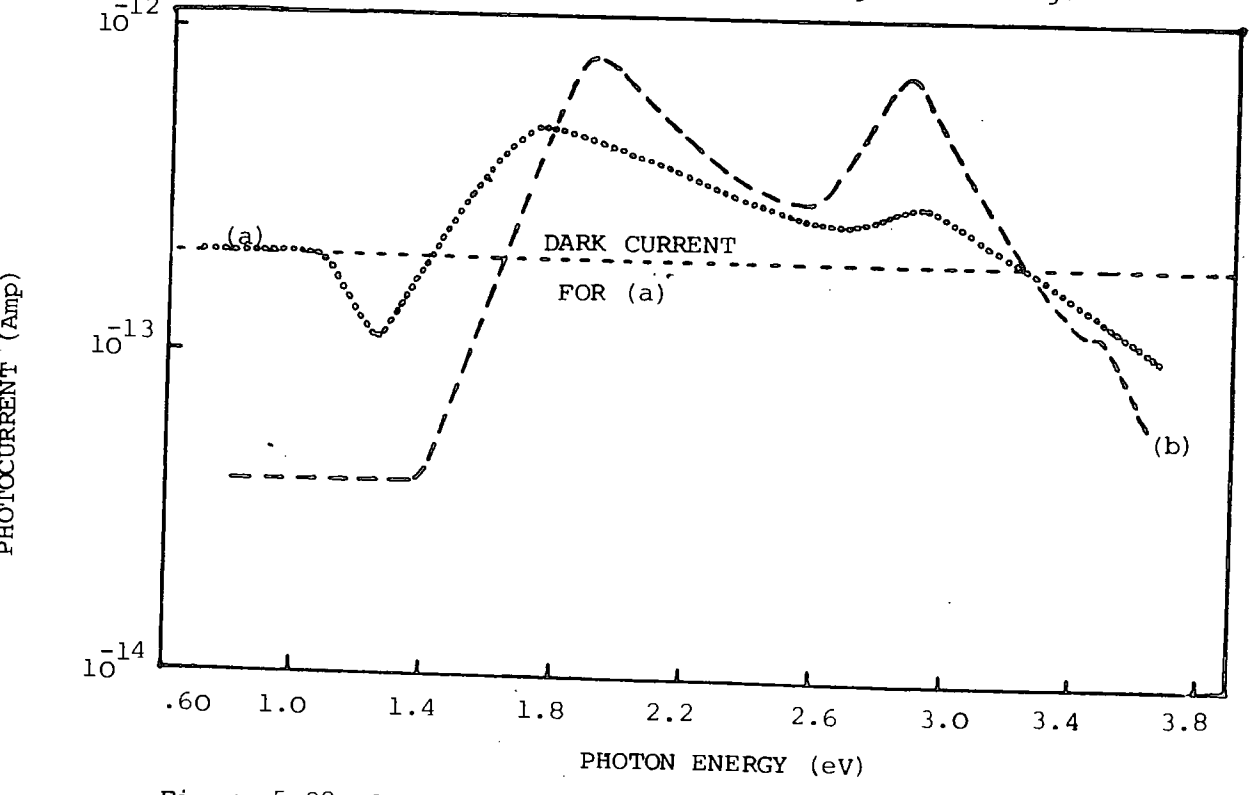

Figure 5.22 :Spectral response of photocurrent at T ≈ 85 K for (a) ZnS (2HT65) and (b) ZnS (1HT69).

shows that the photoexcited electrons have been captured by shallow traps and an exchange of electrons between the traps and the conduction band gives rise to the high dark current. When the sample is re-irradiated immediately afterwards, the electrons are freed from the traps to the conduction band giving a small increase in photocurrent. The first wavelength scan of the sample, generates some holes in the valence band during band to band excitation, which are then captured by Class II centres leading to a slow recombination rate of free electrons. When the sample is excited immediately afterwards at larger wavelengths electrons are released from the traps and holes from the Class II centres at the same time. Thus the recombination rate through Class I centres increases giving a reduction in the photocurrent as shown in the lower energy side of curve (b). The measurements show that there is a shift in peak positions from 1.64 eV to 1.40 eV after thermal cleaning of the sample. It may be that these peaks belong to different types of trapping centre. The conclusive observations are that this sample has thresholds at 0.80, 1.20 and 2.50 eV.

The responses shown in Fig 5.22 are for samples 2HT65 and 1HT69, at liquid nitrogen temperature. Sample 2HT65 showed a negative photocurrent at 1.08 eV, curve (a). This is interesting because it was not necessary to have made a previous illumination before observing this effect. After heating and cooling this sample showed the same response. The other sample 1 HT69 showed a more normal positive response, curve (b), with a first threshold at 1.38 eV, a second at 2.60 eV and a tiny peak near 3.48 eV. A repeat scan again led to quenching of the photocurrent.

The sample doped with gallium led to the curves shown in Fig 5.23. The response (a) was measured at room temperature, with small twin peaks at 0.86 and 0.95 eV, and a broad band with a threshold at 1.10 eV and maximum at 2.06 eV. The twin peaks were reduced in magnitude and finally disappeared after repeated runs, but the broad band remained. There was a negative effect at 1.0 eV at liquid nitrogen temperature and the positive increase in photo-

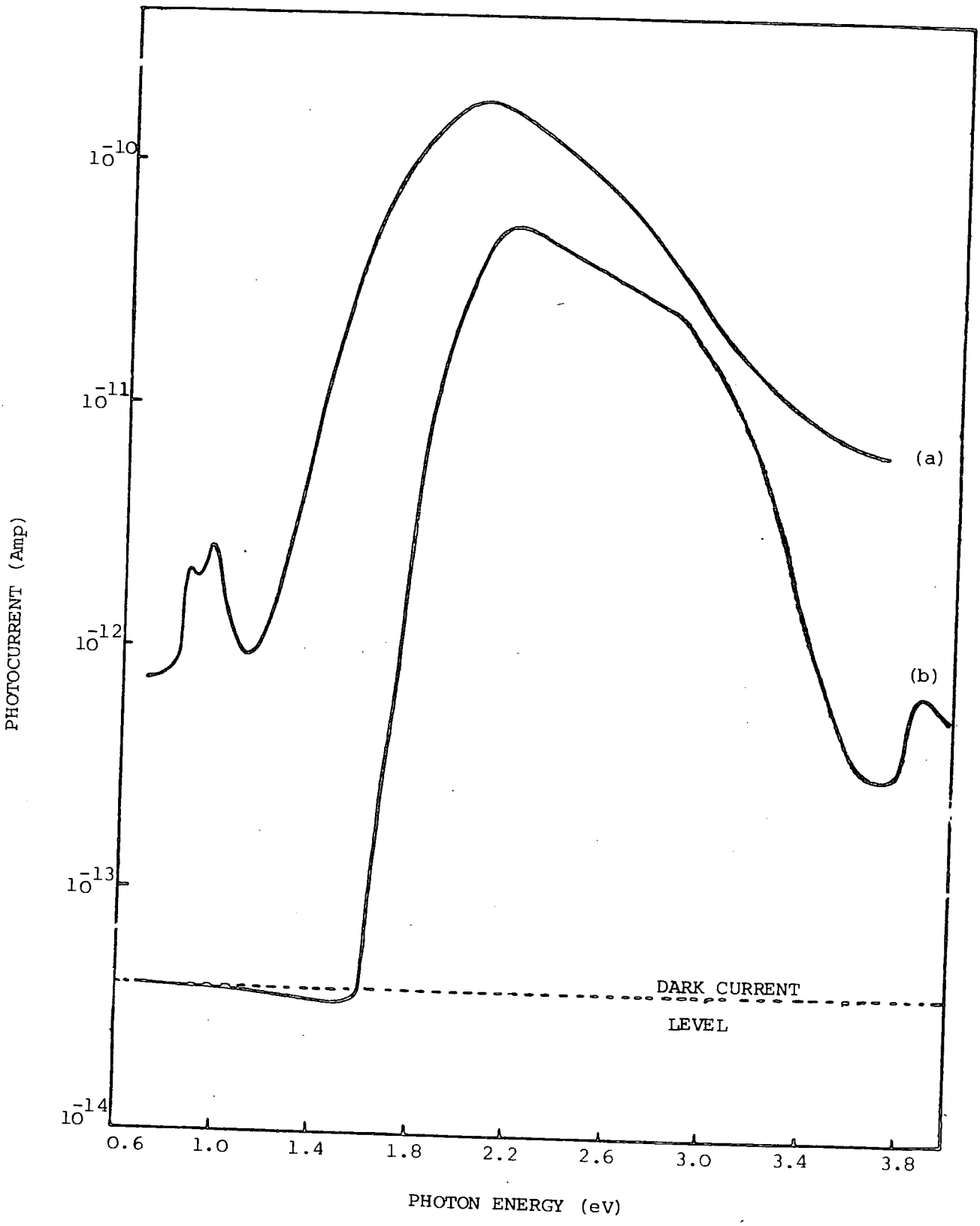

Figure 5.23 : Spectral response of photocurrent for ZnS:Ga (a) at T = 294 K and (b) at T = 85 K.

current began from 1.60 eV, curve (b). This broad band had its maximum at 2.20 eV and a slight change of slope at 2.86 eV. The band gap response near 3.86 eV was also obvious in this sample, although it was never observed in the undoped ZnS.

The results of the measurements of the photoconductivity at liquid nitrogen temperature of the ZnS crystals are summarized in Table 5.3. The values marked with an asterisk (*) are thresholds for the negative photoconductivity effects.

5.7.2 Infra-Red Quenching

For quenching measurements on the ZnS samples, the primary excitation was provided by the 0.365 μm line of a high pressure mercury lamp (UV). The photocurrent excited by this lamp was quenched with infra-red from the monochromator.

The quenching curves obtained are shown in Fig 5.24. Curve (a) is for sample 6HT60, which has only one threshold at 1.25 eV and maximum quenching of 40%, at liquid nitrogen temperature. The sample 2HT65 exhibits quenching at room temperature, curve (b), with one threshold at 0.80 eV and another at 1.20 eV. At liquid nitrogen temperature, this sample shows the quenching effects illustrated in curve (c). The negative quenching threshold is at 0.88 eV and the rising threshold (i.e. positive quenching or actual infra-red quenching) may be at 1.24 or 1.40 eV. This sample has complicated trapping effects, which are also apparent in the photocurrent spectrum, Fig 5.22 (a).

The gallium doped ZnS, sample No. 1HT83, shows simple quenching, curve (d), at nitrogen temperature, with a threshold near 0.82 eV. The maximum quenching was 20%.

The quenching thresholds determined here are listed in Table 5.4. The thresholds found for the undoped sample 2HT65 agree quite well with the results reported by Blount et al (1967) ; and Hemila and Bube (1967), who found levels at 0.80 and 1.20 eV in undoped ZnS, at room temperature.

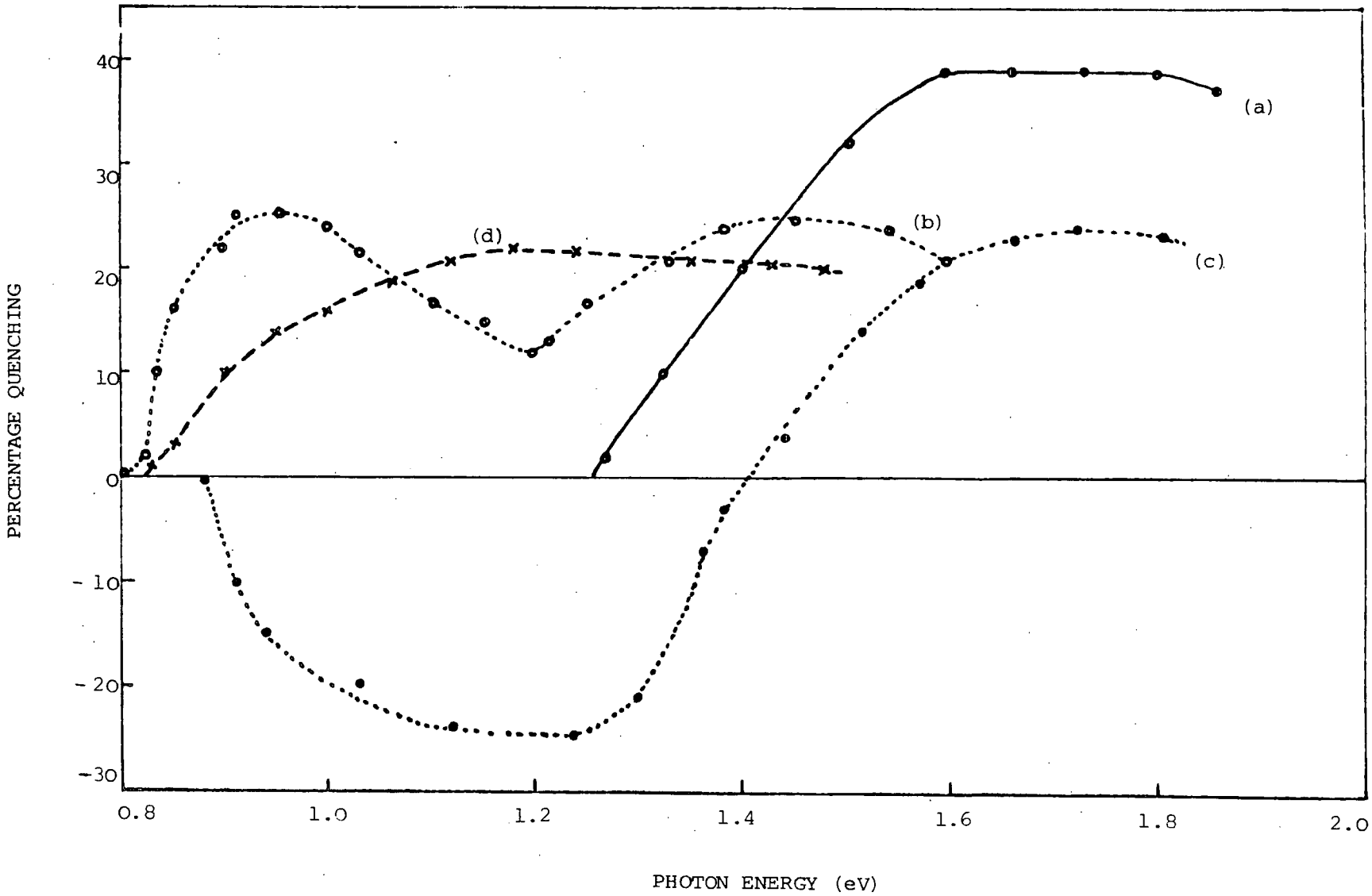

Figure 5.24 : Infra-red quenching of photocurrent for undoped and gallium doped ZnS samples : (a) ZnS (6HT60), T = 85 K, (b) ZnS (2HT65), T = 296 K, (c) ZnS (2HT65), T = 86 K and (d) ZnS: Ga (1HT83), T = 86 K.

TABLE 5.3 : Summary of photoconductivity results from ZnS crystals at L.N.Temp.

Sample	Threshold a (eV)	Threshold b (eV)	Threshold c (eV)	Peak a (eV)	Peak b (eV)	Peak c (eV)
ZnS (6HT60)	0.80 1.06*	1.20	2.50	1.14	1.65	2.88
ZnS (2HT65)	1.08*				1.74	2.90
ZnS (1HT69)		1.38	2.60		1.90	2.88 & 3.48
ZnS:Ga (1HT83)	1.00*	1.60			2.20	3.86

TABLE 5.4 : Summary of IR quenching results from ZnS crystals

Crystal	At Liq. N_2 Temp.		At Room Temperature	
	1st Threshold	2nd Threshold	1st Threshold	2nd Threshold
6HT60	1.25 eV	-	-	-
2HT65	-	1.24 or 1.40	0.80	1.20
1HT83	0.82	-	-	-

5.7.3 Discussion of the ZnS Results

The photoconductivity and IR quenching spectra for ZnS crystals, shown in Figs 5.20-5.24, are very complex. Complications are associated with the contacts as well as with the crystals themselves. The contacts are probably not the real problem, since on several samples, the contacts were repeatedly remade, and the optical measurements remained unchanged. The main factor complicating the photoconductive and quenching behaviour is attributable to excessive trapping effects.

The photoconductive and IR quenching results are summarized in Tables 5.3 and 5.4. The asterisks against some values indicate that they are not necessarily correct. The spectral responses of the photoconductivity have shown that there are many deep levels below the conduction band. Those nearest to the band lie between 0.80 $\sim$ 1.08 eV. The IR quenching measurements which were more accurate indicated levels from 1.25 $\sim$ 1.40 eV in undoped ZnS and from 0.82 eV in ZnS:Ga above the valence band.

A survey of published work indicates some reasonable agreement with our observations.

Samelson and Lempicki (1962) investigating photoluminescence reported levels at 0.17 eV for V_S (sulphur-vacancy), 0.22 eV for Cl_S (Chlorine on a sulphur site), 2.62 eV for V_{Zn}'' (doubly ionized zinc vacancy) and 3.22 eV for V_{Zn}' (singly ionized zinc vacancy), below the conduction band. According to Allen (1964), Cu_{Zn}^{x} in ZnS is 0.60 eV above the valence band and Cu_{Zn}' is slightly higher. Blount et al (1967) and Hemila and Bube (1967) placed sensitizing centres at 0.80-0.97 and 1.20 eV above the valence band in ZnS, from their studies of photoelectric and optical quenching.

Kang et al (1967) found two thresholds in ZnS:Cu,Cl at 2.50 and 3.20 eV in photoconductivity. They also observed a quenching threshold at 0.80 eV which therefore corresponds to the position of a level above the valence band. A very similar quenching threshold was found in our ZnS:Ga crystals.

The energy level of the excited state of the copper acceptor, i.e. the level of the divalent copper ion (Cu^{2+}) giving Cu^{x}_{Zn} centres was put 1.25 eV above the valence band by Suzuki and Shionoya (1971). A level at this energy was found in our undoped ZnS only.

A multilevel band diagram was proposed by Georgobiani et al (1976) for ZnS:Ga from their studies of photoconductivity, luminescence and electro-absorption. The levels reported were 0.513, 0.576, 0.975, 1.79, 1.975, 2.075, 2.515 and 3.18 eV below the conduction band. It was suggested that the levels at 0.513 and 0.575 eV were associated with Ga_{Zn} and that of 3.18 eV with the $(V_{Zn}\text{-}Ga_{Zn})'$ complex. Davies and Nicholls (1979) using the optically detected magnetic resonance (ODMR) technique found the donor, Ga_{Zn}, to lie 0.40 eV below the conduction band, while the 'A' centre or self-activated centre was placed 0.95 eV above the valence band in ZnS:Ga. Nicholls and Davies (1980) have also reported an ionization energy of between 0.40 and 0.60 eV for the indium donor, 0.95 eV for the 'A' centre and 0.70-0.90 eV for unidentified centres above the valence band in ZnS doped with indium.

In conclusion, the infra-red quenching studies on undoped and gallium doped ZnS determined a level 1.25 eV above the valence band associated with copper, and another at 0.82 eV associated with gallium SA centres.

CHAPTER 6

TRANSIENT PHOTOCURRENT AND TRANSIENT PHOTOCAPACITANCE MEASUREMENTS

6.1 INTRODUCTION

An account of the information that can be obtained from the transient photocurrent and transient photocapacitance techniques has been given in Chapter 3. In the present work these techniques have been applied to an investigation of the sensitizing centres (i.e. Class II centres) found in the indium and gallium doped ZnSe crystals. The results and their interpretation are discussed in the present chapter.

The devices used were Schottky diodes with an evaporated layer of gold as the Schottky contact and indium as the Ohmic contact. Most of the samples studied were as-grown crystals of ZnSe, containing 5 ppm and 50 ppm of indium (In) or gallium (Ga). Their resistivities ranged from 92.0 to 10^5 ohm-cm.

All measurements were made at liquid nitrogen temperature ($\approx$ 84 K). The experimental arrangements and apparatus used have already been described in Chapter 4. The intensity of the photon flux employed was in the range from 5×10^{10} to 2×10^{13} photons/cm^2-sec.

6.2 TRANSIENT PHOTOCURRENT MEASUREMENTS

6.2.1 Spectrum of the Photoionization Cross-Section of Holes, (σ_p^o)

The spectral analysis of the photoionization cross-section for the excitation of holes from the deep centres to the valence band, i.e. excitation of electrons from the valence band to the deep centres, will now be described.

Initially, the diodes were reverse biased, although in some experiments zero bias was used. In the first instance the experimental procedure for determining the spectrum of σ_p^o will be described in detail for one particular

device and thereafter only the resultant plots of σ_p^o will be given for the remainder of the devices. The curves in Fig 6.1 are for diode 405-5, fabricated from crystal boule No.405, doped with 50 ppm In. A reverse bias (-2 V) was applied to this diode and radiation with photon energy $h\nu_p$ = 2.45 eV was allowed to fall on the gold film side for four minutes and was then removed. This primary radiation excited some electrons from the deep centres to the conduction band thus emptying some of these centres. Since the temperature was low enough, thermal excitation could be neglected so that after the removal of the radiation some centres would remain empty. When monochromatic secondary illumination with photon energy $h\nu_s$ such that 0.6 eV$\leq h\nu_s \leq$ 1.0 eV was used to irradiate the diode, the centres were refilled, and the photocurrent decayed as illustrated in Fig 6.1. Similar curves were also obtained with the other devices. During the incident primary irradiation, the photocurrent rose at first and then decreased to a slightly small value. Then during irradiation with the secondary illumination $h\nu_s$, as shown in Fig 6.1, the photocurrent rose rapidly before decaying in a matter of seconds. The transient curves as shown in the diagram could only be obtained, if the centres were first emptied using the primary radiation $h\nu_p$. Incidentally, once the centres were emptied, they remained empty and gave similar transient curves up to 20 minutes after the removal of the primary radiation. When the transient photocurrents were plotted on a semilogarithmic scale, straight lines were obtained as shown in Fig 6.2, which are for diode 405-5. From equation (3.20) the slopes of these lines provide a measure of the inverse of the time constants (τ^{-1}), i.e. the optical emission rates ($e_p^o = \sigma_p^o \phi$). Knowing the photon flux ϕ (i.e. No.of incident photons/cm^2-sec) measured with the help of a PIN diode and a thermopile, the photoionization cross-section for holes, σ_p^o, could be determined. The resultant spectrum is shown (by the points)in Fig 6.3. The lowest measured value of the cross-section for this ZnSe sample doped with 50 ppm In was 5.0 x 10^{-16} cm^2 and the maximum value was 5.2 x 10^{-15} cm^2. This

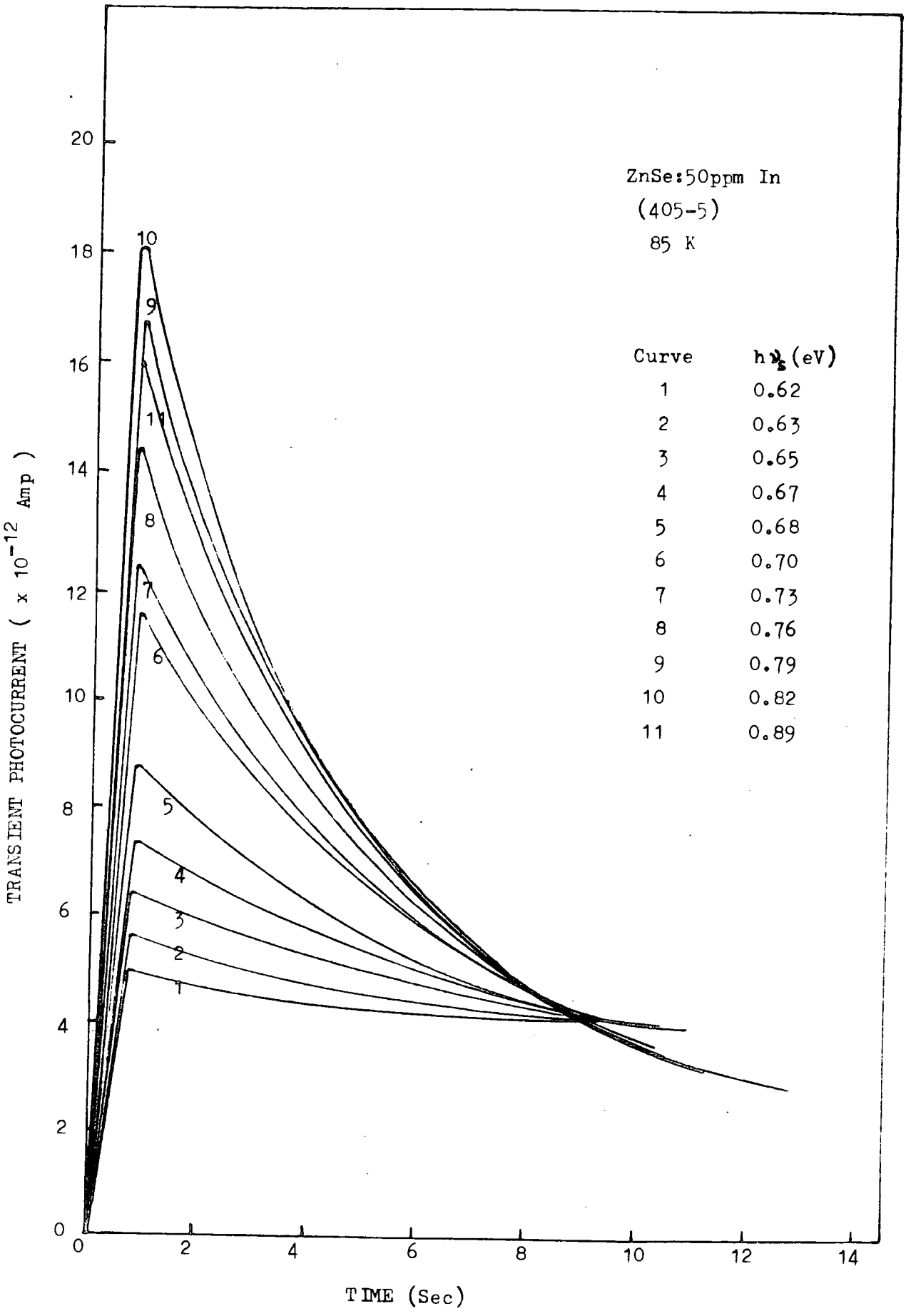

Fig 6.1 : Decay of photocurrent in ZnSe:50ppm In at 85 K due to refilling of deep centres during irradiation with $h\nu_\varepsilon$.

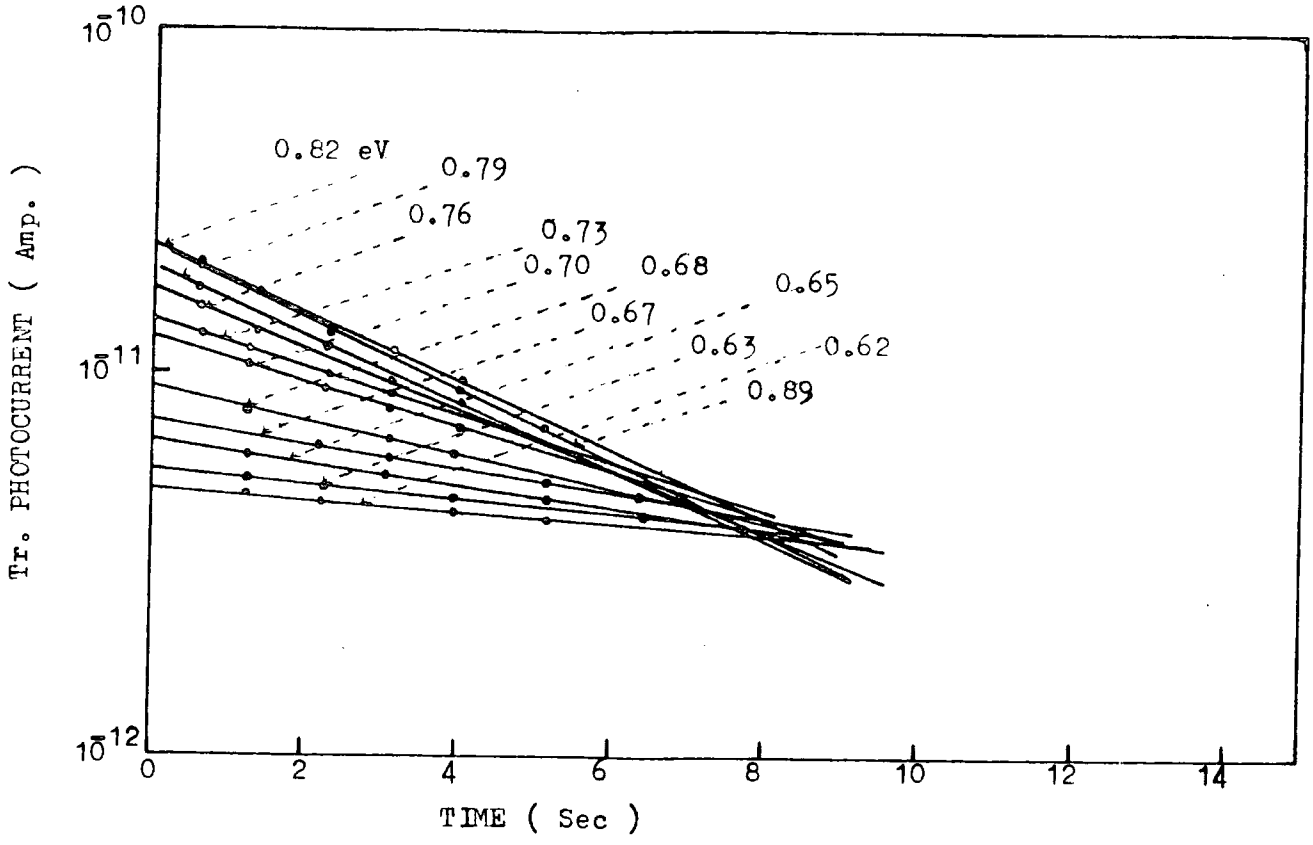

Fig 6.2 : Semi-logarithmic plot of the decay of photocurrent shown in fig 6.1.

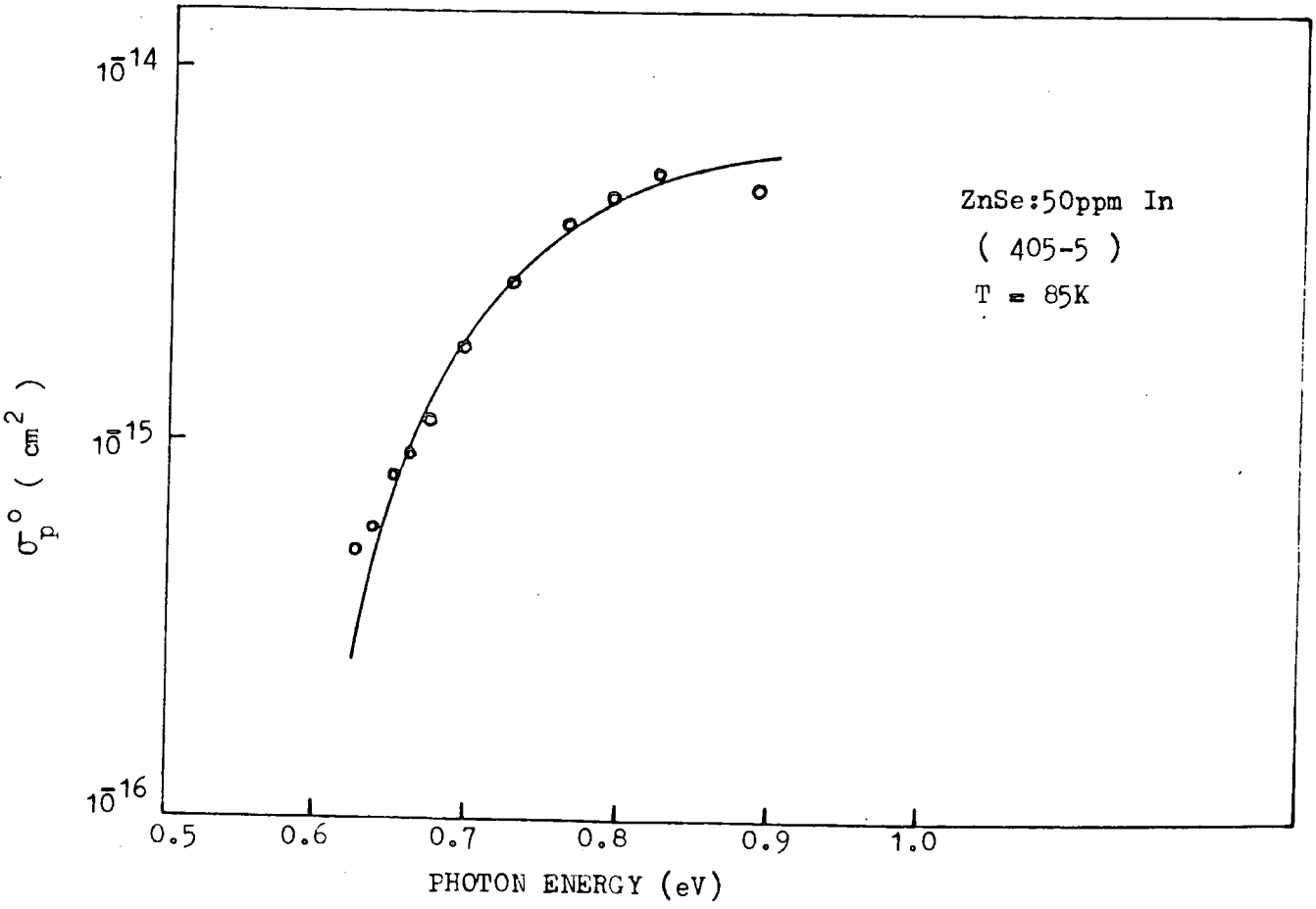

Fig 6.3 : Spectrum of the photoionization cross-section of holes for ZnSe:50ppm In (o). Solid line is the Lucovsky plot.

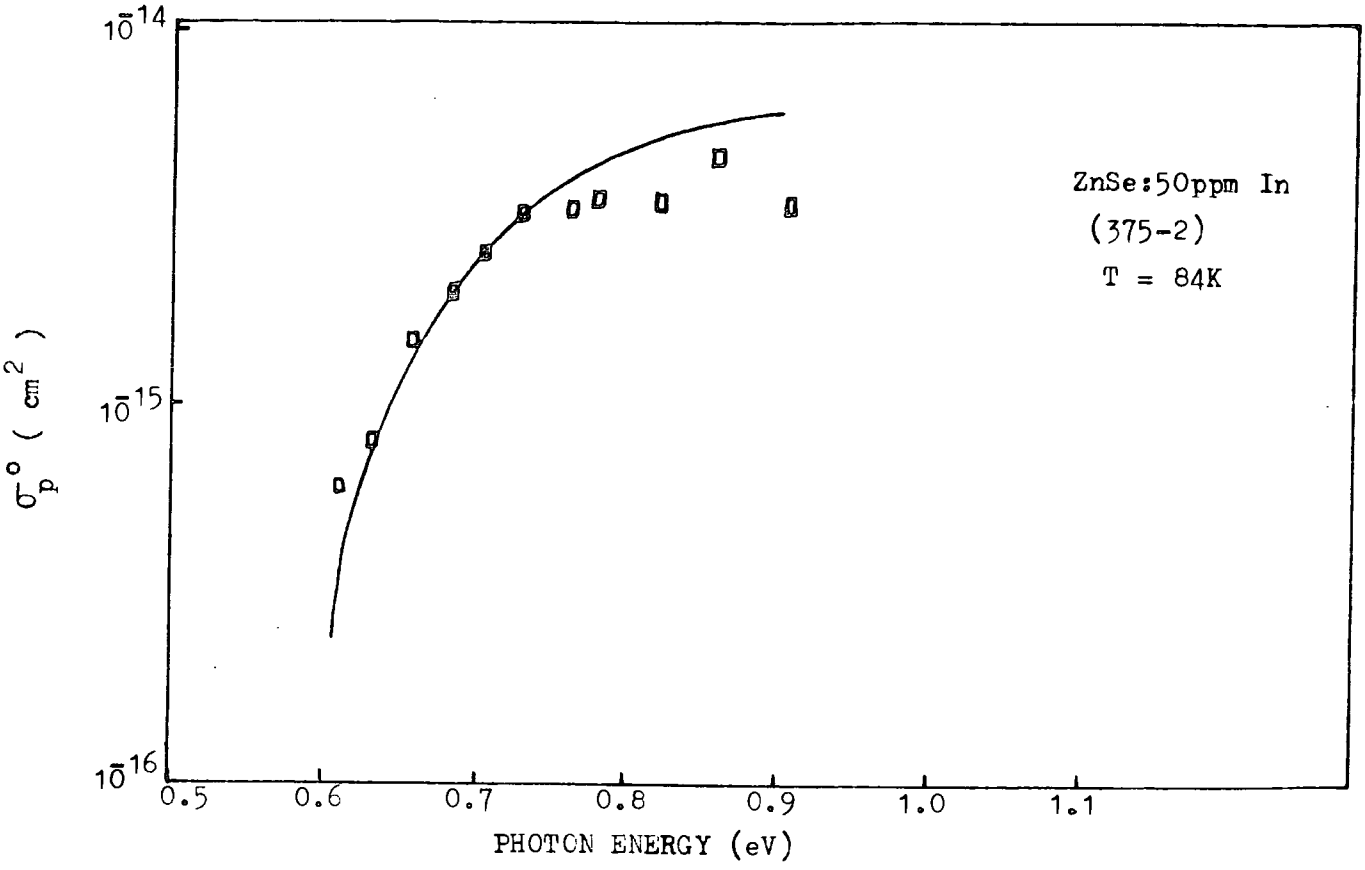

Fig 6.4 : Spectrum of the photoionization cross-section of holes for a diode from a different ZnSe:50ppm In boule

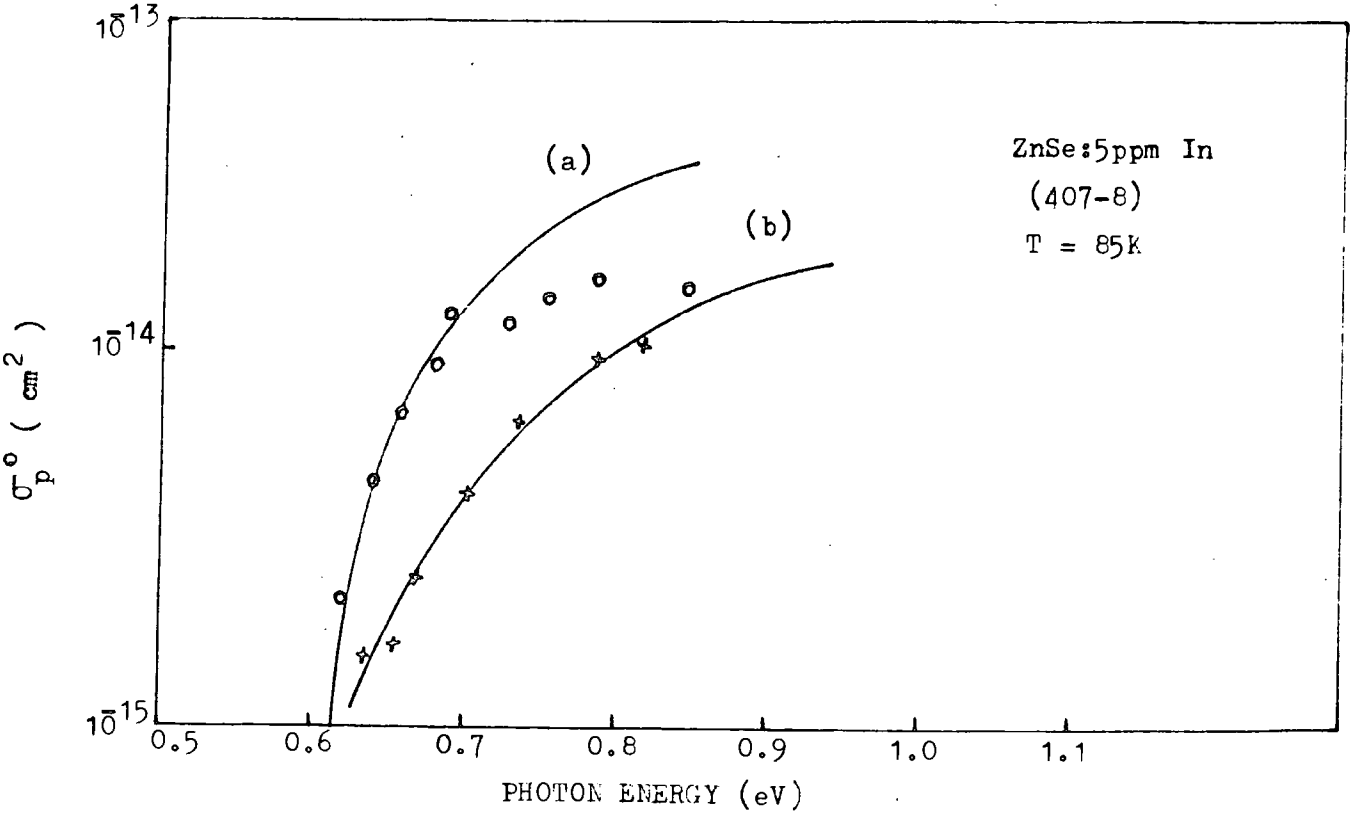

Fig 6.5 : Spectra of the photoionization cross-section of holes for ZnSe:5ppm In (a) using transient photocurrent technique and (b) using transient photocapacitance method (ref 6.3.4) Solid lines are Lucovsky plots.

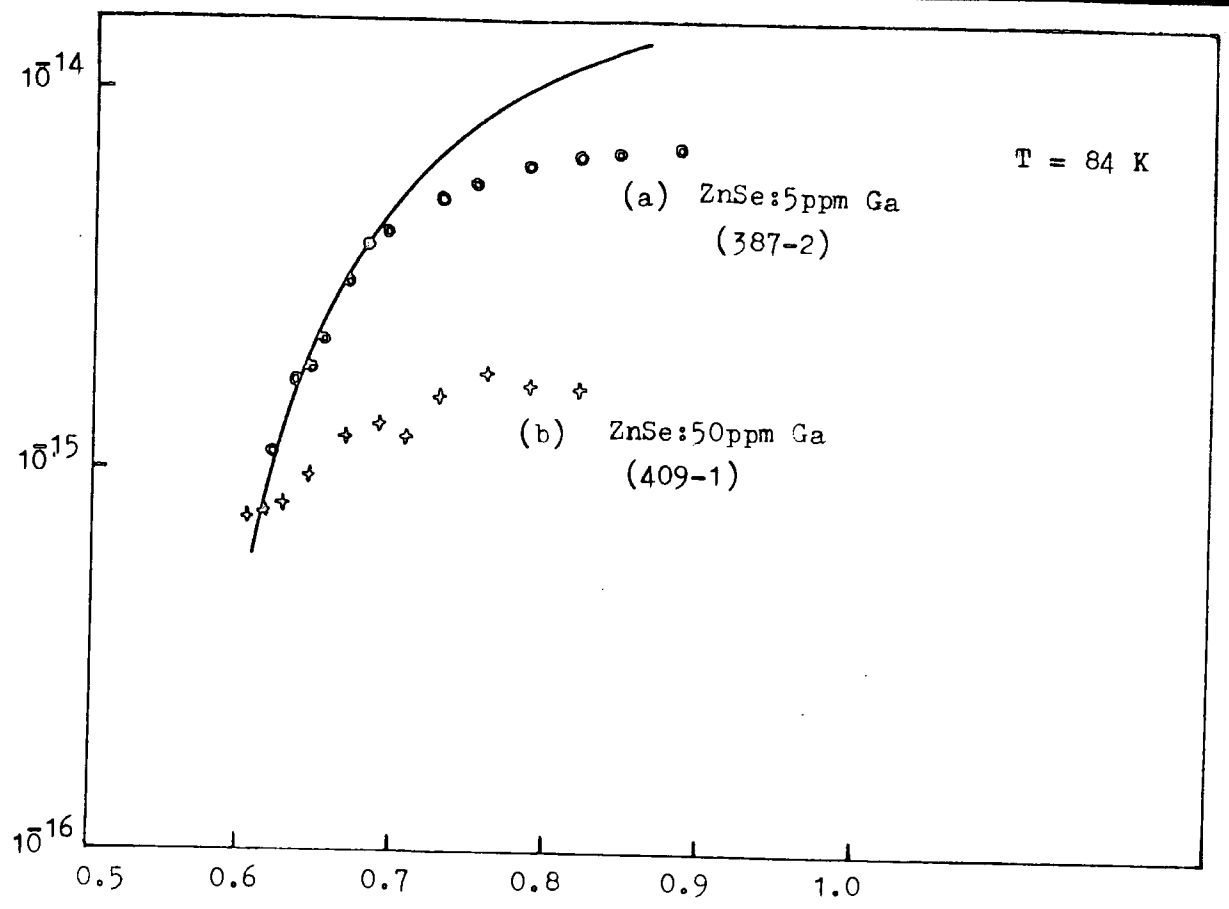

Fig 6.6 : Spectra of the photoionization cross-section of holes for (a) ZnSe:5ppm Ga and (b) ZnSe:50ppm Ga. Solid line is Lucovsky plot.

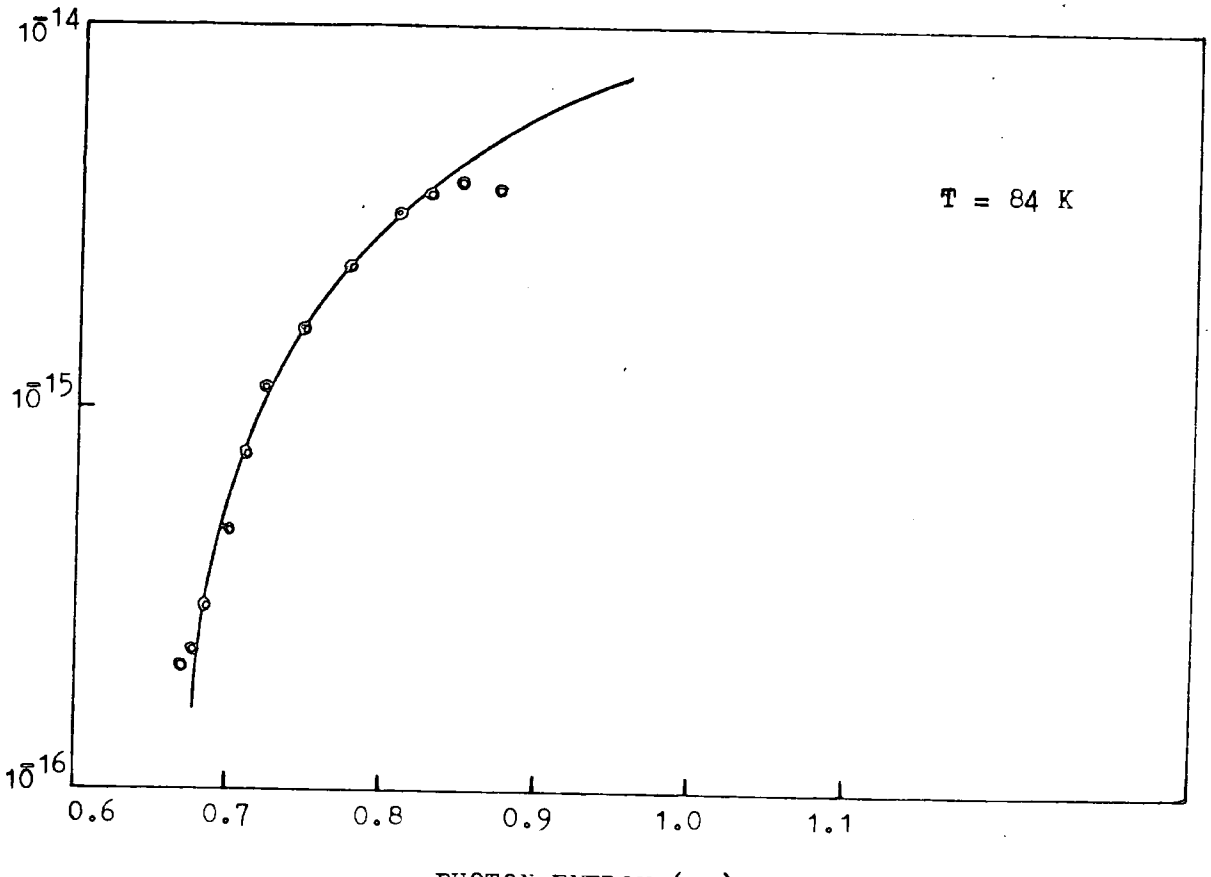

Fig 6.7 : Spectrum of the photoionization cross-section of holes for ZnSe:Cu. Solid line is Lucovsky plot.

spectrum reveals the dominance of one deep level, the position of which (about 0.61 eV above the valence band) can be determined using Lucovsky's model. This will be discussed in section (6.4).

Another diode No.375-2, from crystal boule No.375, doped again with 50 ppm indium, showed the spectrum illustrated in Fig 6.4. Zero bias and primary radiation with $h\nu_p$ = 2.45 eV were used with this diode. The values of lowest and highest photoionization cross-sections were nearly the same as with diode No.405-5. Diode 407-8 was fabricated from crystal boule No.407, doped with 5 ppm indium and this gave the spectrum illustrated in Fig 6.5(a). The bias voltage and $h\nu_p$ were the same as for diode 405-5. The values of σ_p^o were slightly higher for the lightly doped (5 ppm) samples than for the 50 ppm indium doped samples. The lowest and highest values of σ_p^o for sample No.407-8 were 2.1×10^{-15} and 1.5×10^{-14} cm^2 respectively. The threshold energy for filling the level was about 0.61 eV in all these samples (see later).

Two dice from boule No.405 were heat treated in molten zinc at 850°C for one day. They became black in colour and no successful transient photocurrent measurements could be made with them.

The results of the measurements on the gallium doped samples are shown in Fig 6.6. The diode 387-2 was doped with 5 ppm gallium and gave the spectrum shown in Fig 6.6(a) with a range of cross-sections from 1.1×10^{-15} to 7.0×10^{-14} cm^2. The sample with a concentration of 50 ppm gallium, diode No.409-1, led to the spectrum (b) in Fig 6.6. The bias voltage for these diodes was -2V and the value of $h\nu_p$ of the primary radiation used was 2.51 eV. The ionization thresholds were near 0.61 eV in both of these samples.

A measurement was also done on a copper doped ZnSe crystal. The diode No.327-1 was obtained from an undoped ZnSe, boule No.327, and then heated in molten zinc + 1% copper at 850°C for 6 days. The spectrum of photoionization cross-section is shown in Fig 6.7 which gave minimum and maximum values for σ_p^o of 2×10^{-16} cm^2 and 4×10^{-15} cm^2. The ionization threshold ($\sim$ 0.67 eV)

was distinctly higher than the thresholds observed in the indium and gallium doped samples.

6.2.2 Integrated Charge Associated with Refilling of Deep Centres

When the deep centres are filled by irradiation with the secondary illumination $h\nu_s$ ($h\nu_s < \frac{1}{2}Eg$), the charge Q associated with the refilling of the centres can be determined from transient photocurrent plots similar to those in Fig 6.1. Some results are shown in Fig 6.8 for ZnSe containing 5 ppm and 50 ppm In, and in Fig 6.9 (a) for ZnSe containing 5 ppm Ga. These plots show a steady rise from the low energy side, followed by a nearly constant region between 0.75 and 1.20 eV. It was argued by Grimmeiss et al (1976) that such measurements could be used to reveal whether more than one deep level was active. In their experiments on manganese doped ZnSe crystals, there was a second rise for $h\nu_s > 1.0$ eV in the plot of integrated charge versus $h\nu_s$, and they suggested that this was attributable to the involvement of another deep level. Such a rise was not observed in our experiments.

The integrated charge Q can also be used to determine the number of deep centres emptied by the primary radiation in the region $(W-W_o)$. The result for the sample with 5 ppm Ga gives a maximum value of about 10^8, see Fig 6.9(b).

The magnitude of Q depends on the magnitude of the reverse bias. In Figs 6.10 and 6.11, some plots of Q against reverse bias are shown for indium and gallium doped ZnSe crystals. The increase in Q with increasing reverse bias is due to the fact that the reverse bias increases the width of the depletion region (W), and therefore allows more deep centres to take part in the optical processes. The straight lines signify that the deep centres are homogeneously distributed in the bulk of the crystals. The dependence of Q on the time taken to empty the deep centres with the primary radiation $h\nu_p$ is shown in Fig 6.12. The steady state was reached in about four minutes with device 407-9. As discussed earlier the primary radiation $h\nu_p$ empties

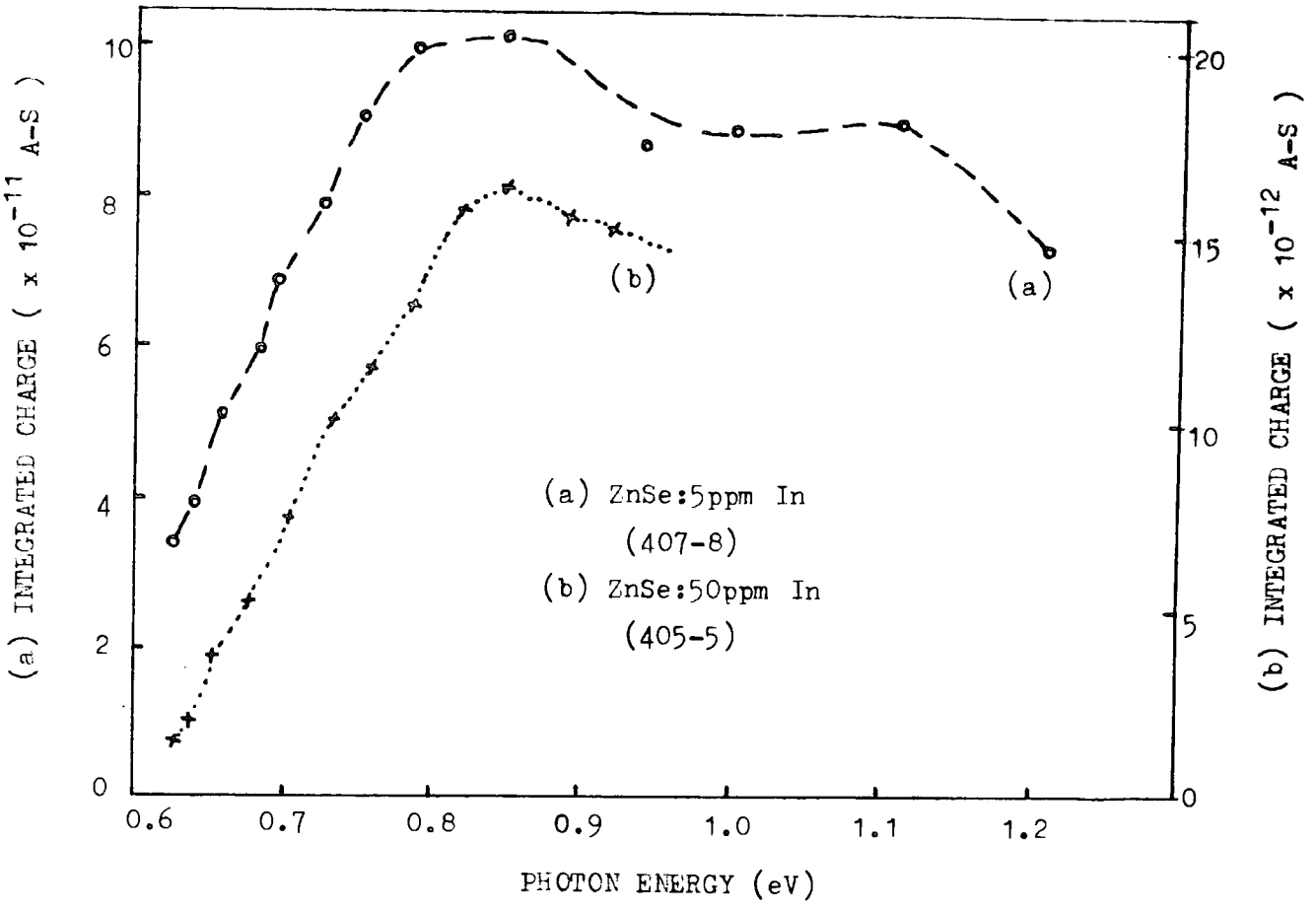

Fig 6.8 : Spectra of the integrated charge (Q) associated with refilling of deep centres for (a) ZnSe:5ppm In and (b) ZnSe:50ppm In.

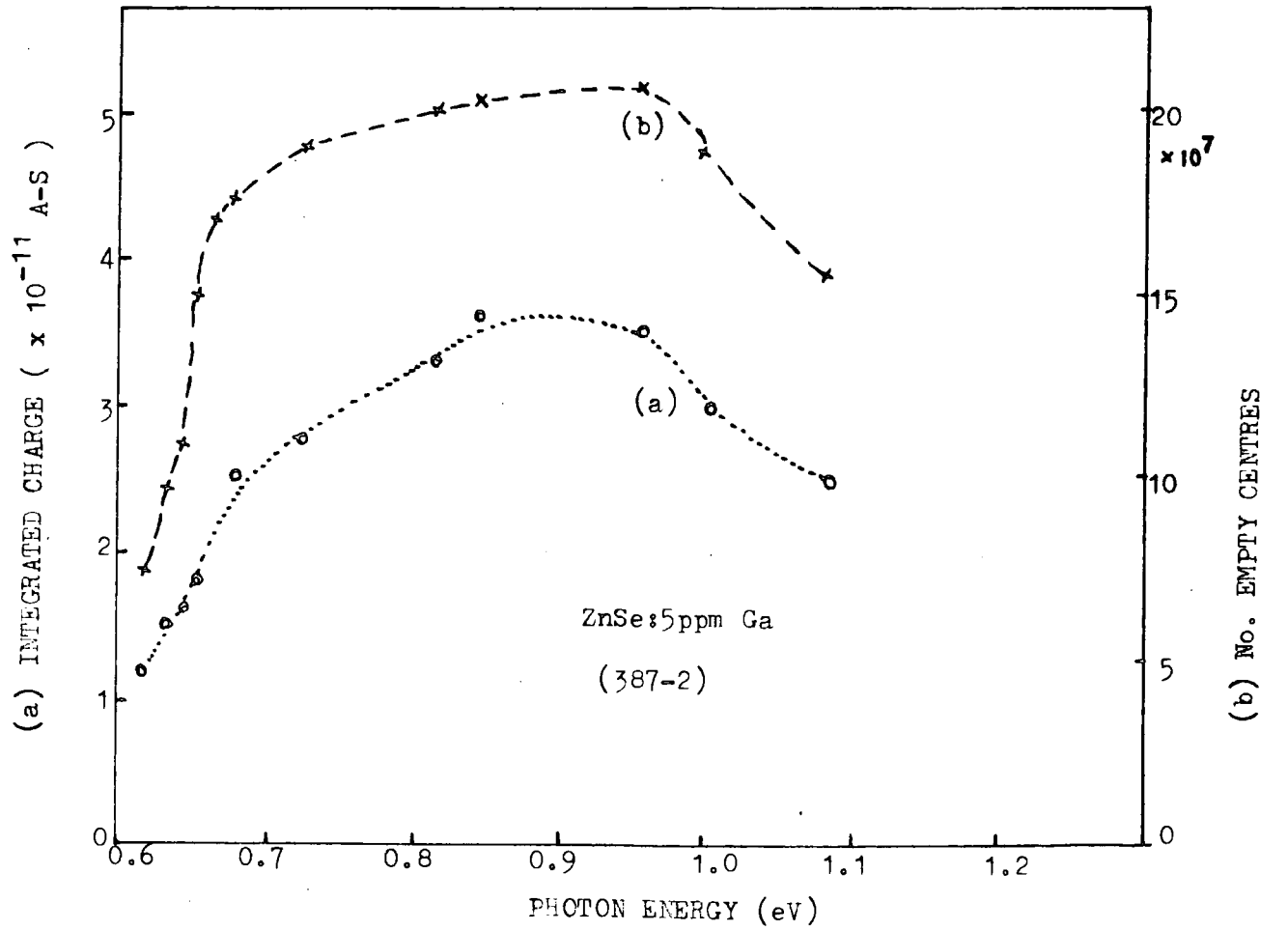

Fig 6.9 : Spectra of the integrated charge (a) and number of empty centres (b) for ZnSe:5ppm Ga.

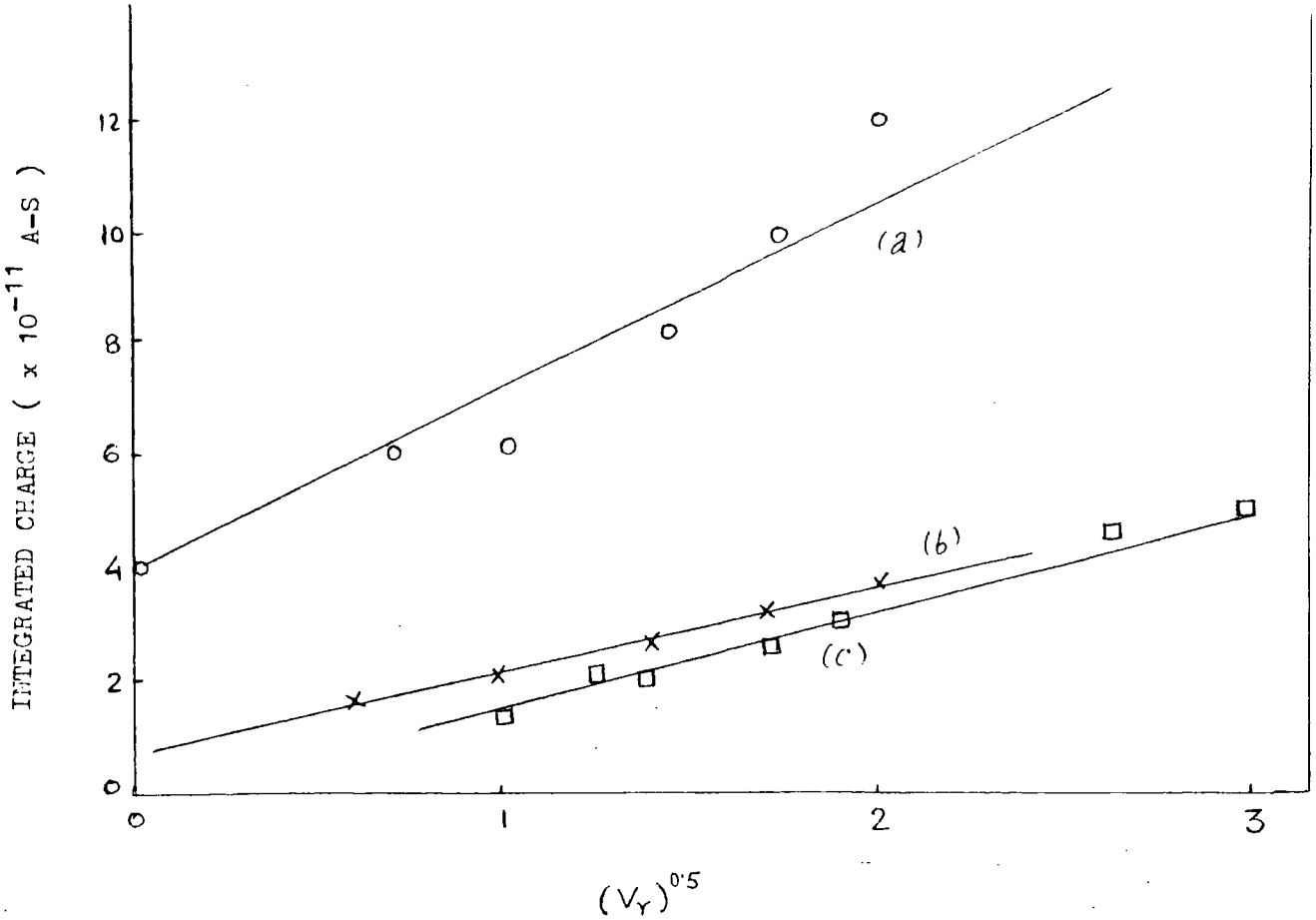

Fig 6.10 : Integrated charge against bias for (a) ZnSe:5ppm In , 407-8 , (b) ZnSe:5ppm In , 407-9 and (c) ZnSe:50ppm In , 405-5.

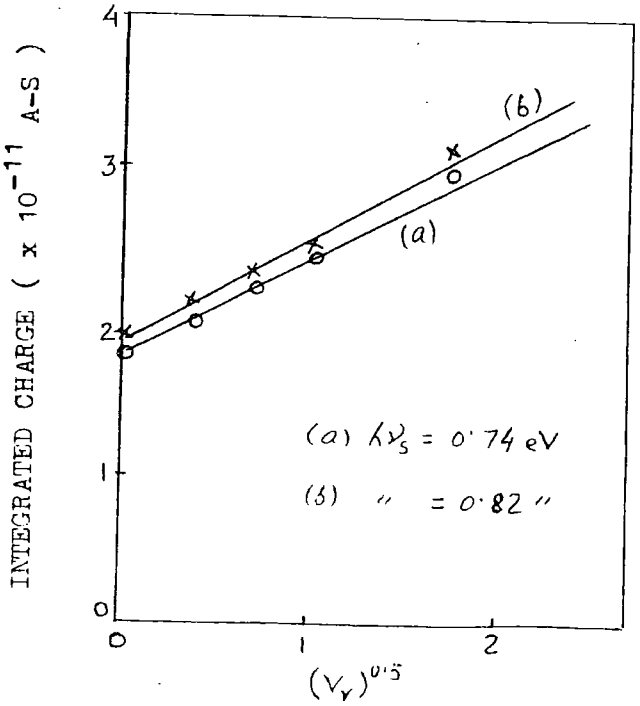

Fig 6.11 : Integrated charge against reverse bias for ZnSe:5ppm Ga at different secondary illuminations ($h\nu_s$).

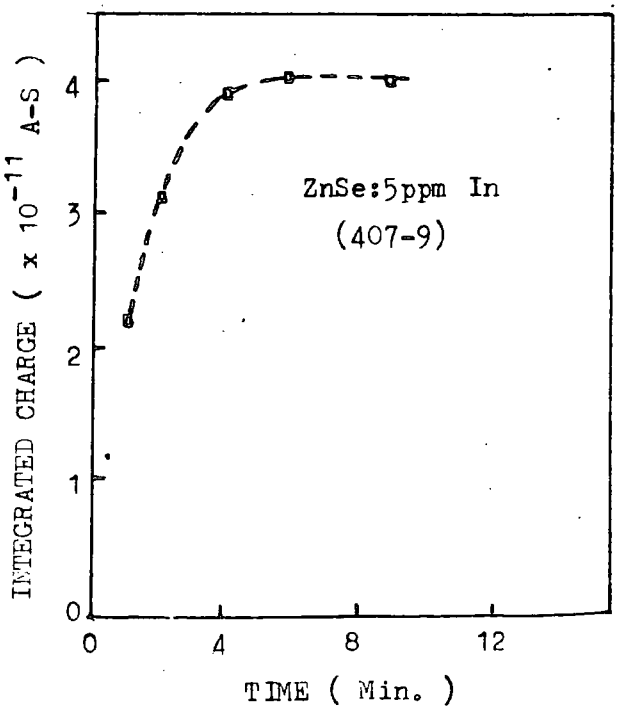

Fig 6.12 : Integrated charge vs. duration of primary excitation ($h\nu_p$ = 2.45 eV) for ZnSe:5ppm In. $h\nu_s$ = 0.67 eV.

the deep centres and the secondary radiation refills them. With primary irradiation of shorter duration a lower density of centres will be available to be filled by $h\nu_s$, and it is clearly important to allow sufficient time for the steady state to be reached.

The plots of integrated charge Q against bias in conjunction with a knowledge of the values of depletion width (derived from C-V measurements, see Chapter 8) have been used to find the concentration per unit volume of deep centres. This is described in the following section.

6.2.3 Concentrations of Deep Centres

As indicated in the preceding section, transient photocurrent measurements can be used to determine the concentrations of the empty centres $p_T(o)$ and concentrations of deep centres N_T, in the different indium and gallium doped ZnSe crystals.

In separate measurements as described in Chapter 8, the values of the depletion width (W) as a function of reverse bias were determined in the dark, at liquid nitrogen temperature.

When Q (section 6.2.2) and W are known for different biases, then the corresponding values of Q and W may be selected at the same bias. These values of Q and W have been plotted on a linear scale, according to eqn.(3.22), as shown in Figs 6.13-6.17. All plots were straight lines, implying that the deep centres were homogeneously distributed throughout the bulk of the crystals.

The depletion width W of a Schottky barrier region consists of the transition region (W_o), which is closer to the neutral region of the bulk of the crystal, and the space charge region ($W-W_o$), which is closer to the gold contact. Only those deep centres which are present in the space charge region respond to the optical emptying and filling processes of the transient photocurrent measurements. The region W_o is inoperative because its centres fill by accepting electrons from the bulk of the crystal, see Braun and Grimmeiss (1973). The plots of Q versus W can be used to find W_o, which according to

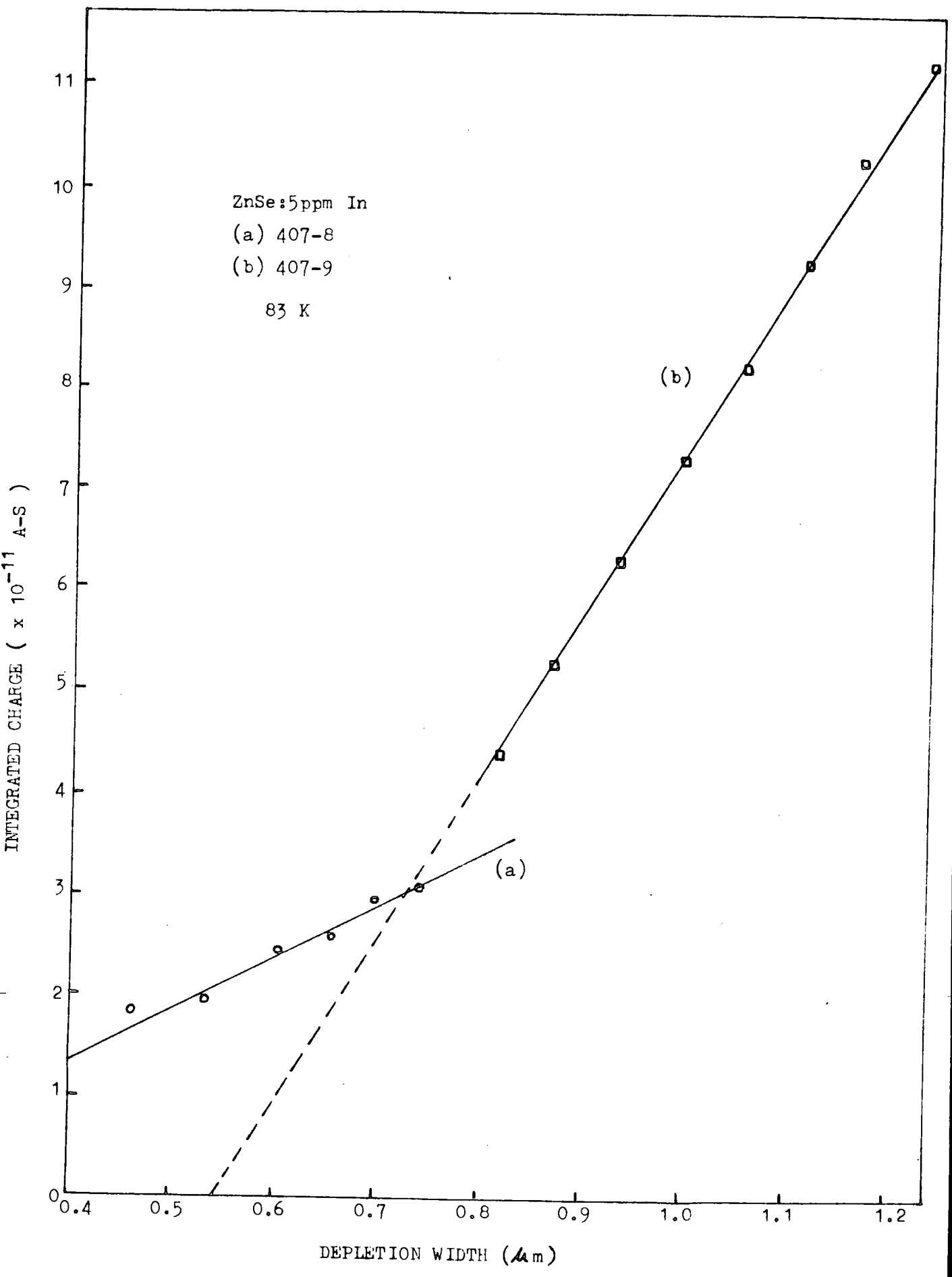

Fig 6.13 : Integrated charge as a function of depletion width for two ZnSe:5ppm In diodes from boule (407).

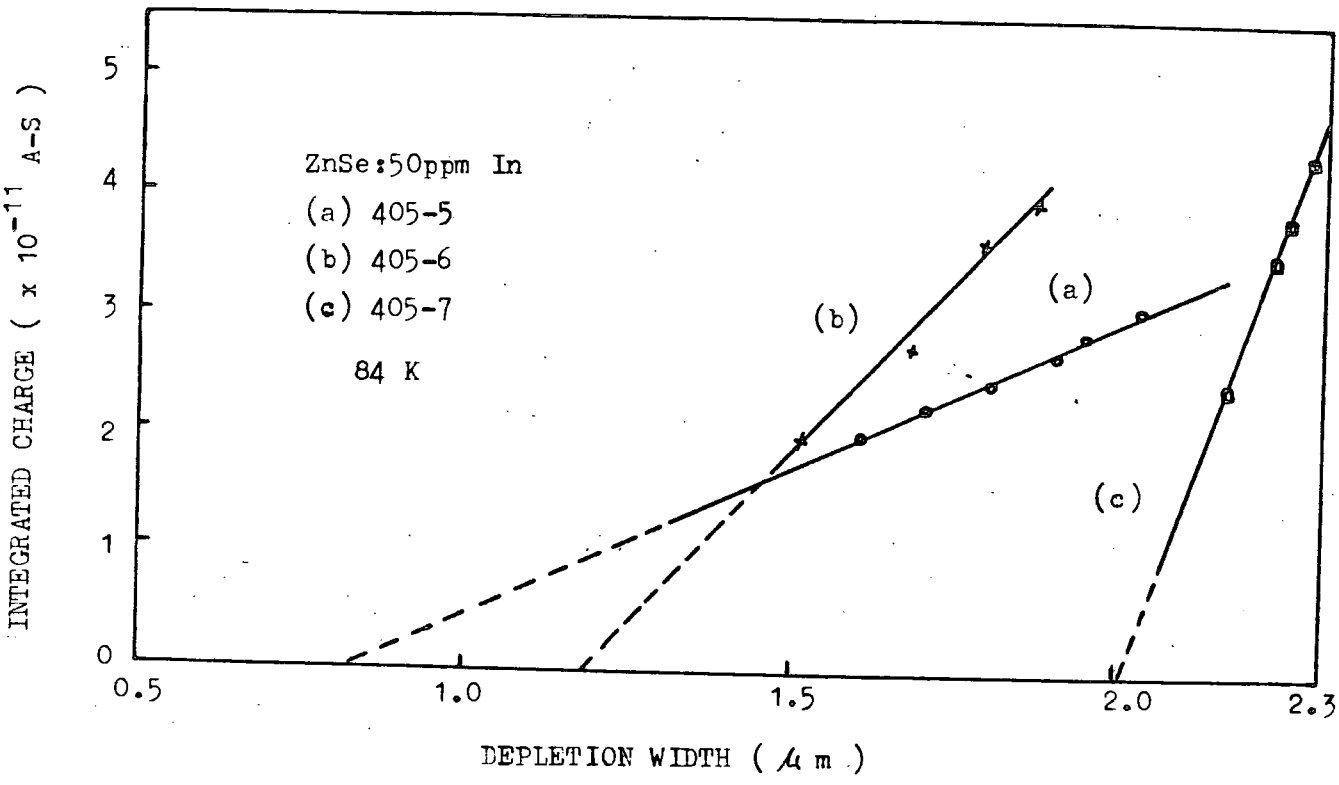

Fig 6.14 : Integrated charge as a function of depletion width for three ZnSe:50ppm In diodes.

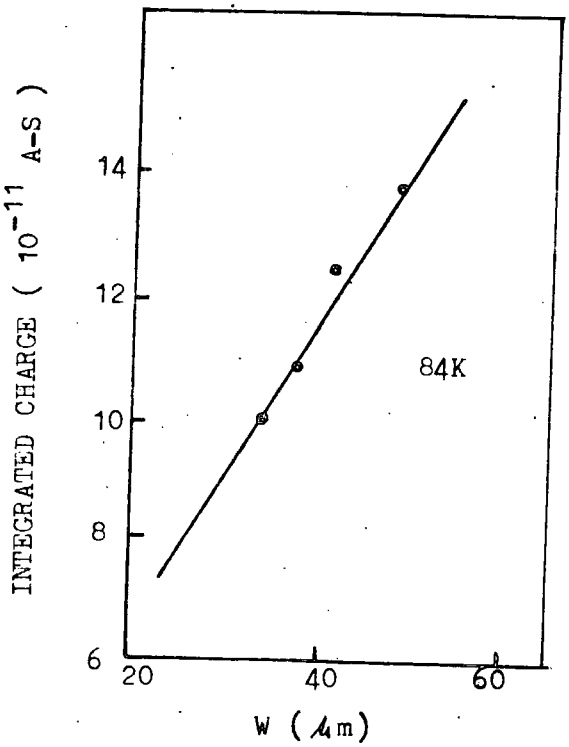

Fig 6.15: Integrated charge as a function of depletion width for ZnSe: 50ppm In , 375-2.

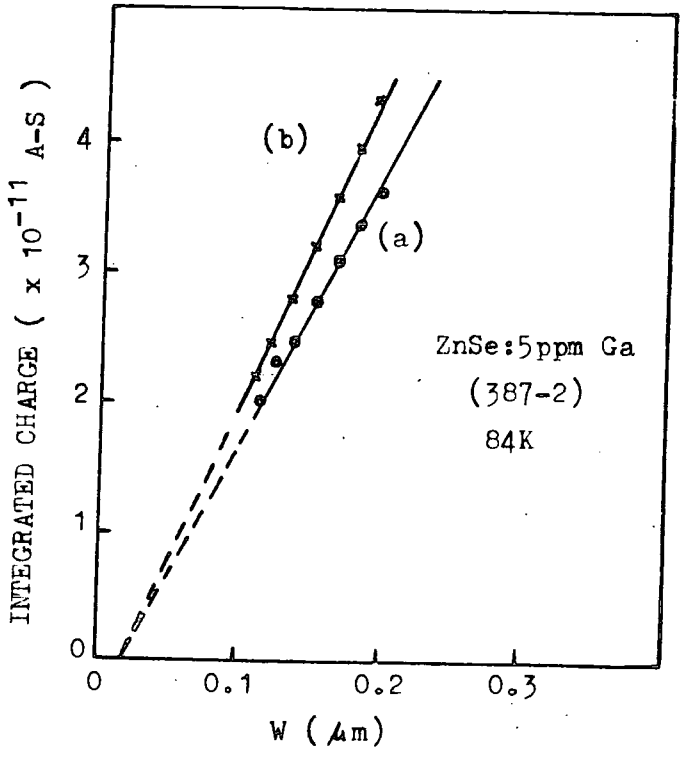

Fig 6.16: Integrated charge as a function of depletion width for ZnSe:5ppm Ga when (a) $h\nu_s$ = .74 eV and (b) $h\nu_s$ = .82 eV.

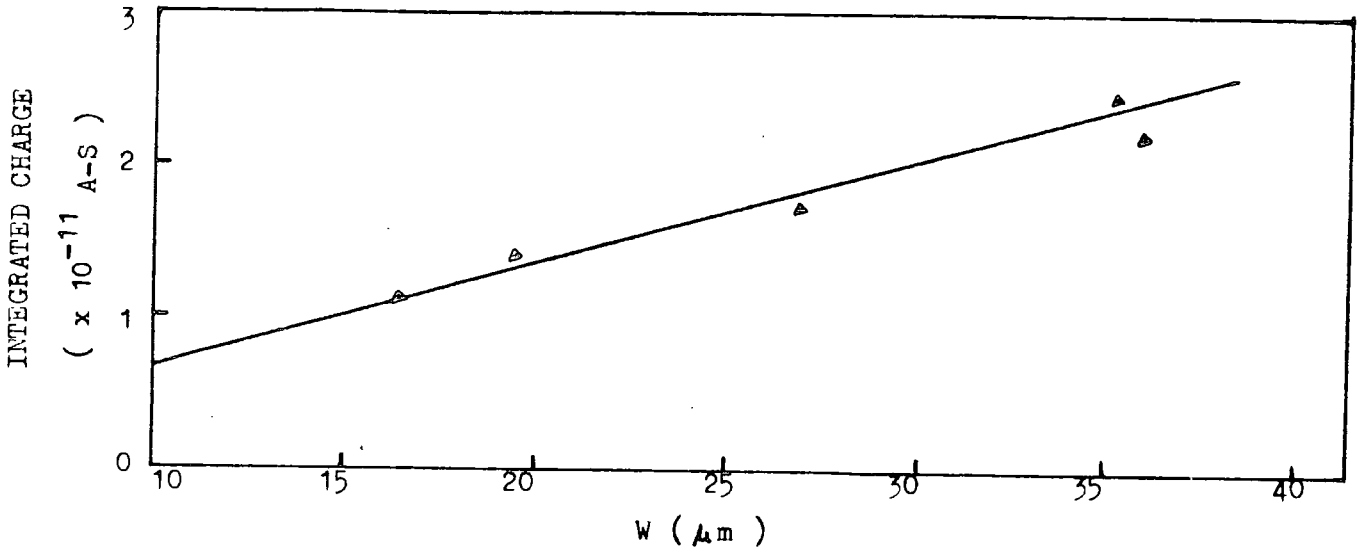

Fig 6.17 : Integrated charge as a function of depletion width for ZnSe:50ppm Ga.

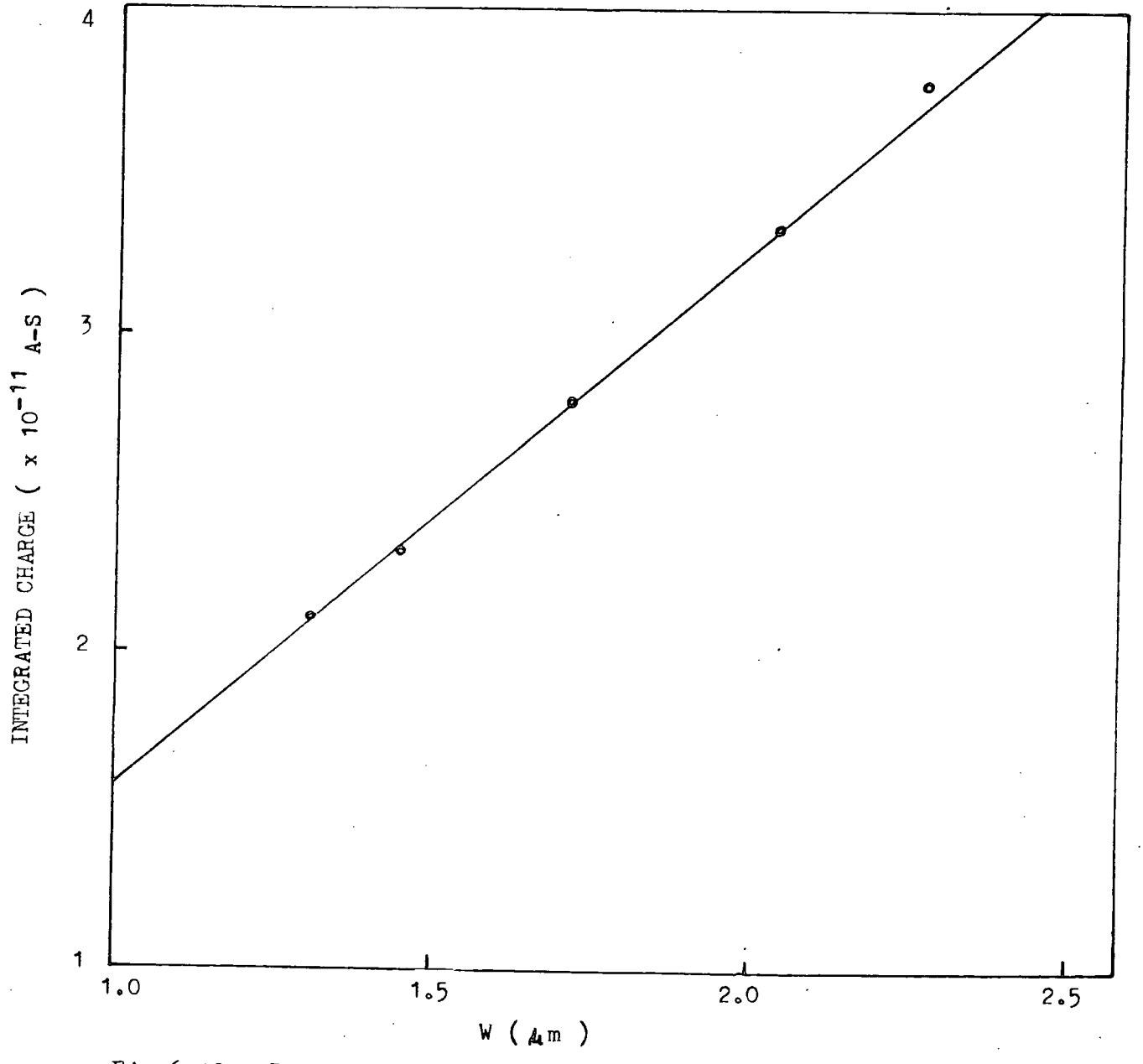

Fig 6.18 : Integrated charge as a function of depletion width for ZnSe:Cu.

eqn. (3.22) is given by the intercept of the straight line on the W-axis. The values of W_o determined in this way are shown in Figs 6.13 - 6.17. They ranged from 0.02 to 5.00 μm for different samples. The high values in some diodes are associated with the high resistivities of those samples. The plots in Fig 6.16 are interesting. Here the centres were refilled using secondary radiation with two different photon energies, but nevertheless the straight lines led to the same value for W_o of 0.02 μm. Thus W_o is a constant factor for a particular device, independent of the change of illumination.

Knowing the values of W_o and using the slopes of the straight lines in eqn. (3.22), it was possible to calculate the concentrations of empty centres $p_T(0)$ following the primary irradiation. Only one sample, doped with 5 ppm In, appeared to satisfy the condition, $e_n^o \approx e_p^o$ at $h\nu \approx 2.40$ eV (see curves a and b in Fig 6.27) where it is possible, as discussed in § 3.4.4, to write $N_T = 2\, p_T(o)$. This gave $N_T = (1.42\text{-}4.46) \times 10^{15}$ cm^{-3}. The calculations of N_T in other samples were not so straightforward, and were determined with the help of Figs 6.27 - 6.28 and eqn. (3.18).

The plot of Q against W for the ZnSe: Cu, diode No. 327-2, is shown in Fig 6.18. This diode gave $p_T(o) = 1.7 \times 10^{16}$ cm^{-3} and $N_T = 2.4 \times 10^{16}$ cm^{-3}.

The results of transient photocurrent measurements taken in conjunction with C-V and transient photocapacitance measurements of different doped samples are shown in Table 6.1. The best results were found in the lightly doped samples with low values of W_o and reasonable concentrations of deep centres, as in 5 ppm indium and gallium doped ZnSe crystals. It is interesting however to note that the concentration of the (0.60-0.61) eV centres decreased with increasing concentration of indium or gallium.

TABLE 6.1 : Data from Photocurrent and Photocapacitance (Transients) Measurements for ZnSe:In or Ga or Cu.

CRYSTAL	DIODE No.	W_o (μm)	$p_T(o)$ (cm^{-3})	N_T (cm^{-3})
ZnSe:5 ppm In	407-8 407-9	0.14 0.54	7.1×10^{14} 2.23×10^{15}	1.42×10^{15} 4.46×10^{15}
ZnSe:50 ppm In	405-5 405-6 405-7	0.86 1.19 2.01	3.3×10^{14} 7.4×10^{14} 6.8×10^{14}	3.7×10^{14} 8.3×10^{14} 7.7×10^{14}
ZnSe:50 ppm In	375-2	5.00	4.4×10^{13}	
ZnSe:5 ppm Ga	387-2	0.02	$(2.81 - 3.00) \times 10^{15}$	$(3.3 - 3.5) \times 10^{15}$
ZnSe:50 ppm Ga	409-1	1.00	9.8×10^{12}	1.1×10^{13}
ZnSe:Cu	327-2	0.52	1.7×10^{16}	2.4×10^{16}

6.3 TRANSIENT PHOTOCAPACITANCE MEASUREMENTS

There now follows a description of the results obtained using the transient photocapacitance technique. Such measurements lead to the spectral distribution of the photoionization cross-section, σ_n^o, for the excitation of electrons from the deep centres to the conduction band in the various indium and gallium doped ZnSe crystals. Measurements can also be manipulated to give the absolute values of the photoionization cross-section of electrons, σ_n^o ; and the concentration of the photoionized centres.

6.3.1 Spectrum of the Photoionization Cross-Section of Electrons, (σ_n^o)

In discussing the evaluation of the photocapacitance measurements, a similar procedure to that adopted when dealing with the transient photocurrents has been employed. Thus the method of determining the photoionization cross-section from the transient photocapacitance measurements will be discussed in detail for one diode, and for the remainder the resultant spectra only will be shown.

With diode No.407-9, prepared from a ZnSe crystal (boule No.407) doped with 5 ppm In, and with zero bias applied, a rise in photocapacitance (ΔC) was observed when the device was irradiated with primary light with $E_g > h\nu_p > E_g/2$, as shown by the curves in Fig 6.19 in region I. When the primary excitation was removed there was a small decrease in the value of ΔC, but the capacitance did not return to its original value. This decrease in the dark is shown in region II. A secondary excitation with light of photon energy $h\nu_s$ = 0.78 eV brought the capacitance back nearly to its starting value, as shown in region III. In the first period,I, during the excitation with $h\nu_p$, the occupancy of the deep centres was changed as dynamic equilibrium was established between the competing processes of ejecting electrons from the deep centres to the conduction band and of exciting electrons from the valence band to the empty centres. This gave rise to an increase in the capacitance of the depletion region of the diode and shows that on balance the deep centres were emptied. But when this excitation was removed, region II, a few of emptied centres were filled thermally or relaxed optically so that there was only a slight decrease in ΔC. Finally, when the centres were filled with electrons excited from the valence band by the secondary irradiation $h\nu_s$, there was a sudden fall in ΔC, region III. In the experiment with diode No.407-9, the energy of the primary excitation, $h\nu_p$, used to empty the centres ranged from 2.20 to 2.65 eV while the secondary excitation ($h\nu_s$ = 0.78 eV) used

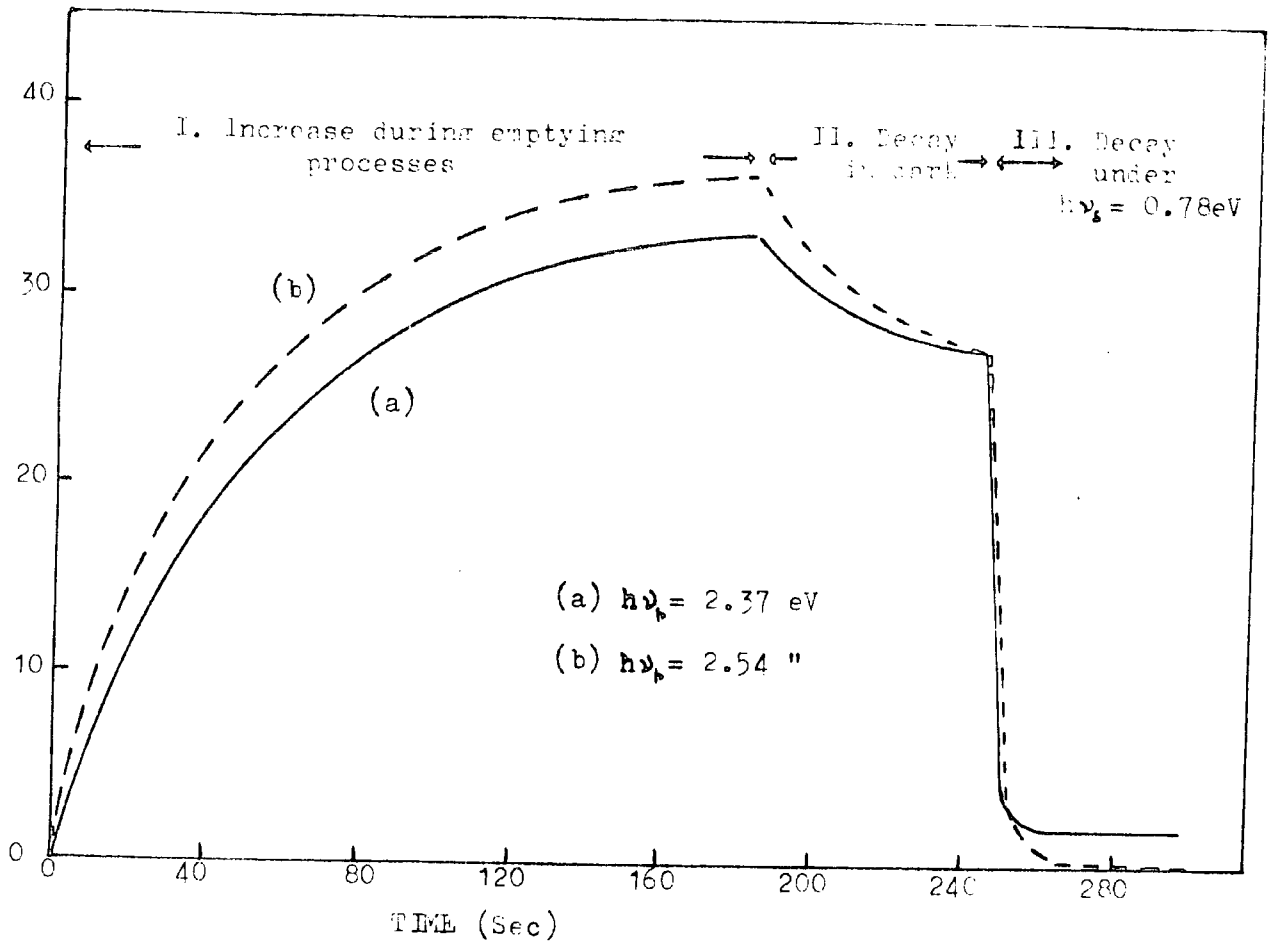

Fig 6.19: Behaviour of the photocapacitance under conditions I, II & III recorded for ZnSe:5ppm In diode.

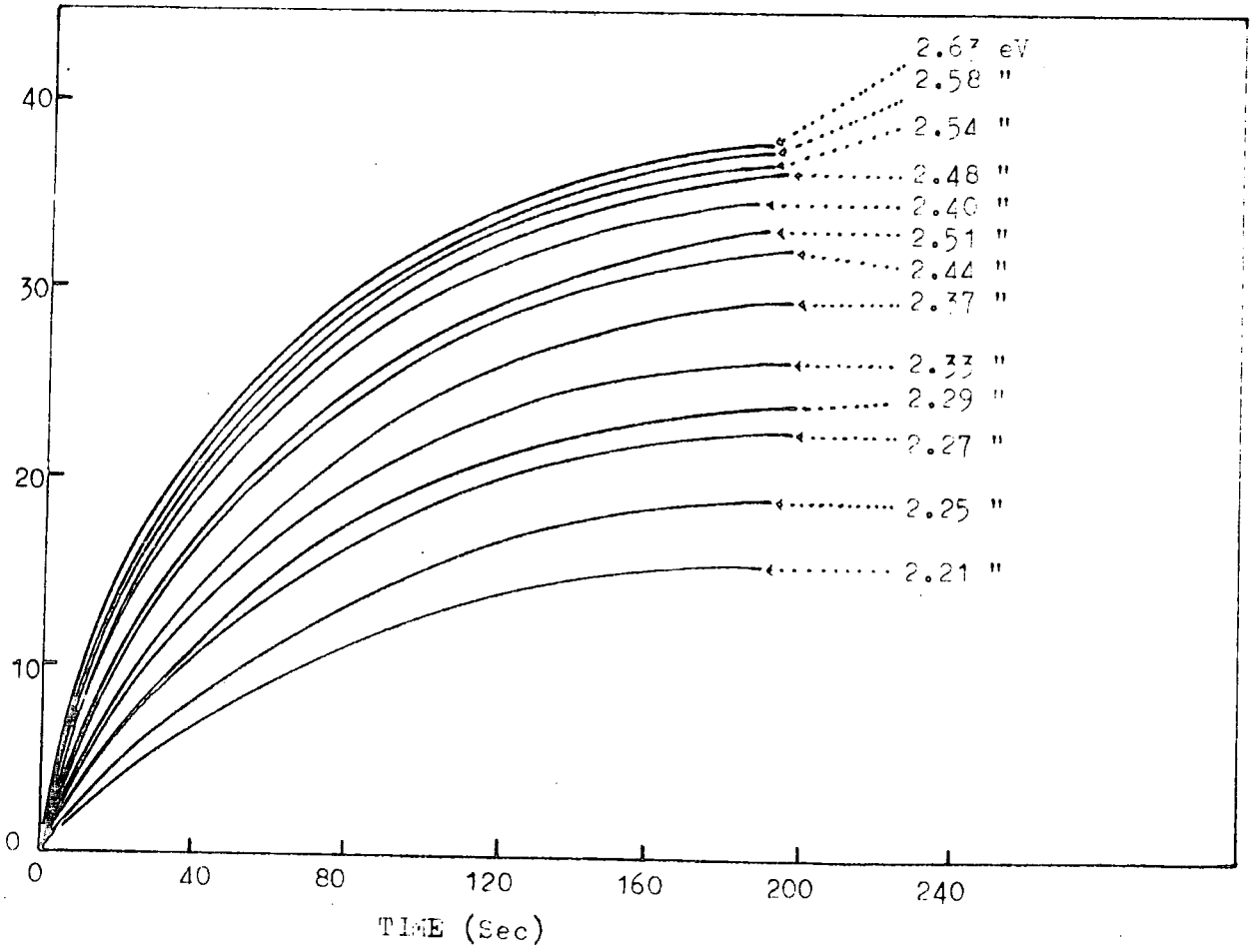

Fig 6.20 : Increase of photocapacitance at different primary excitations for ZnSe:5ppm In diode.

to fill the centres was maintained for two minutes. As a result a series of curves of transient photocapacitance were obtained for each of the primary photon energies ($h\nu_p$), see Fig 6.20. These are time dependent plots, since the rate of emptying the centres varies with the photon energy of the primary irradiation. From eqn. 3.30, a plot of Ln $[C^2(\infty) - C^2(t)]$ against time should yield a straight line. Here $C(\infty) = C_o + \Delta C$, where C_o is the diode capacitance in the dark and $C(t) = C_o + C_t$; C_t is the photocapacitance at any time t. The appropriate plots of the experimental results are shown in Fig 6.21. The inverse of the time constants (τ^{-1}) associated with the emptying of the deep centres were calculated from the slopes of the lines, and when used in eqn. (3.28), knowing the photon flux (ϕ), led to values of the photoionization cross-sections σ_n^o. The experimental spectrum of σ_n^o for diode 407-9 obtained in this way is shown by the points plotted in Fig 6.22. The cross-sections are in arbitrary units and the results suggested the existence of two deep levels, the thresholds of which (2.21 and 2.39 eV) were obtained by fitting the experimental points to Lucovsky's theoretical plots. The appropriate procedure will be discussed later. Since the values of the constant B and concentrations N_T in eqn (3.28) were not known, it was not possible to calculate the absolute values of σ_n^o.

The spectra of σ_n^o as a function of $h\nu_p$ for the other samples are shown in Fig 6.23-6.25. The spectrum in Fig 6.23, is for diode 405-9, fabricated from a ZnSe crystal (boule No.405) doped with 50ppm indium. This sample revealed much more definite evidence of the presence of two deep levels at 2.21 and 2.39 eV below the conduction band. The spectrum was run using two different biases, and no remarkable change was found. When the measurements were done on Zn-extracted samples, no transient photocapacitance measurements were possible, which suggests that the centres responsible had been removed by the Zn-treatment.

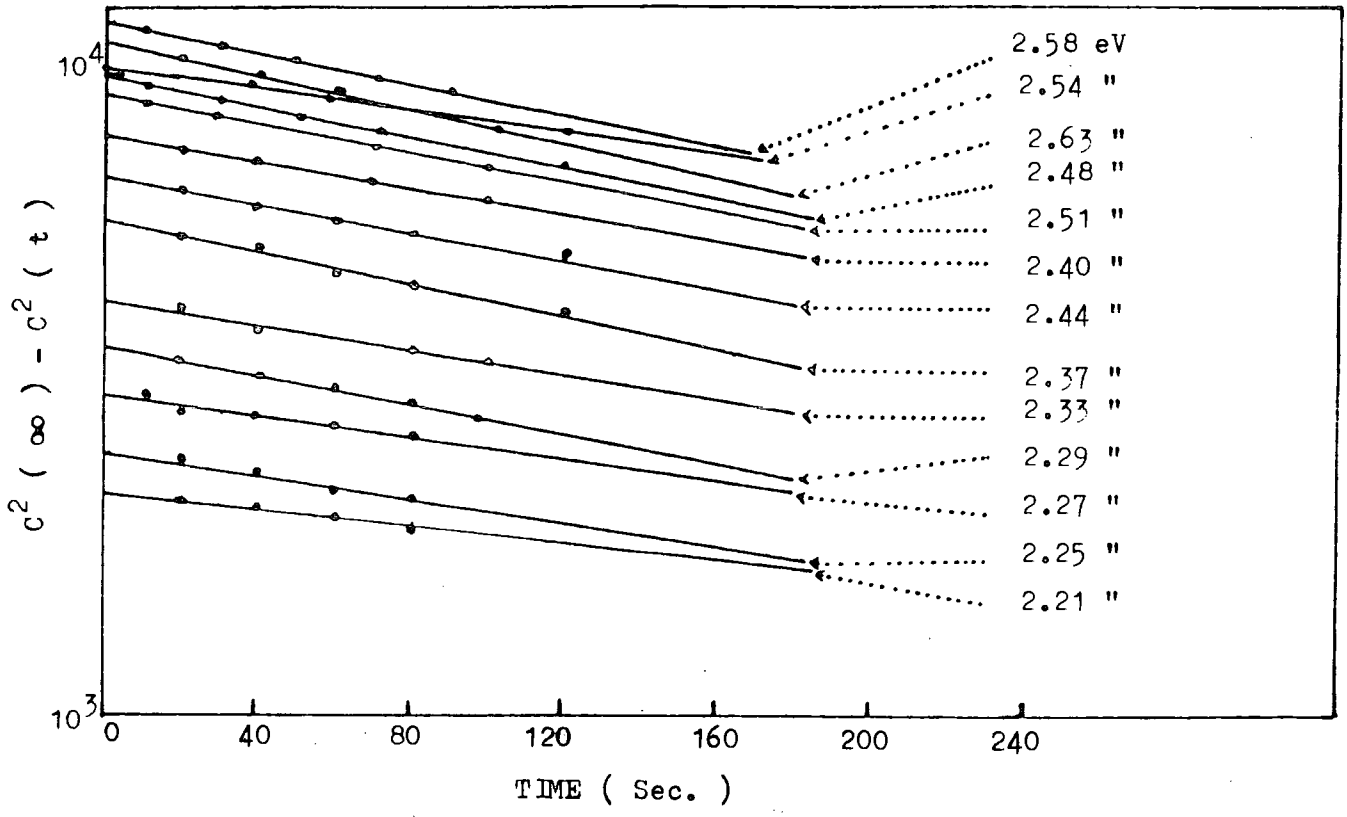

Fig 6.21 : Semi-logarithmic plot of the rise of the photocapacitance shown in Fig. 6.20.

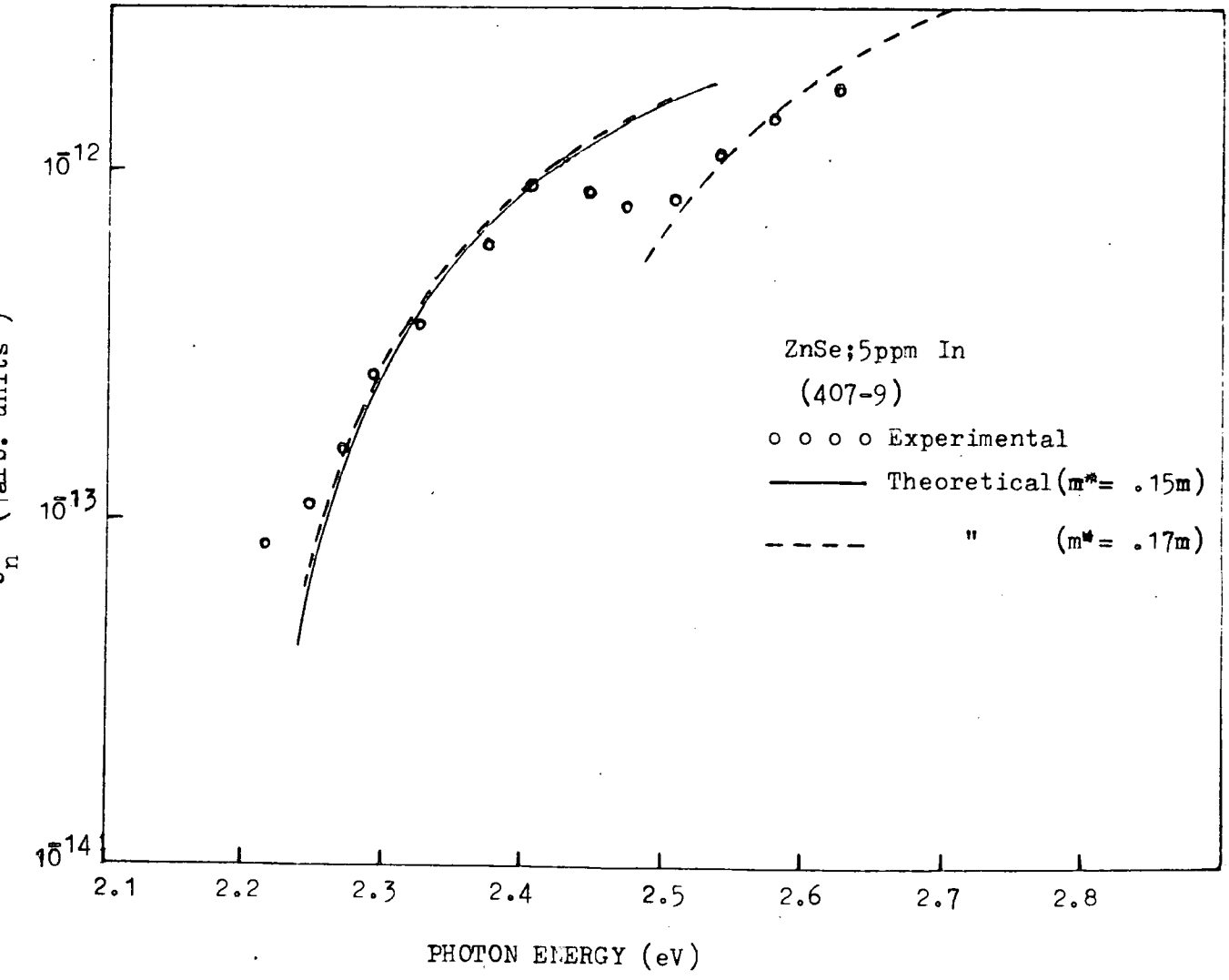

Fig 6.22 : Spectrum of the photoionization cross-section of electrons for ZnSe:5ppm In diode.

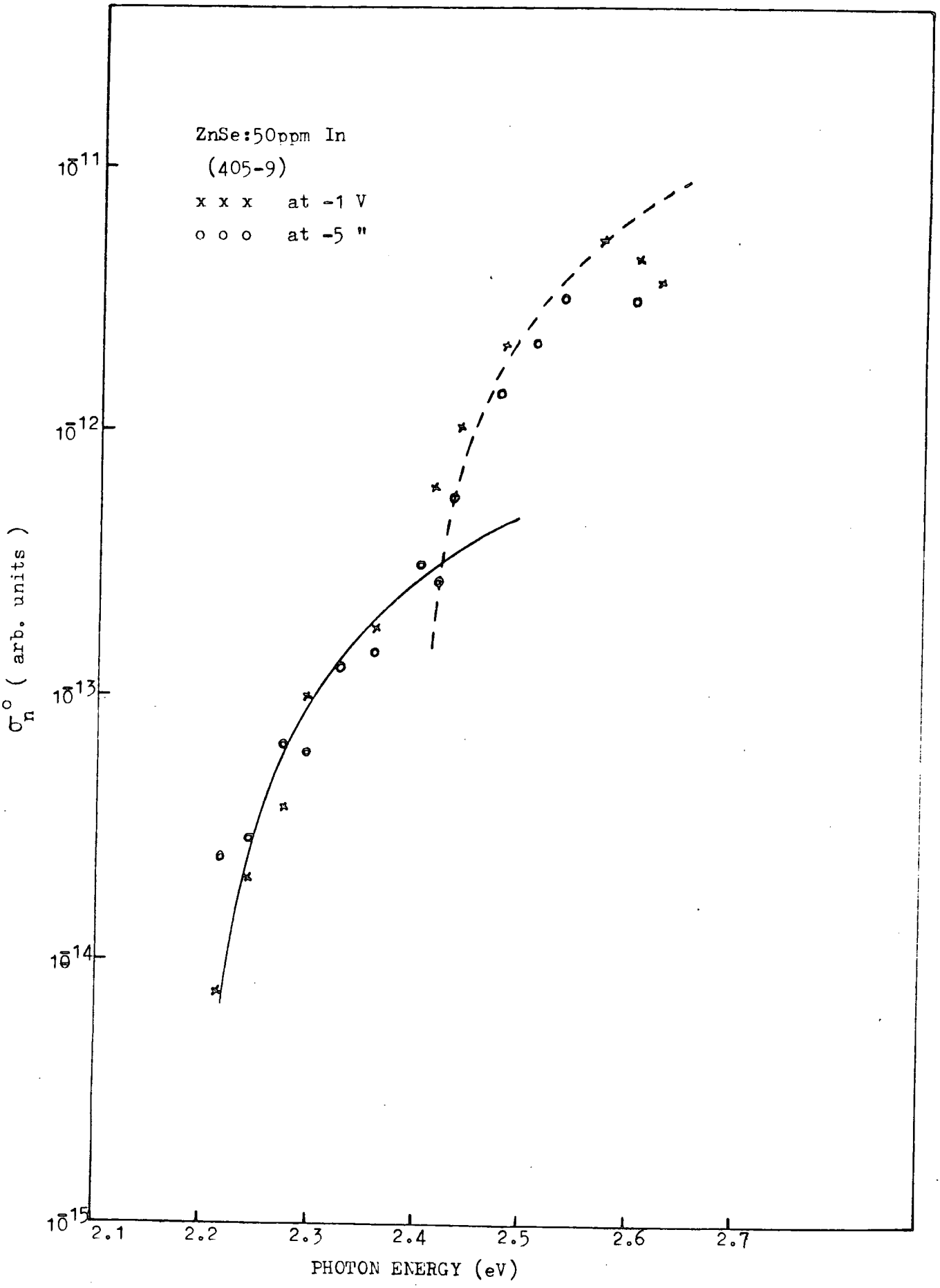

Fig 6.23 : Spectrumof the photoionization cross-section of electrons for ZnSe:50ppm In diode. Solid and broken lines are Lucovsky plots.

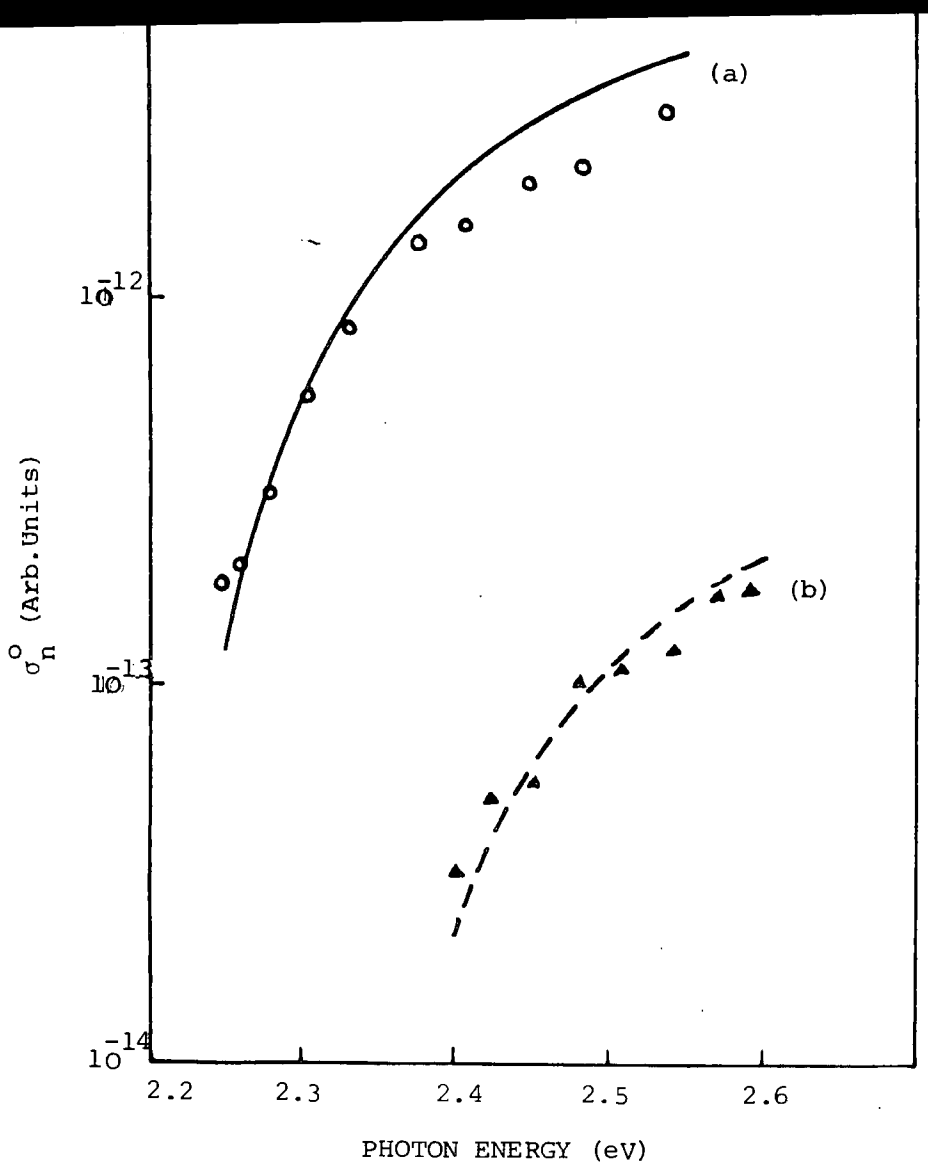

Figure 6.24 : Spectra of the photoionization cross-section of electrons for (a) as grown ZnSe:5 ppm Ga, and (b) after heat treatment in Zn.

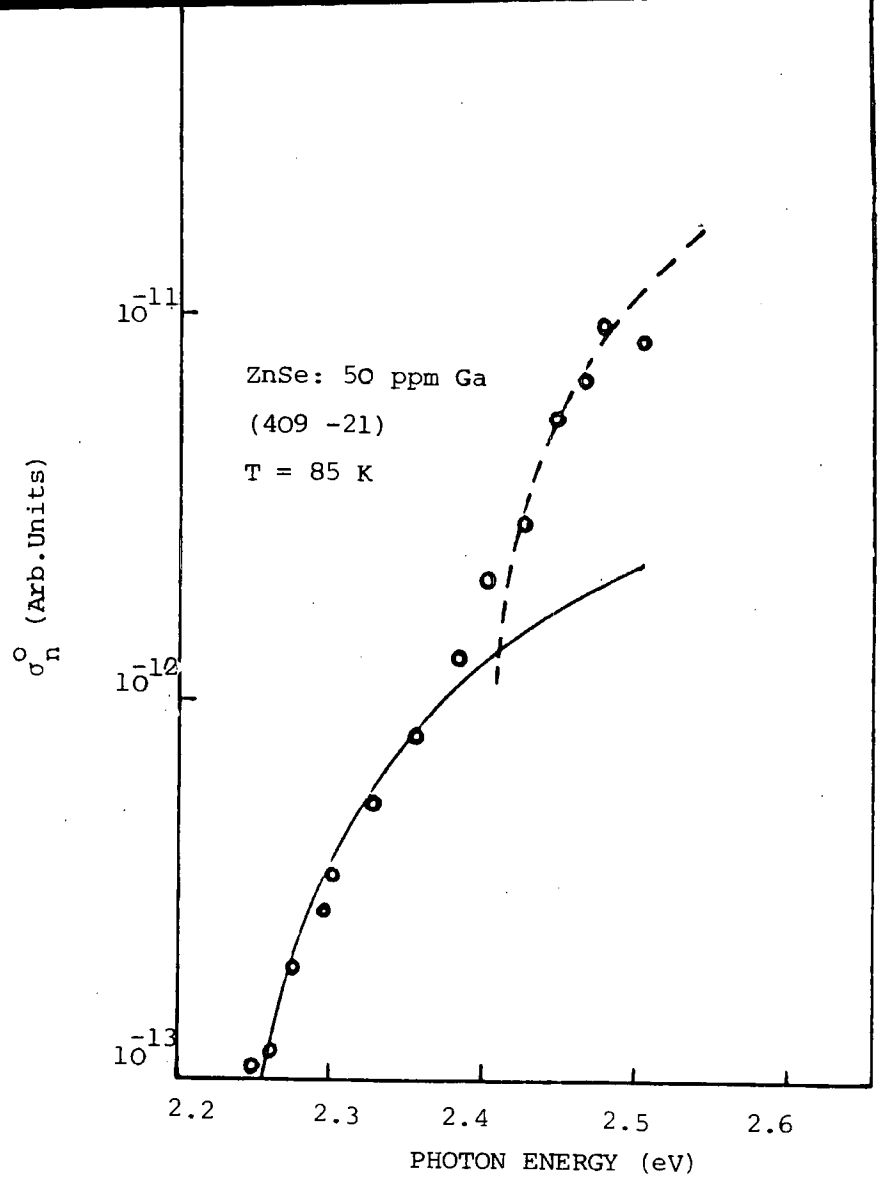

Figure 6.25 : Spectrum of the photoionization cross-section of electrons for ZnSe: 50 ppm Ga.

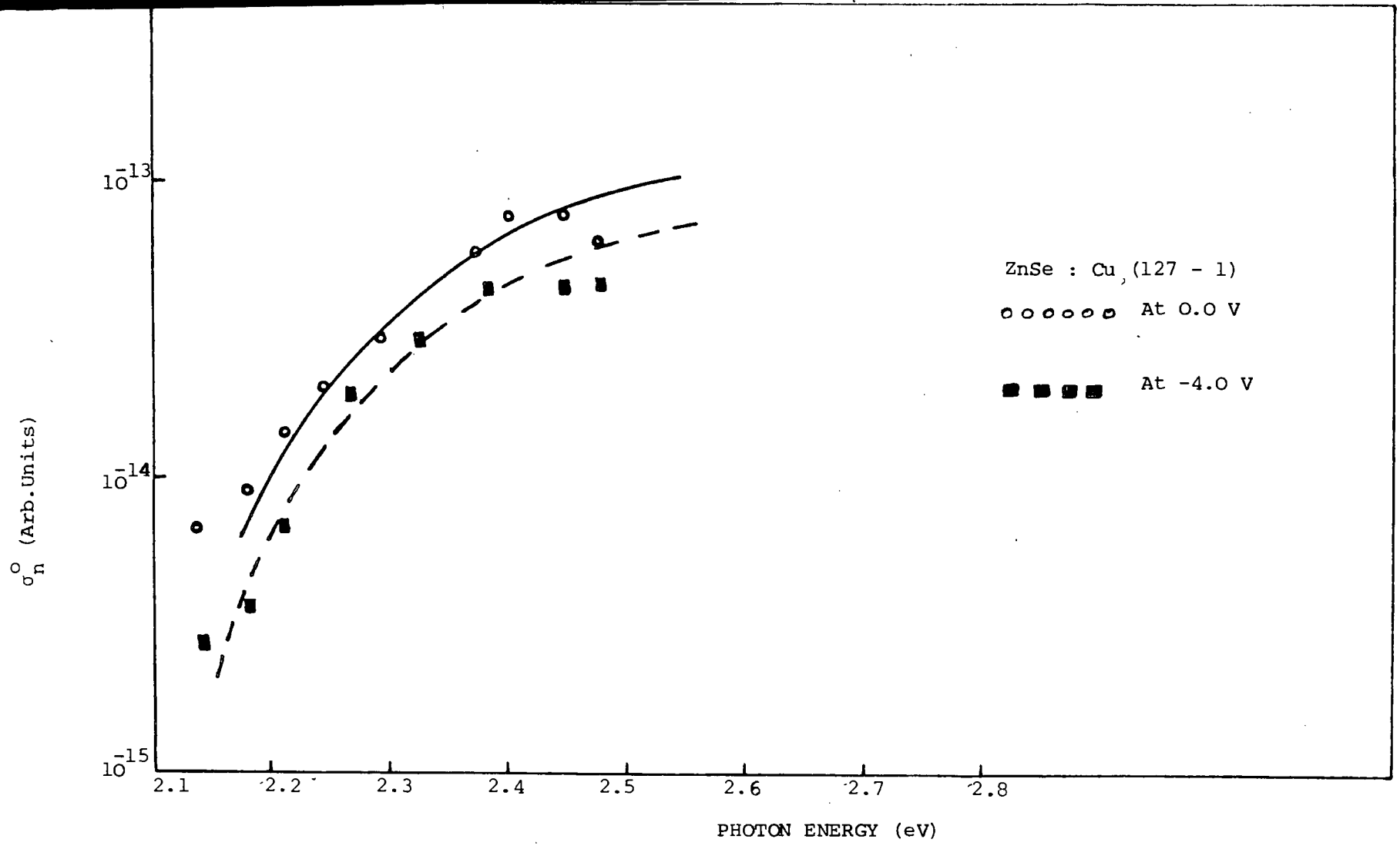

Figure 6.26 : Spectra of the photoionization cross-section of electrons for ZnSe:Cu.

The results for the gallium doped ZnSe samples are shown in Figs 6.24 and 6.25. The spectrum of diode 387-2, obtained from the crystal doped with 5 ppm Ga, as shown in Fig 6.24(a), indicated one deep level at 2.25 eV below the conduction band. When two dice from this crystal boule (No.387) were heat treated in molten zinc at 850°C for one day, the resistivity was reduced from 92 ohm-cm in the as-grown sample to 0.27 ohm-cm ; and after fabricating a device (No.387-X), the spectrum shown in Fig 6.24(b) was obtained. No spectrum was obtained in the lower energy region, and at the same time the whole spectrum shifted downwards. These changes may be associated with a decrease in the concentration of zinc vacancies after the heat treatment or the extraction of unintentional copper impurity. The spectrum of a sample doped with 50 ppm gallium, diode 409-21, is shown in Fig.6.25. This indicates the presence of two deep levels 2.25 and 2.40 eV below the conduction band.

A ZnSe diode in which copper was introduced as described in § 6.2.1, had the spectrum of σ_n^o shown in Fig 6.26. This revealed a deeper level with an ionization threshold between 2.13 and 2.14 eV. This clearly indicates that the levels observed in the experiments on indium and gallium doped diodes were not associated with substitutional copper.

6.3.2 Total Photoionization Cross-Sections

The results of the transient photocurrent and photocapacitance measurements can be combined to yield the spectra of the photoionization cross-sections of electrons and holes. Since the time constant for emptying the deep centres is given by the expression, see eqn. (3.27),

$$\tau = \left[\left(\sigma_n^o + \sigma_p^o \right) \phi \right]^{-1}$$

The photocapacitance response curves, taken together with a knowledge of the photon flux ϕ, give values of $(\sigma_n^o + \sigma_p^o)$. With photon energies, smaller than

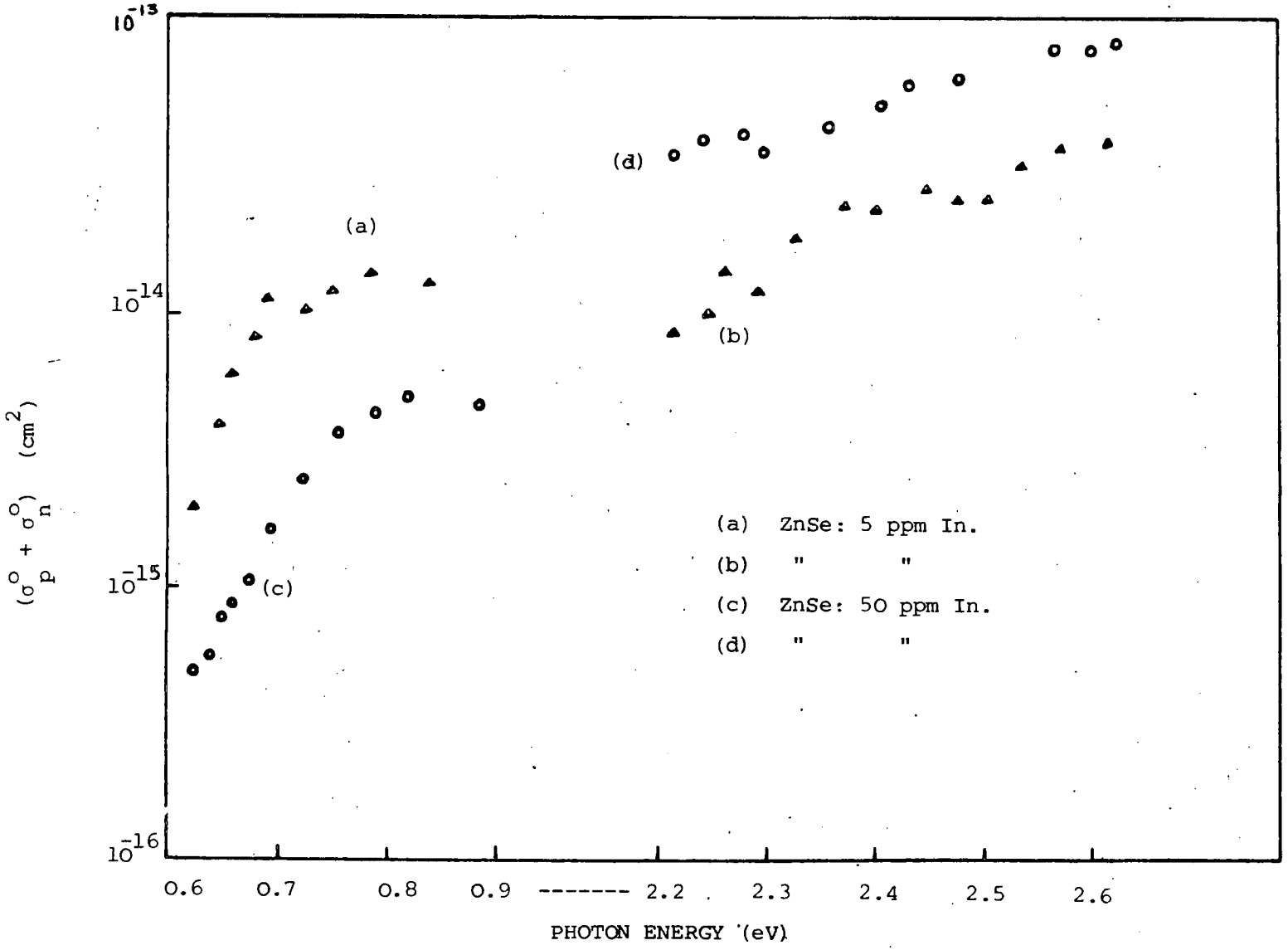

Figure 6.27 : Total photoionization cross-section spectra of holes and electrons, obtained from tr.photocurrent (LHS) and tr.photocapacitance (RHS) techniques.

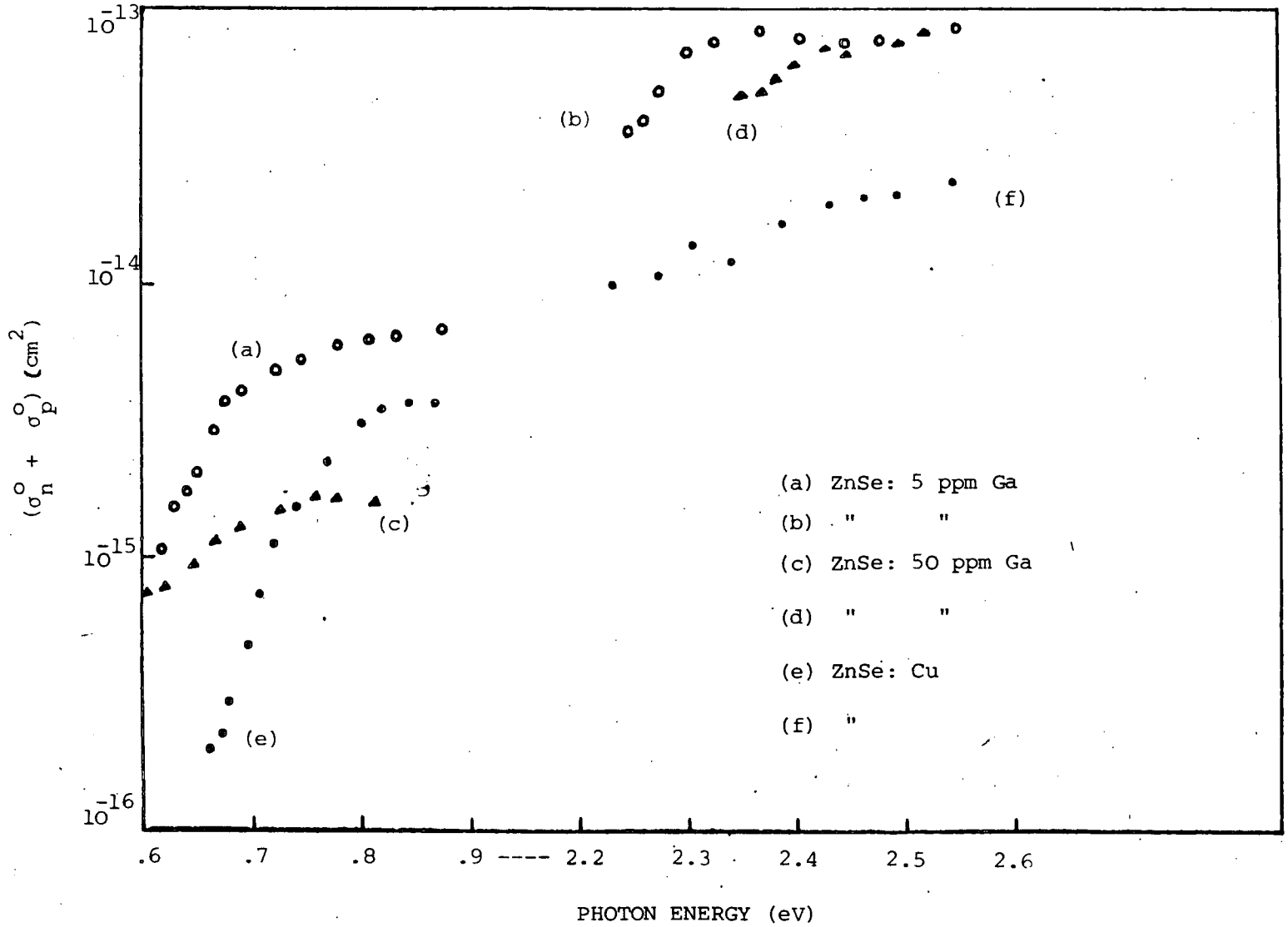

Figure 6.28 : Total photoionization cross-section spectra of holes and electrons, obtained from tr.photocurrent (LHS) and tr.photocapacitance (RHS) techniques.

half the band gap, σ_n^o can be neglected (i.e. there is then no photoexcitation from the deep centres to the conduction band) and $\sigma_n^o + \sigma_p^o = \sigma_p^o$. Then the curves of σ_p^o from Figs 6.3 - 6.7, can be used as values for $\sigma_n^o + \sigma_p^o$. The plots obtained in this way are shown in Figs 6.27 and 6.28. With the exception of the 5 ppm indium doped ZnSe samples, there are considerable differences between the maxima of the spectra obtained from the transient photocurrent measurements and the minima of the spectra obtained from transient photocapacitance measurements. Thus the arguments of Grimmeiss, et al (1976) who found that with $h\nu = 2.48$ eV, $e_n^o \approx e_p^o$ or $\sigma_n^o \approx \sigma_p^o$; in ZnSe: Mn crystals, do not apply to our crystals doped with 50 ppm of In or 5 or 50 ppm of Ga. With photon energies $h\nu > 2.30$ eV, the photoexcitation of electrons dominates over the photoexcitation of holes and $(\sigma_n^o + \sigma_p^o) \approx \sigma_n^o$. As a result the plots in Figs 6.27 and 6.28 give the absolute values of the photoionization cross-section of electrons from the centres to the conduction band. The following minima were found in our measurements : 9.0×10^{-15} cm^2 for ZnSe: 5 ppm In, 4.0×10^{-14} cm^2 for ZnSe:50 ppm In, 3.8×10^{-14} cm^2 for ZnSe: 5 ppm Ga, 5.0×10^{-14} cm^2 for ZnSe: 50 ppm Ga and 1.0×10^{-14} cm^2 for ZnSe:Cu.

6.3.3 Concentrations of Photoionized Deep Centres

Referring to § 3.5.5, Chapter 3, the concentration of photoionized deep centres (Δn), which is equivalent to the term $p_T(o)$, can be calculated by using eqn. (3.31). Measurements of transient photocapacitance combined with capacitance-voltage curves measured in the dark have been used to find the spectral dependence of Δn for the various indium and gallium doped crystals, shown here in Figs 6.29-6.31.

The first response shown in Fig 6.29(a) is for the ZnSe crystal doped with 5 ppm indium, which gave $\Delta n = 3.8 \times 10^{14}$ cm^{-3} at $h\nu = 2.21$ eV. This is to be compared with the value of $p_T(o) = (7.1 - 22.3) \times 10^{14}$ cm^{-3} found from the transient photocurrent measurements for the deep level at the same height

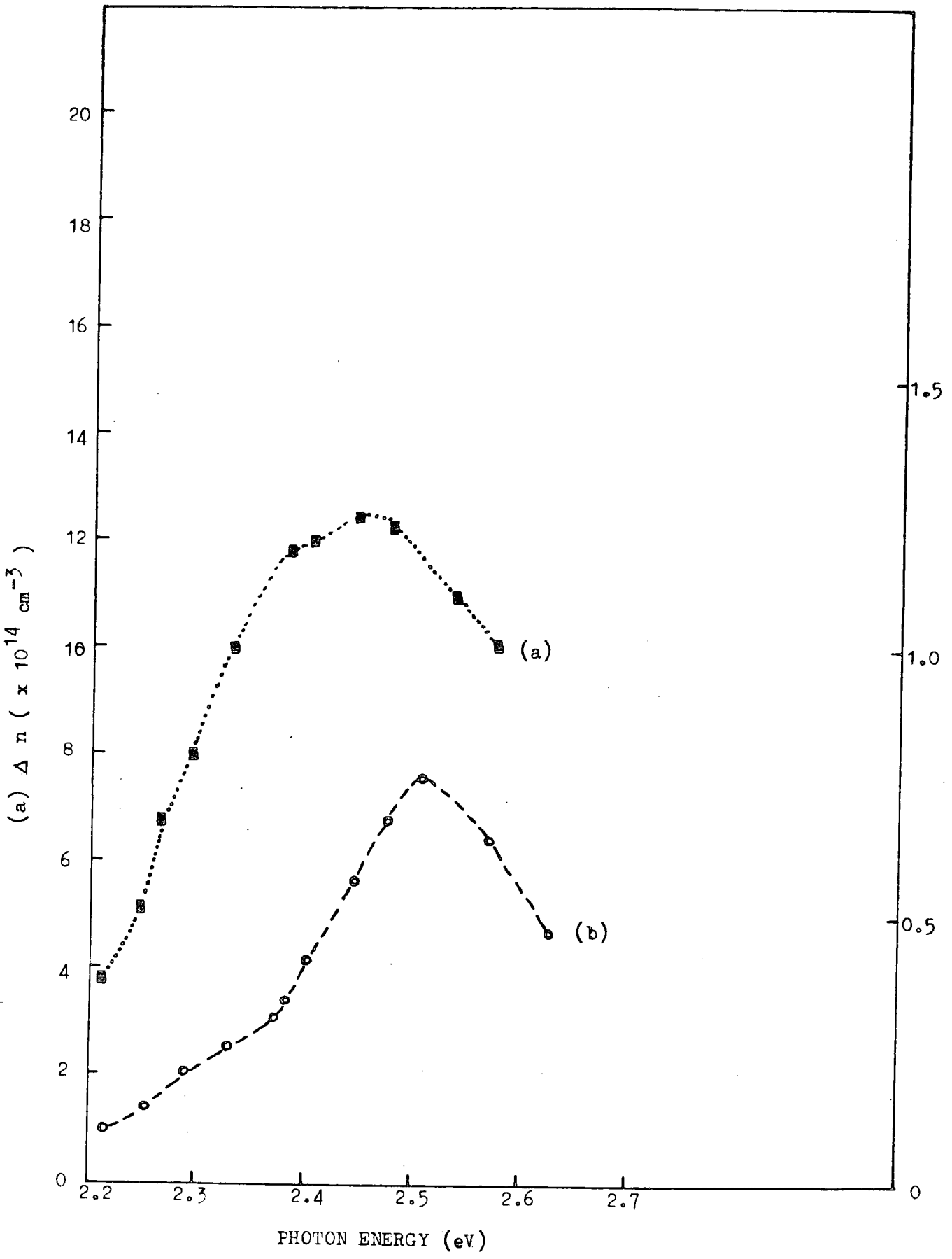

Fig 6.29 : Spectra of the photoionized deep centres for (a) ZnSe:5ppm In and (b) ZnSe:50ppm In.

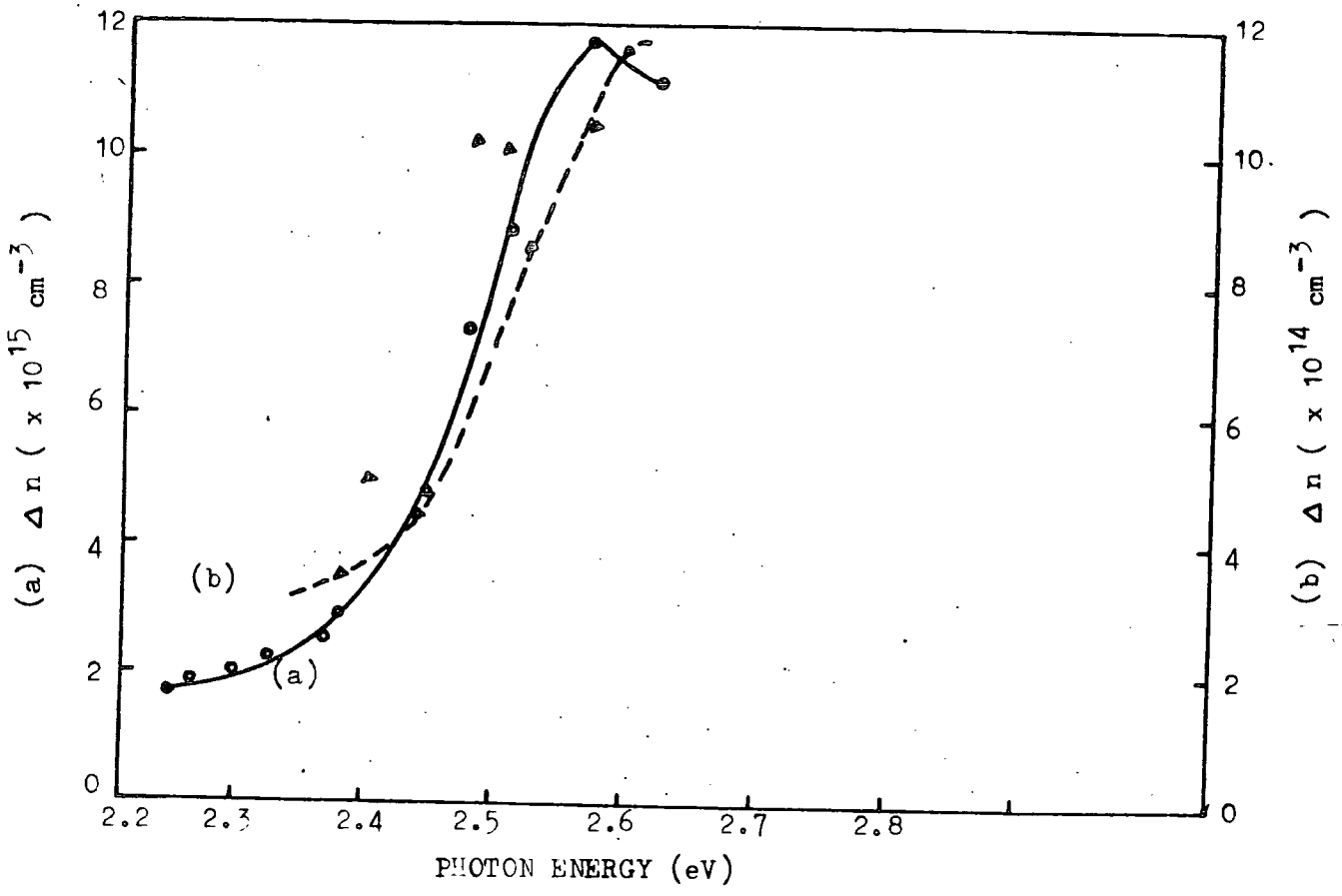

Fig 6.30 : Spectra of the photoionized deep centres for (a) ZnSe: 5ppm Ga as grown and (b) after zinc heat treatment.

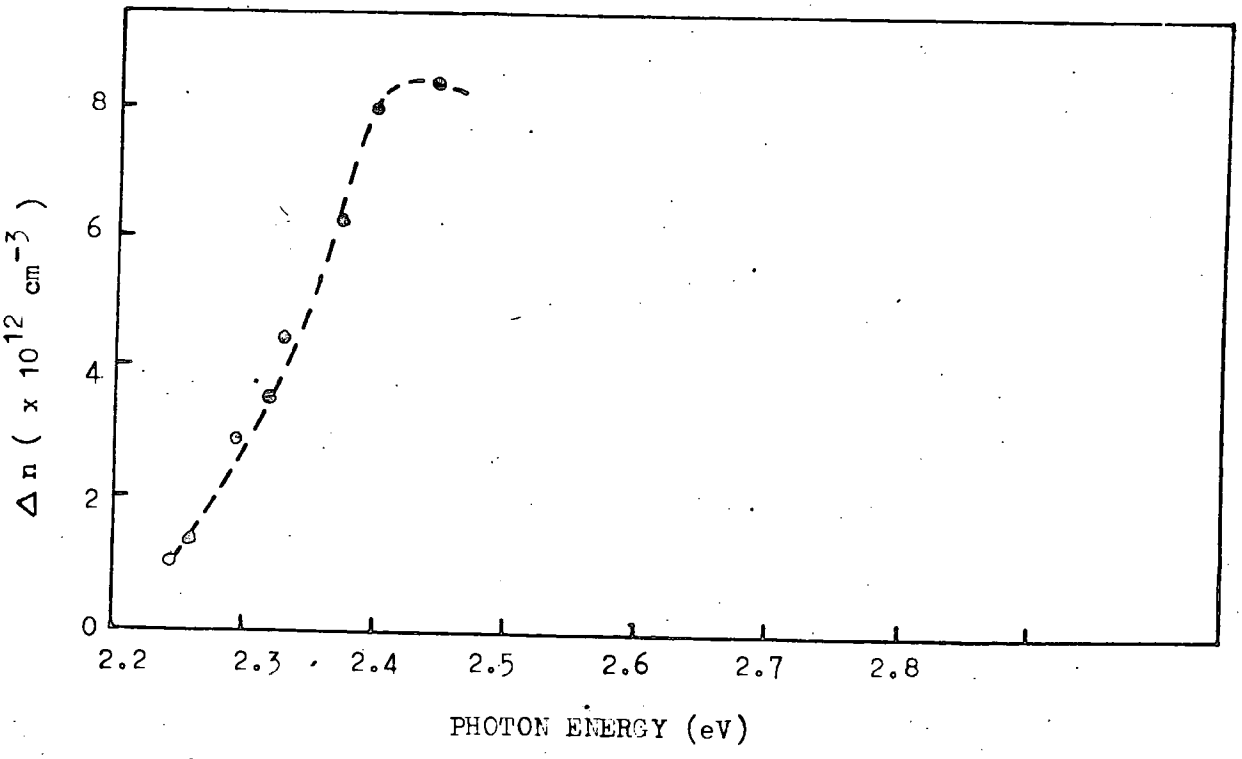

Fig 6.31 : Spectrum of the photoionized deep centres for ZnSe:50ppm Ga.

above the valence band. The values for the sample doped with 50 ppm indium are also shown in Fig 6.29 (b) giving $\Delta n = 1 \times 10^{14}$ cm^{-3} at $h\nu = 2.21$ eV, to be compared with the transient photocurrent values $p_T(o)$ in the range $(3.3\text{-}7.4) \times 10^{14}$ cm^{-3}.

With the sample doped with 5 ppm gallium, $\Delta n = 1.7 \times 10^{15}$ cm^{-3}, see Fig 6.30 (a), at $h\nu = 2.25$ eV and $p_T(o) = (2.81 - 3.00) \times 10^{15}$ cm^{-3}, while the sample heated in molten zinc gave $\Delta n = 3.5 \times 10^{14}$ cm^{-3} at $h\nu = 2.39$ eV, see Fig 6.30 (b) ; and the sample with 50 ppm gallium had $\Delta n = 1.0 \times 10^{12}$ cm^{-3} at 2.25 eV, see Fig 6.31, with $p_T(o) = 9.8 \times 10^{12}$ cm^{-3}.

The concentration of empty centres obtained in this way are clearly in reasonable agreement with concentrations obtained using the transient photocurrent technique.

6.3.4 Locating the Position of the Deep Centres

The photocurrent methods have the drawback that they do not identify whether the centre under study is closer to the conduction or to the valence band, i.e. whether the response obtained is due to electrons or holes. But this point can be resolved by using the capacitance method. It was therefore applied to those diodes on which the transient photocurrent technique had been employed.

Values of σ_p^o can also be determined from transient photocapacitance measurements using the range of energies employed in the transient photocurrent technique. It is argued that when empty deep centres are filled by secondary excitation with $h\nu_s$ in the range of 0.60 - 1.00 eV, the charge Q of the depletion region will change, and with it the capacitance. This photocapacitance technique therefore can be used to identify which band edge the deep centres are nearer to. Only one plot, see Fig 6.5 (b), was completely recorded, and this revealed that the deep centre detected in corresponding transient photocurrent measurements was closer to the valence band, because the photocapacitance decreased under the secondary irradiation

and curves similar to that shown in Fig 6.1 were obtained. This method was also applied to other crystals when the transient photocurrent technique was being used, to check the location of the levels. The conclusion is that all the levels found using the transient photocurrent technique were closer to the valence band.

6.4 LUCOVSKY PLOTS AND THRESHOLD ENERGIES

Equation (2.14), obtained from Lucovsky's theoretical model has been used to calculate the values of σ^{o} ; and the theoretical curves have been fitted to the experimental points to fix the energy thresholds. In the calculation of σ_p^o a value of the hole effective mass of $m_h^* = m_o$ was used in eqn. (2.14), and for σ_n^o a value of $m_e^* = 0.17\ m_o$, see Marple (1964), was taken. Also when the value $m_e^* = 0.15\ m_o$, as reported by Grimmeiss et al (1976) was employed instead, we found no essential difference, see Fig 6.22.

With the sample doped with 5 ppm In, a threshold $\Delta E_p^o = 0.61$ eV was found from the transient photocurrent method, Fig 6.5 (a), indicating that the deep level was 0.61 eV above the top of the valence band. With the transient photocapacitance method, two deep levels with thresholds $\Delta E_n^o = 2.21$ and 2.39 eV, Fig 6.22, were detected. These values of ΔE_n^o gave the positions of the deep levels below the bottom of the conduction band. The level with $\Delta E_{n1}^o = 2.21$ eV is the same as that with $\Delta E_p^o = 0.61$ eV. The difference (Δ) between the width of the band gap ($E_g = 2.80$ eV at liquid nitrogen temperature) and the sum $\Sigma = (\Delta E_p^o + \Delta E_{n1}^o)$ is therefore (Δ) = 0.02 eV. The second value of ΔE_{n2}^o refers to a different level 0.41 eV above the valence band. For the sample with 50 ppm In, the corresponding values of ΔE_p^o and ΔE_{n1}^o were also 0.61 eV (see Figs 6.3 and 6.4) and 2.21 eV (see Fig 6.23) respectively, giving (Δ) = 0.02 eV. The second level at 0.41 eV was also detected in this sample.

With ZnSe doped with 5 ppm Ga, the threshold energies were $\Delta E_p^o = 0.61$ eV, Fig 6.6 (a), and $\Delta E_{n1}^o = 2.25$ eV, Fig 6.24 (a) ; giving a difference (Δ) of 0.06 eV. After heat treatment in molten zinc, the sample displayed a threshold

ΔE^{o}_{n2} at 2.38 eV, Fig 6.24 (b). The curve fitting and hence the determination of the correct threshold was not possible with the transient photocurrent measurements made on the crystal containing 50 ppm Ga, see Fig 6.6 (b), but a rough estimate of the threshold gave ΔE^{o}_{p} = 0.60 eV.

The transient photocapacitance method for ZnSe: 50 ppm Ga sample gave thresholds at ΔE^{o}_{n1} = 2.25 eV and ΔE^{o}_{n2} = 2.40 eV, see Fig 6.25. The difference (Δ) between ($\Delta E^{o}_{n1} + \Delta E^{o}_{p}$) and Eg was 0.05 eV.

The copper doped ZnSe crystal, also gave good theoretical fits with ΔE^{o}_{p} = 0.67 eV and ΔE^{o}_{n} = 2.13 - 2.14 eV, with $\Delta E^{o}_{n} + \Delta E^{o}_{p}$ = 2.80 - 2.81 eV, so that (Δ) = 0.00 - 0.01 eV. In Table 6.2, we have summarized all the measured values. The smallness of (Δ) shows that relaxation effects following the capture or release of charge carriers are small.

TABLE 6.2 : Threshold Energies and Cross-Sections in ZnSe:In or Ga or Cu.

Crystals	$\sigma^{o}_{p_2}$ (cm^2)	ΔE^{o}_{p} (eV)	ΔE^{o}_{n1} (eV)	ΔE^{o}_{n2} (eV)	$\Sigma = \Delta E^{o}_{p} + \Delta E^{o}_{n1}$ (eV)	$(\Delta) = \Sigma - Eg$ (eV)
ZnSe:5 ppm In	2.1×10^{-15}	0.61	2.21	2.39	2.82	0.02
ZnSe:50 ppm In	$(5-6) \times 10^{-16}$	0.61	2.21	2.39	2.82	0.02
ZnSe:5 ppm Ga	1.1×10^{-15}	0.61	2.25	-	2.86	0.06
ZnSe:50 ppm Ga	7.2×10^{-16}	0.60	2.25	2.40	2.85	0.05
ZnSe:Cu	2.0×10^{-16}	0.67	2.13-2.14	-	2.80-2.81	0.00-0.01

6.5 DISCUSSION

In summary, it is clear that the transient photocurrent technique revealed one discrete set of deep centres with a level ΔE_p^o = (0.60 - 0.61) eV above the valence band in ZnSe crystals doped with 5 and 50 ppm of indium or gallium. The technique of transient photocapacitance indicated the presence of two deep levels with electron ionization thresholds of ΔE_{n1}^o = (2.21-2.25)eV, and of ΔE_{n2}^o = (2.39-2.40)eV in indium and 50 ppm gallium doped crystals. There was only one threshold ΔE_{n1}^o = 2.25 eV in ZnSe: 5 ppm Ga.

It seems obvious that the values of ΔE_p^o and ΔE_{n1}^o refer to the same level, because their sum is nearly equal to the band gap energy of the ZnSe. The hole ionization cross-section corresponding to the level ΔE_{n2}^o could not be investigated using the transient photocurrent technique because of the negligible lamp response in the region $h\nu \lesssim 0.50$ eV.

In our studies of photoconductivity and infra-red quenching (see Chapter 5), we found a level (0.54-0.60) eV above the valence band which we have associated with the self-activated (SA) centres in indium and gallium doped ZnSe crystals. The deep level in the region 0.65-0.67 eV was found to be associated with copper contamination. The hole ionization threshold ΔE_p^o = (0.60-0.61) eV investigated here using the transient photocurrent technique is obviously associated with the same self-activated centres which contain zinc vacancies (V_{zn}) and indium or gallium ions substituted at nearest neighbouring zinc site (i.e. In_{zn} or Ga_{zn}). The ionization energies determined in transient photocurrent are slightly greater than those obtained using photoconductivity and IR quenching methods. However, the complementary electron ionization threshold of ΔE_{n1}^o in the range 2.21 - 2.25 eV (or 0.59-0.55 eV above the valence band) as determined by the transient photocapacitance technique agrees very well with the energies found from photoconductivity and IR quenching.

A comprehensive survey of results quoted for copper and SA centres by different researchers is given in Chapter 5 of this thesis. Stringfellow and

Bube (1968) put the self-activated centres at between 0.50 and 0.60 eV, Cu^{1+}(i.e. Cu'_{zn}) at 0.72 eV, and Cu^{2+} (i.e. Cu^{x}_{zn}) at 0.35 eV, above the valence band of ZnSe. Grimmeiss et al (1977-1979) using capacitance spectroscopy described Cu-related acceptor states 0.68 eV above the valence band which they had originally claimed (Grimmeiss et al, 1976) to be associated with manganese in ZnSe:Mn.

Birchak et al (1976) also attributed a 0.68 eV level to copper in ZnSe. Yu and Park (1973) thought that levels between 0.65 and 0.75 eV above the valence band were due to zinc vacancies and complexes containing zinc vacancies ; whereas Jones and Woods (1974) suggested much higher values for SA centres in ZnSe:In at 0.83 eV above the valence band. Dunstan et al (1980) using optically detected magnetic resonance (ODMR) technique found levels between 0.60 and 0.70 eV above the valence band in undoped and chlorine doped ZnSe crystals, and attributed them to associated zinc vacancy defects and SA-centres.

Our experiments on copper doped and undoped ZnSe crystals using IR quenching, and both the photocurrent and photocapacitance transient techniques put the Cu^{1+} level in ZnSe between 0.65 and 0.67 eV above the valence band, which is very close to many reported values. In indium or gallium doped ZnSe crystals we found the dominant acceptors at (0.55-0.61) eV above the valence band, which we believe to be attributable to zinc vacancy complexes or simply SA acceptor centres, on the basis of the agreement with work reported by others. This level is definitely not due to copper because it is less deep and is dominant in the indium and gallium doped samples.

The second level at (0.40-0.41)eV above the valence band is shallower than the SA level. Several workers including Stringfellow and Bube (1968), Jones and Woods (1974) and, Adachi and Machi (1975) have reported a level between 0.35 and 0.37 eV as the neutral copper (Cu^{2+}) acceptor. In comparison with this, the level at (0.40-0.61) eV found by us is definitely different

and deeper, and since it appears in the indium and gallium doped samples, it is suggested that it is attributable to some indium or gallium acceptor-like complex.

Russell et al (1981) suggested that normally at low concentrations the indium should go to Zn-sites and behave as a simple donor. But at high concentrations because of charge compensation, the In^{3+} ions are compensated by V_{zn}^{2-} or V_{zn}^{1-} vacancies. The first vacancy will produce $(V_{zn}^{--} - In_{zn}^{+})^{-}$ complex centres and the second will create $(V_{zn}^{-} - In_{zn}^{+})^{o}$ centres. The $(V_{zn}-In_{zn})^{-}$ configuration has one extra negative charge and should be farther from the valence band than $(V_{zn}- In_{zn})^{o}$ which is neutral. If this explanation is correct then the levels at (0.55-0.61) eV should be related to $(V_{zn}-In_{zn})^{-}$ centres and those at $\sim$ 0.41 eV to $(V_{zn}-In_{zn})^{o}$ complexes.

There are other possibilities, see Russell et al (1981) and Ray and Kröger (1978), who discussed the observations that with indium or gallium doping, there is no linear relation between impurity concentration and conductivity, unlike the situation with the other group III dopant aluminium which is normal. Higher concentrations of indium or gallium lead to an increase in the resistivities of the crystals and both sets of investigators suggest that at higher concentrations the indium or gallium might occupy selenium sites and thus form multiple acceptors which should compensate the donors and decrease the conductivity. Simple geometrical arguments using the concept of ionic radii support this suggestion. For example, the ionic radii of Zn^{2+}, Se^{2-}, Al^{3+}, In^{3+} and Ga^{3+} are 0.74, 1.91, 0.51, 0.81 and 0.62 Å respectively. The ZnSe crystals used in this work were grown from the vapour phase, with indium or gallium added to the charge. With zinc in the reservoir a small zinc over pressure at the growing interface is obtained and selenium vacancies would therefore be created together with a smaller concentration of zinc vacancies in the growing boule. Since the ionic radius of Zn^{2+} is larger than that of Al^{3+}, aluminium can readily occupy zinc sites and increase the n-type

conductivity of ZnSe. With indium, however, which has a larger radius than zinc, substitution on zinc sites is more difficult. Thus at higher concentrations some of the excess selenium vacant sites could be occupied with indium and, $In_{se}^{'''}$ multiple acceptors would then result. The same argument might be advanced for gallium, but because of its smaller radius it is more likely to substitute on zinc sites with reasonable solubility. Thus it is distinctly possible that the level at (0.40-0.41) eV above the valence band is due to In_{se}^{3-} or Ga_{se}^{3-}. This suggestion is supported by the results from samples with the higher concentrations of indium or gallium where the response in transient photocapacitance from this level was much more pronounced compared with that in the lightly doped samples.

The concentration N_T of the SA centres was observed to decrease as the concentration of indium or gallium was increased, see Table 6.1. However, in the more highly doped samples, the indium or gallium contributes to an increase in the concentration of the (0.40-0.41)eV level.

The absolute values of the photoionization cross-sections of holes, σ_p^o, reported here are higher than those measured by Grimmeiss et al (1976,1977) in their copper or manganese doped ZnSe. The higher values are a consequence of the high measured emission rates ($e_p^o \alpha \frac{1}{\tau}$) of holes from the centres ΔE_p^o. The emission rates of electrons from these centres were also large. This may be observed in Figs 6.1 and 6.20. Values of $\sigma_p^o \gtrsim 10^{-16}$ cm^2 are not unreasonable however particularly since Suda and Bube (1981) studying Cu_xS-CdS samples found values of $\sigma_p^o \gtrsim 10^{-16}$ cm^2 for the copper level in CdS. Another factor to take into account is that the higher cross-sections found here might be due to the influence of other competing centres during decay transients. However, the exact explanation remains uncertain.

CHAPTER 7

STEADY STATE PHOTOCAPACITANCE MEASUREMENTS

7.1 INTRODUCTION

The photoconductivity and I-R quenching techniques and the various transient methods, described in Chapters 5 and 6 respectively, are best suited for the investigation of deep levels. In the present chapter measurements of steady state photocapacitance are described which allow many shallow, as well as deep levels, to be identified. Shallow defects particularly have been investigated using the technique described by Marfaing et. al (1974), (see Chapter 3, § 3.2.2).

Most of the work was done on ZnSe doped with indium or gallium, but a few results were also obtained for undoped and copper doped crystals. The effects of varying the temperature, frequency, bias, doping concentration and Zn-treatment, on photocapacitance have been studied and are discussed below.

The measurements were carried out on Schottky diodes fabricated from $3 \times 3 \times 1$ mm^3 dice, with gold contacts covering a 2 mm^2 area. The monochromator providing the illumination was driven extremely slowly. In some runs point-by-point plotting was also used, where time was allowed (up to 4 minutes) for the photocapacitance to reach a steady state value. Before moving to the next wavelength the photocapacitance was returned to its initial value by appropriate irradiation in the infra-red.

7.2 TEMPERATURE DEPENDENT PHOTOCAPACITANCE

The temperature dependence of the photocapacitance (ΔC) for different indium, gallium and copper doped ZnSe crystals has been measured in the range 82-293 K. All responses at liquid nitrogen temperature were larger and better resolved than those at room temperature. This is illustrated in Figs. 7.1 and 7.2. The photocapacitance spectrum, for diode No. 405-14, ZnSe : 50 ppm In, at room temperature is shown in Fig. 7.1(a). The dark capacitance level was 32.6×10^2 pf/$_{cm^2}$ and the wavelength scan revealed a single threshold at 2.15 eV. At liquid nitrogen temperature, the dark capacitance level dropped to 1.8×10^2 pf/$_{cm^2}$ and excitation gave a well resolved spectral dependence, with thresholds at 2.22, 2.40, 2.61 and 2.74 eV; see Fig. 7.1(b). In curve (b) two responses have been shown, the solid line curve was obtained by scanning the wavelength at a very slow speed, and the dotted curve was obtained using the point-by-point method. Obviously there was little difference between the two techniques. In another diode (No. 409-6), on ZnSe doped with 50 ppm gallium, the dark capacitance was 31.4×10^2 pf/$_{cm^2}$ and the room temperature photo-capacitance response, as shown in Fig. 7.2(a), had a threshold at 2.16 eV. Again at liquid nitrogen temperature, the dark capacitance dropped to 1.40×10^2 pf/$_{cm^2}$ and the photocapacitance as a function of photon energy was as shown in Fig. 7.2(b). As usual the solid line and dotted curves shown here were obtained using a slow scan and by the point-by-point methods respectively. Both techniques revealed similar thresholds which were at $h\nu$ = 2.25, 2.48, 2.54, 2.63 and 2.74 eV.

As discussed in Chapter 3, the capacitance of the depletion region is temperature dependent, see eqn. (3.4b),

$$C = \left(\frac{q \varepsilon_s N_d}{2} \right)^{\frac{1}{2}} \left(V_{do} + V_r - \frac{kT}{q} \right)^{-\frac{1}{2}}$$

and, C increases as T increases. Even if we use the depletion approximation,

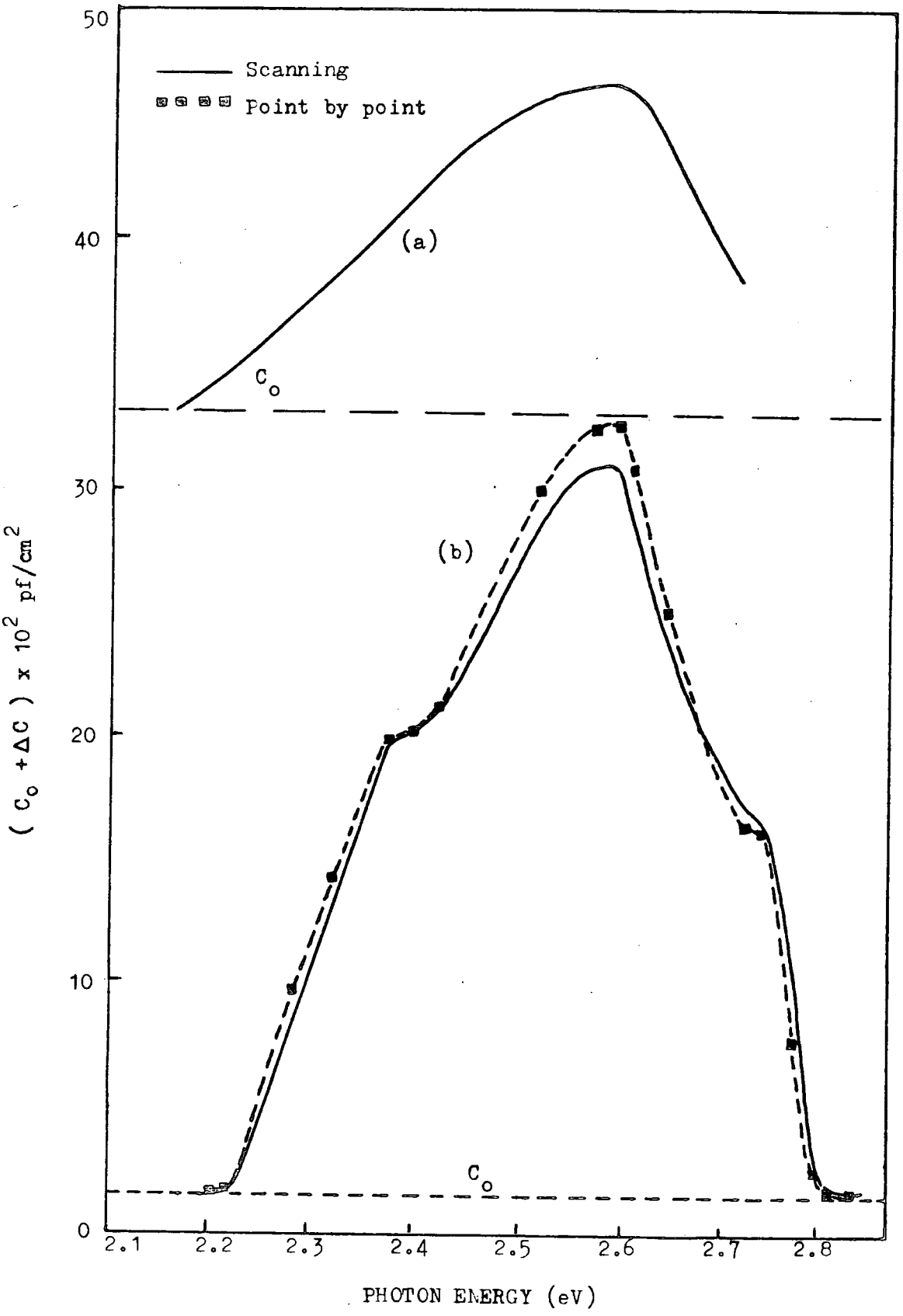

Fig 7.1 : Photocapacitance spectra for ZnSe:50ppm In (a) at room temperature and (b) at liquid nitrogen temperature. C_o is dark capacitance level.

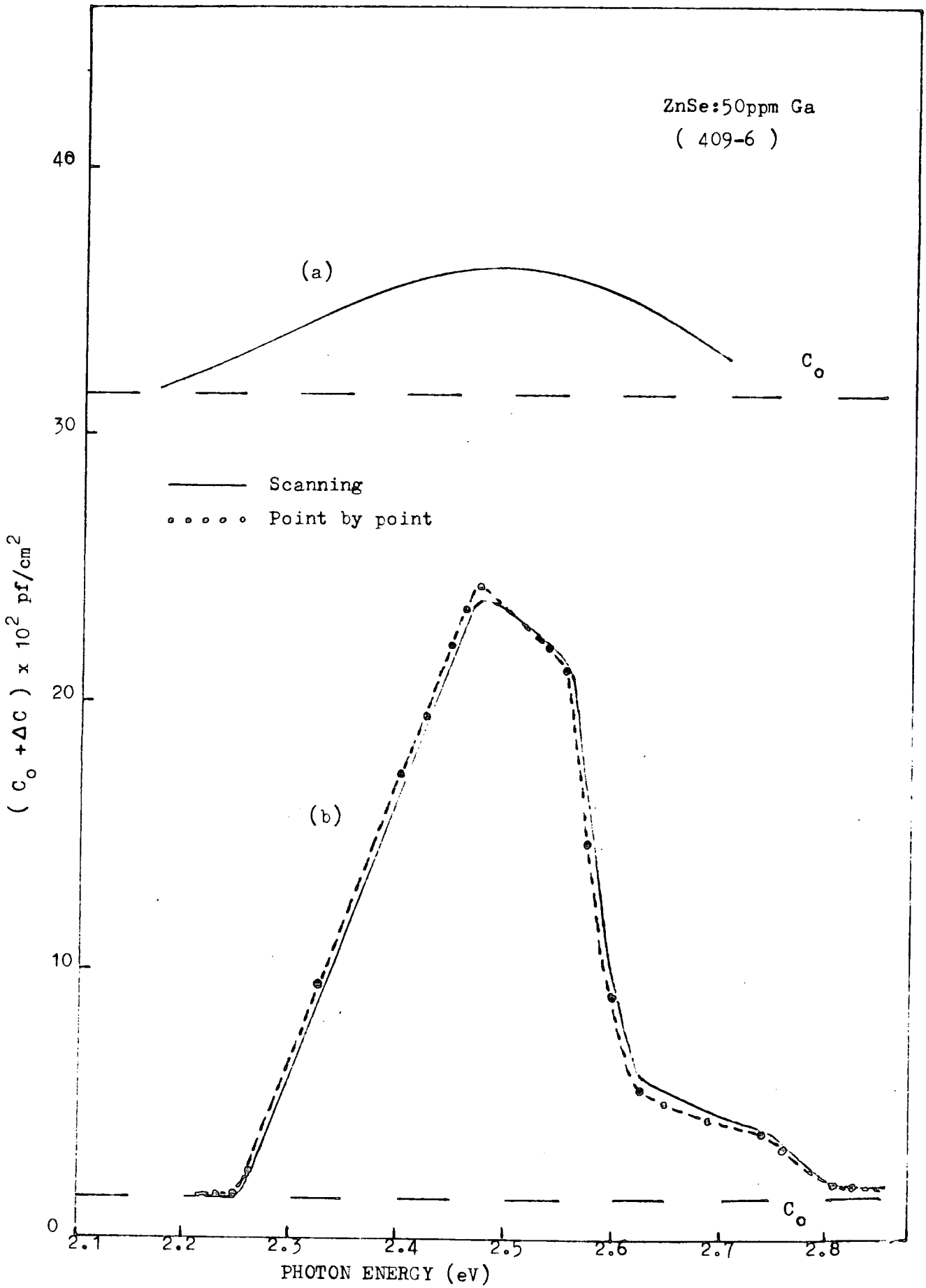

Fig 7.2 : Photocapacitance spectra for ZnSe:50ppm Ga, (a) at room temperature and (b) at liquid nitrogen temperature. C_o is dark capacitance level.

the capacitance of the depletion region, see eqn. (3.7a), shows a temperature dependent character due to the variation in the concentration of uncompensated donors N_d. At low temperature, the charge carriers freeze out into the shallow donors (in an n-type semiconductor) decreasing N_d, so that the width of the depletion region increases, producing a lower capacitance. The dark capacitance levels, C_o, in Figs. 7.1 and 7.2 follow this trend, but in photocapacitance the reverse was observed. The photocapacitance was much larger at low temperature. This is not clearly understood, but parameters such as impurity concentrations, capture and emission rates, absorption coefficient etc. are undoubtedly involved. At low temperature thermal capture and emission rates are negligible, and since the dark capacitance, C_o, was less at low temperature, the resolution in the photocapacitance spectrum was greatly improved and details were much more pronounced.

In order to see how the photocapacitance and the apparent positions of the defect levels varied with temperature, some preliminary measurements were made with increasing temperature starting at 82 K. In Fig. 7.3, the photocapacitance (ΔC) measured at four different temperatures for diode No. 405 - 12, formed on ZnSe doped with 50 ppm In, is illustrated by curves (a), (b), (c) and (d). At higher temperatures the shapes of the responses differ from the low temperature responses, and the values of ΔC decreased as the temperature increased. The first threshold on the low energy side shifted slightly from 2.22 to 2.20 eV as the temperature increased from 82 to 185 K, this is also illustrated in Fig. 7.4(a). At lower temperatures, there were four thresholds in the spectra associated with different deep and shallow centres, which are listed in Table 7.1(a).

The temperature dependence of the photocapacitance of a device on ZnSe : 50 ppm Ga, diode No. 409-7, is illustrated in Fig. 7.5, at six different temperatures. A shift in the threshold position on the low

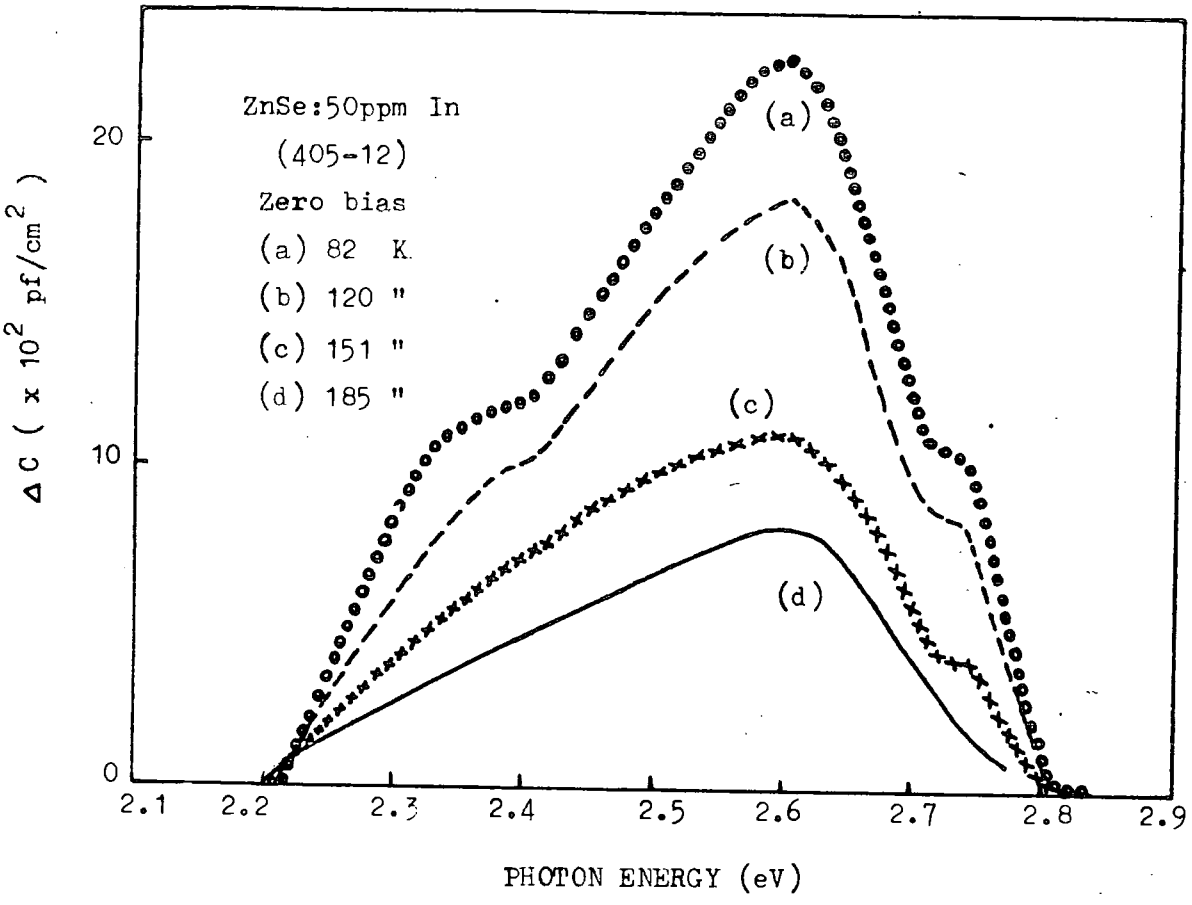

Fig 7.3 : Photocapacitance spectra for ZnSe:50ppm In at different temperatures.

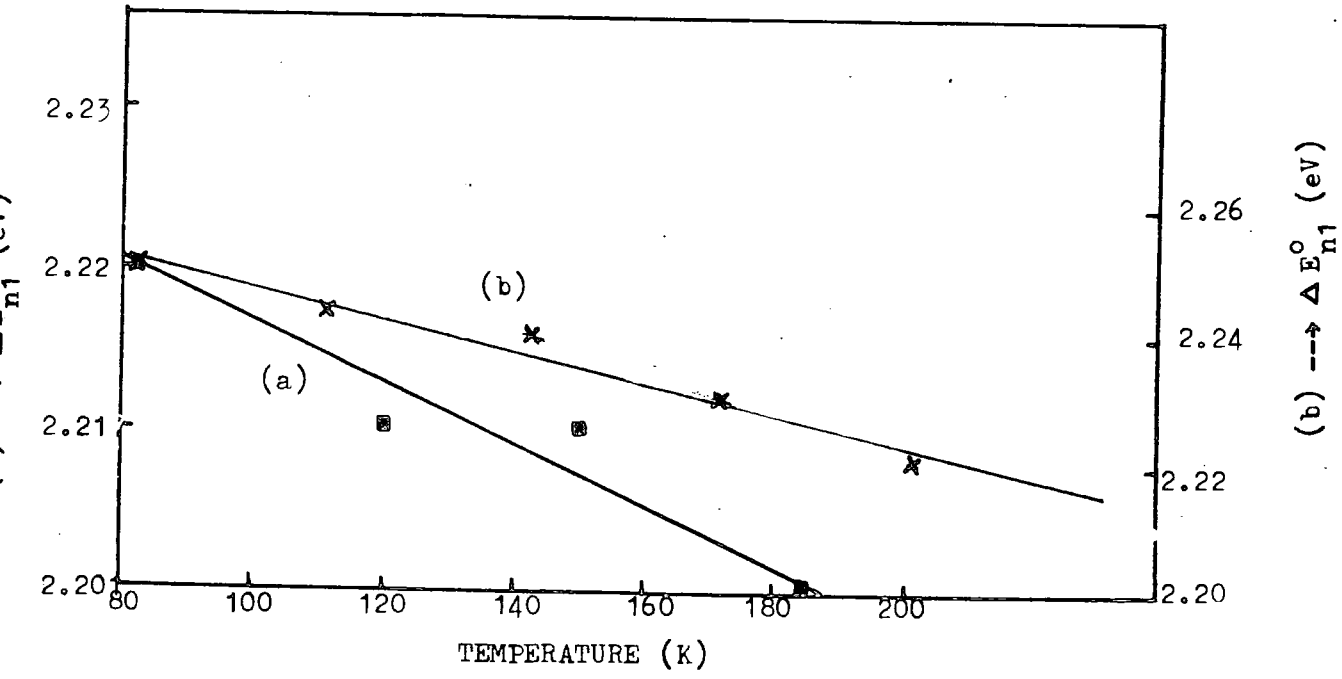

Fig 7.4 : Temperature dependence of optical thresholds
(a) ZnSe:50ppm In (see Fig. 7.3)
(b) ZnSe:50ppm Ga (see Fig. 7.5).

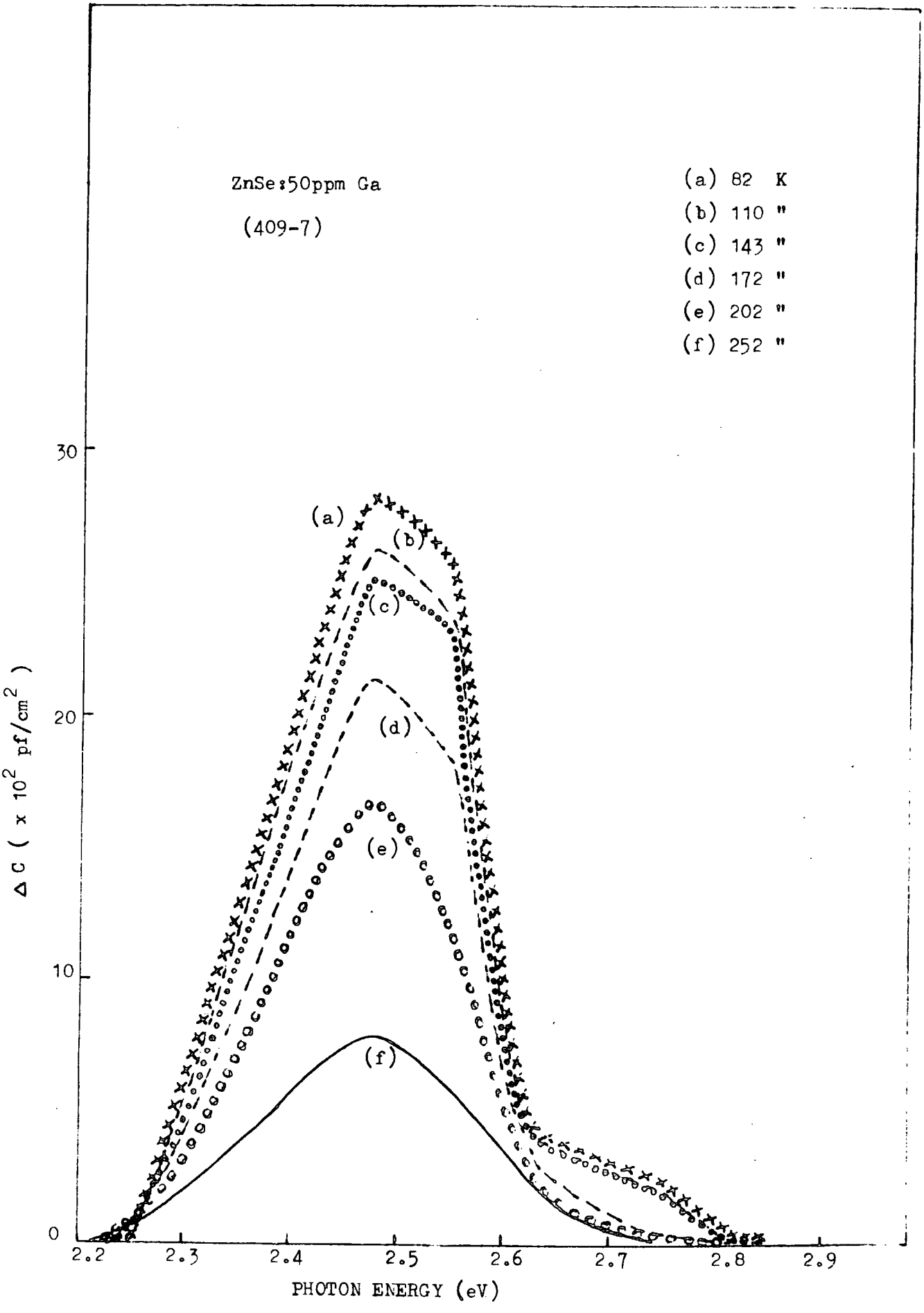

Fig 7.5 : Photocapacitance spectra for ZnSe:50ppm Ga at different temperatures.

TABLE 7.1 (a) : OPTICAL THRESHOLD POSITIONS AT DIFFERENT TEMPERATURES FOR ZnSe : 50 ppm In and ZnSe : Cu

Sample	Temp. (K)	Above V.B. (eV) / Below C.B. (eV)	Above V.B. (eV) / Below C.B. (eV)	Above V.B. (eV) / Below C.B. (eV)	Below C.B. (eV)
ZnSe : 50 ppm In (405-12)	82	0.58 / 2.22	0.40 / 2.40	2.61 / 0.19	0.03
	120	0.59 / 2.21	"	2.61 / 0.19	"
	151	0.59 / 2.21	"	"	"
	185	0.60 / 2.20	x	x	"
ZnSe : Cu (327-2)	83	0.67 / 2.13	0.12 / 2.68	2.48 / 0.32	0.02
	117	"	"	"	"
	148	"	"	"	"

TABLE 7.1 (b) OPTICAL THRESHOLD POSITIONS AT DIFFERENT TEMPERATURES FOR ZnSe : Ga

Sample	Temp. (K)	Above V.B. (eV) / Below C.B. (eV)	Above V.B. (eV) / Below C.B. (eV)	Above V.B. (eV) / Below C.B. (eV)	Above V.B. (eV) / Below C.B. (eV)	Below C.B. (eV)
ZnSe : 50 ppm Ga (409-7)	82	0.55 / 2.25	2.48 / 0.32	2.54 / 0.26	2.63 / 0.17	0.03
	110	0.56 / 2.24	"	"	"	"
	143	0.56 / 2.24	"	"	"	"
	172	0.57 / 2.23	"	"	"	x
	202	0.58 / 2.22.	"	x	"	x
	252	0.59 / 2.21	"	x	x	x
ZnSe : 100 ppm Ga (382-11)	83	0.53 / 2.27	x	2.55 / 0.25	2.62 / 0.18	0.03
	113	"	x	2,54 / 0.26	"	"
	125	"	x	"	"	"
	169	"	x	2.52 / 0.28	"	x

energy side of the spectrum was observed, which moved from 2.25 to 2.21 eV when the temperature was increased from 82 to 252 K. The shift in this threshold position is plotted in Fig. 7.4(b). All energy levels observed at different temperatures in this sample are listed in Table 7.1(b). In another device on gallium doped ZnSe, with a concentration of 100 ppm, diode No. 382-11, the photocapacitance curves shown in Fig. 7.6 were obtained. The first threshold was at 2.27 eV, practically the same energy as the first threshold in ZnSe : 50 ppm gallium. No shift with temperature was observed, but this may have been due to the very low magnitude of the photocapacitance obtained with this high resistance sample which reduced the resolution. A decrease in photocapacitance with increasing temperature, was also observed with this sample, as was obtained in samples doped with 50 ppm indium and gallium. The threshold levels observed at different temperatures for this sample are listed in Table 7.1(b).

These studies show that steady state photocapacitance measurements must be made at low temperatures, if the positions of different donors and acceptors with respect to the band edges are to be determined.

In ZnSe : 50 ppm In, low energy thresholds at 2.22 and 2.40 eV were observed at T = 82 K, see Fig. 7.1 (b), corresponding to two deep acceptors with levels at 0.58 and 0.40 eV above the valence band. This assumes that the bandgap energy at $\tilde{\sim}$ 82 K was 2.80 eV. The defects are identified as acceptors because the photocapacitance increased when they were emptied. Two more thresholds were also obvious in this sample at higher energies, one at 2.61 and the other at 2.74 eV. If donors in the depletion region are ionized in thermal equilibrium, then when they are filled optically with electrons, the photocapacitance will decrease. This happened with the thresholds at 2.61 and 2.74 eV. The corresponding donor depths therefore were 0.19 and 0.03 eV. The depth of the shallow donor (i.e. 0.03 eV) was determined using the Marfaing technique described in Chapter 3. The

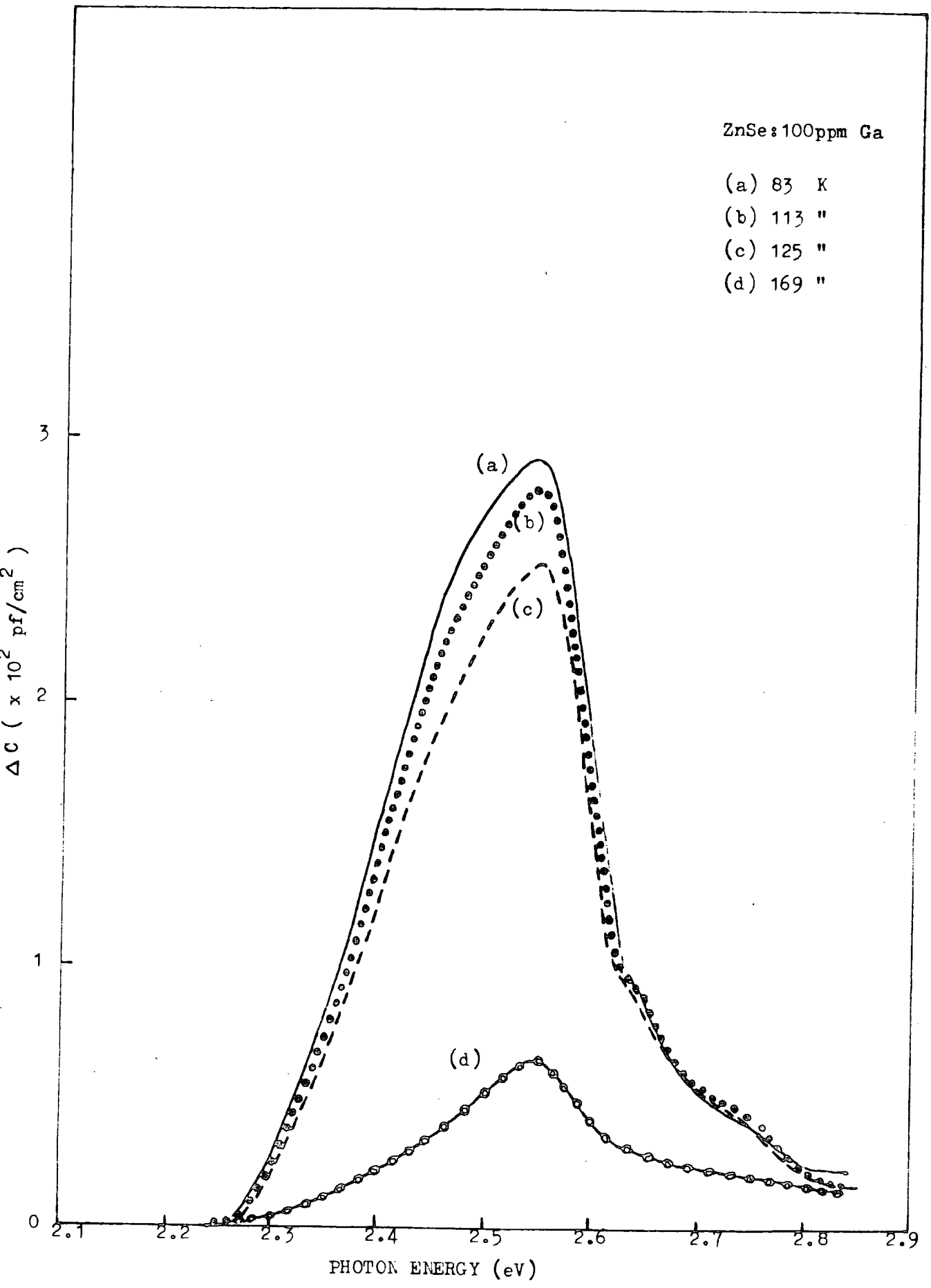

Fig 7.6 : Photocapacitance spectra for ZnSe:100ppm Ga at different temperatures.

same procedure was adopted for the determination of the positions of the donors and acceptors in ZnSe doped with 50 ppm gallium. The threshold with $h\nu$ = 2.25 eV, see Fig. 7.2(b), put the deep acceptor level at 0.55 eV above the valence band. Numerous donor levels were observed in this sample with energies of 0.32, 0.26, 0.17 and 0.03, corresponding to thresholds of $h\nu$ = 2.48, 2.54, 2.63 and 2.74 eV. The sample with a higher concentration (100 ppm) of gallium, (Fig. 7.6), had its low energy threshold at 2.27 eV giving the position of the deep acceptor at 0.53 eV above the valence band. The donors with $h\nu$ = 0.25, 0.18 and 0.03 eV were associated with thresholds at 2.55, 2.62 and 2.74 eV, see table 7.1(b).

A comparative investigation was done on copper doped ZnSe, diode 327-2, which had the temperature dependent photocapacitance illustrated by curves (a), (b) and (c) in Fig. 7.7. A large increase was observed at $h\nu$ = 2.13 eV which was associated with a deep acceptor lying 0.67 eV above the velence band. A shallow acceptor at 0.12 eV above the valence band was also indicated, associated with the sharp increase near $h\nu$ = 2.68 eV. Two donors, one at 0.32 eV and the other some 0.02 eV below the conduction band are also suggested by the two sudden decreases at $h\nu$ = 2.48 and 2.76 eV, respectively. The temperature dependence of the photocapacitance was similar to that of the other samples, i.e. ΔC decreased slightly as the temperature increased. The levels found for this sample at different temperatures are given in Table 7.1(a).

The low energy thresholds in both the indium or gallium (50 ppm) doped devices shifted from higher to lower energies as the temperature increased. This is attributable to changes in the band gap with temperature. Similar threshold shifts have been reported by Grimmeiss et al (1976) in Mn-doped ZnSe.

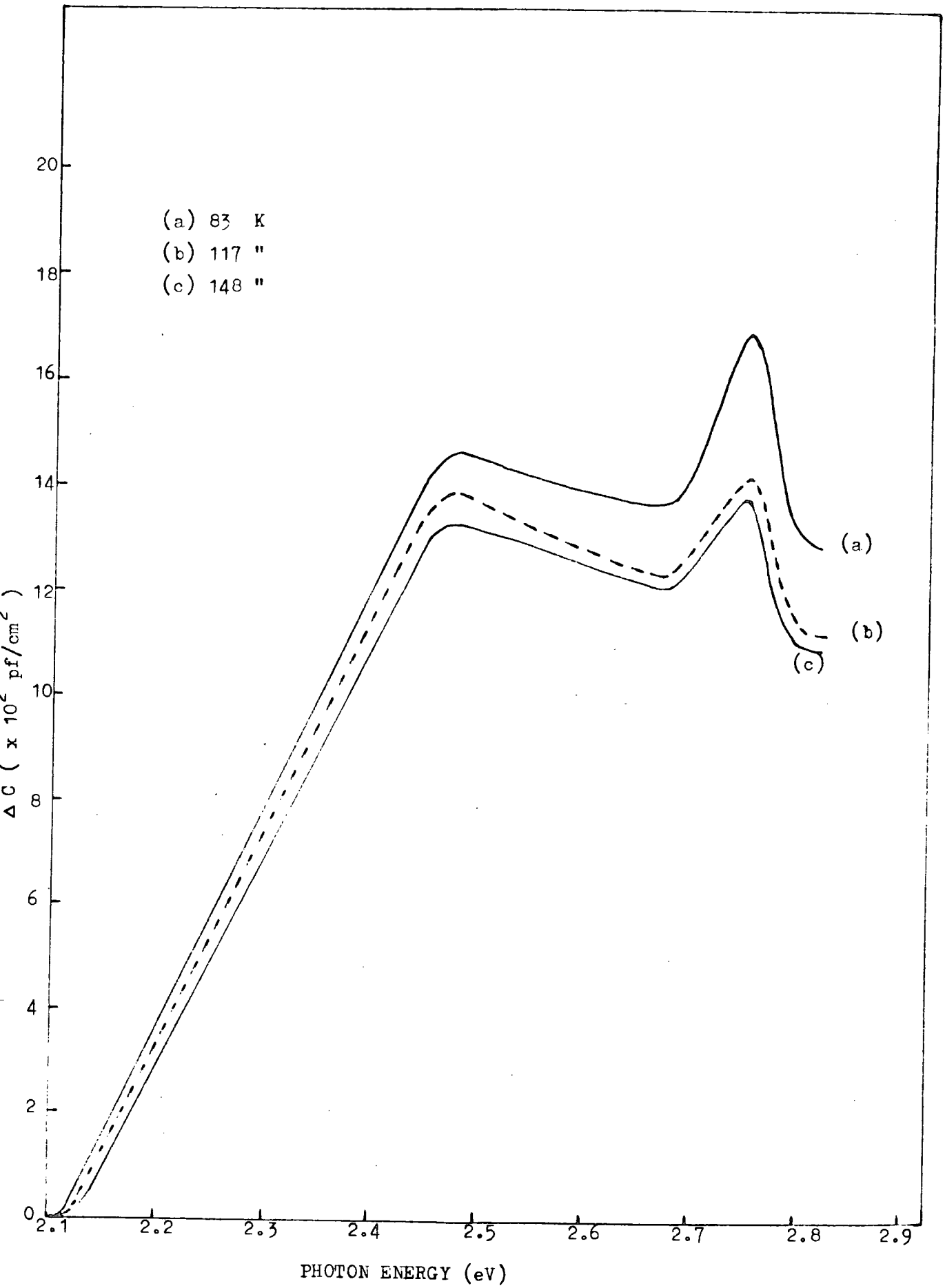

Fig 7.7 : Photocapacitance spectra for ZnSe:Cu at different temperatures.

7.3 FREQUENCY AND BIAS DEPENDENCE OF THE PHOTOCAPACITANCE

(a) Frequency Dependence

In this section the effect of varying the measuring frequency on the photocapacitance is described. There is a considerable literature on the frequency dependence of the dark capacitance, but there is very little about photocapacitance. For example, Roberts and Crowell (1970), Beichler, et al (1980), Viktorovitch and Jousse (1980) and, Viktorovitch (1981) described the frequency dependence of the dark capacitance of Schottky diodes, while Sah and Reddi (1964) and Kimerling (1974) studied the effects in p-n junctions. These authors describe how the occupancies of the band gap states and interface states are modulated by frequency and thus make a contribution to the capacitance of the barrier region. In the absence of gap states, or if no modulation were taking place, the measured capacitance would be, see eqn. (3.7a), $\varepsilon_{s/w}$. However, the gap states do not fill or empty instantaneously during modulation and these processes depend on how ω_s (the signal frequency) compares with the inverse of the time constant of the traps . At low frequencies, the traps follow the signal variations and contribute to the capacitance, see eqn. (3.10), Chapter 3. In Schottky diodes the measured capacitance is a function of the depletion region capacitance (C_D), trap capacitance (C_T) and surface state capacitance (C_S), see Chapter 3. At high frequencies, where traps do not follow the signal, C_T and C_S are negligible and the measured capacitance is simply the capacitance of the depletion region, see Viktorovitch, Jousse (1980) and Rhoderick (1980).

Experimentally, Vincent et al (1975) and Beichler, et al (1980) and many others, have found that the measured capacitance of a diode is inversely proportional to signal frequency. As the frequency decreases the capacitance increases indicating the positive contribution of gap or interface states. This type of behaviour was also a feature of our photocapacitance measurements.

The photocapacitance spectra measured in the range of frequencies from 200 to 20 kHz, at liquid nitrogen temperature, are illustrated in Fig. 7.8, for a diode on ZnSe : 50 ppm In, obtained from boule No. 405. The high frequency responses are similar to that illustrated in Fig. 7.1, as described before; but at 20 kHz, Fig. 7.8 (g), the response shows a new feature with no indication of the presence of donors or acceptors, on excitation with photons with near bandgap energies. Another diode on ZnSe with the same indium concentration, but cut from a different boule No. 375, had the frequency dependent photocapacitance shown in Fig. 7.9. This particular crystal had a high resistivity in comparison with the previous one (diode No. 405-8) and this probably explains the low magnitude of the photocapacitance. The spectral response curve at 20 kHz for diode No. 375-6 was different from those measured at high frequencies and again showed no sign of the familiar thresholds for near bandgap excitation. Instead new thresholds were observed, corresponding to donor levels at 0.12 and 0.31 eV. All the thresholds found in diodes (405-8) and (375-6) at different frequencies are tabulated in Table 7.2(a).

The highest values of the photocapacitance at 2.50 - 2.60 eV, plotted against measuring signal frequency, are shown in Fig. 7.10. The curves clearly illustrate the pattern of an increase in photocapacitance with decreasing frequency. The low frequency response is probably a measure of the contribution of the interface and gap states.

Similar behaviour was also observed in gallium doped ZnSe crystals. Fig. 7.11 shows the frequency dependence of the photocapacitance curve in diode No. 409 - 5, on ZnSe with 50 ppm gallium. In another device on ZnSe with 100 ppm gallium, diode No. 382-1, the measured photocapacitance was as shown in Fig. 7.12. The high resistivity of this sample was again responsible for the low values of photocapacitance. The low frequency

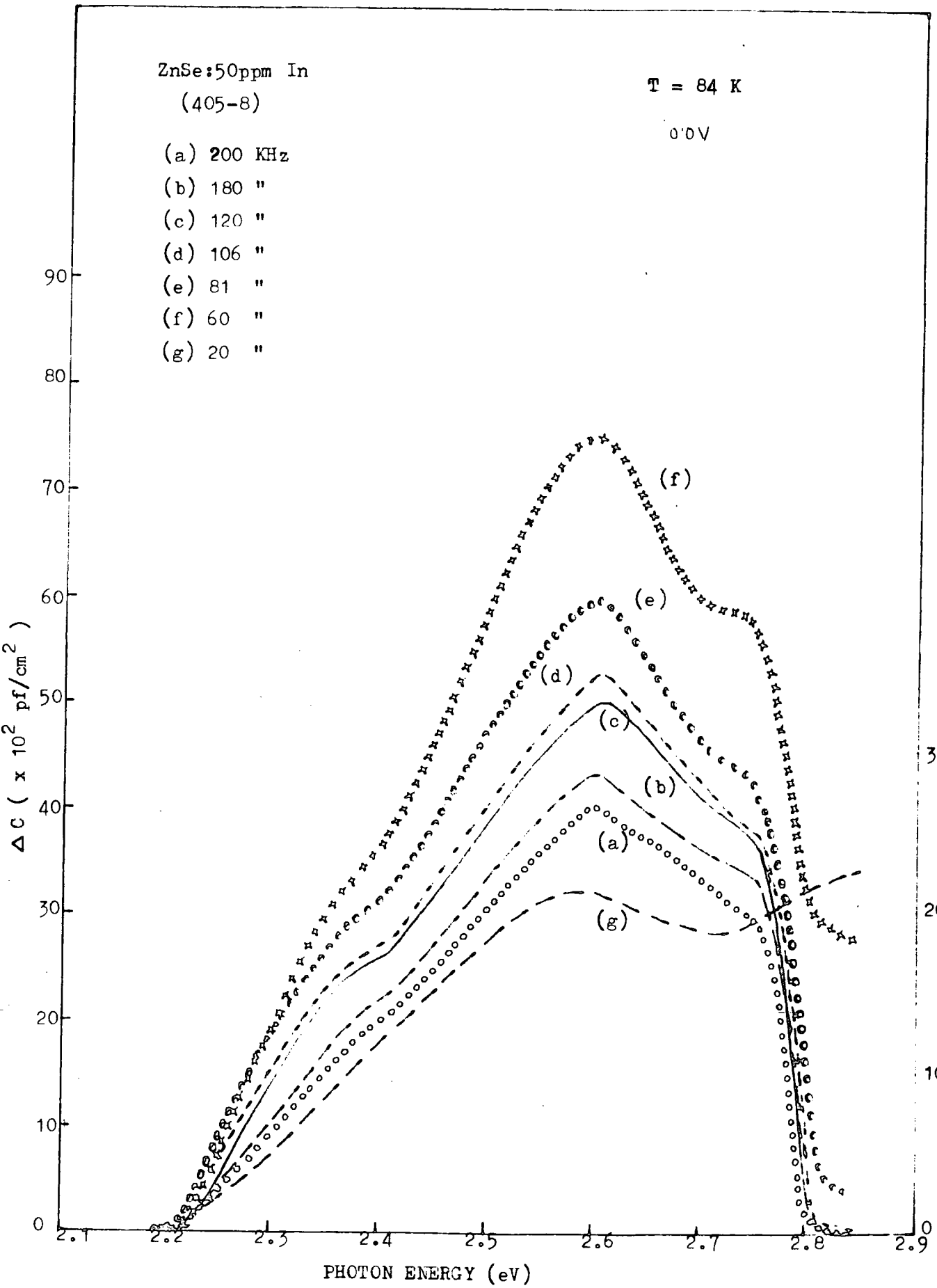

Fig 7.8 : Photocapacitance spectra for ZnSe:50ppm In at different measuring signal frequencies.

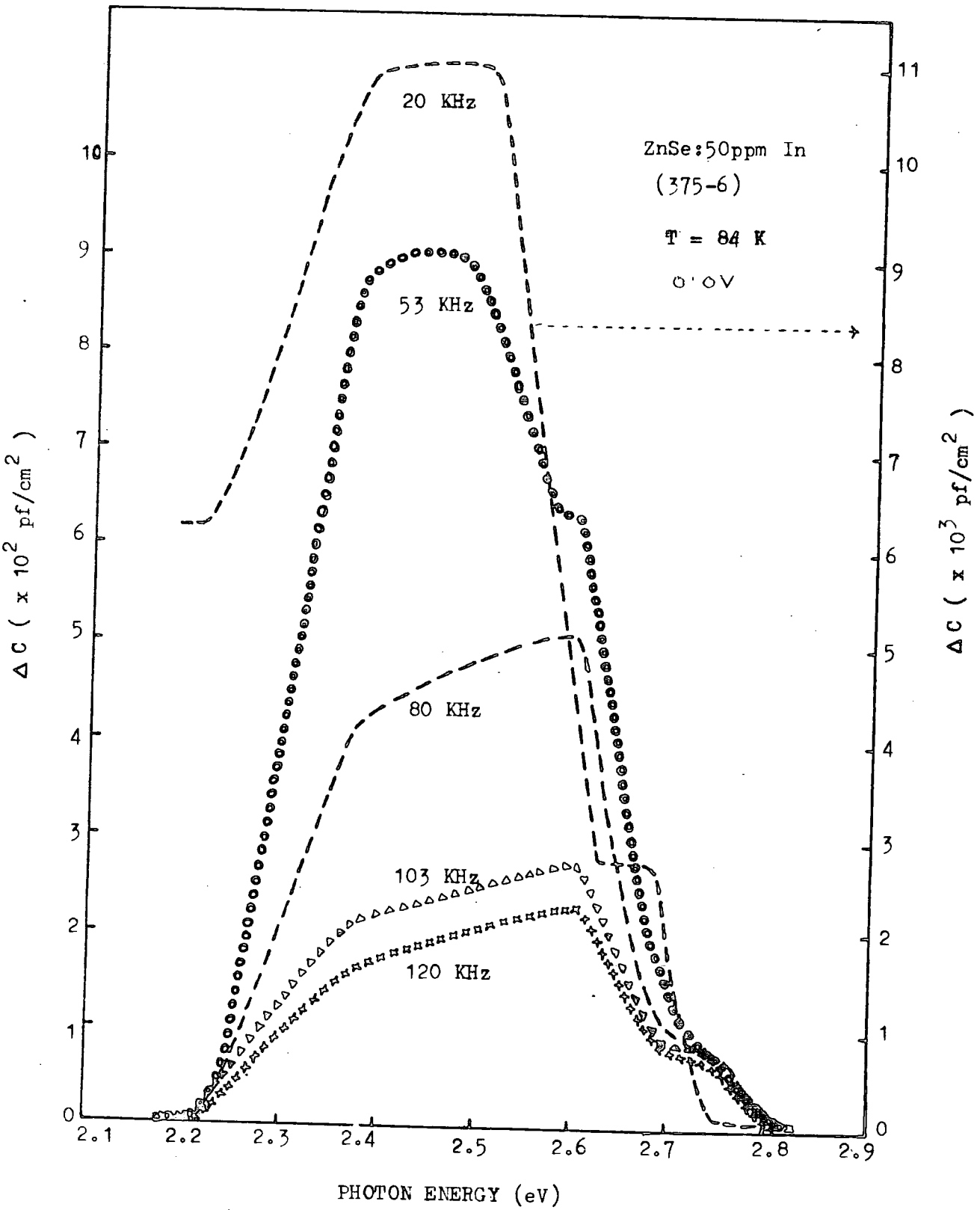

Fig 7.9 : Photocapacitance spectra for ZnSe:50ppm In at different measuring signal frequencies.

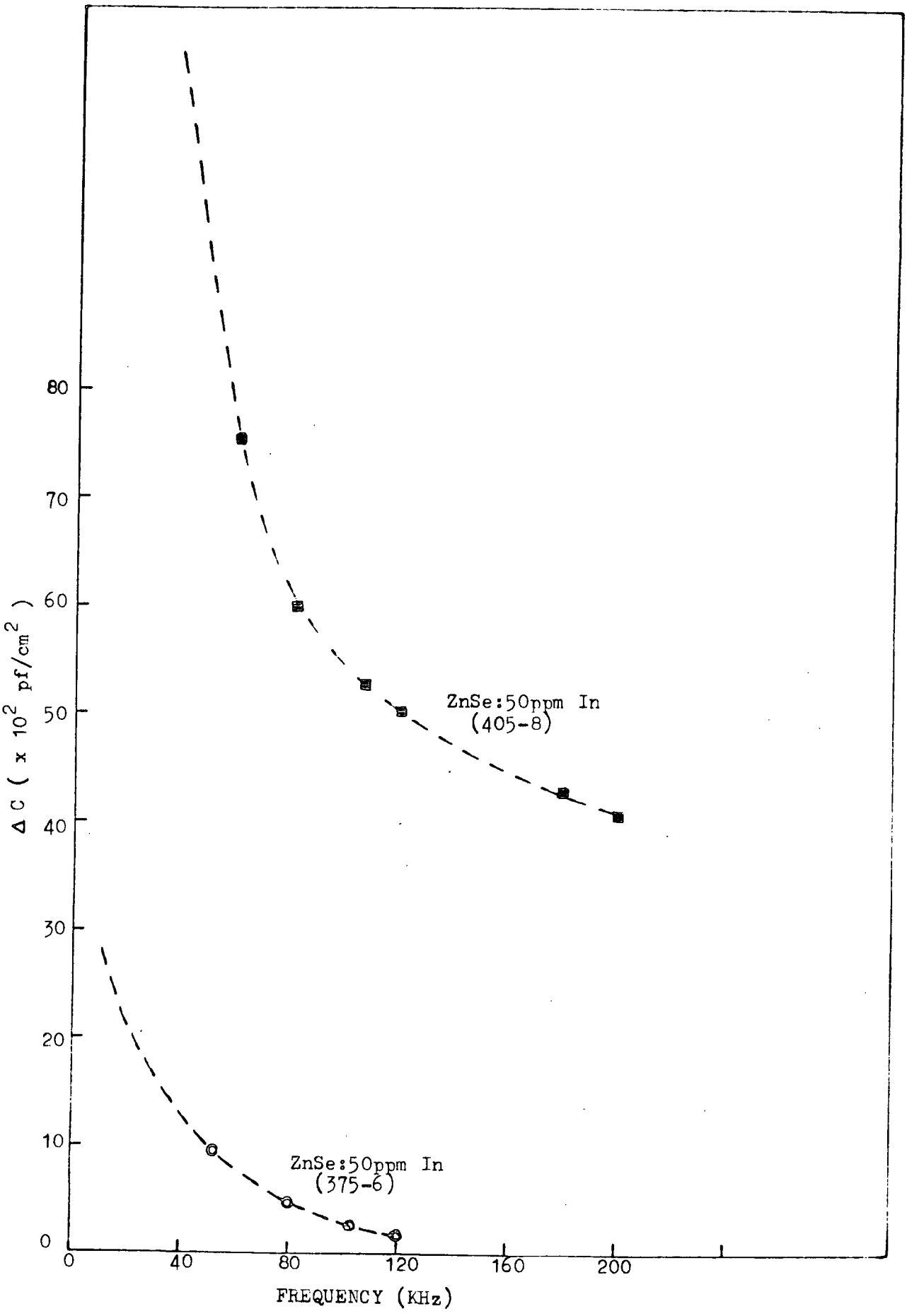

Fig 7.10 : Plot of maximum peak value photocapacitance (from Figs. 7.8 & 7.9) against measuring signal frequency.

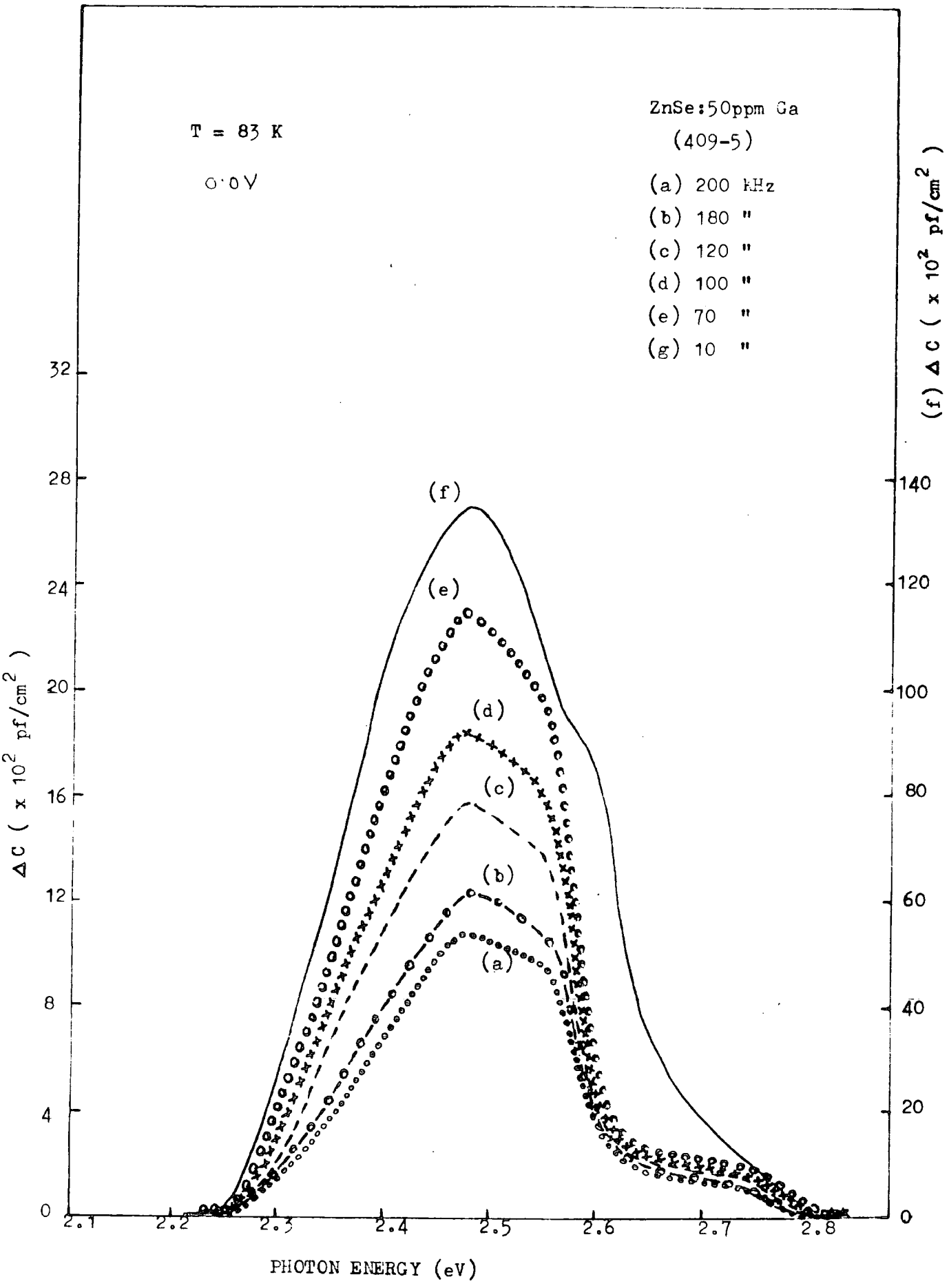

Fig 7.11 : Photocapacitance spectra for ZnSe:50ppm Ga at different measuring signal frequency

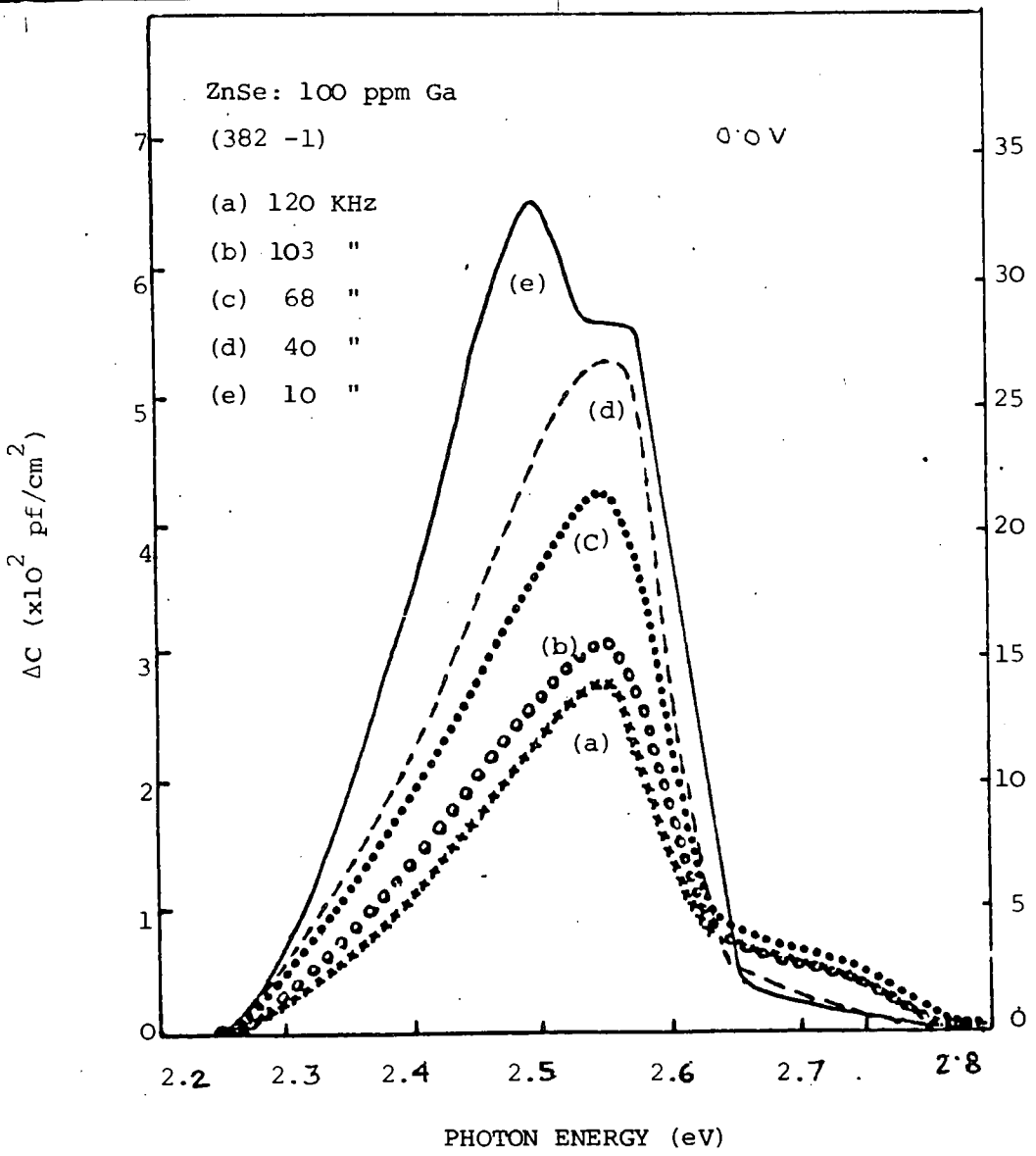

Figure 7.12 : Photocapacitance spectra for ZnSe:100 ppm Ga at different measuring signal frequency.

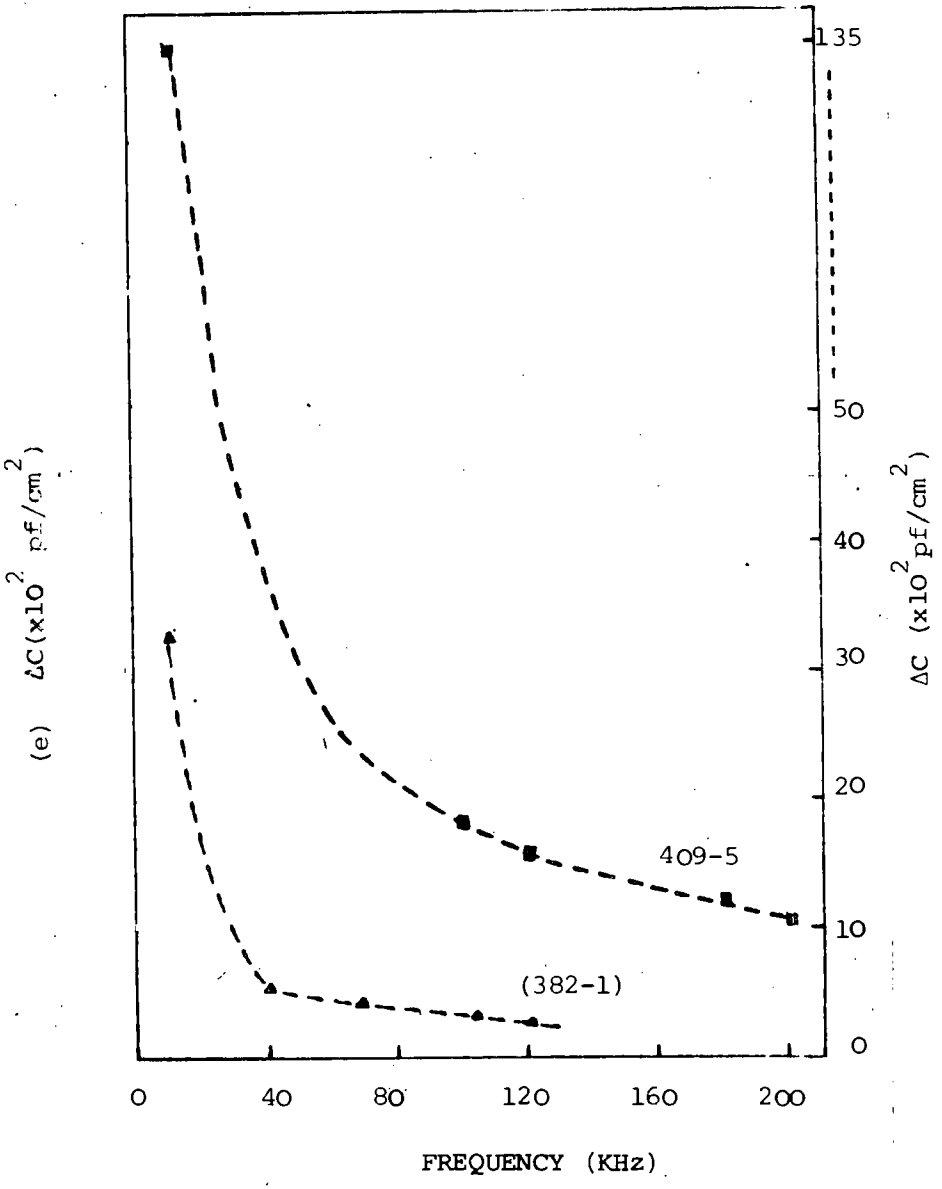

Figure 7.13 : Plot of maximum peak value photocapacitance (from Figs 7.11 & 7.12) against measuring signal frequency.

TABLE 7.2(a) OPTICAL THRESHOLD POSITIONS AT DIFFERENT MEASUREMENT FREQUENCIES FOR ZnSe : In

Sample	Frequency (KHz)	Above V.B. (eV) / Below C.B. (eV)	Above V.B. (eV) / Below C.B. (eV)	Above V.B. (eV) / Below C.B. (eV)	Above V.B. (eV) / Below C.B. (eV)	Below C.B. (eV)
ZnSe : 50 ppm In (405 - 8)	200	0.58 / 2.22	0.41 / 2.39	2.61 / 0.19		0.03
	180	"	"	"		"
	120	"	"	"		"
	106	"	"	"		"
	81	"	"	2.60 / 0.20		"
	60	"	"	"		0.02
	20	"	x	x		x
ZnSe : 50 ppm In (375 - 6)	120	0.58 / 2.22	0.42 / 2.38	2.60 / 0.20	x	0.03
	103	"	"	"	x	"
	80	"	"	"	x	"
	53	"	x	2.48 / 0.32	2.60 / 0.20	"
	20	0.59 / 2.21	x	2.49 / 0.31	2.68 / 0.12	x

TABLE 7.2 (b) OPTICAL THRESHOLD POSITIONS AT DIFFERENT MEASUREMENT FREQUENCIES FOR ZnSe : Ga

Sample	Frequency (KHz)	Above V.B. (eV) / Below C.B. (eV)	Above V.B. (eV) / Below C.B. (eV)	Above V.B. (eV) / Below C.B. (eV)	Above V.B. (eV) / Below C.B. (eV)	Below C.B. (eV)
ZnSe : 50 ppm Ga (409 - 5)	200	2.25 / 0.55	2.48 / 0.32	2.55 / 0.25	2.63 / 0.17	0.03
	180	"	"	"	"	"
	120	"	"	"	"	"
	100	"	"	"	"	"
	70	"	"	"	"	"
	10	"	"	2.58 / 0.22	x	x
ZnSe : 100 ppm Ga (382 - 1)	120	2.27 / 0.53	2.54 / 0.26	2.62 / 0.18		0.03
	103	"	"	"		"
	68	"	"	"		"
	10	"	2.50 / 0.03	2.57 / 0.23	2.65 / 0.15	x

responses in both diodes were peculiar. The inverse relation between photocapacitance and frequency was obvious and is illustrated in Fig. 7.13. The different thresholds at different frequencies observed in 50 and 100 ppm gallium doped diodes are tabulated in Table 7.2(b).

The frequency response of the photocapacitance appears to have two parts : (a) a smooth rise in photocapacitance as the frequency decreases from 200 kHz and, (b) a steeper exponential increase at much lower frequencies. The small and smooth increase in the photocapacitance with decreasing frequency, in the higher frequency range is dominated by the depletion region capacitance. However, at lower frequencies surface states begin to contribute to the capacitance (for example in the region near 60 kHz). This is supported by the work of Ozsan and Woods (1975, 1977), who proposed that there is always an insulating oxide layer between the gold and the semiconductor ZnSe in Schottky devices, when prepared on chemical etched surfaces. In the presence of an insulating layer the role of surface states at low frequency is important.

(b) Bias Dependence

The space charge region, $W-W_o$, which is close to the barrier contact of the Schottky diode is bias dependent and most active in optical phenomena, Braun and Grimmeiss (1973). An increase in reverse bias increases the width of the space charge region and in turn the number of ionized defect centres. The photocapacitance should change accordingly if the centres are distributed throughout the bulk of the crystal. In order to study this the photocapacitance - bias responses shown in Figs. 7.14 - 7.18 were recorded. Before making the measurements the deep acceptors were filled by a preliminary illumination lasting for at least 3 minutes.

The responses for diode 405 - 9, doped with 50 ppm indium, are shown in Fig. 7.14, where biases between 0 and -6 volt were applied. The

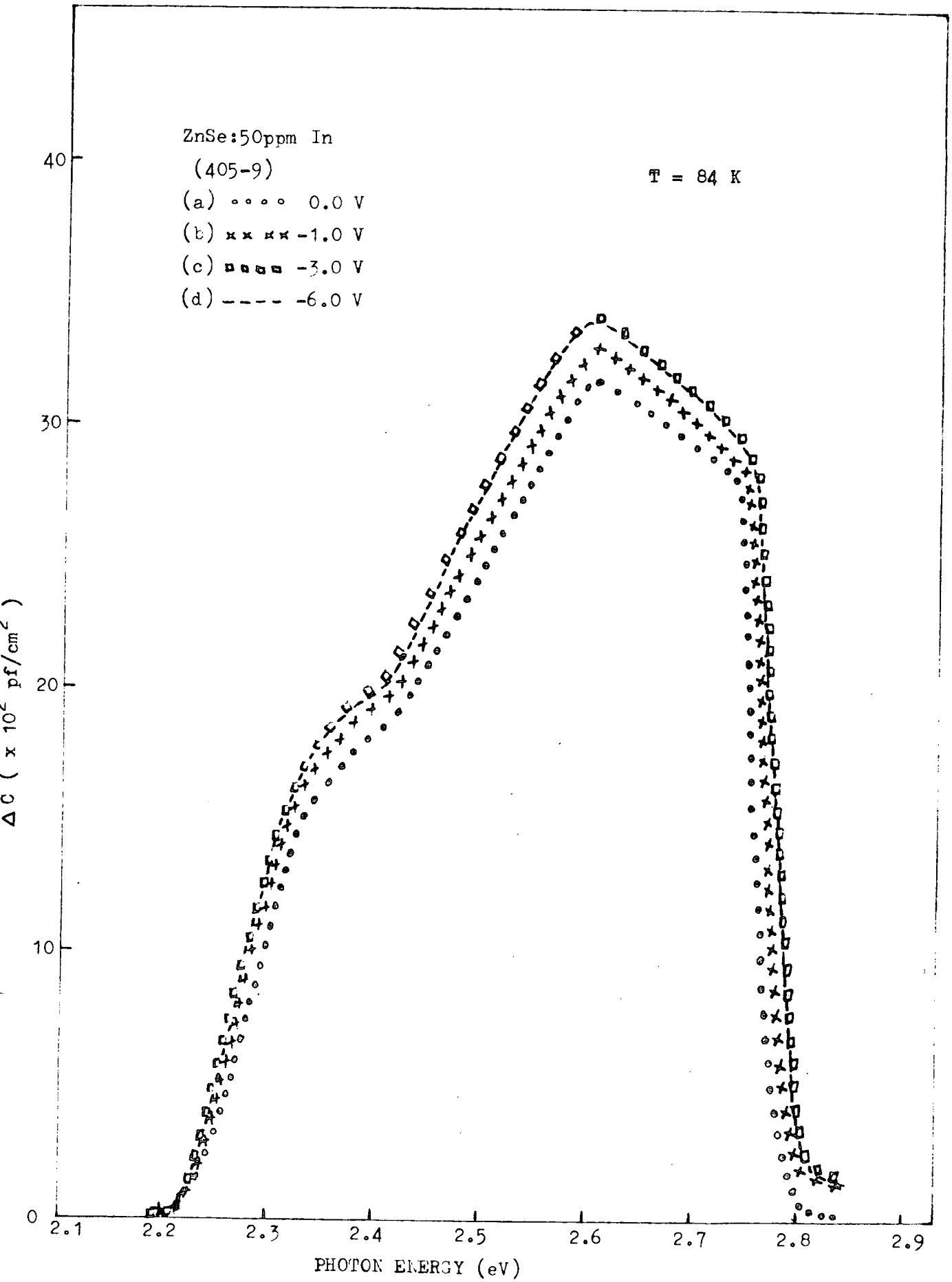

Fig 7.14 : Photocapacitance spectra for ZnSe:50ppm In at different reverse bias.

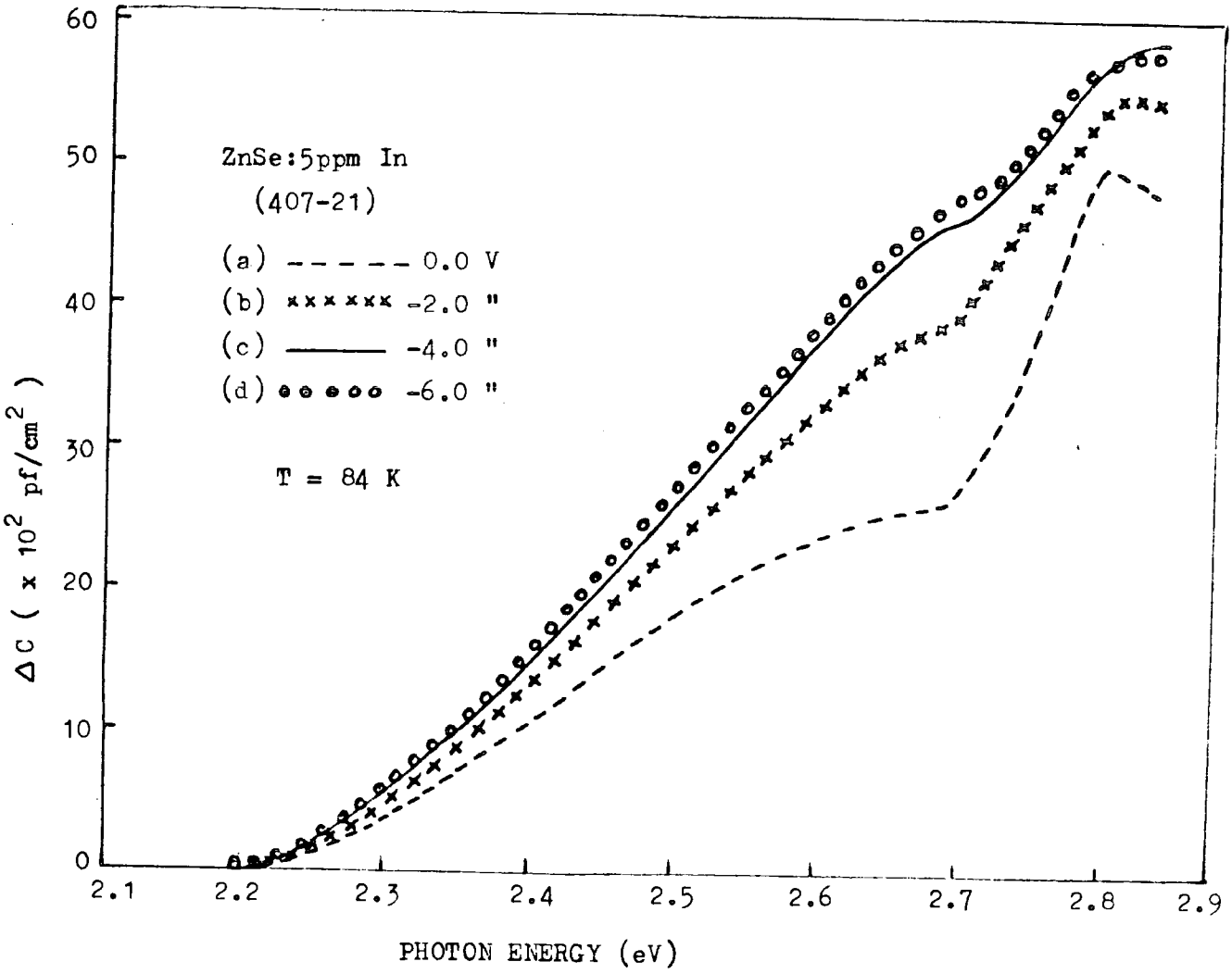

Fig 7.15 : Photocapacitance spectra for ZnSe:5ppm In at different reverse bias.

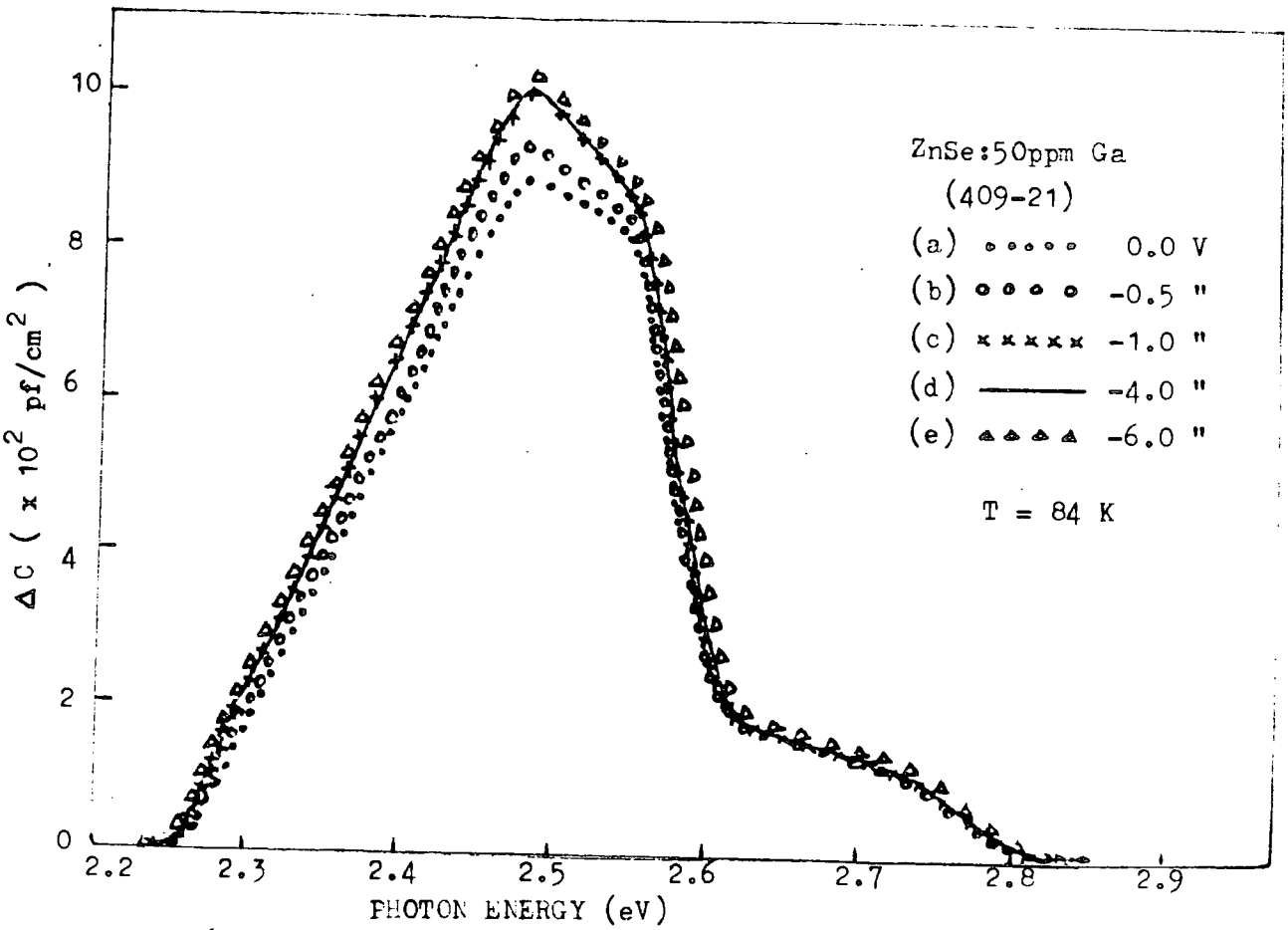

Fig 7.16: Photocapacitance spectra at different reverse bias for ZnSe:50ppm Ga.

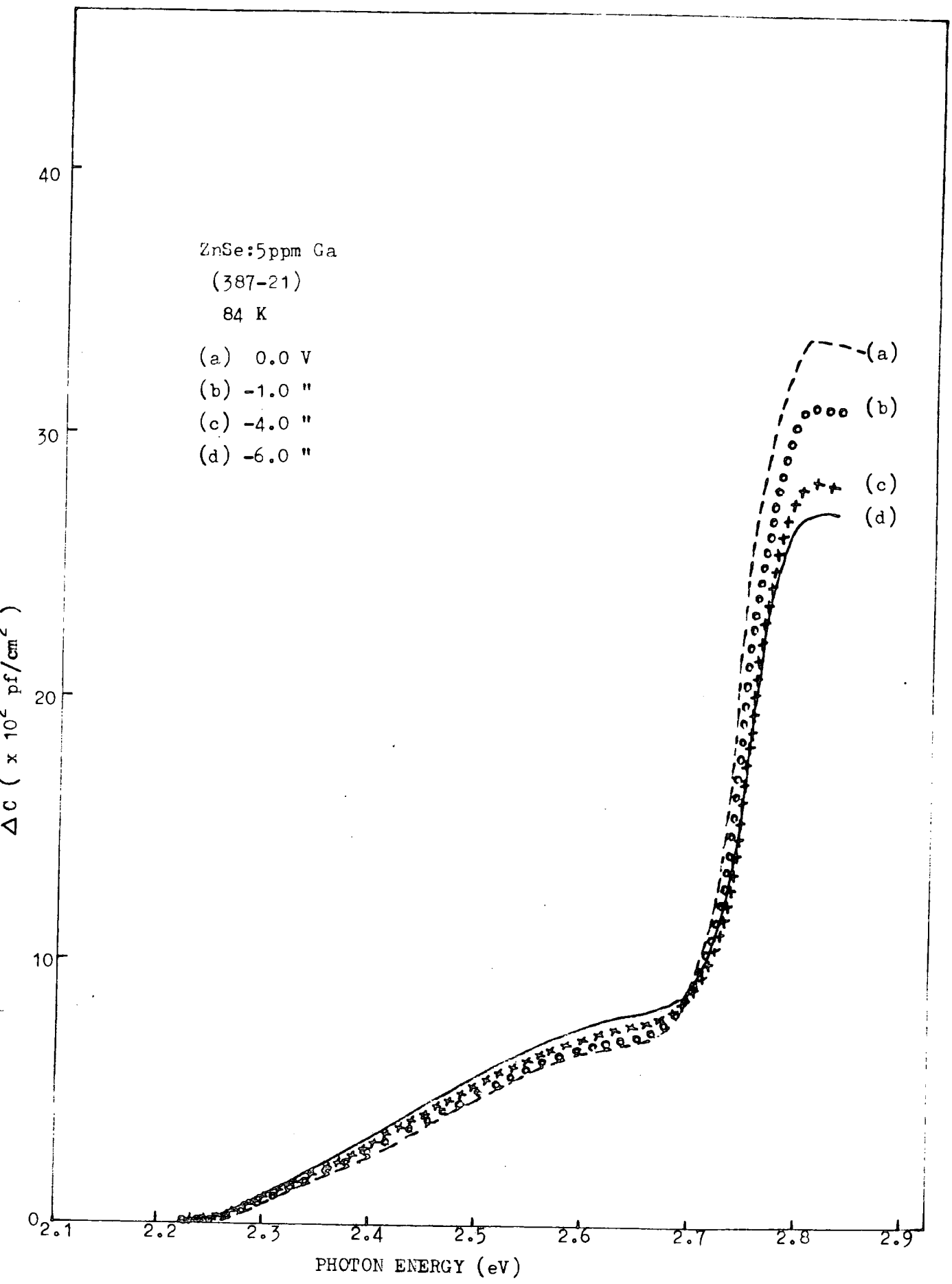

Fig 7.17: Photocapacitance spectra for ZnSe:5ppm Ga at different reverse bias.

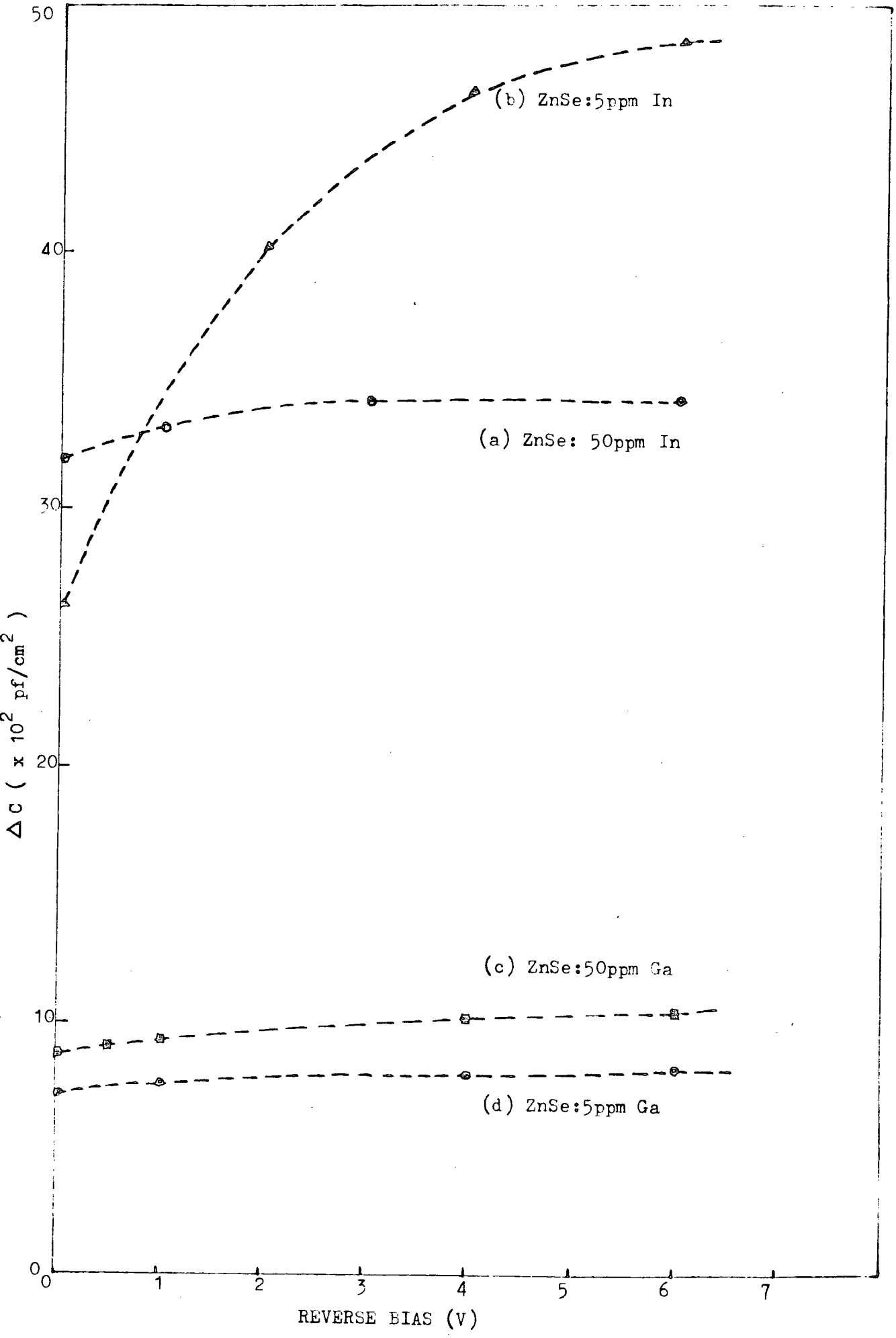

Fig 7.18: Dependence of photocapacitance (see Figs 7.14-7.17) on reverse bias for different samples.

photocapacitance corresponding to centres with thresholds at 2.22 and 2.40 eV increased slightly with increasing reverse bias which showed that these centres were present in the bulk. The maximum photocapacitance at $h\nu \sim 2.60$ eV at different biases extracted from Fig. 7.14 is plotted in Fig. 7.18(a). This shows that the photocapacitance increased by 7% when the bias changed from 0 to -3V and thereafter no change was observed when the bias increased to -6V. With a lightly (5 ppm In) doped diode, No. 407 - 21, the bias dependent photocapacitance was as illustrated in Fig. 7.15. The photocapacitance response corresponding to the low energy threshold ($h\nu$ = 2.22 eV) increased with increasing bias, (see Fig. 7.18b), while the response associated with the threshold near 2.68 eV was very prominent at zero bias, but less pronounced as the reverse bias was increased.

In diode 409 - 21, ZnSe : 50 ppm Ga, the maximum value of photocapacitance near $h\nu \sim 2.48$ eV increased slightly with increasing reverse bias, Fig. 7.16. This is also illustrated in Fig. 7.18(c). With ZnSe : 5 ppm Ga, diode 387 - 21, the photocapacitance response with a threshold at $h\nu \sim 2.25$ eV related to the deep acceptor showed a slight increase with bias, see Figs. 7.17 and 7.18 (d). However, the response at higher photon energy near the bandgap was similar to that found in ZnSe : 5 ppm In in that it decreased with increasing reverse bias.

These measurements suggest that the deep acceptors associated with the 2.22 or 2.25 eV thresholds in the indium or gallium doped ZnSe are present in the bulk of the crystal. The diodes showed negligibly small changes in the photocapacitance associated with donor levels. This type of behaviour has been discussed by Lindquist and Bube(1972) in their studies of photocapacitance in Cu_2S - CdS heterojunctions. According to them, bias independence demonstrates that the centres responsible for photocapacitance are localized in the depletion region at zero bias, i.e. near the surface.

7.4 INFRA-RED QUENCHING OF PHOTOCAPACITANCE

An investigation of deep acceptors (i.e. Class II centres) present in the indium and gallium doped ZnSe was also carried out using infra-red quenching of photocapacitance (IQ-PHCAP). The infra-red quenching of photocurrent (IQ-PC) in these samples has already been described, see Chapter 5. The main difference between the two methods lies in the range of the resistivities of the samples which can be measured. The IQ-PHCAP technique is useful for low resistivity samples where Schottky diodes are easily fabricated. On the other hand IQ-PC technique can be used with high resistivity samples. During the photocapacitance quenching measurements the centres were first emptied using continuous primary irradiation, then they were filled with electrons from the valence band excited by the infra-red. The spectral distributions were recorded at liquid nitrogen temperature with zero bias using the step-by-step method and are shown in Figs. 7.19 - 7.22.

The first curve drawn in Fig. 7.19 belongs to diode 407 - 17, fabricated from 5 ppm indium doped ZnSe. This was a comparatively low resistivity sample so that an investigation of the sensitizing centres by photocurrent quenching was impossible, however the photocapacitance quenching technique proved successful. When the centres had been emptied, curve (a) was recorded by irradiating the sample with tungsten light passing through combined 0.44 μm band pass and infra-red absorbing filters. The low energy threshold was at 0.59 eV and the maximum infra-red quenching was 91% at $h\nu_s \tilde{\sim}$ 0.80 eV. When the primary excitation was passed through combined 0.52 μm and I-R absorbing filters the maximum quenching was 96% and the low energy quenching threshold was at 0.60 eV; see curve (b). With a device on ZnSe doped with 20 ppm indium, diode No. 413-17, the quenching spectrum shown in Fig. 7.20 (a) was obtained. The quenching began at $h\nu_s$ = 0.59 eV and increased to a maximum value 77.7% at $h\nu_s \sim$ 1.0 eV.

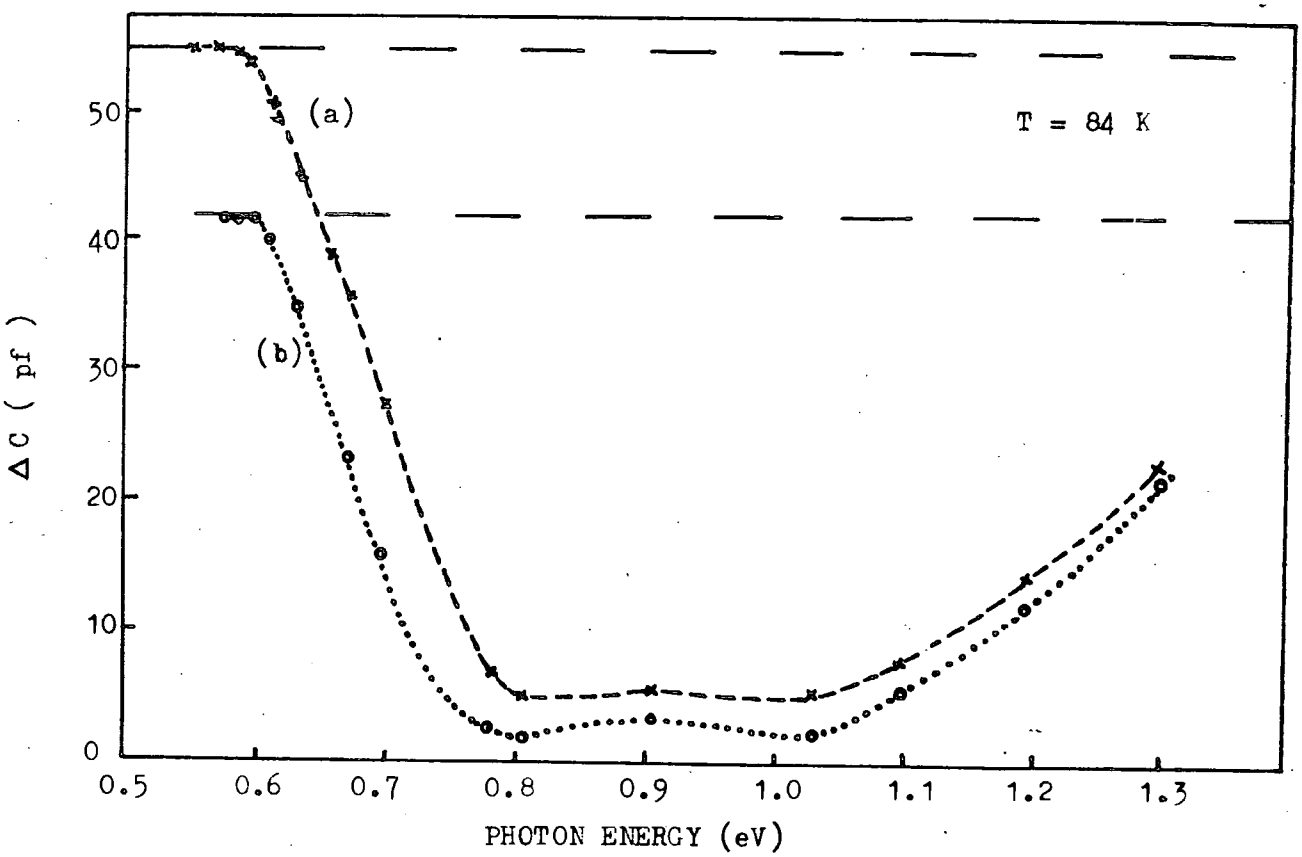

Fig 7.19 : Infra-red quenching of photocapacitance for ZnSe:5ppm In at different primary excitations (a) using 0.44 μm + IR abs. filters, and (b) using 0.52 μm + IR abs. filters.

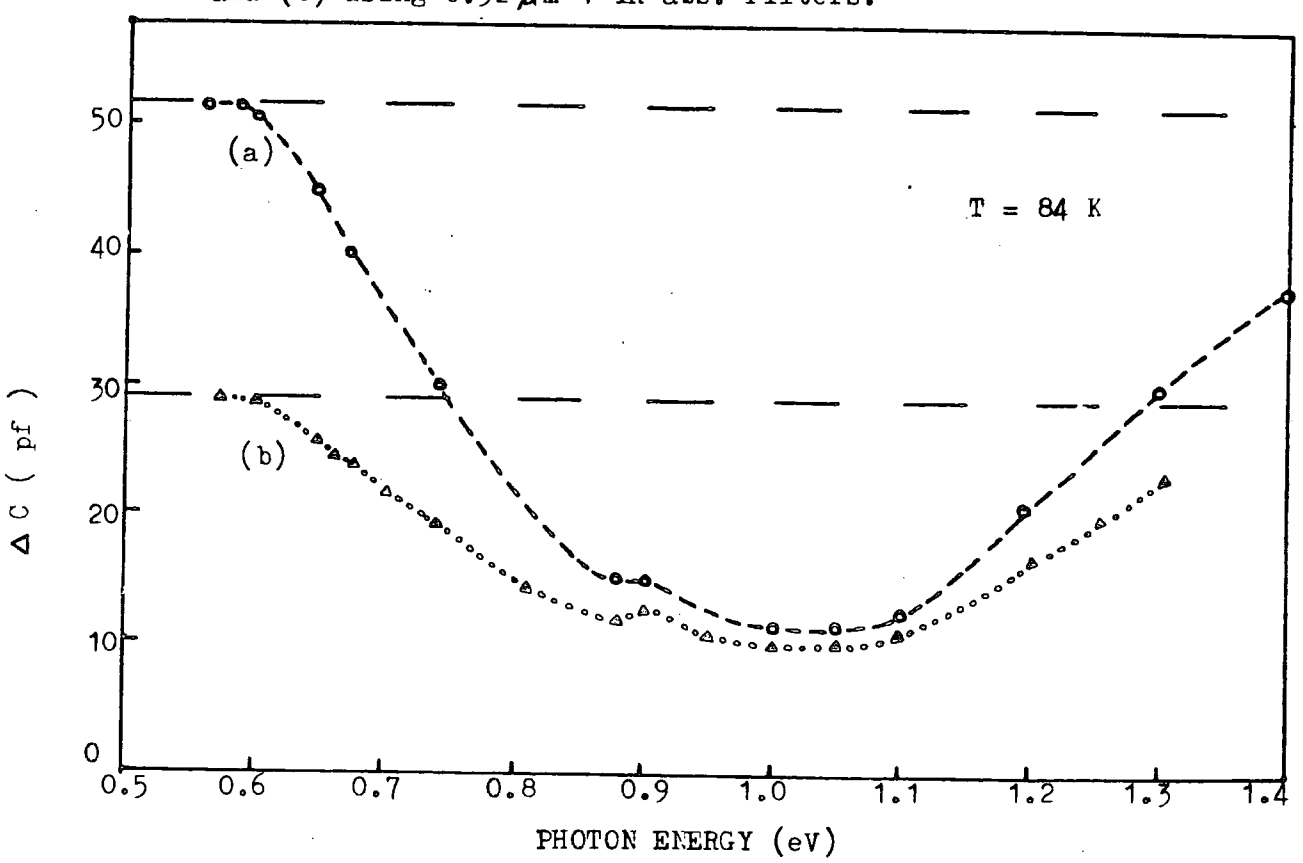

Fig 7.20 : Infra-red quenching of photocapacitance for (a) ZnSe:20ppm In and (b) ZnSe:50ppm In.

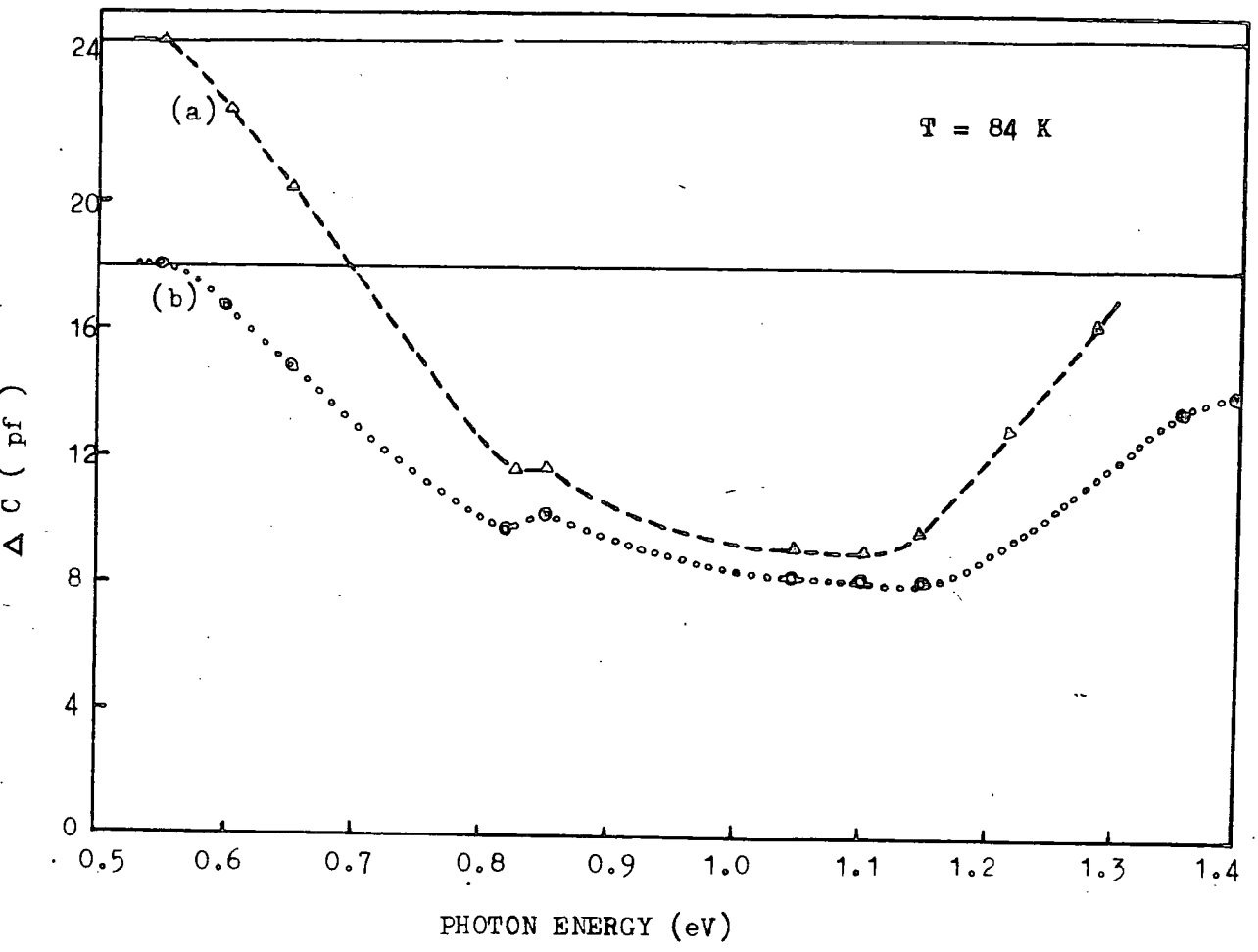

Fig 7.21 : Infra-red quenching of photocapacitance for (a) ZnSe:5ppm Ga and (b) ZnSe:50ppm Ga.

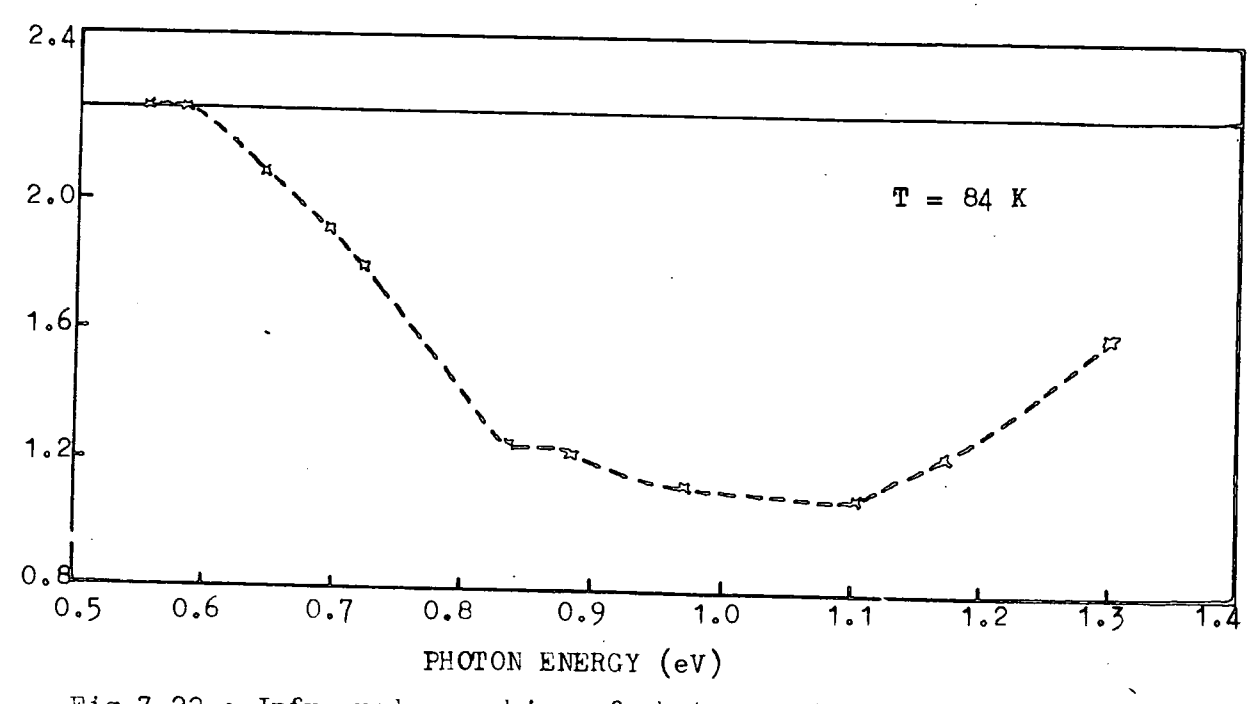

Fig 7.22 : Infra-red quenching of photocapacitance for ZnSe:100ppm Ga.

In a sample containing 50 ppm indium, diode 405-17, a similar distribution of infra-red quenching of the photocapacitance excited by light passing through 0.52 μm B.P. +IR abs. filters (also used for diode 413-17 for excitations) was obtained with 62.5% maximum quenching near ∿1.0 eV, and a low energy threshold near $h\nu_s$ = 0.60 eV, see Fig. 7.20(b). In all these samples only one threshold at 0.59 - 0.60 eV was apparent which gives the position of the deep acceptor at this energy above the valence band. It coincides with the values discussed in previous chapters. The maximum quenching was found in samples containing lower concentrations of indium. This suggests that the concentration of the deep acceptor is large in the lightly doped samples, and that it decreases as the content of indium increases. This result is in excellent agreement with the conclusions drawn from the transient photocurrent measurements described in Chapter 6.

Similar quenching curves were obtained with gallium doped ZnSe. Diode 387-23, containing 5 ppm gallium, had the response shown in Fig. 7.21(a) with a threshold at 0.55 eV and maximum quenching of the order of 64% at $h\nu_s \sim$ 1.0 eV. Curve (b) in the same figure is for diode No. 409-23 on ZnSe : 50 ppm Ga. The threshold position was similar to that in ZnSe : 5 ppm Ga, but the magnitude of the maximum quenching was less at 56%. For the sample doped with 100 ppm gallium which had the highest resistivity, a maximum quenching of 52% was obtained, and the threshold had shifted slightly to 0.58 eV, see Fig. 7.22. These diodes showed that the quenching decreased as the concentration of gallium increased, which is a similar effect to that observed in indium doped ZnSe. The trend to reduced quenching agrees with our earlier findings in Chapter 6, namely that a second deep acceptor was formed as the indium or gallium concentration was increased so that the concentration of the SA acceptor decreased. The second acceptor could not be investigated by the infra-red quenching technique because of the limitations of our source in the infra-red. The hump near ∿ 0.85 eV is due to a decrease in the intensity of secondary source at this energy.

7.5 EFFECT OF DOPING CONCENTRATION ON THE SPECTRAL DISTRIBUTION OF PHOTOCAPACITANCE

The effective study of donors using the photocapacitance technique was only straight forward in devices prepared on the material more highly doped with indium or gallium. The samples containing 5 ppm of these dopants had a complex behaviour which did not indicate the presence of any donor-like defects.

The spectral distribution of the photocapacitance of a number of indium doped devices is shown in Fig. 7.23. Curve (a) is for a diode with 5 ppm indium, No. 407-9. This has its first threshold at 2.22 eV and the second at 2.67 eV, with a very high photocapacitance response $\Delta C = 85.6 \times 10^2 pf/cm^2$ near 2.81 eV. In this device no decrease in ΔC corresponding to the filling of donors was observed. Diode No. 413-2, containing 20 ppm indium, had the photocapacitance spectrum illustrated by curve (b). The low energy threshold is unchanged, but a change of slope similar to that in ZnSe : 50 ppm In, is obvious near 2.40 eV. The spectrum also shows sudden decreases in ΔC at 2.60 and 2.75 eV which suggest donor levels. For comparison the corresponding spectra for two 50 ppm indium doped devices are also shown in Fig. 7.23, curves (c) and (d). Inspection of the curves reveals that (1) the magnitude of the photocapacitance is large in the lightly doped 5 ppm sample (low resistance) and low in the heavily doped 50 ppm samples (high resistance). The photocapacitance decreased as the resistance of the sample increased; (2) the sudden decreases in photocapacitance associated with donors are not observed in the 5 ppm sample, and (3) the threshold at 2.40 eV and the appearance of the acceptor at 0.40 eV is dependent on the indium concentration.

Similar results were obtained for gallium doped devices, see Fig. 7.24. Curve (a) is for a sample doped with 5 ppm gallium, diode No. 387-10, and shows two thresholds one at 2.25 eV and the other at 2.67 eV, followed by a fast rise ending near 2.80 eV with $\Delta C = 45 \times 10^2 pf/cm^2$. This curve is

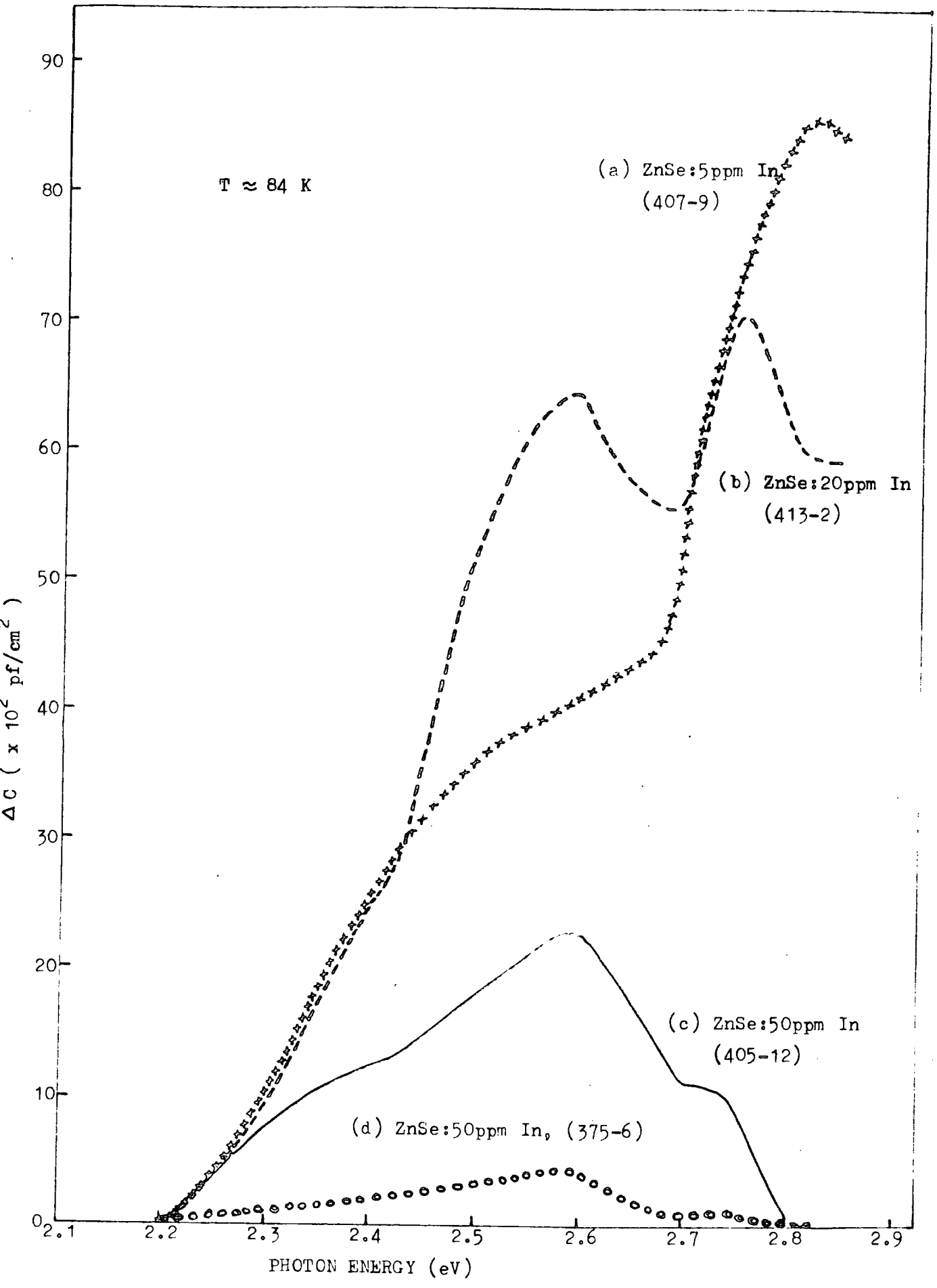

Fig 7.23 : Relative plots of the photocapacitance spectra for different indium doped ZnSe samples.

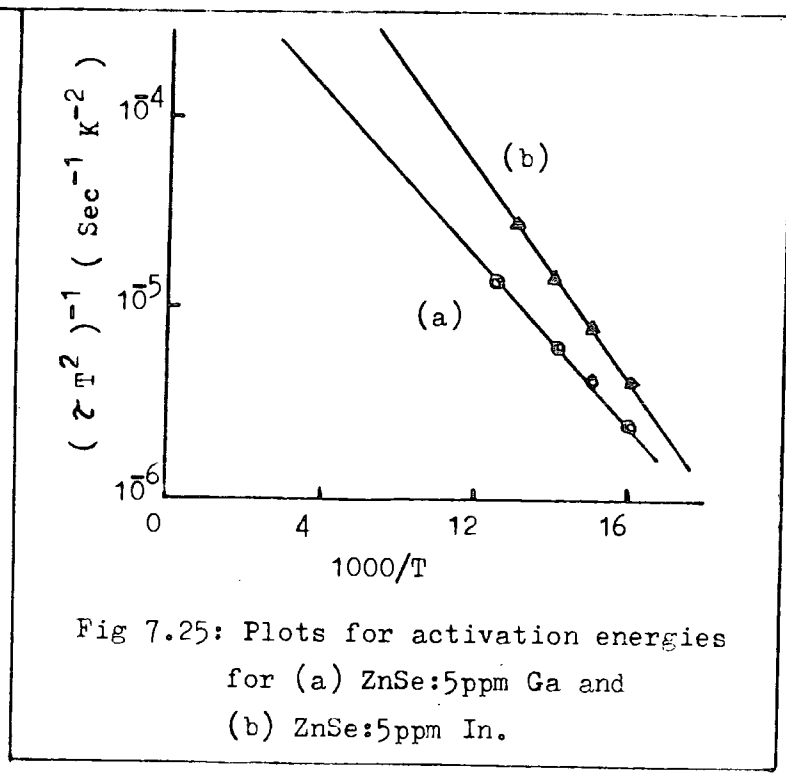

Fig 7.25: Plots for activation energies for (a) ZnSe:5ppm Ga and (b) ZnSe:5ppm In.

(a) ZnSe:5ppm Ga (387-10)

(b) ZnSe:50ppm Ga (409-8)

(c) ZnSe:100ppm Ga (382-4)

45
40
35
30
25
20
15
10
5
0

2.1 2.2 2.3 2.4 2.5 2.6 2.7 2.8 2.9

PHOTON ENERGY (eV)

Fig 7.24: Relative plots of the photocapacitance spectra for ZnSe:Ga.

similar in shape to curve (a) of Fig. 7.23 for ZnSe : 5 ppm In. Corresponding photocapacitance spectra for diodes (409-8) and (382-4) with 50 and 100 ppm gallium prepared at the same time as diode 387-10, are depicted by curves (b) and (c) in Fig. 7.24.

The effect on the photocapacitance of increasing the doping concentration is not entirely understood but a few possible suggestions are as follows:

(a) Low Density of Ionized Donors

A decrease in photocapacitance is associated with the filling of ionized donors in the optically active space charge region ($W - W_o$). With low resistivity devices (containing 5 ppm In or Ga) the Fermi-level (E_F) in the bulk is much closer to the conduction band and the optically active ($W - W_o$) region is narrow. This leads to a low total number of ionized donors. The optical filling of these donors when electrons are excited from the valence band would give a small decrease in photocapacitance which is swamped by the persistent increase due to the emptying of the deep acceptors with their long time constants.

(b) Influence of Hole Trapping

Electron-hole pairs are produced when photons with energy near the bandgap of ZnSe are absorbed or when two step optical generation occurs. The electrons flow away from the barrier into the bulk of the semiconductor, and the optically generated holes, are trapped in the deep acceptors, as they try to pass through the depletion layer to the metal contact, see Suda and Kurita (1979). The trapped holes reduce the concentration of ionized deep acceptors (N_A^-) and consequently the capacitance of the depletion region is increased because $C \alpha (N_D^+ - N_A^-)$.

(c) Shallow Acceptors

The two effects discussed above might be simultaneously responsible for the persistent rise in the photocapacitance of lightly doped material near the bandgap. However the question arises as to why there is a

threshold at 2.67 eV with a sharp rise in the photocapacitance. This sharp rise appears to be associated with a shallow acceptor some 0.13 eV above the valence band.

In an attempt to identify this acceptor some photocapacitance decay curves were studied at different temperatures. First the centres were emptied by irradiating with light of energy $h\nu = 2.72$ eV. Then this radiation was cut-off and the decay curve was measured. According to the expression,

$$\frac{1}{\tau} = \sigma_p \; v_p \; N_V \; e^{-\Delta E/kT},$$

where τ = Time constant

σ_p = Capture cross-section of hole

$v_p = \left(\frac{3\,kT}{m^*}\right)^{\frac{1}{2}}$ = Thermal velocity of hole,

$N_V = 2\left(\frac{2\pi m^* kT}{h^2}\right)^{3/2}$ = Effective density of states in the velence band,

ΔE = Activation energy,

k = Boltzmann constant,

T = Temperature (K), and

m^* = Effective density of states in the valence band;

the time constant can be obtained by plotting ln ΔC against decay time. Then a plot of ln $\frac{1}{\tau T^2}$ versus $1000/T$ should yield a straight line from the slope of which the activation energy, ΔE, can be determined. Such a plot for the ZnSe : 5 ppm Ga, diode 387-14, is shown in Fig. 7.25 (a),

giving ΔE = 0.03 eV. Using the above expression the capture cross-section for holes, σ_p, was found to be 1.74 x 10^{-25} Cm^2. In addition the diode 407-17, fabricated from ZnSe doped with 5 ppm of indium led to an acceptor ionization energy ΔE = 0.027 eV, determined from the slope of the straight line, (b) in Fig. 7.25. The corresponding value of σ_p was 5.1 x 10^{-24} Cm^2. Such small values of cross section suggest a neutral or positively charged centre.

7.6 PHOTOCAPACITANCE AFTER ZINC EXTRACTION

Some photocapacitance spectra were also recorded on indium or gallium doped samples which had been heated in molten zinc. The colour of samples (containing concentrations > 50 ppm In or Ga) changed from yellow-orange to black, see Appendix. The photocapacitance spectra were completely different from those found in devices on unannealed samples. The results are discussed below.

7.6.1 Effect of Zinc Annealing Time

The photocapacitance curves for diodes on ZnSe doped with 50 ppm indium are plotted in Fig. 7.26. The dice had all been heated in molten zinc at 850°C for different periods of time before the diodes were prepared. The diodes (405-Z1), (405 - Z2) and (405 - X) were on dice heated for 5, 15 and 24 hours, respectively. All the diodes were fabricated at the same time. Curves (a) and (b) show the photocapacitance (ΔC) for diode 405 - Z1, with zero and - 4.0V bias; curve (c) is for diode 405 - Z2 also at zero and curve (d) is for diode 405 - X at zero bias. All these curves show the threshold for the rise in the photocapacitance near 2.65 eV, corresponding to a level $\sim$ 0.15 eV above the valence band. The magnitude of the photocapacitance was larger with the samples treated for the shorter times. This behaviour is more clearly illustrated by Fig. 7.27, which shows that after a sample had been heated for five days no photocapacitance effect could be observed, i.e. $\Delta C \rightarrow 0$.

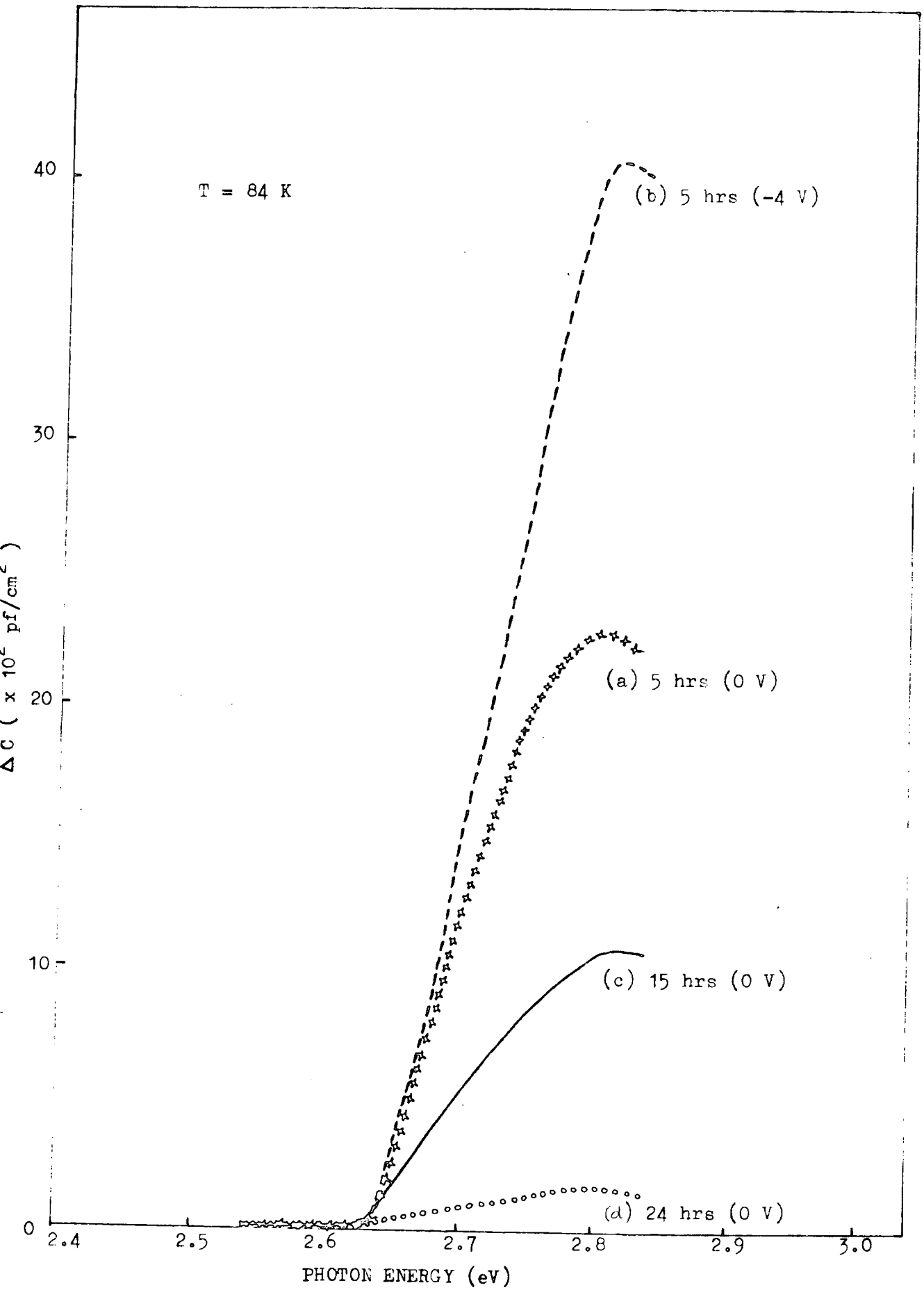

Fig 7.26 : Photocapacitance spectra for ZnSe:50ppm In samples after heat-treatment in molten zinc at different periods.

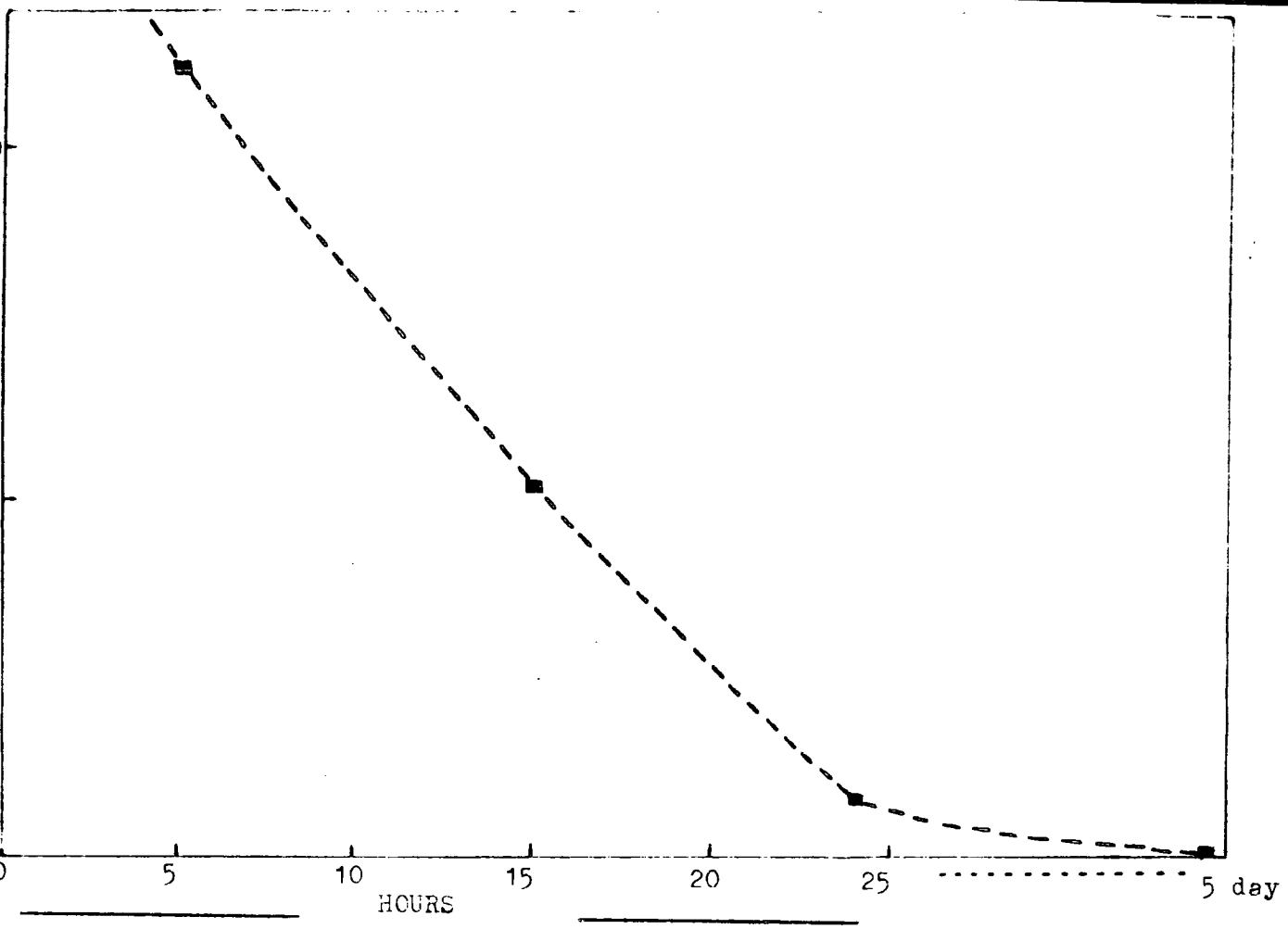

Fig 7.27 : Plot of peak value photocapacitance (see Fig 7.26) against zinc heat treatment time obtained at zero bias.

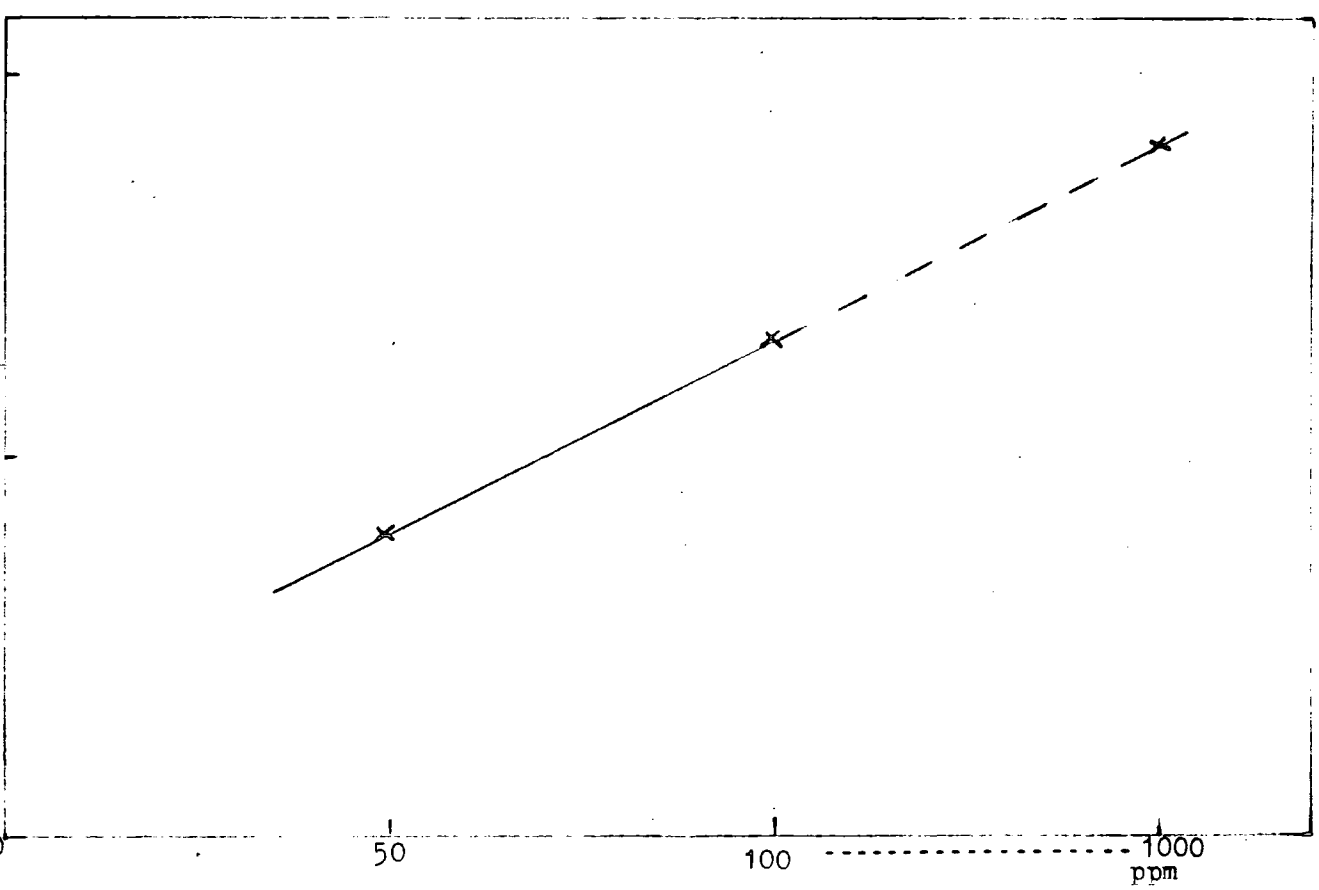

Fig 7.30 : Plot of photocapacitance (see Figs 7.26,7.28,7.29) maxima obtained at zero bias against doping concentration.

7.6.2 Effect of doping concentration

The photocapacitance spectra in Figs. (7.28) and (7.29) are for diodes on zinc treated samples containing 100 and 1000 ppm indium. These dice had been heated in zinc at 850°C for 24 hours. Since as grown samples with comparable concentrations of indium (In) had a very high resistivity, no photocapacitance measurements could be made with these samples. However, after zinc treatment the measured responses were as shown in Figs. (7.28) and (7.29). The curves were measured at different biases. Although the diodes were not fabricated at the same time a difference in the photocapacitance level was noticed. The photocapacitance obtained at zero bias for devices on samples heated for one day (50, 100 and 1000 ppm In) are shown in Fig. 7.30. An increase in photocapacitance, ΔC, was apparent for devices containing increasing concentrations of indium. The acceptor level appeared to be at 0.12 eV in the 100 ppm and 0.15 eV in 1000 ppm samples.

7.6.3 Measurements on ZnSe : Ga

The photocapacitance spectra on gallium doped ZnSe samples after heating in zinc for one day were also measured and are shown in Fig. 7.31. The diodes (387-X) and (382-2Z) were on 5 and 100 ppm gallium samples respectively. Curve (a) for diode 387-X and curve (b) for 382-2Z had different magnitudes and the large increase in photocapacitance at 2.63 eV was similar to that found in the indium doped samples after zinc-treatment. The acceptor level found from this threshold is 0.17 eV above the valence band in both samples. The photocapacitance response associated with the deep acceptors was reduced but not completely absent.

7.6.4. Zn-Treatment of Undoped ZnSe

As a control, an undoped ZnSe sample was also heated in a zinc melt at 850°C for six days. There was no blackening and the resistivity was reduced to 100 ohm-cm. After fabricating a diode No. 327-1Z, the photocapacitance spectra at different biases were as shown in Fig. 7.32. The low energy

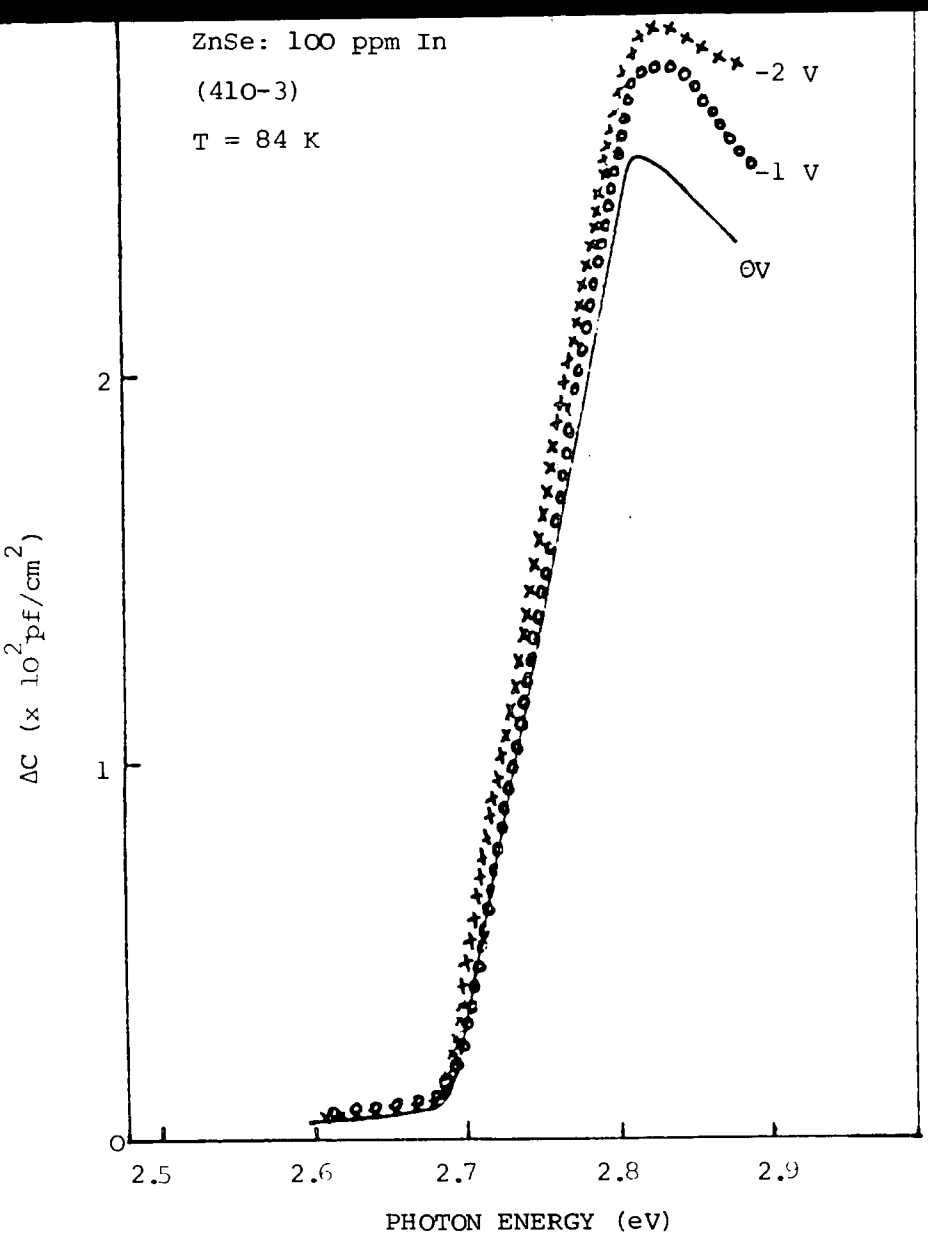

Figure 7.28 : Photocapacitance spectra of ZnSe: 100 ppm In sample after heat-treatment in molten zinc, at different reverse bias.

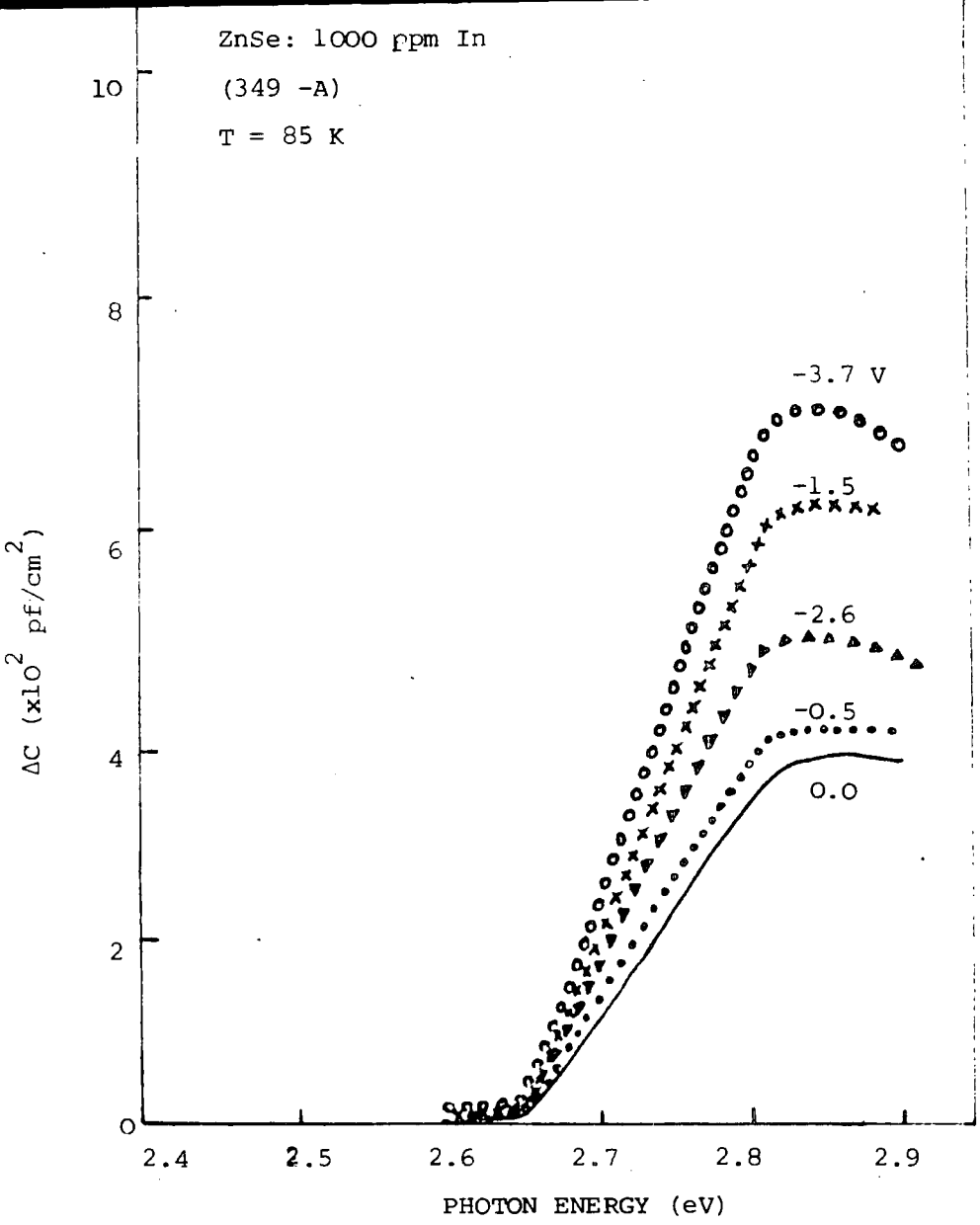

Figure 7.29 : Photocapacitance spectra of ZnSe: 1000 ppm In sample after heat-treatment in molten zinc, at different reverse bias.

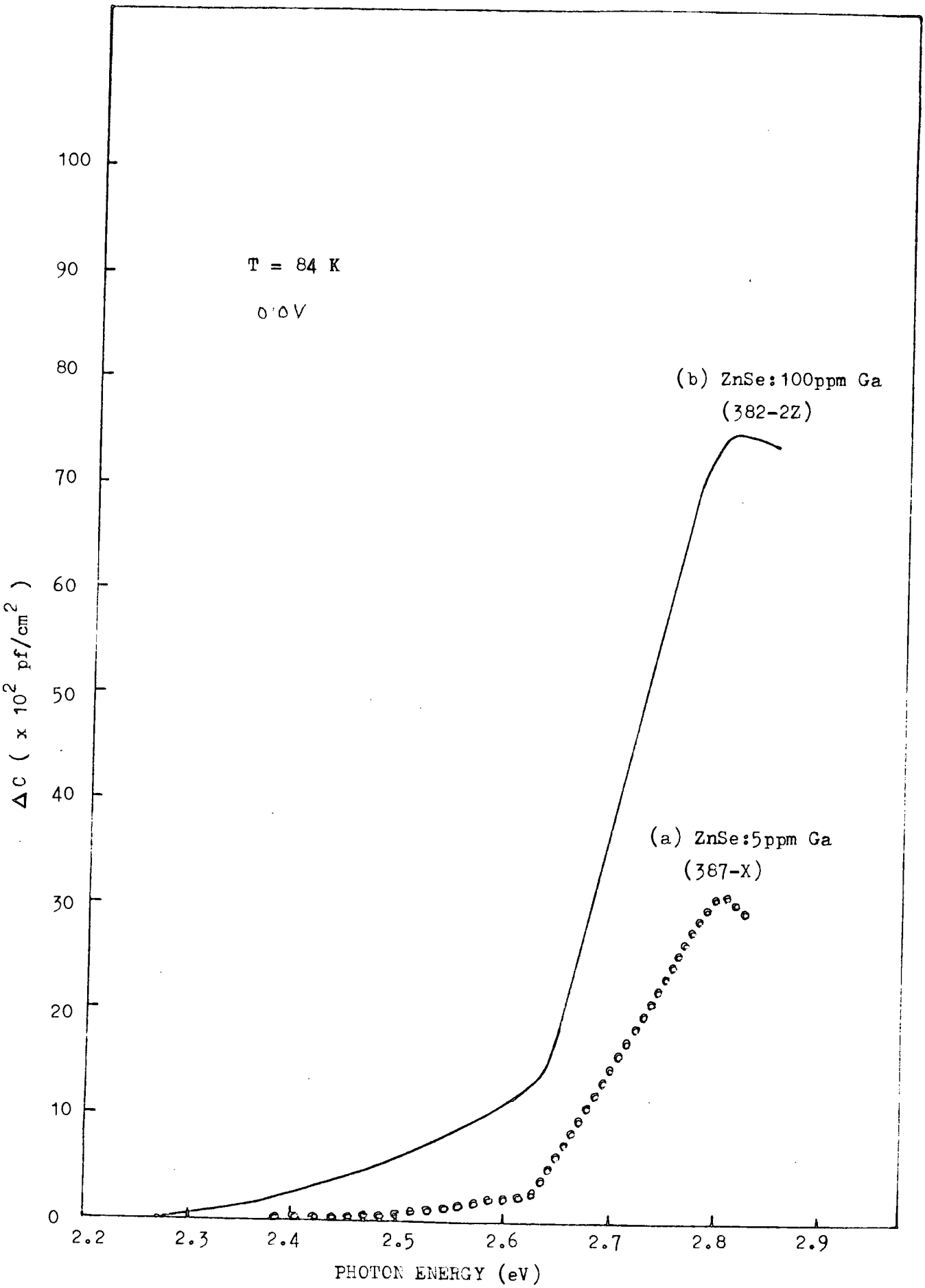

Fig 7.31: Photocapacitance spectra of gallium doped ZnSe after zinc heat-treatment.

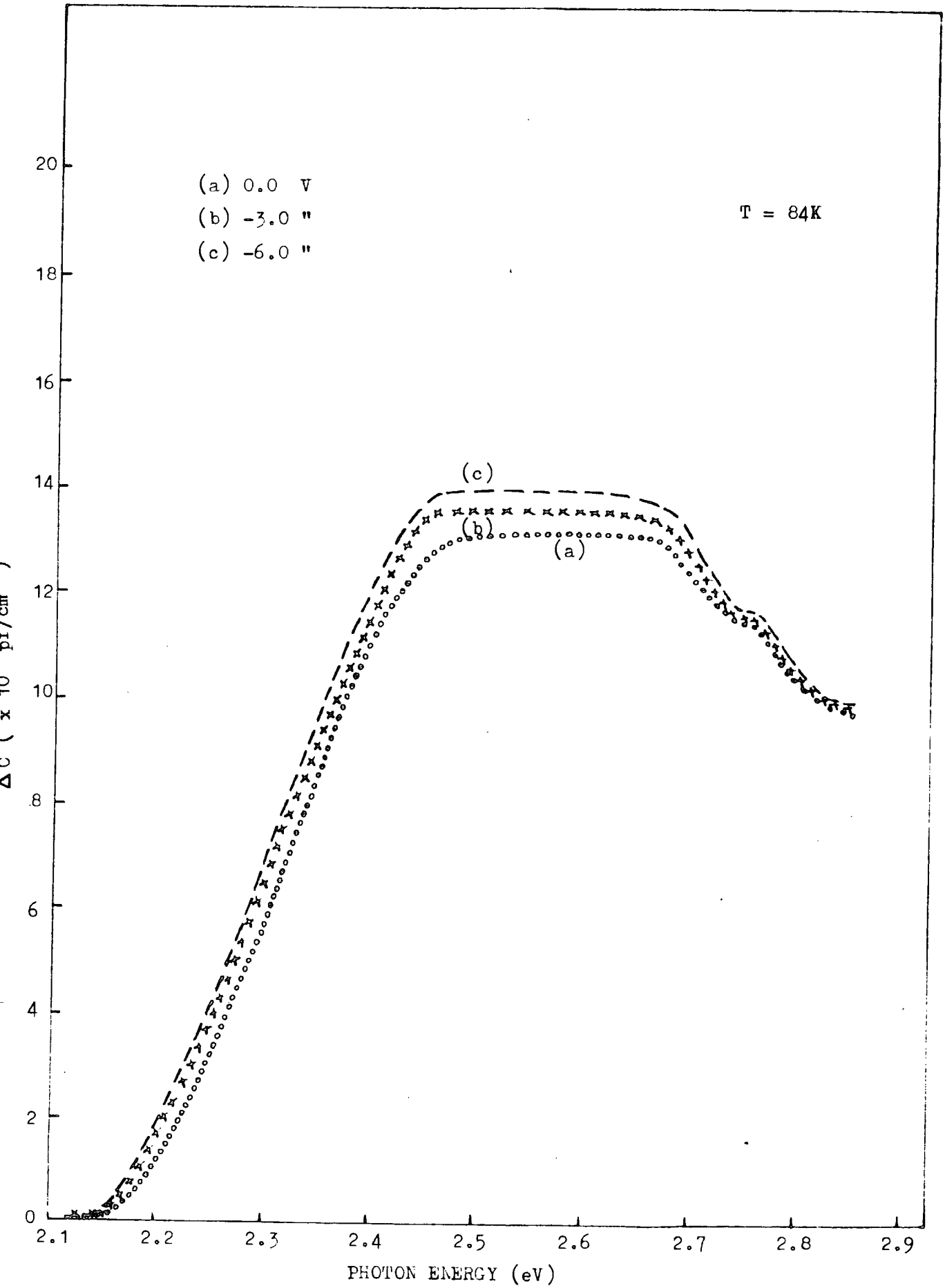

Fig 7.32 : Photocapacitance spectra of undoped ZnSe after zinc heat-treatment.

threshold at 2.13 eV gives rise to a large photocapacitance, which is associated with the deep acceptor at 0.67 eV above the valence band. This is due to copper. It is surprizing that the zinc-treatment did not remove all the unintentional copper completely. Unlike the photocapacitance spectra with zinc treated samples of indium or gallium doped ZnSe, this diode showed two abrupt decreases at 2.67 eV and 2.76 eV corresponding to donors lying 0.13 and 0.02 eV below the conduction band.

7.7 CONCLUSION AND DISCUSSION

The main interest in steady state photocapacitance as discussed in this chapter was to investigate shallow centres in indium or gallium doped ZnSe. The measurements were successful and for the first time the photocapacitance technique has been used to identify shallow donors or acceptors in ZnSe. In the past, photoluminescence, thermally stimulated conductivity (TSC), Hall and electrical conductivity and many other techniques, have been used to determine the activation energies of shallow centres, and it is interesting that our results are in general in good agreement with published values.

The photocapacitance measurements were carried out at different temperatures, frequencies and bias and in summary the results were as follows:

(a) Larger photocapacitance values were obtained at lower temperatures,

(b) At low frequency the photocapacitance was large,and with increasing the frequency the overall photocapacitance decreased, and

(c) The photocapacitance increased with increasing reverse bias.

The energy levels associated with deep and shallow centres, obtained from steady state photocapacitance measurements on different doped and undoped ZnSe are tabulated in Table 7.3. Indium doped ZnSe contained two donor levels, one 0.20 eV and the other (0.02-0.03) eV below the conduction band, although with ZnSe : 5 ppm In the technique failed to reveal any donor level. The deep acceptor with a level at 0.58 eV above the valence band was common in ZnSe : In with all concentrations, but the acceptor lying

TABLE 7.3 SUMMARY OF ENERGY LEVELS OBTAINED FROM STEADY STATE PHOTOCAPACITANCE MEASUREMENTS AT T ∿ 82 K

CRYSTAL	A1 (eV)	A2 (eV)	D1 (eV)	D2 (eV)	D3 (eV)	D4 (eV)
ZnSe : 5 ppm In	0.58	0.13	-	-	-	-
ZnSe : 20 ppm In	"	0.40	0.02	0.20	-	-
ZnSe : 50 ppm In	"	0.40 - 0.42	0.03	0.19	-	-
ZnSe : 5 ppm Ga	0.55	0.13	-	-	-	-
ZnSe : 50 ppm Ga	"	-	0.03	0.17	0.26	0.32
ZnSe : 100 ppm Ga	0.53	-	"	0.18	0.25 - 0.26	-
ZnSe : Cu	0.67	0.12	0.02	-	-	0.32
ZnSe (Undoped)	"	-	"	0.13	-	-

A = Acceptor above V.B.

D = Donor below C.B.

(0.40 - 0.42) eV above the valence band appeared in the more heavily doped 20 and 50 ppm indium samples only. With 5 ppm indium a shallow acceptor 0.13 eV above the valence band was observed. Gallium doped ZnSe showed the same pattern in photocapacitance with doping concentration and the sample containing the lowest (5 ppm Ga) concentration showed no photocapacitance corresponding to donors. A series of donors at 0.32, 0.26, 0.17 and 0.03 eV in ZnSe: 50 ppm Ga and $\sim$ 0.26, 0.18 and 0.03 eV in ZnSe : 100 ppm Ga, below the conduction band were found. The deep acceptor with a level (0.54 $\pm$ 0.01) eV above the valence band was found in most samples. It was thought that a higher gallium content would introduce a similar deep acceptor to that found in the indium doped samples at (0.40 - 0.42) eV, but no such deep level was found. In the transient photocapacitance measurements (see Chapter 6) such a level was identified in ZnSe : 50 ppm Ga, but it was not so dominant as in ZnSe : 50 ppm In. As with ZnSe : 5 ppm In, a shallow acceptor level some 0.13 eV above the valence band was found in samples with 5 ppm gallium.

Measurements were also made on undoped and copper doped ZnSe samples. A shallow donor, with a level 0.02 eV below the conduction band, was found in both the undoped and copper doped samples. A deeper donor at 0.32 eV, which also appeared in ZnSe : 50 ppm Ga, was evident in ZnSe : Cu; while a donor level at 0.13 eV was only apparent in undoped ZnSe. Two acceptors one at 0.67 eV and the other at 0.12 eV above the valence band were found in ZnSe : Cu, whereas in undoped material only the 0.67 eV acceptor appeared.

Hydrogenic model and neutral donors:-

According to the hydrogenic or Coulombic potential, the donor binding energy in ZnSe is, see Yamaguchi et al (1977) and Woodbury and Aven (1974),

$$E_D = \frac{m^*_e e^2}{2\hbar^2 \varepsilon^2} = 28.1 \pm 1.4 \text{ meV},$$

where $m^*_e = 0.17\, m_o$, m_o is the rest mass of electron, ε is the static dielectric onstant ($\varepsilon = 9.1\, \varepsilon_o$, ε_o is the dielectric constant in vacuum). Values close to this were found in all our indium and gallium doped samples. Indium or gallium in its atomic state has '3' valence electrons in the outermost shell. The first electron is removed when it occupies a Zn-site to form $(In_{Zn})^+$ or $(In_{Zn})^{\cdot}$ and $(Ga_{Zn})^+$ or $(Ga_{Zn})^{\cdot}$ donors. According to Ray and Kröger(1978), trivalent metal atoms substituting for zinc in ZnSe are expected to act as shallow donors. Such behaviour also occurs with aluminium. The first shallow donor at 0.03 eV below the conduction band in both indium or gallium doped ZnSe is a neutral donor. This value is very close to those determined by Merz et al (1972) from photoluminescence. Merz et al. reported values of 0.029 ± 0.006 eV for indium and 0.028 ± 0.006 eV for gallium neutral donors in ZnSe. Jones and Woods (1976) using measurements of the electrical conductivity and Hall coefficient found the ionization energy of the shallowest level in indium doped ZnSe to be 0.021 eV. The corresponding value in gallium doped ZnSe was 0.065 eV. Recently, however, Blanconnier et al (1981) have found values much closer to those of Merz et al, i.e. 0.028 eV for indium and 0.027 eV for gallium donors.

Ionized Donors:-

The ionization energy of the second electron from the substitutional centres of indium or gallium is larger and should give rise to deeper levels. The donor levels at 0.20 eV and (0.17 - 0.18) eV below the conduction band were only found in the indium or gallium doped samples, so it may be said with certainty that these levels are also associated with substitutional impurities of indium or gallium. The empty centres may be of the form $(In_{Zn})^{++}$ or $(Ga_{Zn})^{++}$.

Activation energies of comparable magnitude have been reported by several workers in ZnSe containing similar and different dopants. Jones and Woods (1976) from electrical conductivity and Hall measurements on ZnSe doped either with indium or gallium, found donor-levels at 0.20 eV in ZnSe : In and 0.13 eV in ZnSe : Ga, below the conduction band. In another investigation, Jones and Woods (1974) located a donor between 0.20 and 0.30 eV in chlorine doped ZnSe, which they associated with the chlorine. Aven and Segall (1963) have also reported a donor in Cl-doped ZnSe some 0.19 eV below the conduction band. In bromine doped ZnSe a donor level at 0.21 eV was found by Bube and Lind (1958).

Selenium vacancies and zinc interstitials:-

If one selenium ion is missing from its proper site in the ZnSe lattice, it will give rise to a doubly ionized selenium vacancy, $(V_{se})^{++}$, which could act as a deep donor. After capturing an electron a singly ionized centre, $(V_{ge})^{+}$, is formed which lies closer to the conduction band and forms a shallow (ionized) donor. Aven (1971) reported that the low resistivity n-type conduction of ZnSe crystals heat treated in molten zinc was dominated by the shallow native donor level at 0.021 eV below the bottom of the conduction band. Igaki and Satoh (1979) from measurements of Hall coefficient and electrical conductivity found activation energies in the range 0.02 - 0.025 eV which they attributed to Se- vacancies or Zn- interstials.

From Deep Level Transient spectroscopy (DLTS) studies of ZnSe and $ZnS_x\ Se_{1-x}$, Shirakawa and Kukimoto (1980) explained the dominant electron traps they observed at 0.30 eV by assuming that the responsible defects were anion vacancies.

Most investigators have reported the presence of two types of donor in crystals subjected to the zinc-extraction process. Although there is no great unanimity of opinion as to the depth of the corresponding energy

levels, a summary of the available evidence would suggest that the shallower of the two donor levels lies between 0.008 and 0.023 eV below the conduction, near the position expected for a hydrogenic donor level. The second level is deeper and lies between 0.10 and 0.19 eV below the conduction band. This second level has been attributed variously to a Cl donor level by Aven and Segall (1963), and to a native double acceptor by Lorenz et al. (1963) and Aven (1964). Fukuda and Fukai (1967) also suggested that a native defect was responsible for the shallower level.

Our photocapacitance measurements revealed a level at 0.32 eV in ZnSe : 50 ppm Ga and at 0.32 eV in ZnSe : Cu, below the conduction band which might be a doubly ionized selenium vacancy. The shallow donor at 0.02 eV is very close to that observed by Aven and by Igaki and Satoh. A donor with an ionization energy of 0.13 eV was also present in our zinc-extracted, undoped ZnSe.

Shallow acceptor:-

The hydrogenic or Coulombic value of the acceptor binding energy in ZnSe is, see Yamaguchi, et al. (1977),

$$E_A = \frac{m^*_h e^4}{2\hbar^2 \varepsilon^2} = 115 \text{ meV}$$

Shallow acceptors with levels at 0.13 eV above the valence band in ZnSe doped with 5 ppm indium or gallium and 0.12 eV in copper doped ZnSe, have been found consistently in our studies. These values are very close to the theoretical value (0.115 eV). Other workers, for example Yu and Park (1973) found a shallow acceptor at $\sim$ 0.10 eV in undoped ZnSe, heat treated in selenium vapour. They attributed this level to zinc vacancies or zinc-vacancy-complexes.

The most obvious candidate for a shallow acceptor at a zinc site in ZnSe is substitutional lithium (Li), which has a covalent radius very

close to that of Zn, see Anderson (1960) and should therefore fit easily into the ZnSe lattice. Merz et al. (1973) established the energetic position of the Li_{Zn} acceptor as 0.114 eV by analyzing donor acceptor pair discrete line spectra. There is no certainty about the identity of the 0.12 - 0.13 eV levels found in our measurements, but they could clearly be associated with substitutional lithium.

Self activated centres:-

The self-activated acceptor centre as previously described is a zinc vacancy in association with a substitutional donor on a zinc site, for example, $(V_{Zn} - In_{Zn})'$ or $(V_{Zn} - Ga_{Zn})'$ complex centres. These complexes are very similar to acceptor complexes found in chlorine doped ZnSe by Holton et al (1965) using luminescence and spin resonance techniques. A zinc vacancy and substitutional gallium donor complex was proposed by Boley et al (1975). Sethi and Mathur (1978) have also reported such a complex in indium doped ZnSe crystals.

The SA centre in ZnS is defined to be responsible for the characteristic blue luminescence in ZnS : Al. A variety of techniques, including optically detected magnetic resonance, Nicholls, et al (1979), have been used to show that this luminescence results from DAP (donor-acceptor pair) transitions involving shallow Al donors and the A-centres, $V_{Zn} - Al_{Zn}$ associates. A broad band luminescence centred at 2.03 eV has been similarly attributed to self-activated emission in ZnSe : Cl by Bryant and Manning (1974), and in ZnSe:Ga by Fugita et al (1979) and identified using the ODMR technique in ZnSe:Al, see Dunstan et al (1977). Vincent (1980) found two bands, green and red at 555 nm and 625 nm respectively, at liquid nitrogen temperature, in ZnSe:In or Ga crystals. The red band was attributed to SA luminescence.

Our results are based on electrical observations, which located one level at 0.58 eV in indium doped, and one at $\sim$ 0.54 eV in gallium doped ZnSe crystals. From these results alone it would be difficult to identify

the levels, but by making comparisons with the work of others we can definitely say that they are attributable to self-activated centres. They are not associated with copper because we identified the copper level at 0.67 eV above the valence band.

Complex Acceptor:-

The acceptor lying about ∿ 0.41 eV above the valence band as described in Chapter 6, is dependent on the concentration of indium or gallium in ZnSe. It's presence was more obvious when the doping concentration increased. Ray and Kröger (1978) in explaining their results, obtained from electrical measurements of gallium doped ZnSe, considered the possible existence of complex acceptors, such as $(Ga_{Zn} - Ga_{Se})'$, $(Ga_{Zn} - Ga_{Se})''$ or $(Ga_{Se})'''$; which would be singly, doubly or triply ionized acceptors respectively. A possible triply charged acceptor, formed when indium is substituted at a selenium site, $(In_{Se})'''$, was also discussed by Sethi and Mathur (1978). Boley et al (1975) and Russell et al (1981) have discussed the possibilities of an acceptor formed by singly ionized zinc vacancy and substitutional gallium or indium, i.e. a $(V_{Zn} - Ga_{Zn})^{\circ}$ or $(V_{Zn} - In_{Zn})^{\circ}$ centre.

The level at ∿ 0.41 eV may be a complex of any one of these. As previously described in Chapter 6, we think $(In_{Se})'''$ or $(Ga_{Se})'''$ acceptors are more probable, in view of the radii of participating elements.

Copper Centres:

Copper sometimes is a very undesirable contaminant and produces deep multi-level acceptors, which also contribute to the compensation of undoped crystals. The presence of copper in ZnSe has been extensively investigated by several workers mainly using photoluminescence techniques. Yamaguchi and Shigematsu (1978) have shown that ZnSe crystals containing lower copper concentrations emitted the copper-red (Cu-R) band peaking at 6350 A° at 90K,

while those with higher copper concentrations exhibited the copper-green (Cu-G) emission at 5330 A^{o}. Copper was introduced by leaving crystals in molten zinc containing copper. The critical copper concentration for the appearance of the green emission was $Cu/_{Zn} = 10^{-4}$ (mole ratio). Moreover, at the high concentrations the blue band-edge emission and the self-activated yellow-orange emission decreased appreciably with increasing copper concentration.

Nearly ~~ten~~ fifteen years ago, Stringfellow and Bube (1968) suggested that the red emission at 1.97 eV is the result of a transition from the conduction band to a deep acceptor 0.72 eV above the valence band; while the green emission (2.34 eV) was produced by a transition between the conduction band and another acceptor level 0.35 eV above the valence band. Furthermore, the acceptor level at 0.72 eV was identified as a singly negatively charged copper ion on a zinc site (Cu'_{Zn}), while the second copper level at 0.35 eV was supposed to be neutral (Cu^{x}_{Zn}). Jones and Woods (1974) and Gezci and Woods (1975) also attributed the red and green bands to copper centres, but they placed these two levels at 0.86 eV and 0.46 eV above the valence band, because they took the value of the bandgap at liquid nitrogen temperature to be 2.80 eV instead of 2.70 eV as assumed by Stringfellow and Bube.

The green emission at 530 nm in ZnSe has been studied by optically detected magnetic resonance (ODMR), Patel et al (1981). Observations of hyperfine structure showed unequivocally that copper ions were involved with the emission. The spectrum was attributed to Cu^{2+} (Cu^{x}_{Zn}) either at the zinc substitutional site or at the interstitial site that is surrounded by four selenium ions. The acceptor level was put at $\sim$ 0.20 eV above the valence band.

There have been a large number of investigations into the nature of the copper centres in ZnSe, and there is a fair amount of conflicting

evidence. Nonetheless our present result that copper forms at least one acceptor level 0.67 eV above the valence band is in good agreement with several authors, and particularly with the research of Grimmeiss et al (1977 - 1979) who found the Cu'_{Zn} centre 0.68 eV above the valence band of ZnSe.

CHAPTER 8

THE EFFECTS OF DOPING ON SCHOTTKY DIODE PARAMETERS

8.1 INTRODUCTION

The characteristic behaviour of a Schottky diode is determined by the resistivity of the crystal, if all the other factors such as preparation etc. are the same. A comprehensive study, of nearly 20 samples of indium or gallium doped ZnSe devices, has been carried out to determine how the various Schottky diode parameters, such as N_d, V_{do}, ϕ_c, ϕ_p, W, E, $\Delta\phi$ and E_F, vary with doping concentrations. In most of the diodes with low dopant concentrations ($\sim$ 5 ppm) consistent results were obtained. But with the diodes fabricated from crystals containing 50 ppm or more impurity, which had high resistivities, the results were more complicated. Since all the results for good diodes of a particular type were similar, the discussion in this chapter is restricted to those.

8.2 CAPACITANCE-VOLTAGE MEASUREMENTS

The dark capacitance (C) of various Schottky diodes was measured as a function of reverse bias (V_r). The measurements helped in understanding the properties of the crystals when doped with different concentrations of indium or gallium. The experimental procedure has already been described in Chapter 4. The capacitance was measured with a small A.C. voltage of 28 mV peak-to-peak at a frequency of 120 kHz.

UNCOMPENSATED DONOR CONCENTRATION :- The concentrations of uncompensated donors N_d, ($N_d = N_D^+ - N_A^-$, N_D^+ = con. of ionized donors, N_A^- = con. of ionized acceptors), in different samples were determined from plots of C^{-2} versus V_r, see Figs 8.1-8.5, using eqn.(3.6). Since these plots are between C^{-2} in $(pf)^{-2}$

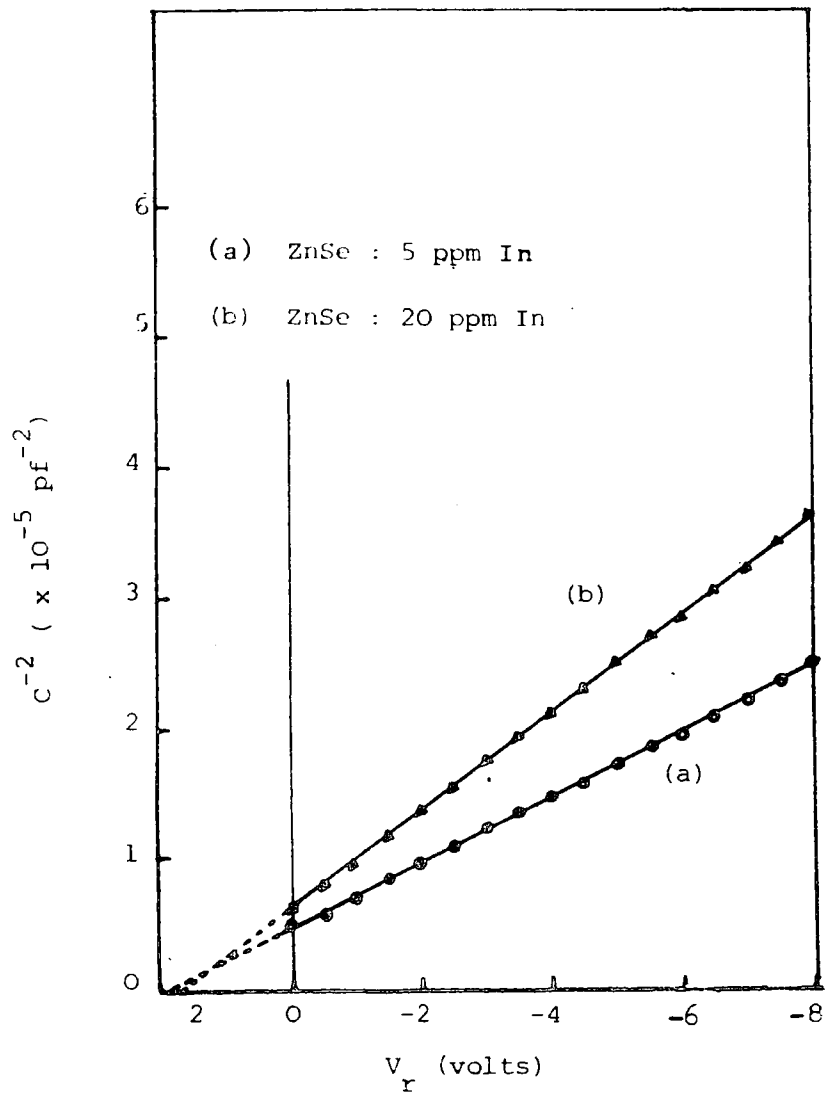

Fig. 8.1 C^{-2} vs V_r plots at T ∿ 294 K

(a) ZnSe : 5 ppm In, and
(b) ZnSe : 20 ppm In, diodes

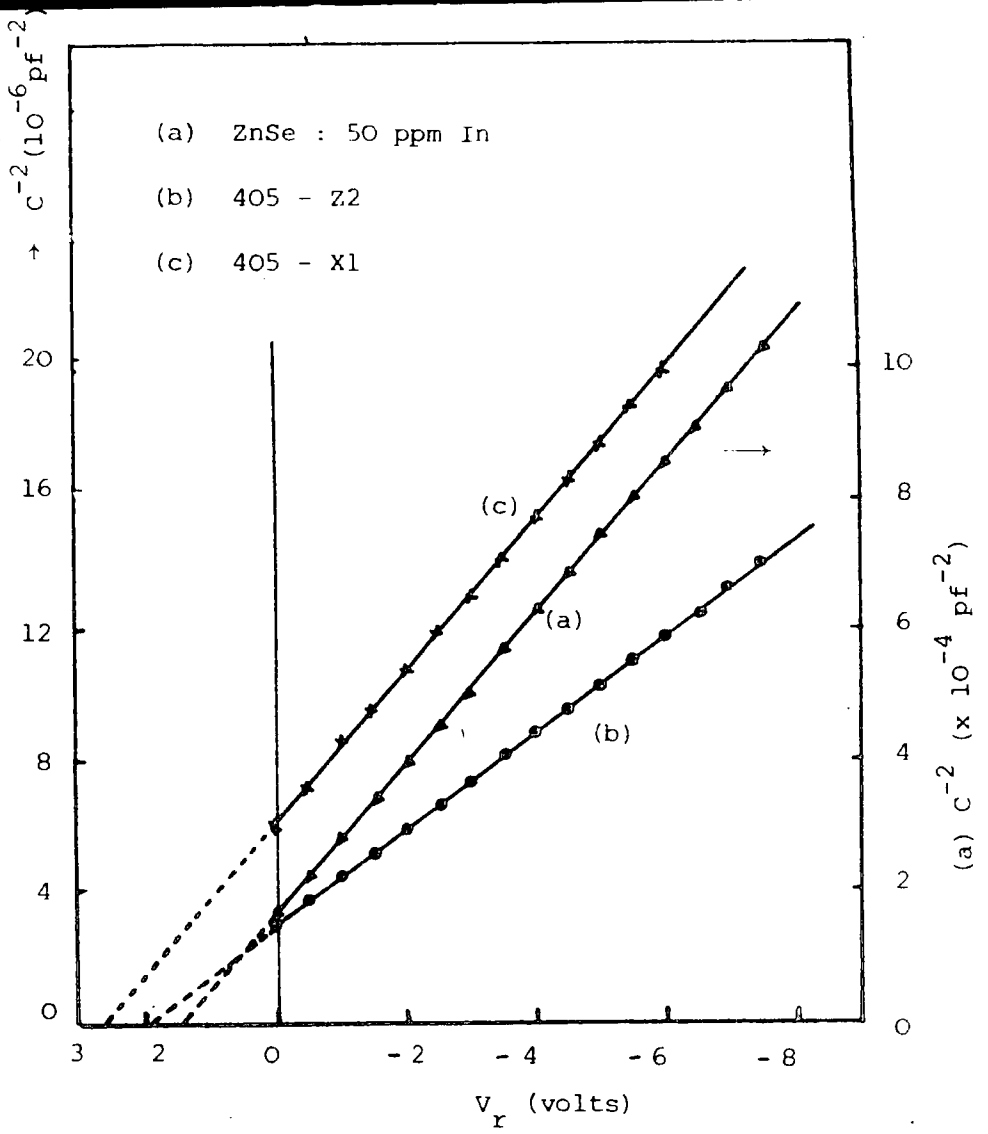

Fig. 8.2. C^{-2} vs V_r plots at T ∿ 294 K for ZnSe: 50 ppm In

(a) As grown sample
(b) After heat treatment in Zn (405-Z2)
(c) After heat treatment in Zn (405 - X1)

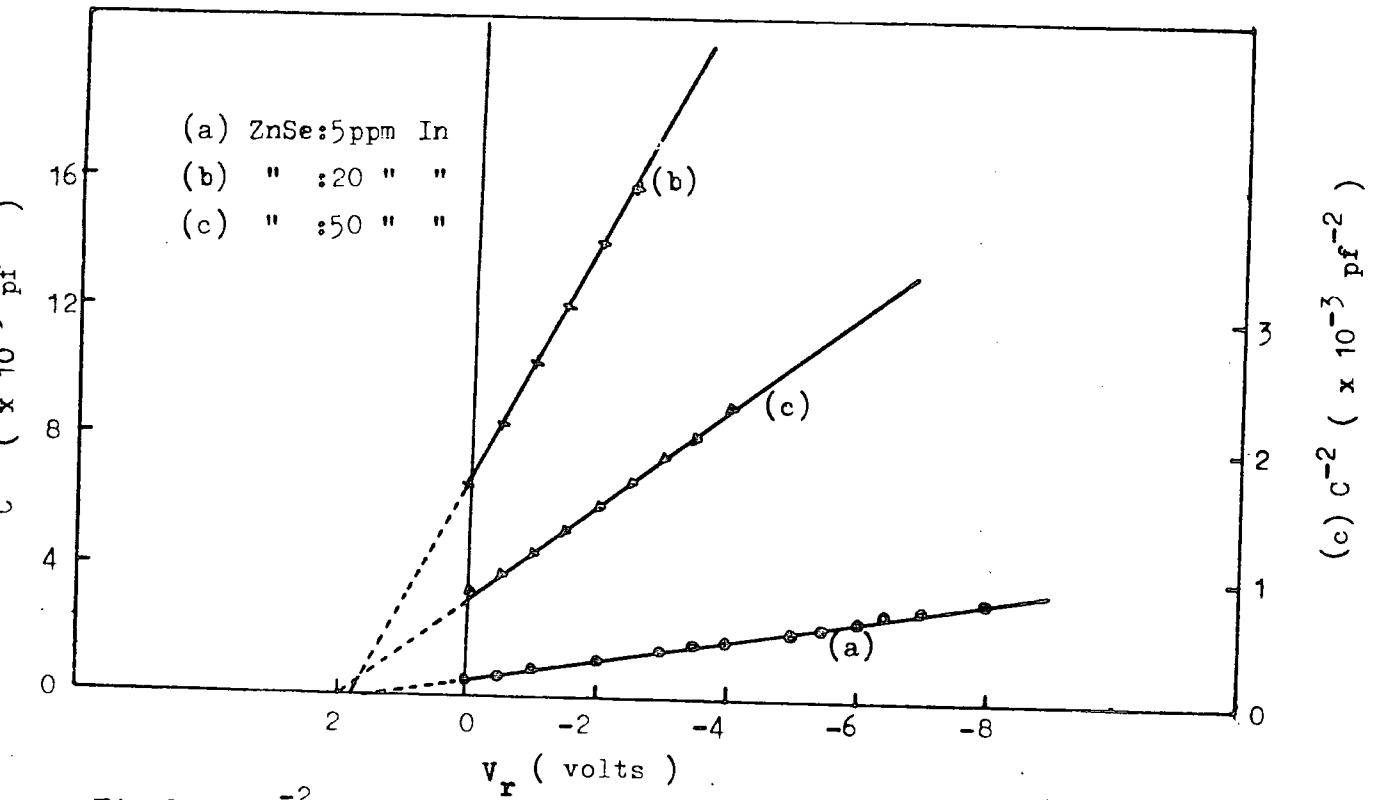

Fig 8.3 : C^{-2} versus V_r plots for ZnSe Schottky diodes at T ~ 85K.

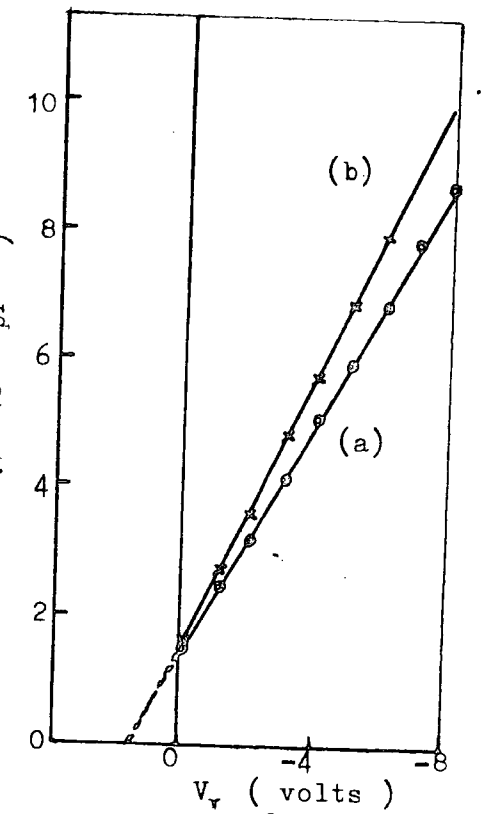

Fig 8.4:: C^{-2} vs V_r plots for ZnSe:5ppm Ga at (a) T = 294K and (b) T = 85K

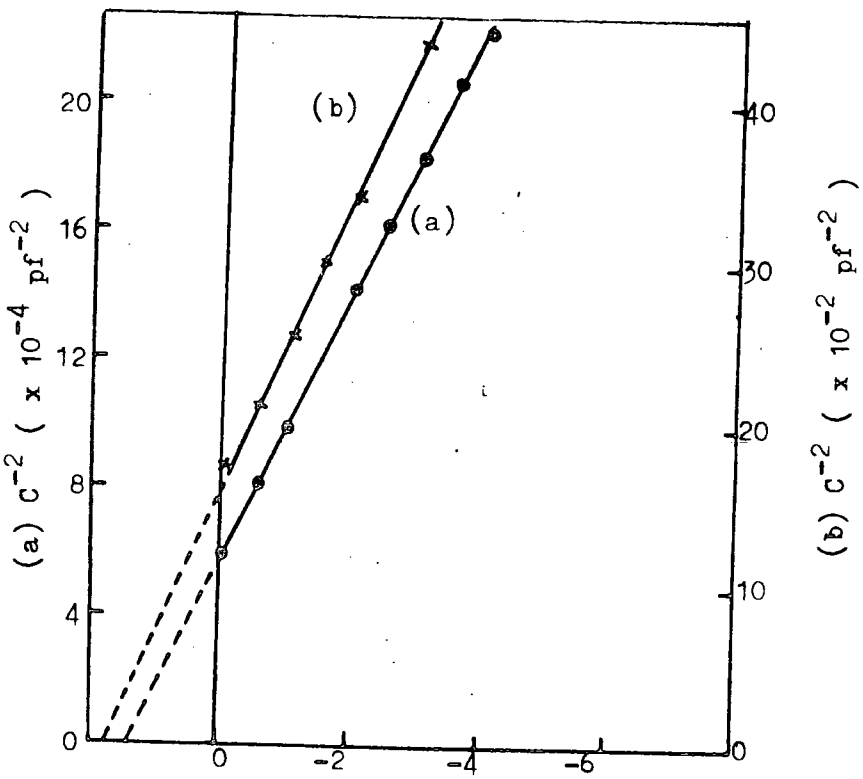

Fig 8.5 : C^{-2} vs V_r plots for ZnSe: 50ppm Ga diode at (a) T = 294K and (b) T = 85K.

and the reverse bias in volts, eqn. (3.6) is rewritten in the form,

$$N_d = \frac{2d\ (V_r)}{q\ \varepsilon_s d(C^{-2})\ A^2} \qquad (3.6')$$

where A is the area of the gold contact, to give the correct value of N_d.

For indium doped diodes the plots of C^{-2} versus V_r are shown in Figs. 8.1-8.3. At room temperature, the diode 407-20, fabricated from 5 ppm indium doped ZnSe, gave $N_d = 1.64 \times 10^{16}$ cm^{-3}, and diode 413-20, with 20 ppm indium, had $N_d = 2.73 \times 10^{15}$ cm^{-3}, obtained from curves (a) & (b) in Fig 8.1 respectively. For a 50 ppm indium doped sample, diode 405-9, gave $N_d = 6.8 \times 10^{14}$ cm^{-3} which was deduced from curve (a) in Fig 8.2. Much higher values of N_d were found in samples containing 50 ppm indium after they had been heated in molten zinc. Diode 405-Z2, Fig 8.2(b), gave $N_d = 2.32 \times 10^{16}$ cm^{-3} and device 405-X1, Fig 8.2(c), gave $N_d = 1.1 \times 10^{17}$ cm^{-3}. The diodes 405-Z2 and 405-X1 were fabricated on samples heated in molten zinc at 850°C for 15 and 24 hours, respectively. At liquid nitrogen temperature, values of $N_d = 1.24 \times 10^{16}$ cm^{-3} for ZnSe: 5 ppm In, 6×10^{14} cm^{-3} for ZnSe:20 ppm In and 4.1×10^{12} for ZnSe: 50 ppm In were found. The plots of C^{-2} versus V_r at this temperature are shown in Fig 8.3.

The plots of C^{-2} versus V_r for gallium doped samples are shown in Figs 8.4 and 8.5. The diode 387-20, ZnSe: 5 ppm Ga, had $N_d = 4.5 \times 10^{16}$ and 4.29×10^{16} cm^{-3} at room and liquid nitrogen temperatures, as obtained from curves (a) and (b) in Fig 8.4. With ZnSe: 50 ppm Ga, diode 409-7, a large difference in N_d was observed, varying from 4.9×10^{15} cm^{-3} at room temperature to 1.7×10^{12} cm^{-3} at liquid nitrogen temperature, see Fig 8.5.

All diodes showed straight lines in C^{-2} versus V_r plots, which suggests that the uncompensated donors were uniformly distributed in the depletion region. The decrease in N_d at lower temperature was observed in different diodes studied here and is attributed to incomplete donor ionization (free carrier freeze-out).

The uncompensated donor concentration, evaluated from the C^{-2} versus V_r plots, is equivalent to the free-carrier concentration (n) determined from Hall-effect measurements. A number of investigators have used the latter technique to measure the carrier concentrations in ZnSe variously doped with indium or gallium. Jones and Woods (1976) and Sethi and Mathur (1978) found that the carrier concentration decreased as the concentration of indium dopant increased. Using samples cut from the same boules as ours, Vincent (1980) reported from Hall measurements that the values of n dropped from $\sim 10^{16}$ to $\sim 10^{10}$ cm^{-3} while the doping concentration of indium increased from 5 to 1000 ppm. We conclude that the capacitance-voltage technique was successful and our results were in good agreement with earlier findings. As has been demonstrated in the preceding experimental chapters, a higher indium or gallium content does not necessarily lead to an increased concentration of donors. Instead it gives rise to at least two different acceptors. The acceptors compensate any possible increase in the density of donors with the result that there is a decrease in the number of uncompensated donors.

FERMI LEVEL:- The position of the Fermi-level, E_F, i.e. the difference between the bottom of the conduction band and top of the Fermi-level, can be calculated with the help of eqn. (3.16),

$$E_F = \frac{kT}{q} \ln \frac{N_c}{N_d}, \quad (eV) \qquad (3.16)$$

where, $\frac{kT}{q}$ = 0.0252 volts at T = 293 K,

$\frac{kT}{q}$ = 0.0072 " " T = 84 K,

N_c = Effective density of states in the conduction band,

= 1.7×10^{18} cm^{-3} at T = 293 K

= 2.6×10^{17} cm^{-3} at T = 84 K.

By using values of N_d in eqn.(3.16), the depths of the Fermi-level below the conduction band were found as given in Table 8.1, for different

Crystal	E_F (eV)		V_{do} (eV)		ϕ_c (eV)	
	∿ 293 K	∿ 84 K	∿ 293 K	∿ 84 K	∿ 293 K	∿ 84 K
ZnSe: 5ppm In (407-20)	0.117	0.022	1.875	1.657	1.887	1.560
ZnSe: 20 ppm In (413-20)	0.162	0.044	1.675	1.907	1.758	1.895
Zn Se:50 ppm In (405-9)	0.197	0.046	1.425	2.007	1.568	2.002
405 - Z2	0.108	-	2.025	-	2.069	-
405 - X1	0.069	-	2.675	-	2.494	-
ZnSe: 5ppm Ga (387-20)	0.019	0.013	1.625	1.525	1.559	1.538
ZnSe:50 ppm Ga (409-7)	0.147	0.086	1.425	1.807	1.484	1.880

TABLE 8.1 : Data from C-V Measurements for ZnSe : In & ZnSe : Ga

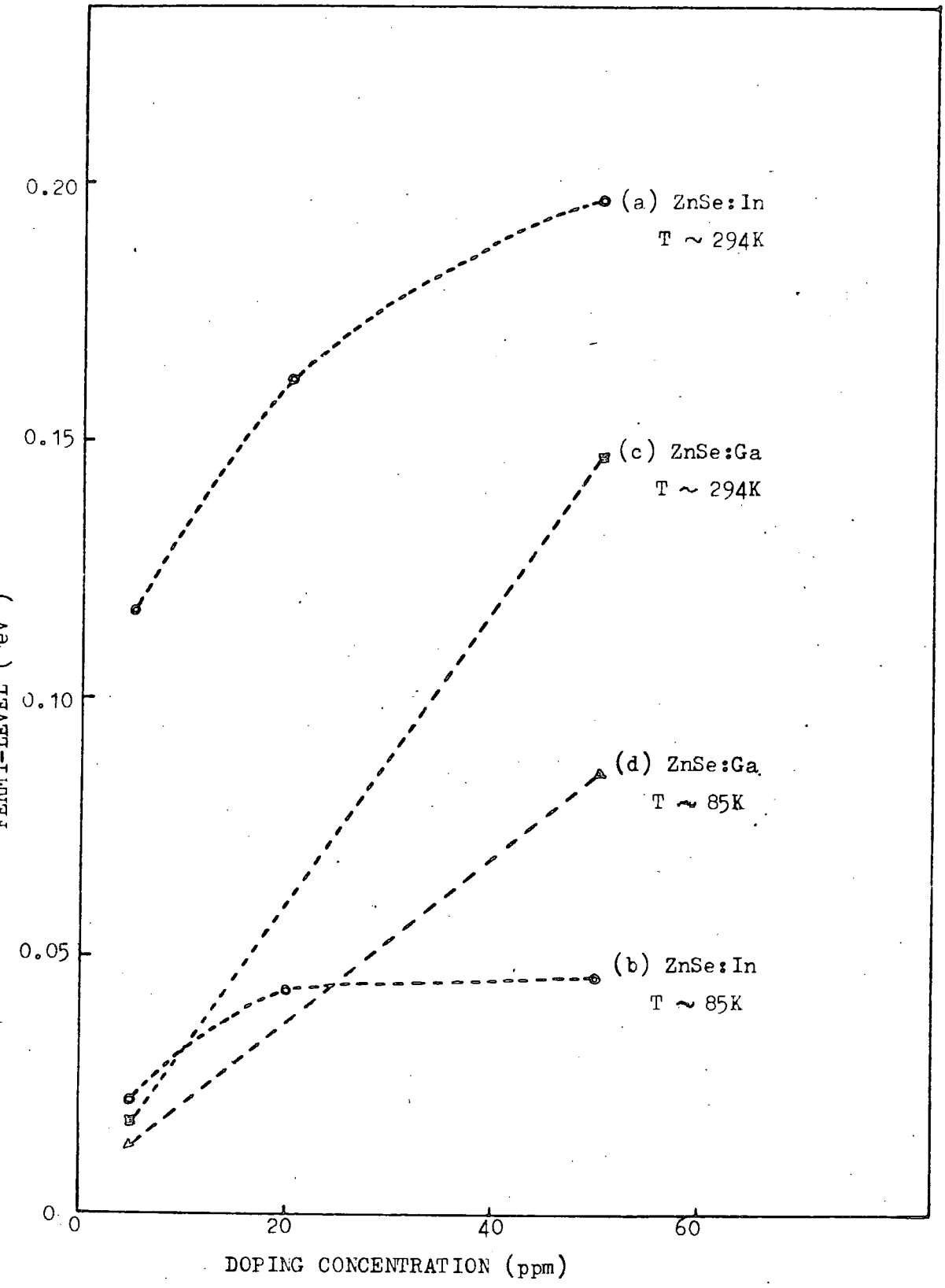

Fig 8.6 : Dependence of Fermi-levels on In or Ga doping concentration for (a) ZnSe:In, at 294K; (b) ZnSe:In, at 85K (c) ZnSe:Ga, at 294K and (d) ZnSe:Ga, at 85K.

indium or gallium doped samples. The Fermi-levels were closer to the conduction band in lightly doped ZnSe and moved further into the bandgap as the doping (in ppm) concentration increased. The dependence of E_F on the concentrations of indium or gallium is illustrated in Fig 8.6.

The variations are in fair agreement with the resistivities of the respective crystals.

DIFFUSION POTENTIAL AND BARRIER HEIGHT:- As has been described in Chapter 3, the C^{-2} versus V_r plots could be used to determine the barrier height (ϕ_c) of the Schottky diodes. According to eqn.(3.15),

$$\phi_c = V_{do} + E_F \quad (eV) \qquad (3.15')$$

ϕ_c = Barrier height determined from C-V measurements.

and $$V_{do} = V_i + \frac{kT}{q} .$$

The values of the diffusion potential (V_{do}) or band bending, see Fig 3.1, were determined by observing the intercept on the voltage axis in Figs. 8.1-8.5. The results are tabulated in Table 8.1, and showed that the more heavily (50 ppm) doped samples have the smallest band bending in comparison to the lightly doped samples which have a larger bending or diffusion potential. This effect reflects the different resistivities of the samples.

The knowledge of the diffusion potential and the Fermi-level can be used now in eqn.(3.15')to calculate the barrier height ϕ_c. The results obtained in this way are listed in Table 8.1. At room temperature ($\sim$ 293 K), ϕ_c was 1.887 eV for ZnSe: 5 ppm In and decreased to 1.568 eV for ZnSe: 50 ppm In. Similarly there was a difference between the barrier heights of gallium doped samples as shown in the table.

According to eqn (3.1), the barrier height depends on the metal work function (ϕ_m) and the electron affinity (χ_s) of the semiconductor and should be a constant. But in practice this does not often happen for many reasons. The metal work function might be changed as a result of the image force and the electric field in the barrier region, see Sze (1969). Bardeen (1947) showed that in the absence of surface states or in the presence of a sufficiently small surface state density, the barrier height should be a linear function of the metal work function. However, Crowell et al (1965), Rhoderick (1980) and many others have shown that there is always an insulating layer of considerable thickness between the metal and the semiconductor interface, which would influence the barrier height. A dependence of the barrier height on donor concentration has been demonstrated by Archer et al (1968) and Archer and Yep (1970) for diodes formed with Au contacts on n-type Si with $10^{14}\ cm^{-3} < N_d < 2 \times 10^{19}\ cm^{-3}$. They expressed the view that since the space charge of the depletion region depends on the donor concentration, the barrier height of a Schottky diode should depend on the donor concentration, due to the electric field in the semiconductor at the interface.

ELECTRIC FIELD AND BARRIER LOWERING:- The maximum electric field, E_{max}, at the interface of the metal-semiconductor contact under zero bias is given by,

$$E_{max}^2 = \frac{2q N_d}{\varepsilon_s} \left(V_d - \frac{kT}{q} \right) . \qquad (3.3)$$

Also, the lowering of the potential barrier by an amount $\Delta\phi$, (Schottky effect), as a result of combining effects of the image force and electric field is according to Sze (1969),

$$\Delta\phi = \left(\frac{q E_{max}}{4 \pi \varepsilon_o} \right)^{\frac{1}{2}}$$

where, $\varepsilon_o = 8.85 \times 10^{-14}$ F/cm.

Crystal	E_{max} (V/cm)		Δφ (eV)		W (μm)	
	∿ 293 K	∿ 84 K	∿ 293 K	∿ 84 K	∿ 293 K	∿ 84 K
ZnSe: 5ppm In (407-20)	1.13×10^5	9.25×10^4	0.105	0.115	0.33	0.36
ZnSe: 20ppm In (413-20)	4.33×10^4	2.18×10^4	0.079	0.056	0.38	1.25
ZnSe: 50ppm In (405-9)	1.99×10^4	1.84×10^4	0.054	0.051	1.01	2.40
405 - Z2	-	-	-	-	0.13	-
405 - X1	3.5×10^5	-	0.225	-	0.15	0.18
ZnSe: 5ppm Ga (387 - 20)	1.73×10^5	2.06×10^5	0.158	0.172	0.19	0.20
ZnSe: 50ppm Ga (409 - 7)	5.36×10^4	1.14×10^3	0.088	0.013	1.50	2.52

TABLE 8.2 : Data from C-V Measurements for ZnSe : In & ZnSe : Ga at zero bias.

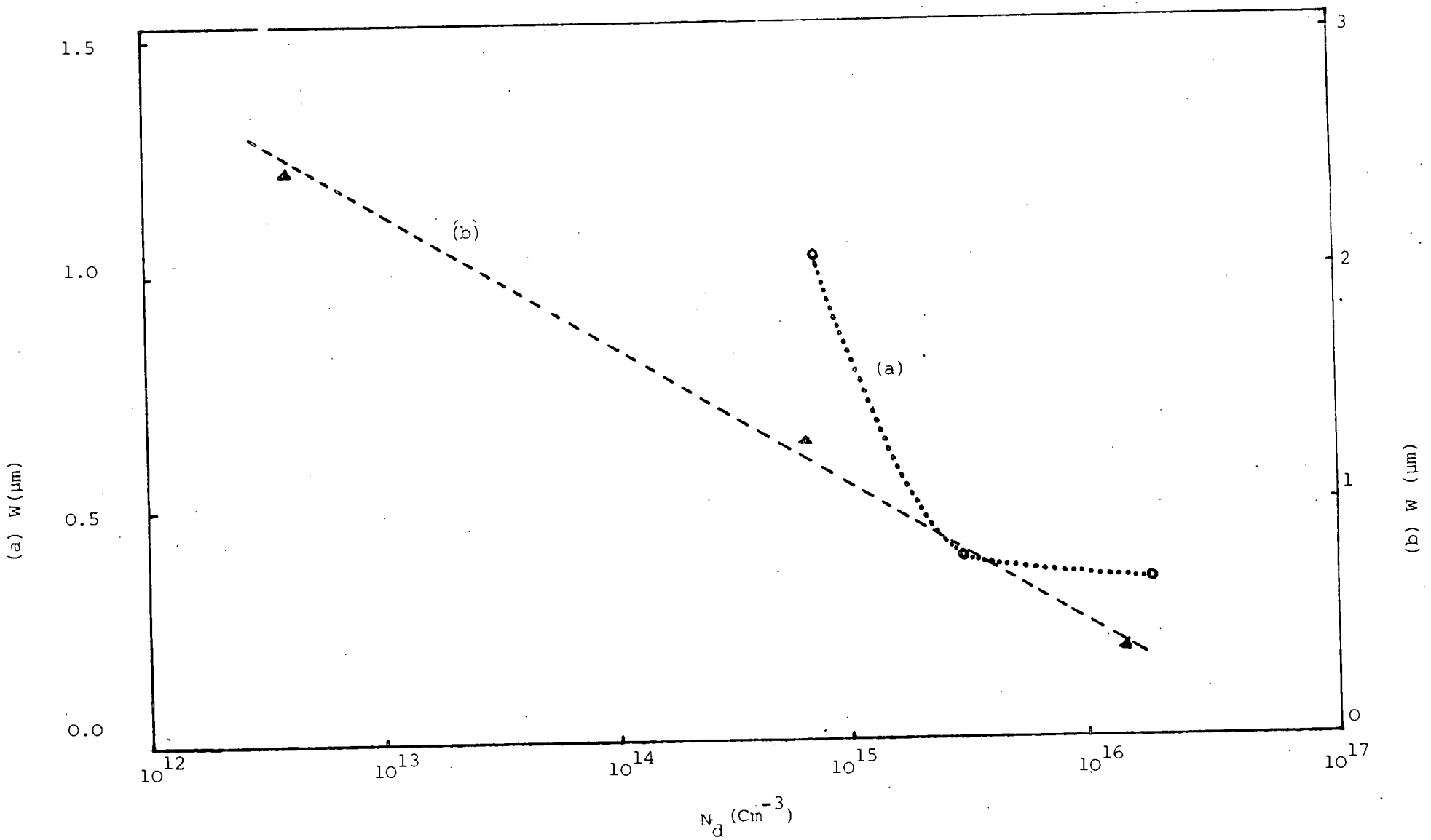

Fig. 8.7: Dependence of depletion width on the concentration of uncompensated donors for Au- ZnSe : In Schottky diodes, at zero bias.

(a) T ∿ 296K (b) T ∿ 85K.

The values of E and $\Delta\phi$ calculated from the above two expressions are recorded in Table 8.2. In general the magnitude of the electric field decreased as the concentration of indium or gallium increased. Since a decrease in the concentration of uncompensated donors was found in these samples, a decrease in E with increasing doping concentration (in ppm) is obviously expected.

The barrier lowering was large for lightly doped samples and small for highly doped samples. Evidently barrier lowering does not explain all the measured differences in barrier heights.

DEPLETION WIDTH:- The depletion width (W), Fig 3.1, of the Schottky diode should increase when the reverse bias is increased. Such measurements were employed as a part in Chapter 6, in the investigations of the concentration of deep centres. The width of the depletion region is determined from eqn (3.7a), rewritten in the form,

$$W = \frac{\varepsilon_s A}{C}, \quad (\mu m) \qquad (3.7a')$$

using $\varepsilon_s = 76.641 \times 10^{-14}$ F/cm,

$A = 2 \times 10^{-2}$ cm^2,

and knowing C from C-V measurements.

The values of W at zero bias for different indium or gallium doped samples are given in Table 8.2. Some results are plotted in Fig 8.7. The samples with the higher donor concentrations N_d (more lightly doped) had the narrower depletion regions and hence sharper band bending.

8.3 PHOTOELECTRIC MEASUREMENTS

Although C-V measurements can give an approximate estimate of the barrier height in a Schottky diode, the most accurate values are derived from photoelectric measurements. The appropriate theory is given in section 3.1.6 (a). The procedure is to measure the short circuit photocurrent per

incident photon, R, for different wavelengths of incident monochromatic light, and to plot absolute values of $\sqrt{R}$ against $h\nu$. This provides a measure of $h\nu_o \equiv \phi_p$ from the intercept on the energy axis. Absolute values of the incident photon flux (ϕ) were recorded as described in Chapter 6. The required values of R were obtained by dividing the measured photocurrent by the photon flux. The plots of $\sqrt{R}$ against $h\nu$ for indium or gallium doped samples are shown in Figs 8.8-8.10. The barrier heights obtained at room and liquid nitrogen temperatures are given in Table 8.3.

The measured barrier heights were lower at room temperature and higher at liquid nitrogen temperature. The temperature dependence of the barrier height has been studied by several workers. Crowell et al (1964) measured the temperature dependence of gold-silicon barriers using the photoelectric method and found that ϕ_p was a decreasing function of temperature. Arizumi and Hirose (1969) also found the height of gold-silicon barriers to decrease more or less linearly with increasing temperature. This has been explained in terms of the presence of surface states, and of the variation in the bandgap energy with temperature, using the relation, see Rhoderick (1980),

$$\phi_{bn} \approx E_g - \phi_o,$$

where ϕ_o is the neutral level for surface states (see Chapter 3). Since the bandgap energy in general increases with decreasing temperature, the barrier height should increase.

The measurements showed a decrease in barrier height as the concentration of indium or gallium decreased. This is in contrast with the barrier heights obtained by C-V measurements. The comparison of the barrier heights determined by these two methods will be discussed in the next section. In all Fowler plots some points were found at energies less than the threshold ($h\nu_o$) which are most probably associated with the tunnelling of photoexcited

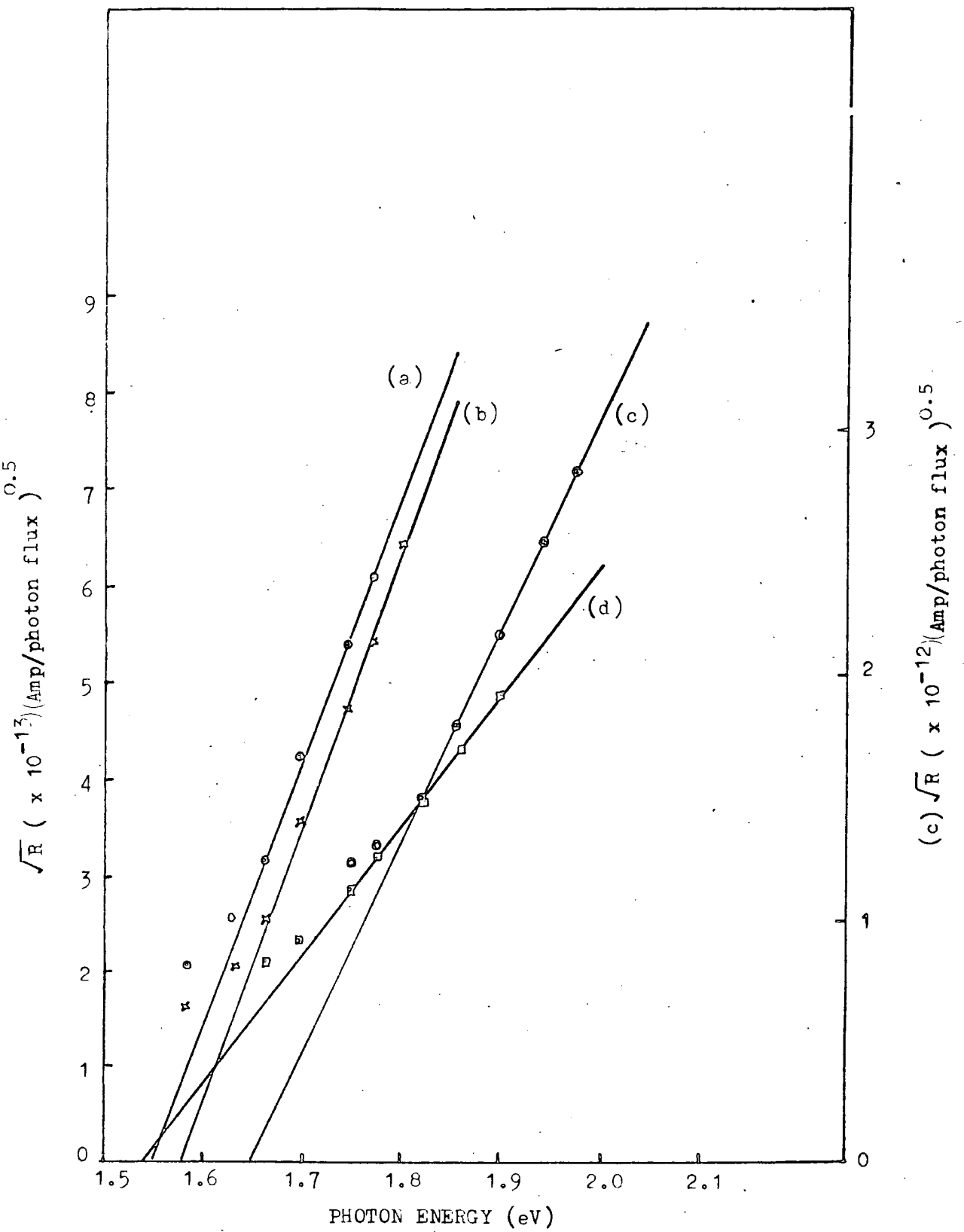

Fig 8.8 : Barrier height determination from photoelectric method at room temperature for ZnSe Schottky diodes containing (a) 5ppm, (b) 20ppm, (c) 50ppm In. and (d) 405-XI.

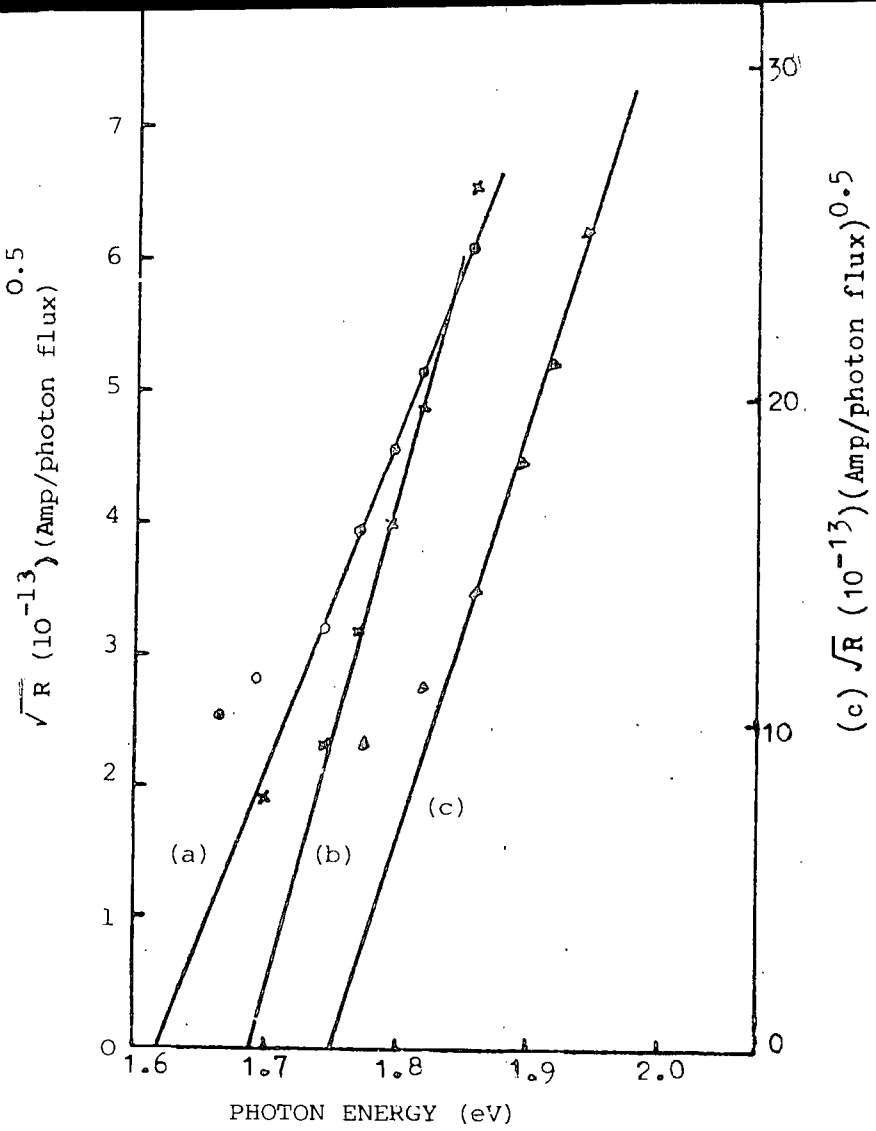

ig. 8.9 Barrier height determination from photoelectric method at T~84K for ZnSe Schottky diodes containing

(a) 5 ppm, (b) 20 ppm and (c) 50 ppm In.

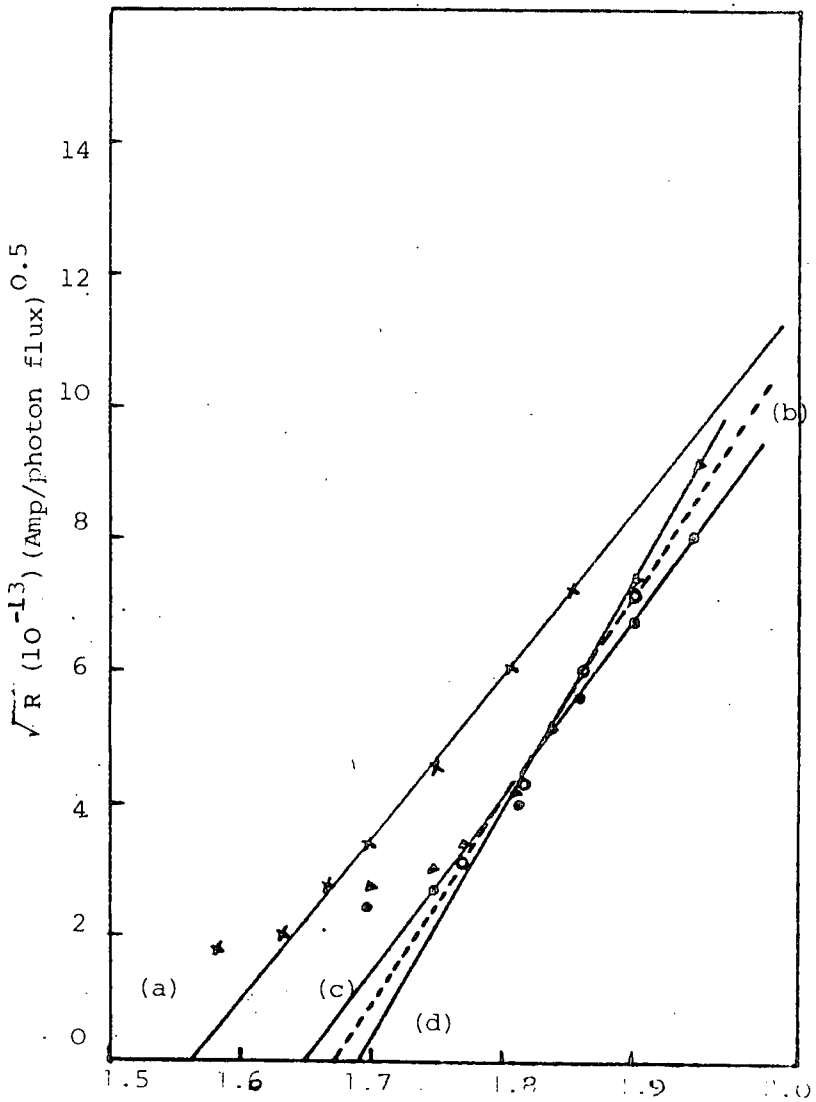

Fig. 8.10 Barrier height determination from photoelectric measurements of Schottky diodes for ZnSe : 5 ppm Ga (a) at T = 294K, (b) at T = 84K, and for ZnSe : 50 ppm Ga (c) at T = 294K, (d) at T = 84K.

electrons from the metal into the semiconductor. The barrier lowering, $\Delta\phi$, seems to be one source of the differences in the barrier heights of differently doped diodes. The lightly doped samples have low resistivity and therefore high concentrations of uncompensated donors, such diodes exhibit a large barrier lowering, so that an electron excited from the Fermi-level of the metal needs to acquire less energy to reach the semiconductor. In contrast the more heavily doped samples, have higher resistivities and lower N_d, so that the barrier lowering is less and net barrier heights are large.

TABLE 8.3

Crystal	ϕ_p (eV)	
	∿ 294 K	∿ 84 K
ZnSe: 5 ppm In	1.55	1.62
ZnSe: 20 ppm In	1.58	1.69
ZnSe: 50 ppm In	1.65	1.75
405 - X1	1.54	-
ZnSe: 5 ppm Ga	1.54	1.67
ZnSe: 50 ppm Ga	1.65	1.69

8.4 COMPARISON OF THE BARRIER HEIGHTS MEASURED BY C-V AND PHOTOELECTRIC METHODS

The values for the barrier heights, obtained from C-V and photoelectric measurements, are larger than the theoretical value 1.11 eV (determined from the difference of the metal work function and the electron affinity of the semiconductor), as well as the experimental value 1.40 eV reported by Swank et al (1969) for an Au-ZnSe contact prepared in ultra-high vacuum. On the other hand Özsan and Woods (1975 & 1977) using etched crystals measured a barrier of 1.63 eV in their Au-ZnSe system, but Grimmeiss et al (1976) reported a value of ϕ_{bn} = 1.51 eV in their ZnSe sample. There are two main problems with the C-V and photoelectric methods :

(1) The polishing and etching treatment prior to the deposition of gold leads to the formation of a semi-insulating oxide-layer, up to 240 Å thick, so that MIS rather than MS devices are prepared, see Özsan and Woods. The presence of an i-layer is the root cause of the difference between the values of ϕ_c and ϕ_p. In the absence of interface and surface state effects, the barrier heights measured from C-V and photoelectric methods will be equal, see Crowell and Roberts (1969).

(2) In the photoelectric method, the photoelectric current sometimes includes the current generated from deep levels, so that accurate measurements remain a problem. The influence of deep acceptor levels was avoided by Grimmeiss et al (1976) in their ZnSe:Mn samples by using light with $h\nu < 1.85$ eV. We also adopted this precaution with our indium and gallium doped ZnSe samples.

A comparison of the barrier heights measured by the C-V and photoelectric methods plotted as functions of uncompensated donor concentration (N_d), at room temperature is illustrated in Fig 8.11. A similar comparison of ϕ_c and ϕ_p against N_d, for Schottky barrier heights of Au contacts to n-type Si has been given by Archer and Yep (1970), and for MIS devices, by Crowell and Roberts (1969). The changes in the two barrier heights with variations in N_d,

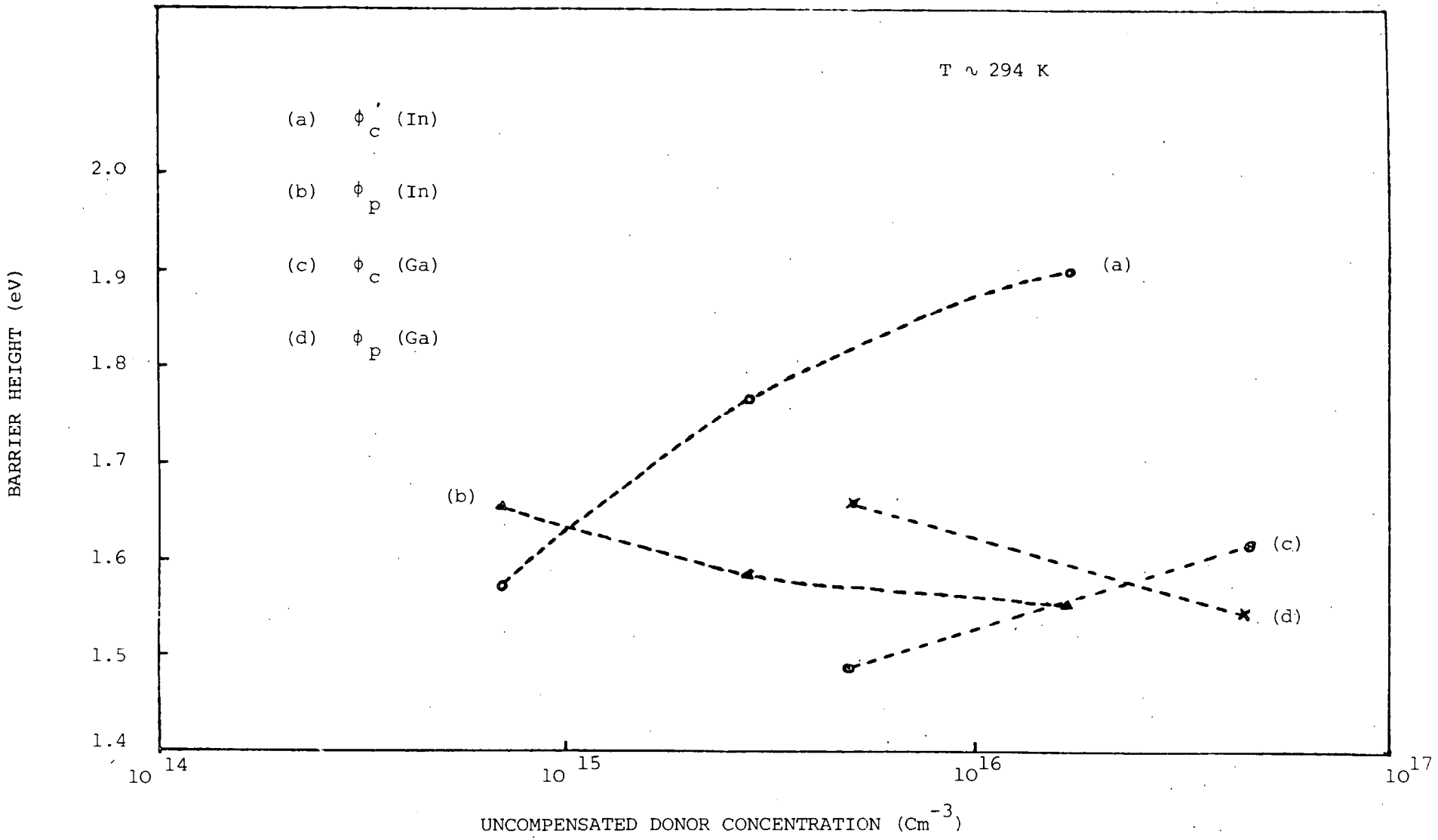

Fig. 8.11 Comparison of the barrier heights determined by C-V and photoelectric methods for In or Ga doped ZnSe diodes

in our samples, follow a pattern similar to that described by the above authors. Crowell and Roberts showed that the dependence of barrier height ϕ_b, on electric field E is given by

$$\frac{d\,\phi_b\,(E)}{dE} = -\varepsilon\left[\, q\, n_{ss} + \frac{\varepsilon_i}{\lambda_i}\,\right]^{-\frac{1}{2}} \qquad (8.1)$$

where,

E, see eqn (3.3) is directly proportional to N_d,

ε = The static permittivity of semiconductor,

ε_i = The permittivity of the i-layer,

n_{ss} = The density of semiconductor surface states,

and

λ_i = The thickness of the i-layer

Equation (8.1) includes the effects of surface states and of an interfacial layer. It suggests that the barrier height should decrease with increasing values of E and N_d. The barrier height may be relatively independent of E if n_{ss} is large, or if λ_i is small. The barrier height ϕ_b shown in the above equation is the true barrier height ϕ_p measured by the photoelectric method. In contrast the C^{-2} versus V_r plots only give an apparent barrier height, ϕ_c, and according to Crowell and Roberts, the two barrier heights are related by

$$\phi_c \equiv V_i + U = \phi_p - E\left\{\frac{d\phi_b}{dE}\right\} + \left\{\frac{q\,N_d}{2\,\varepsilon}\right\}\left\{\frac{d\phi_b}{dE}\right\}^2 \qquad (8.2)$$

where

$$U \equiv \frac{kT}{q}\left[\, 1 + \ln\frac{N_c}{N_d}\,\right]$$

and V_i is the voltage intercept.

In eqn (8.2) the term $\left\{ \frac{d\phi_b}{dE} \right\}$ is negative so that barrier heights measured by the C-V method are larger than those derived from photoelectric measurements. ϕ_c will also increase when E or N_d increase.

The two expressions (8.1) and (8.2) can readily explain our results on indium and gallium doped samples. As shown in curves (b) and (d) in Fig 8.11, the barrier heights measured by the photoelectric method decrease and follow eqn. (8.1) as the density of uncompensated donors increases. On the other hand the barrier heights obtained by the C-V method are in agreement with eqn (8.2), and increased with increasing N_d, see curves (a) and (c) in the same diagram.

According to eqn (8.2), $\phi_c > \phi_p$, and this is true in our results on low resistivity samples. However, in the more heavily doped samples with 50 ppm indium or gallium, $\phi_c < \phi_p$. Crowell and Roberts (1969) have analyzed such a situation in terms of the influence of a deep donor level. For this case the true barrier height can be deduced from the following relationship:

$$\phi_p = V_i + U + \frac{N_t \left[E_t - U + (kT/q) \ln g \right]}{N_d + N_t} \qquad (8.3)$$

where,

N_t = Deep donor density

E_t = Depth of deep donor level from the conduction band edge,

and g = Donor degeneracy factor.

From the above results, if ϕ_c $(\equiv V_i + U) > \phi_p$, this is evidence for surface state and interface effects, eqn (8.2). If $\phi_c < \phi_p$, this is evidence for the existence of an appreciable density of deep lying impurities, eqn (8.3). Equality of ϕ_c and ϕ_p implies that either the ideal case obtains or that interface states are compensated by the effects of deep lying impurities.

8.5 CONCLUSION

A large number of ZnSe crystals, containing between 5 and 250 ppm of indium or gallium, were used to fabricate Schottky diodes for this investigation. The resistivity of the samples was the dominant feature and as described in the preceding chapters, it increased with increasing doping concentration, due to compensation effects. Fairly good Schottky diodes were obtained on samples containing 5 to 50 ppm of indium or gallium with resistivities of the order of $\sim 10^2$ to 10^4 ohm cm, at room temperature. The increasing resistivity set a limit to the experimental study. Nevertheless, the following pattern of behaviour was observed, which agreed quite well with earlier reported work :

(1) The uncompensated donor or free carrier concentration, N_d, is large for lightly (5 ppm) doped samples and small for heavily (50 ppm) doped ones. This study supports the results reported earlier in this thesis that higher concentration of indium or gallium contributed to the creation of an extra acceptor at $\sim$ 0.41 eV above the valence band which compensated the donors and increased the resistivity.

(2) The position of the Fermi-level varied with the resistivity and temperature of the material. The Fermi-level was closer to the conduction band for samples containing lower concentrations of indium or gallium.

(3) The diffusion potential, V_{do}, was inversely proportional to the doping concentration or directly proportional to the uncompensated donor concentration. This shows that lightly doped samples had comparatively sharp band bending.

(4) Large depletion widths were recorded for the most heavily doped devices.

(5) Devices on lightly doped samples have a large electric field at the interface and a large barrier lowering effect, due to the higher values of N_d.

(6) The barrier heights ϕ_c and ϕ_p determined by the capacitance-voltage and photoelectric methods, respectively, were dependent on the doping concentration. The value of ϕ_c increased with increasing N_d or decreasing indium or gallium concentrations, whereas ϕ_p decreased.

CHAPTER 9

CONCLUSIONS

9.1 SUMMARY OF RESULTS

The main aim of the research reported in this thesis has been to investigate indium and gallium doped ZnSe to determine whether acceptors as well as donors are formed by these impurities. In addition, nominally pure crystals and samples doped with copper, chlorine, and copper and chlorine have been examined for comparison.

For this purpose crystals were grown in the departmental laboratory, using the vapour phase technique. The concentrations of indium or gallium in ZnSe were determined by atomic absorption analysis.

The resistivities of different as-grown crystals varied from 92 to 10^{13} ohm-cm, and this created severe problems preventing the use of a single photoelectric technique to determine the position of impurity levels in all crystals. Since measurements of steady state photoconductivity and infra-red quenching could be employed with high resistivity (ρ) samples, these techniques were used on simple bulk specimens with resistivities $\rho \gtrsim 10^4$ ohm-cm. at room temperature. On the other hand, Schottky diodes were made on low resistivity ($\rho \lesssim 10^4$ ohm-cm) crystals and transient photocurrent and various photocapacitance techniques were exploited.

Measurements of I-R quenching of photoconductivity on high resistivity samples revealed the following deep acceptors :

S.N.	$E_A - E_V$ (eV)	Crystal
1.	0.65 $\pm$ 0.02	Nominally pure & ZnSe:Cu
2.	0.56 $\pm$ 0.01	ZnSe : Cl
3.	0.58 $\pm$ 0.01	ZnSe : In
4.	0.54 - 0.60	ZnSe : Ga
5.	0.82 & 1.25	ZnS : Ga & ZnS : Cu

Here $E_A - E_V$ is the difference between the acceptor level and the top of the valence band. The deeper (0.65 ± 0.02) eV level is due to Cu'_{Zn} centres; the levels at (0.56 ± 0.01), (0.58 ± 0.01) and (0.54 - 0.60) eV are for self-activated centres, associated with $(V_{Zn} - Cl_{Se})'$, $(V_{Zn} - In_{Zn})'$ & $(V_{Zn} - Ga_{Zn})'$ centres, in ZnSe. With ZnS the value of $E_A - E_V$ = 1.25 eV is for copper impurity, while 0.82 eV is for the self-activated centres, $(V_{Zn} - Ga_{Zn})'$. The measurements of steady state photoconductivity were inconclusive, although the spectral response curves showed the presence of many defect centres.

As mentioned earlier, the main object of the research was the study of indium and gallium doped ZnSe. These crystals were highly compensated, and increased concentrations of indium or gallium led to increased resistivities. The uncompensated donor concentrations, $N_D^+ - N_A^-$, were determined from C-V measurements on Schottky diodes, fabricated on these crystals. The values of $(N_D^+ - N_A^-)$ and corresponding room temperature resistivities of ZnSe crystals doped with different concentrations of indium or gallium are given below :

S.N.	Crystal	$N_D^+ - N_A^-$ (cm^{-3})	ρ (ohm-cm)
1.	ZnSe: 5 ppm In	1.64×10^{16}	7×10^2
2.	ZnSe:20 "	2.73×10^{15}	8×10^3
3.	ZnSe:50 "	6.8×10^{14}	5.1×10^4
4.	ZnSe: 5 ppm Ga	4.5×10^{16}	92
5.	ZnSe:50 "	4.9×10^{15}	2.9×10^3

The table clearly shows that the free carrier concentration, or $N_D^+ - N_A^-$, decreased and resistivities increased, when more indium or gallium was incorporated in the ZnSe. The reduction in free electron concentration is attributed to several self-compensating effects. Ray and Kröger (1978) and Sethi and Mathur (1978) have reported similar effects in gallium and indium doped ZnSe. We have attempted to understand the compensation mechanism by

investigating the defects formed by adding indium or gallium.

Using the photocurrent and photocapacitance transient techniques, as advocated by Grimmeiss et al (1976), and with the help of Lucovsky's theoretical plot, we have accurately located one deep acceptor at 0.59 eV and another at 0.41 eV above the valence band in indium doped ZnSe. The second level was more pronounced in samples with higher indium content, which strongly suggested that indium contributed to enhancing this acceptor. This was well supported by the calculation of the concentration of the 0.59 eV acceptor, which decreased from $N_T \simeq 3 \times 10^{15}$ cm^{-3} in ZnSe : 5 ppm In to $N_T \simeq 6 \times 10^{14}$ cm^{-3} in ZnSe: 50 ppm In. In gallium doped crystals the self-activated acceptor was at 0.55 eV above the valence band in all doping concentrations. The concentration N_T also dropped from 3.4×10^{15} cm^{-3} in ZnSe : 5 ppm Ga to 1.1×10^{13} cm^{-3} in ZnSe : 50 ppm Ga. This suggests that gallium behaves similarly to indium. In higher doping concentrations (i.e. 50 ppm Ga) an additional level was found at about 0.40 eV above the valence band from transient photocapacitance measurements, but this was not supported by measurements of steady state photocapacitance. According to Yamaguchi et al (1977) the solubilities of indium and gallium in ZnSe are different and depend on the atomic radii of the different constituents, hence rather more gallium atoms might be expected to sit on zinc sites than indium atoms do. This conforms with the observation that the compensating effect was slightly less pronounced when gallium was used as the dopant.

It has been established by several authors that there are always some unavoidable acceptor levels present in n-type ZnSe, such as zinc vacancies and copper impurities, which can adopt various charge states, e.g. neutral (Cu_{Zn}^{x}), singly charged ($Cu_{Zn}^{'}$ and $V_{Zn}^{'}$) or doubly charged ($V_{Zn}^{''}$). These deep acceptors compensate the donors (i.e. selenium vacancies, zinc interstitials, etc) and give rise to high resistivity in ZnSe. Indium and gallium are group IIIa elements and are known to introduce substitutional donors, but our work, and

that of several others has established that these dopants are not so well behaved as the other group IIIa element aluminium. Compensation in indium or gallium doped ZnSe is very strong and increases with increasing concentration. It appears that acceptors other than that associated with the self-activated centre are involved. As inferred by previous workers, it is argued that some of the indium (gallium) atoms replace selenium ions in the lattice and then acceptor complexes such as $(In_{Zn}\text{-}In_{Se})'$ or $(Ga_{Zn}\text{-}Ga_{Se})'$, $(In_{Zn}\text{-}In_{Se})''$ or $(Ga_{Zn}\text{-}Ga_{Se})''$ and $(In_{Se})'''$ or $(Ga_{Se})'''$ could be formed. The level at 0.41 eV might be associated with one of these complexes, which compensate the donor concentration with increasing indium or gallium content.

The measurements of steady state photocapacitance revealed the presence of a variety of donor levels, for example at 0.03 and 0.20 eV below the conduction band in ZnSe: In and 0.03 and 0.18 eV in ZnSe:Ga. Oddly we failed to detect any donors in lightly (5 ppm) doped crystals using the photocapacitance technique, but instead a shallow acceptor 0.13 eV above the valence band was found. This needs further investigation.

Peculiar characteristics were found, when samples containing 50 ppm or more concentration of indium or gallium were heated at 850° C in molten zinc. They became black in colour and no deep levels were found. Examination in the transmission electron microscope revealed that the blackening effect is associated with the formation of precipitates probably in the form of In_2Se or In-Zn alloy (see Appendix).

9.2 MODEL

At this stage when the whole work has been summarized, it would be appropriate to represent the results in a pictorial diagram, i.e. a model, comprising the various defect levels and parameters of Schottky barrier region. The model as shown in Fig 9.1, is for a Schottky diode fabricated on ZnSe doped with 50 ppm indium or gallium, at liquid nitrogen temperature. It is not possible to construct a general model, satisfying all doping concentrations.

The energy level diagram illustrates the positions of two donors,

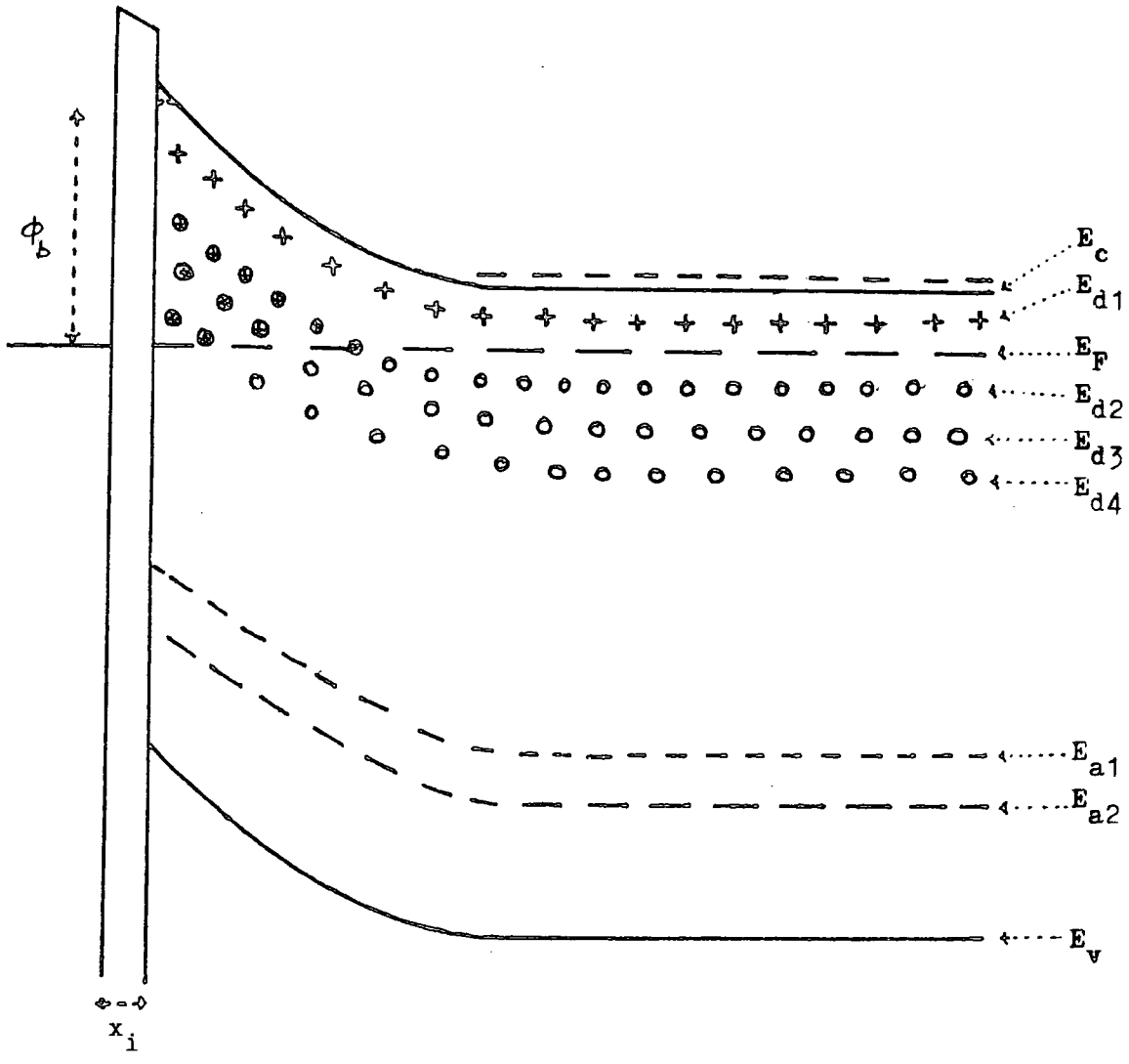

Fig 9.1 : PROPOSED MODEL FOR Au - ZnSe : 50 ppm In or Ga SYSTEM

$E_c - E_{d1}$ = 0.03 eV and $E_c - E_{d2}$ = 0.19 eV, and two acceptors, $E_{a1} - E_v$ = 0.58 - 0.59 eV and $E_{a2} - E_v$ = 0.40 - 0.42 eV, in ZnSe: 50 ppm In. The Fermi-level was at 0.046 eV below the conduction band and suggests that the shallow level 0.03 eV lay above it in the bulk as well as in the depletion region. All levels are ionized (i.e. donors positively and acceptors negatively) in the space-charge region because of the band bending. The barrier height determined by the photoelectric method for this diode was 1.75 eV.

According to Özsan and Woods (1975, 1977) there is always an insulating layer on ZnSe after it has been etched in bromine in methanol. Its thickness, x_i, shown here is not known, but according to Özsan and Woods it should be of the order of 240 Å.

In ZnSe doped with 50 ppm gallium, six impurity levels were observed. There is one shallow donor with $E_c - E_{d1}$ = 0.03 eV which is above the Fermi-level ($E_c - E_F$ = 0.086 eV) of the sample. The deep donors at $E_c - E_{d2}$ = 0.17 eV, $E_c - E_{d3}$ = 0.26 eV and $E_c - E_{d4}$ = 0.32, are well below the Fermi-level in the bulk (neutral region) but are ionized in the space-charge region, $W-W_o$ = 1.52 μm. The deep acceptors are at $E_{a1} - E_v$ = 0.55 eV and $E_{a2} - E_v$ = 0.40. The barrier height for this diode was 1.69 eV.

The characteristic data for both samples is summarised in Table 9.1.

TABLE 9.1 : Experimentally determined values for the model shown in Fig 9.1.

	ZnSe : 50 ppm In	ZnSe : 50 ppm Ga
ϕ_p (ϕ_b)	1.75 eV	1.69 eV
$E_c - E_F$	0.046 eV	0.086 eV
$E_c - E_{d1}$	0.03 eV	0.03 eV
$E_c - E_{d2}$	0.19 eV	0.17 eV
$E_c - E_{d3}$	-	0.26 eV
$E_c - E_{d4}$	-	0.32 eV
$E_{a1} - E_v$	0.58 - 0.59 eV	0.55 eV
$E_{a2} - E_v$	0.40 - 0.42 eV	0.40 eV
$E_c - E_v$	2.80 eV	2.80 eV

9.3 P-TYPE CONDUCTION AND COMPENSATION

Past experience clearly suggests that it is very difficult to grow low resistivity p-type ZnSe. The results of Bhargava et al (1979), Neumark (1979), Kosai et al (1979), Neumark (1980) and many others, have shown that all of the acceptor impurities (Li, Na, P) which have been tried in attempts to achieve type conversion gave very weak or inconclusive p-type conduction in ZnSe. Robinson and Kun (1975) claimed to have obtained highly conductive p-type layers on n-type ZnSe by in-diffusion of either indium or gallium, but their work has never been repeated successfully. Their explanation for p-type conversion was that indium and gallium may be present in both monovalent and trivalent states as reported by Raüber and Schneider (1966), and that these ions could act as acceptors in their monovalent state. However, Ray and Kröger (1978) refute this explanation.

ZnSe, like most of the II-VI compounds, is an n-type semiconductor and when group IIIa elements are added, these should behave as singly charged donors by substituting for zinc atoms on zinc sites and hence the conductivity should increase with increasing dopant concentration. This is what happens with aluminium doping, but a decrease in conductivity is found when high concentrations of indium or gallium are added as described in this thesis. This unusual behaviour may be associated with the phenomenon of self-compensation. Many years ago, de Nobel (1959) discussed self-compensation in CdTe by native defects, and it has commonly been accepted to be the main cause preventing the predominantly n-type materials ZnS , ZnSe, CdS or CdSe, from being prepared p-type, or p-type ZnTe from being made n-type.

Aven et al (1961) found that ZnSe doped with gallium was weakly n-type, suggesting that most of the donors were compensated by zinc vacancies. Wagner and Lorenz (1966) reported that the resistivity of heavily doped ZnSe: Ga was much higher than comparably doped ZnSe: Al. Jones and Woods (1976) also found

similar behaviour with indium or gallium doped ZnSe. Many workers have shown that zinc vacancies and unintentional copper impurities give rise to deep acceptors which compensate donors, leading to low conductivity material. This approach does not seem to be applicable in our indium or gallium doped ZnSe, because from atomic absorption analysis, see Chapter 4, we found no trace of copper in these crystals. Also the compensation in our crystals was doping profile dependent. Sethi and Mathur (1978) and Sethi et al (1978a, 1978b) from Hall measurements on indium doped ZnSe also observed a strong reduction in the carrier concentration with increasing indium concentration ; they concluded that doping of ZnSe with indium resulted in increasing compensation due to the formation of complex acceptor centres. Ray and Kröger (1978) have explained the compensation in ZnSe:Ga in terms of complex acceptors formed in association with gallium. Their approach is most applicable to the problem of compensation in our crystals.

Type conductivity can be determined from thermo-electric power measurements, but the direction of easy-current flow in a Schottky diode can also be used to determine whether the semiconductor is n- or p-type. All diodes prepared and examined in this work with gold as the metal contact have shown that n-type conduction dominated without exception. These findings are in full agreement with previous work (i.e. thermoelectric power and Hall measurements) done on these crystals previously by Vincent (1980).

We conclude that indium or gallium cannot be used to produce p-type ZnSe. Our work suggests that these impurities give rise to deep acceptors rather than shallow ones.

9.4 FUTURE WORK

In the investigations reported in this thesis, several donors and acceptors, associated with indium or gallium in ZnSe crystals have been observed. The conductivities of the samples were dependent on the doping concentration. This was the major handicap in analysing all types of crystals with concentrations of

indium (gallium) ranging from 5 to 1000 ppm with any single technique. Our observations suggest that the deep acceptor some 0.41 eV above the valence band is responsible for the pronounced compensation. Unfortunately, the observations were limited to samples doped with 50 ppm indium (gallium). With higher concentrations Schottky diodes could not be prepared.

With the high resistivity samples, the technique of infra-red quenching of photocurrent could be employed to investigate levels closer to the valence band, if a proper source of excitation were available. Photoluminescence and optically detected magnetic resonance (ODMR) techniques could also probably be used with success. The latter experimental methods are also suited to the study of other deep and shallow centres. Studies of photoluminescence emission and excitation at liquid helium temperatures would be very helpful in confirming the presence of the shallow acceptor 0.13 eV above the valence band in lightly (5 ppm In or Ga) doped ZnSe as well as in locating shallow donors.

Recently infra-quenching of photocapacitance has been used in analyzing deep acceptors and this would be very useful in determining absolute values of cross-sections and concentrations of deep acceptors in low resistivity samples. These measurements in conjunction with those from the transient photocurrent technique, will give a better understanding about the deep acceptor levels. Constant photocapacitance (CPT) is another successful technique which could be employed. The deep level transient spectroscopy (DLTS) technique is a practical method for small bandgap materials but it can also be used with advantage on materials with larger bandgaps such as ZnSe.

APPENDIX

ELECTRON MICROSCOPE STUDY OF PRECIPITATES

1. INTRODUCTION

The as-grown crystals of ZnSe doped with indium or gallium were yellowish-brown and transparent. However, the crystals containing 50 ppm or more indium or gallium, after being heated in molten zinc at 850°C, became black in colour and opaque. The electrical properties of the doped material were changed completely by the zinc treatment, and became quite different from those of undoped crystals subjected to the same treatment, see Chapter 7.

In the present chapter an account is given of a Transmission Electron Microscope (TEM) study of the precipitates formed in indium doped crystals following heat treatment in zinc.

2. TEM STUDIES

The specimens were chemically polished in a solution of chromium trioxide in phosphoric and hydrochloric acids (see Hemmatt and Weinstein,1967), to produce regions that were very thin (less than a few thousand Angstroms) in order to allow the electron beam to pass through and produce clear images and diffraction patterns. The instrument used was a JEM 120 Transmission Electron Microscope.

The TEM examination of the as-grown indium doped specimens revealed a defect structure which was indistinguishable from that of undoped as-grown ZnSe, see Cutter et al (1976). Similar defect structures were also observed in ZnSe samples, doped with 5 & 20 ppm indium, which had been heated at 850° C in molten zinc for five days. To illustrate the various features observed in these samples, micrographs of ZnSe: 5 ppm In after zinc-treatment, are shown in Figs A1.1 and 1.2. The lighter region on the right-hand side in Fig A1.1 is the thin edge of the sample and thickness fringes or extinction contours lie

parallel to it. The micrograph in Fig A1.2 is from a similarly treated specimen from the same boule and also shows thickness fringes, but it contains one twin band. Twin bands were the defects most frequently encountered in this material. The frequency of the twinning varied enormously from sample to sample. Dislocations and stacking faults were not encountered in any of this group of samples. It was obvious that grown-in indium had a negligible effect on the crystal structure.

While the defect content of lightly doped (5 & 20 ppm indium) specimens did not appear to be affected by the zinc treatment, see Figs A1.1 & 1.2, this process gives rise to precipitates and other defects in samples doped with 50 ppm of indium or more. In Figs A(1.3-1.5), the micrographs are of samples, taken from ZnSe: 50 ppm In, boule 405, which had been heated in liquid zinc at 850^{o}C for 5 days. In particular, the precipitates were found to decorate all the twin boundaries as well as the intrinsic stacking faults and dislocations, which were formed as a consequence of the heat treatment given to these crystals. The micrograph in Fig A1.3 shows precipitates, appearing as regions of dark contrast superimposed on the stacking fault fringes extending from one partial dislocation to the other. The row of small dots away from the stacking fault at A may also be precipitates. In another similarly treated specimen from the same boule (405), some larger precipitates may be clearly seen to be decorating a stacking fault lying between the two partial dislocations (A & B) see Fig A1.4. A dislocation decorated by precipitates is shown at C in Fig A1.5. In general, after zinc treatment, all specimens containing 50 ppm In were found to contain precipitates but for this concentration of indium, it was not possible to define their shape.

The precipitates began to show definite morphologies when samples with higher indium concentration were heated in molten zinc at 850^{o}C. The micrographs in Figs A1.6 & 1.7 are from a heat treated specimen of 250 ppm indium doped ZnSe, obtained from boule 408. In fact, most of the precipitates observed

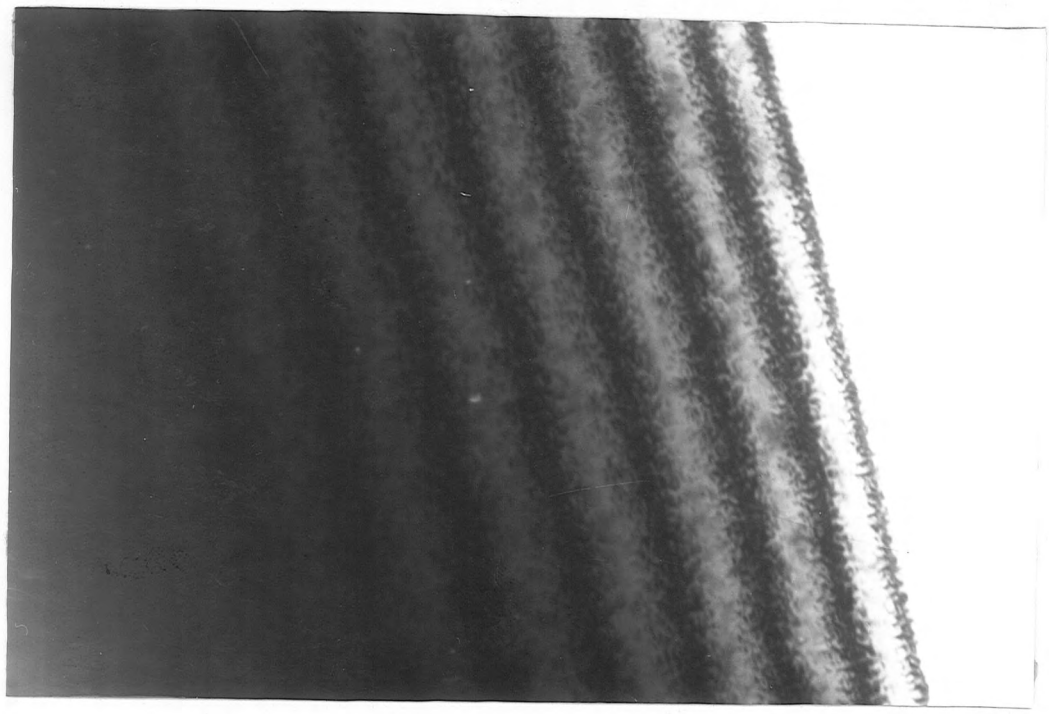

Fig A1.1 : Micrograph of ZnSe:5ppm In after zinc-treatment , showing thickness fringes. (X 30000)

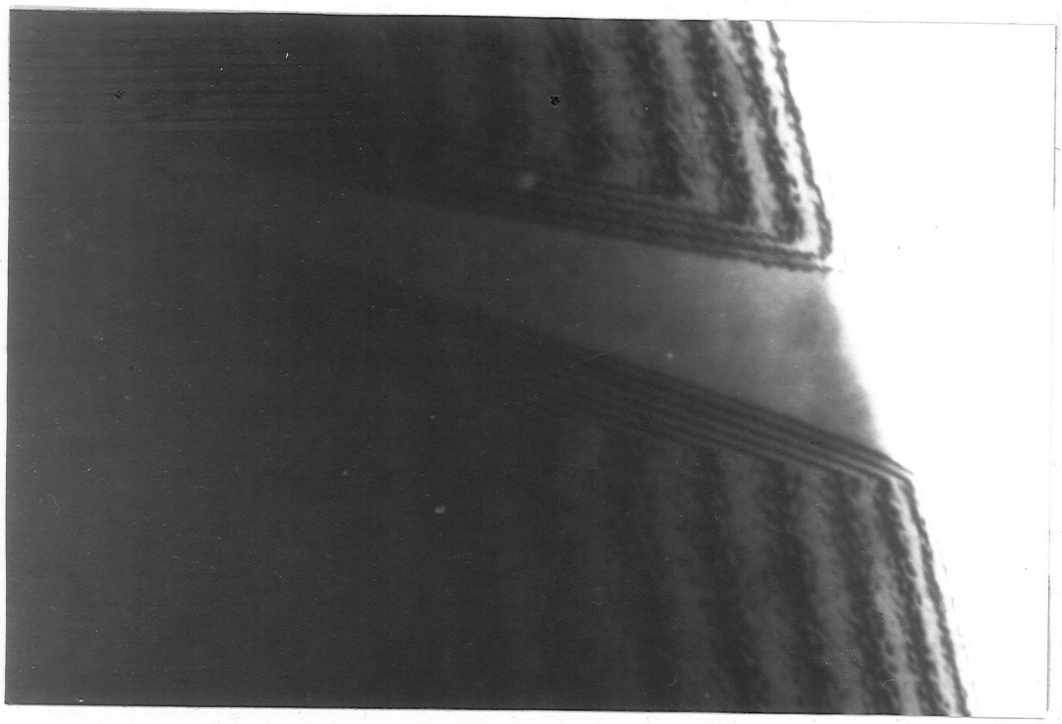

Fig A1.2 : Micrograph of ZnSe:5ppm In after zinc-treatment , showing thickness fringes and one twin band. (X 30000)

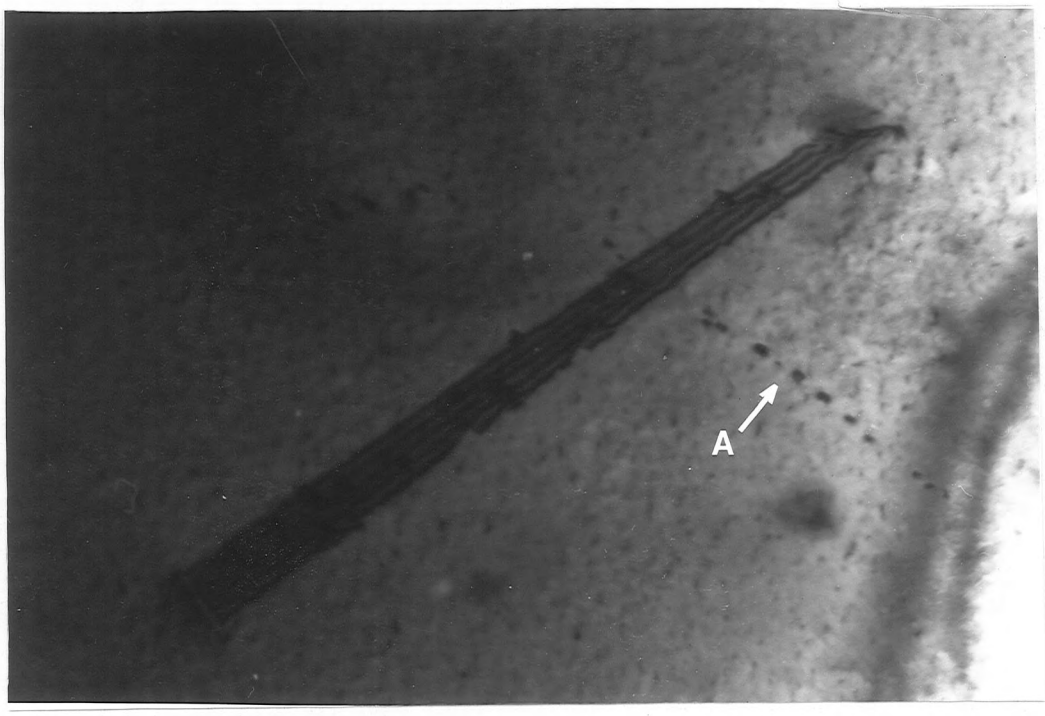

Fig A1.3 : Micrograph of ZnSe:50ppm In after zinc-treatment , showing precipitates , a stacking fault and partial dislocations. (X 52000)

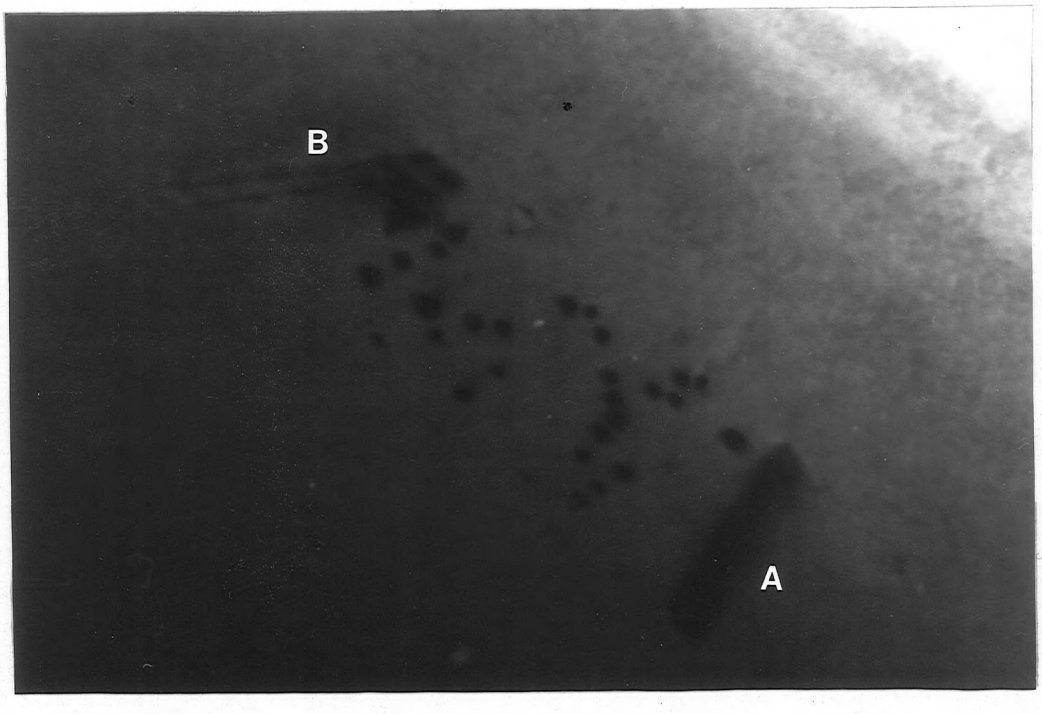

Fig A1.4 : As in fig A1.3 but of a different region with the diffraction conditions selected to eliminate the stacking fault fringe contrast. (X 52000)

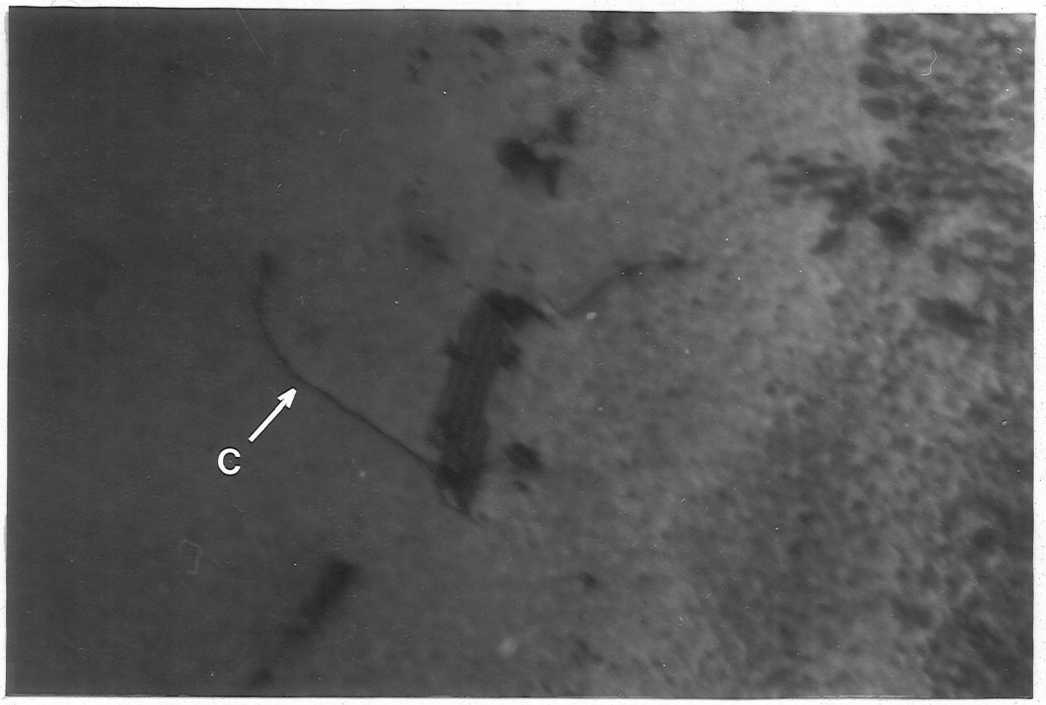

Fig A1.5 : Micrograph of ZnSe:50ppm In after zinc treatment , showing precipitates decorating dislocation (C) and stacking fault. (X 52000).

Fig A1.6 : Micrograph of ZnSe:250ppm In after zinc-treatment , showing spherical precipitates decorating a stacking fault. (X 52000)

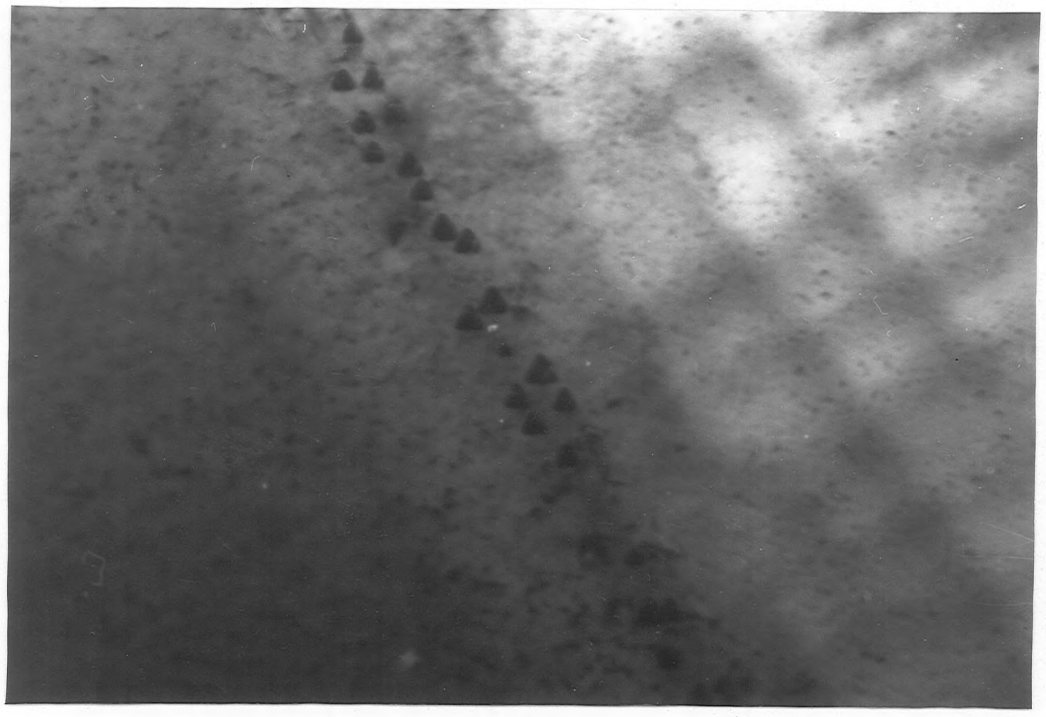

Fig A1.7 : Micrograph of ZnSe:250ppm In after zinc treatment , showing triangular precipitates decorating a grain boundary. (X 52000)

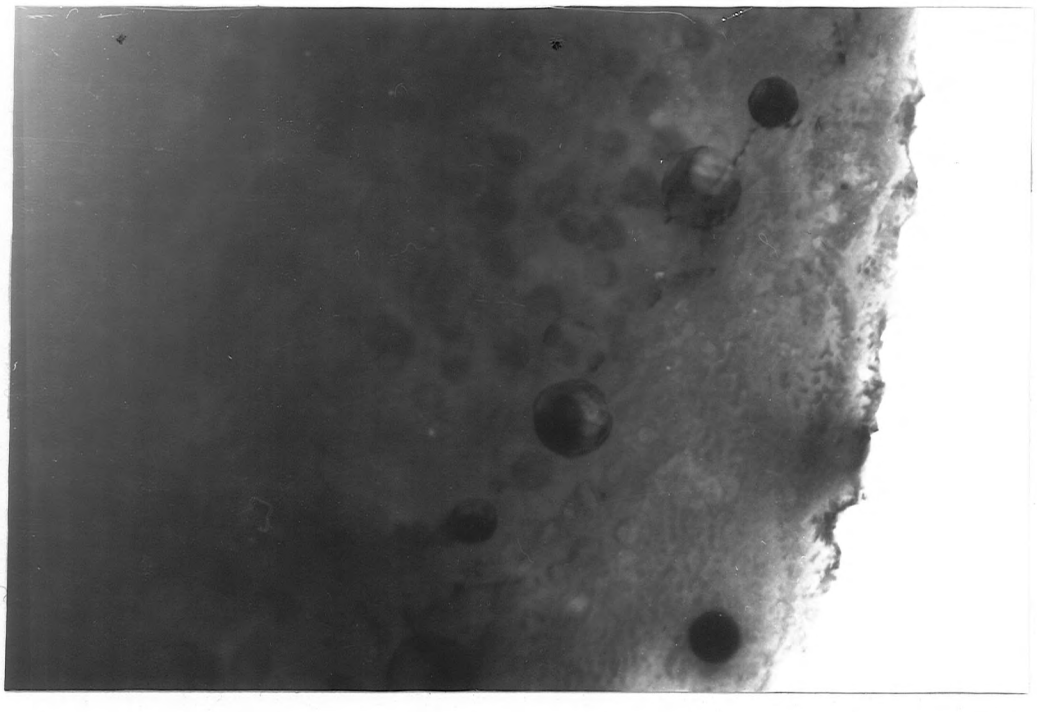

Fig A1.8 : Micrograph of ZnSe:1000ppm In after zinc-treatment , showing large spherical precipitates lying along a twin boundary. (X 52000)

in specimens containing 250 ppm indium showed a well developed shape. Precipitates having spherical shapes are shown in Fig Al.6 ; they decorate a stacking fault. A different specimen from the same boule contained precipitates with a triangular shape, see Fig Al.7, which decorated a grain boundary. It was interesting that when precipitates decorated stacking faults, they were normally spherical, but when they were located at twin or grain boundaries they were often triangular in shape. The actual cause of this difference in morphology was not obvious.

As expected, the largest precipitates were formed in the heat-treated samples of crystals that contained 1000 ppm indium which was the highest concentration of indium used in this study (boule 349). The precipitates decorating stacking faults were either spherical or had a fourfold symmetry. It was in this heavily doped crystal that random precipitation in the absence of any other defect was most evident. The spherical precipitates lying along the twin boundary in Fig Al.8, were the largest observed in this study, being about 2000 Å in diameter.

The important points relating to precipitates in this study were as follows :

(1) Precipitates were only observed in samples containing 50 ppm or more of indium after zinc treatment at 850°C.

(2) The concentration of the precipitates increased with increasing indium concentration.

(3) In crystals with indium concentrations > 50 ppm the precipitates had definite shapes, while some were spherical, others exhibited three or fourfold symmetry.

(4) The precipitates formed preferentially in association with crystallographic defects such as stacking faults, twin and grain boundaries and dislocations.

3. DISCUSSION AND CONCLUSION

Many workers have previously observed the formation of precipitates in gallium or indium doped ZnSe after zinc heat treatment. Ray and Kröger (1978) suggested that GaSe precipitates were formed when gallium doped ZnSe samples were annealed near 1000°C. After annealing at lower temperatures ($\sim$ 800°C) the precipitations were most probably due to Ga_2Se or (Ga,Zn) alloy. In a quite separate investigation Jones and Woods (1976) also noticed that indium or gallium doped ZnSe, after being heated in molten zinc at 850° C, became black and opaque. Examination in the optical microscope revealed that the opacity was attributable to a mass of small precipitates of various shapes with micrometre dimensions. The conclusion was that the indium or gallium was completely precipitated by the zinc treatment, and decorated what were probably dislocations, grain boundaries or voids. However, no photographic evidence or detailed description of the precipitates, was given.

In a recent paper Russell et al (1981) discussed in detail the precipitation effects in indium doped ZnSe. Their study and the present work have shown that the as-grown indium-doped crystals contained long thin twins as the major crystallographic defect, and that the incorporation of indium during growth, even in concentrations up to 1000 ppm, had no noticeable effect on the defect structure. Heating in zinc at 600°C produced the first detectable precipitation effects in crystals containing at least 250 ppm indium, but this treatment did not affect the defect structure either.

Pronounced precipitation occurred in crystals containing more than 50 ppm indium, after they had been heated in molten zinc at 850°C. In such crystals all the twin boundaries, grain boundaries and stacking faults were found to be decorated with precipitates. Some dislocations were decorated, but others were not. It would appear that the stacking faults were caused by the presence of indium because undoped crystals heated in molten zinc did not contain stacking faults. Presumably the indium is ejected from zinc sites

during the heat treatment, and then during cooling to room temperature, thermal stress, enhanced by the presence of indium, causes stacking faults and dislocations to be formed. Once formed they provide regions for the preferential nucleation and precipitation of the indium. Random precipitates were invariably smaller than the precipitates observed at stacking faults in the same sample. This suggests that precipitates had to attain a minimum size to produce sufficient stress to nucleate a stacking fault. The observation also implies that precipitates at stacking faults once nucleated would grow faster. Preferential precipitation would occur at existing growth twins and grain boundaries.

The precipitates may consist of indium metal, but more probably are of indium-zinc alloy or a compound of indium and selenium, in accordance to the suggestion of Ray and Kröger (in the case of precipitation in gallium doped ZnSe). One might speculate that the small spherical precipitates are of indium-zinc alloy, whereas those with a definite crystallographic morphology might be In_2Se in epitaxial registry with the host lattice. Although some precipitates observed in the TEM exhibited three and fourfold symmetry, it may well be that all of them had a basic tetrahedral shape, giving rise to triangular or square sections depending on the angle of incidence of the electron beam and the orientation of the crystal lattice containing the defects.

REFERENCES

Adachi, S and Machi, Y (1975)

Jpn. J. Appl. Phys. 14, 10, p.1599.

Adachi, S and Machi, Y (1976)

Jpn. J. Appl. Phys. 15, 8, p.1513.

Adachi, S and Machi, Y (1978)

Jpn. J. Appl. Phys. 17, 1, p.135.

Adams, W.G. and Day, R.E. (1876)

Proc. Roy. Soc. 25, p.113.

Alfrey, G.F. and Cooke, I. (1957),

Proc. Phys. Soc. 70B, p.1096.

Allen, J.W. (1964)

Proc. 7th. Int. Conf. on Semiconductors, Paris, (Dunod Cie Paris) p.781.

Allen, J.W, Livingstone, A.W. and Turvey, K. (1972),

Solid-St.Electron. 15, p.1363.

Anderson, R.T. (1960)

Chemical Periodicity (Reinhold, New York)

Archer, R.J., Yep,T.O. and Murray, K. (1968)

Tech. Rep. "Control of thin film interface barriers" contract

No. F.33615-68-C-1054, AF Avionics Lab.

Archer, R.J. and Yep, T.O. (1970)

J. Appl. Phys. 41, 1, p.303.

Arizumi, T. and Hirose, M. (1969).

Jpn. J. Appl.Phys. 8, p.749.

Aven, M, Marple, D.T.F. and Segall, B. (1961)

J. Appl. Phys. 32, 10, p.2261.

Aven, M and Woodbury, H.H. (1962)

Appl.Phys. Lett. 1, 3, p.53.

Aven, M and Segall, B. (1963)

Phys. Rev. 130, p.81.

Aven, M (1964)

Bull. Am. Phys. Soc. 9, p.248.

Aven, M (1971)

J. Appl.Phys. 42, 3, p.1204.

Bardeen, J (1947)

Phys. Rev. 71, p.717.

Bebb, H.B. and Chapman, R.A. (1967)

J. Phys. Chem. Solids, 28, p.2087.

Beichler, J, Fuhs, W, Mell, H and Welsch, H.M. (1980)

J. Non.Cryst. Solids. 35 & 36, p.587.

Berezin, A.A. and Kirii, V.B. (1970)

Sov. Phys. Sol. St. 11, p.1709.

Bhargava, R.N, Herko, S.P. and Fitzpatrick, B.J. (1979)

Bull. of the Am.Phys. Soc. 24, 1, p.402.

Birchak, I, Serdyuk, V.V. and Chemeresyuk, G.G. (1976)

Phys. Stat. Solidi (a), 33, K145.

Björklund, G. and Grimmeiss, H.G. (1971)

Solid-St. Electronics, 14, p.589.

Blanconnier, P, Hogrel, J.F, Jean-Louis, A.M. and Sermage, B (1981)

J. Appl.Phys. 52, 11, p.6895.

Blount, G.H, Fisher, M.W, Morrison, R.G. and Bube, R.H. (1966)

J. Electrochem. Soc. 113, p.690.

Blount, G.H, Sanderson, A.C. and Bube, R.H. (1967)

J. Appl.Phys. 38, 1, p.4409.

Boley, J.C, Blanconnier, P, Herman, A, Ph.Ged, Henoc, P and Noblanc, J.P.(1975)

J. Appl.Phys. 46, 8, p.3549.

Braun, F. (1874)

Pogg. Ann. 153, 556.

Braun, S, Grimmeiss, H.G. and Allen, J.W. (1972)

Phys. Stat. Solidi, 14, p.527.

Braun, S, and Grimmeiss, H.G. (1973)

J. Appl.Phys. 44, p.2789.

Braun, S. and Grimmeiss, H.G. (1974)

J. Appl.Phys. 45, p.2658.

Bryant, F.J. and Manning, P.S. (1974)

J. Phys. & Chem. Solids, 35, p.97.

Bube, R.H. and Lind, E.L. (1958)

Phys. Rev. 110, 5, p.1040.

Burr, K.F. and Woods, J. (1971)

J. Cryst.Growth, 9, p.183.

Chapin, D.M, Fuller, C.S. and Pearson, G.L. (1954)

J. Appl.Phys. 25, 5, p.676.

Chung, C.H. and Tai, C.H. (1976)

J. Lumin. 12/13, p.913.

Cohen, M.L. and Bergstresser, T.K. (1966)

Phys. Rev. 141, p.789.

Cowley, A.M. (1966)

J. Appl.Phys. 37, p.3024.

Crowell, C.R, Spitzer, W.G, Howarth L.E. and Labate, E.E. (1962)

Phys. Rev. 127, p.2006.

Crowell, C.R, Sze, S.M. and Spitzer, W.G. (1964)

Appl.Phys. Lett. 4, p.91.

Crowell, C.R, Shore, H.B. and LaBate, E.E. (1965)

J. Appl.Phys. 36, p. 3843.

Crowell, C.R. and Roberts, G.I. (1969)

J. Appl. Phys. 40, 9, p.3726.

Cutter, J.R, Russell, G.J. and Woods, J. (1976)

J. Cryst. Growth, 32, p.179.

Cutter, J.R, and Woods, J. (1979)

J. Cryst. Growth, 47, p.405.

Davies, J.J.and Nicholls, J.E. (1979)

J. Phys. C: Sol.St. Phys. 12, p.3329.

Dean, P.J, Henry C.H. and Frosch, C.F. (1968)

Phys. Rev. 168, p.812.

Dean, P.J, Venghaus, H, Pfister, J.C, Schaub, B. and Marine, J. (1978)

J. Lumin. 16, p.363.

De Nobel, D (1959)

Philips Res. Rep. 14, p.361.

Dunstan, D.J, Nicholls, J.E, Cavanett, B.C, Davies, J.J. and Reddy, K.V.(1977)

Solid St. Comm. 24, p.677.

Dunstan, D.J, Nicholls, J.E, Cavanett, B.C. and Davies, J.J. (1980)

J. Phys. C: Solid St.Phys. 13, p.6409.

Eckett, P, Madelung, O and Treuch, J. (1967)

Phys. Rev. Letters 18, p.656.

Fitzpatrick, B.J, Werkhoven, C.J, McGee, T.F, III, Harnack, P.M, Herko, S.P,

Bhargava, R.N. and Dean, P.J. (1981)

IEEE Trans. Electron Devices ED-28, 4, p.440.

Fowler, R.H. (1931)

Phys. Rev. 38, p.45.

Fujita, S, Mimoto, H. and Noguchi, T. (1979)

J. Appl.Phys. 50, p.1079.

Fukuda, Y. and Fukai, M. (1967).

J. Phys.Soc.Japan, 23, p.902.

Georgobiani, A.N, Ozerov, Yu V, Strumban, E.E. and Anisimov, V.V.(1976)
Physica St.Solidi (a) 35, p.251.

Gezci, S. and Woods, J (1975)
J. Lumin. 10, p.267.

Grimmeiss, H.G. and Olofson, G.O. (1969)
J. Appl.Phys. 40, p.2526.

Grimmeiss, H.G. (1974)
Proc. of the Conf. Metal-Semiconductor Contacts, Manchester. Inst. of Phys. Conf. Ser. No.22, p.187.

Grimmeiss, H.G. and Ledebo, L-A° (1975)
J . Appl.Phys. 46, 5, p.2155.

Grimmeiss, H.G. and Ovren, C. and Allen, J.W. (1976)
J. Appl.Phys. 47, 3, p.1103.

Grimmeiss, H.G. (1977)
Ann. Rev. Mat. Sci. p.341.

Grimmeiss, H.G, Ovren, C, Ludwig, W. and Mach, R. (1977)
J. Appl.Phys. 48, 12, p.5122.

Grimmeiss, H.G, Ovren, C. and Mach, R. (1978)
Inst. of Phys. Conf. Ser. No.43, p.372.

Grimmeiss, H.G, Ovren, C. and Mach, R. (1979)
J. Appl.Phys. 50, p.6328.

Gudden, B,and Pohl, R. (1928)
Z.Phys. 48, 384.

Heine, V. (1972)
Proc. Roy.Soc.A 331, p.307.

Hemila, S.O. and Bube, R.H. (1967)
J. Appl.Phys. 38, 13, p.5258.

Hemmatt, N. and Weinstein, M. (1967)
J. Electrochem. Soc. 114, p.851.

Henry, C.H. (1971)

Phys. Rev. B4, p.2453.

Henry, C.H, Nassau, K. and Shiever, J.W. (1971)

Phys. Rev. B4, p.2453.

Henry, C.H. (1973)

J. Luminescence, 7, p.127.

Herman, J.M. and Sah, C.T. (1973)

J. Appl.Phys. 44, p.1259.

Hertz, H. (1887)

Ann. d. Phys. 31, p.983.

Holton, W.C, De Wit, M. and Estle, T.L. (1965)

Int.Symp. Luminescence, Munich, p.454.

Hughes, A.L. and DuBridge, L.A. (1932)

Photoelectric Phenomena, 352, 466, McGraw Hill Book Company,Inc.

Hughes, A.L. (1936)

Rev. Mod.Phys. 8, p.294.

Ijaki and Satoh (1979)

Jpn. J. Appl.Phys. 48, 10, p.1965.

Jones, G. and Woods, J (1974)

J. Luminescence 9, p.389.

Jones, G. and Woods, J (1976)

J. Phys. D, 9, p.799.

Kang, C.S, Beverley, P, Phipps, P. and Bube, R.H. (1967)

Phys. Rev. 156,3, p.998.

Kaufman, R.G. and Dowbar, P. (1974)

J. Appl.Phys. 45, 10, p.4487.

Kimerling, L.C. (1974)

J. Appl.Phys. 45, 4, p.1839.

Kohn, W. (1957)

Solid St. Phys. 5, Ch.4.

(F. Seitz and D.Turnbull, Eds).

Academic Press, New York.

Kosai, F, Fitzpatrick, B.J, Grimmeiss, H.G, Bhargava, R.N. and Neumark,G.F.(1979)

Appl.Phys. Lett. 35 (2), p.194.

Kovalenko, A.V, Klimenko, S.M, Kushnir, A.S, Omelchenko, S.A, Shlambur, I.V. and Yakunin, AYa(1979)

Sov.Phys. Semicond. 13, 7, p.977.

Kukimoto, H, Henry, C.H. and Merritt, F.R. (1973)

Phys.Rev. B7, 6, p.2486.

Larson, D.M. (1969)

Phys.Rev. 187, p.1147.

Lawther, C. and Woods, J (1978)

Phys. Stat. Solidi (a), 50, p.491.

Lindquist, P.F. and Bube, R.H. (1972)

J. Appl.Phys. 43, 6, p.2839.

Lempicki, A, Birman, J, Samelson, H. and Neumark, G. (1961)

Proc. Int.Conf.Sem.Phys. (Prague 1960) p.768.

Lewis, K.L. and Hill, J. (1980)

Proc. 7th Int.Conf. on Chem.Vap.Deposition, p. 629.

Lorenz, M.R, Aven, M. and Woodbury, H.H. (1963)

Phys. Rev. 132, p.143.

Lucovsky, G. (1965)

Solid St.Communications, 3, p.299.

Mandel, G. (1964)

Phys.Rev. 134, p.A1073.

Marfaing, Y, Lascaray, J. and Triboulet, R. (1974)

Int. Phys.Conf. Ser.No.22, Manchester, p.201.

Marple, D.T.F. (1964)

J. Appl.Phys. 35, p.1879.

Merz, J.L, Kukimoto, H, Nassau, K. and Shiever, J.W. (1972)

Phys. Rev. B6, p.545.

Merz, J.L, Nassau, K. and Shiever, J.W. (1973)

Phys. Rev. B8, p.1444.

Milnes, A.G. (1973)

Deep Imp.in Semicond.

(John-Wiley & Sons, New York).

Moss, T.S. (1952)

Photoconductivity in the elements

(Academic Press, New York).

Mott, N.F. (1938)

Proc.Cambridge Phil.Soc. 34, p.569.

Neumark, G.F. (1979)

Bull. Am.Phys. Soc. 24, p.402.

Neumark, G.F. (1980)

J. Appl.Phys. 51, p.3383.

Nicholls, J.E, Davies, J.J, Cavenett, B.C, James, J.R. and Dunstan, D.J.(1979)

J.Phys. C: Solid St.Phys. 12, p.361.

Nicholls, J.E. and Davies, J.J. (1980)

J.Phys. C: Solid St. Phys. 13, p.2393.

Nitsche, R. (1960)

J.Phys. Chem.Sol.17, p.163.

Nix, F.C. (1932)

Rev. Mod.Phys. 4, p.723.

Okumura, T. and Ikoma, T. (1974)

Appl.Phys. Lett. 25, 10, p.572.

Oẗzsan, M.E. and Woods, J. (1974)

Appl.Phys. Lett. 25, p.488.

Oẗzsan, M.E. and Woods, J. (1975)

Solid St. Electronics, 18, p.519.

Oẗzsan, M.E. and Woods, J. (1977)

Solid St.Electronics, 20, p.343.

Papadopoula, A.C, Jean-Louis, A.M. and Charil, J. (1978)

J.Cryst. Growth, 44, p.587.

Patel, J.L, Davies, J.J. and Nicholls, J.E. (1981)

J.Phys. C: Solid St.Phys, 14, p.5545.

Piper, W.W. and Polich, S.J. (1961)

J. Appl.Phys. 32, p.1278.

Prener, J.S. and Williams, F. E. (1956a)

J. Electrochem.Soc.103, p. 342.

Prener, J.S. and Williams, F.E. (1956b)

J. Chem.Phys. 25, p.361.

Prener, J.S. and Weil, D.J. (1959)

J. Electrochem.Soc. 106, p.409.

Pollard, E.R. and Hartke, J.L. (1969)

Bull. Am.Phys. Soc. Ser. II, 14, p.115.

Raüber, A. and Schneider, J. (1966)

Phys. Stat.Sol.18, p.125.

Ray, A. K. and Kröger, F. A. (1978)

J. Electrochem.Soc. 125, 8, p.1355.

Reynolds, D.C, Pedrotti, L.S. and Larson, O.W. (1961)

J. Appl.Phys. 32, 10, p.2250.

Rhoderick, E.H. (1980)

Metal-Semicond. Contacts

(Clarendon Press, Oxford)

Roberts, G.I. and Crowell, C.R. (1970)

J. Appl.Phys. 41, 4, p.1767.

Robinson, R.J. and Kun, Z. K. (1975)

Appl.Phys. Lett, 27, 2, p.74.

Russell, G.J. and Woods, J. (1979)

J. Cryst.Growth, 47, p.647.

Russell, G.J. Vincent, B. and Woods, J. (1981)

Phys. Stat. Sol (a), 63, p.573.

Sah, C.T. and Reddi, V.G.K. (1964)

IEEE Trans.Electron Devices, ED-11, p.345.

Sah, C.T, Forbes, L, Rosier, L.L. and Tasch, A.F, JR. (1970)

Sol.Stat.Electronics, 13, p.759.

Sah, C.T, Ning, T.H, Rosier, L.L. and Forbes, L (1971)

Sol.Stat. Communications 9, p. 917.

Samelson, H. and Lempicki, A. (1962)

Phys. Rev. 125, 3, p.901.

Schottky, W. (1938)

Naturwiss, 26, p.843.

Schottky, W. and Spenke, E. (1939)

Wiss. Veroff Siemens-Werken, 18, 225.

Segall, B. and Marple, D.T.F. (1967)

Physics and Chem. of II-VI Compounds (Edited by M.Aven and J.S.Prener, North Holland, Amsterdam), p.318.

Sethi, B.R. and Mathur, P.C. (1978)

Phys. Stat. Sol (a), 46, p.717.

Sethi, B.R. and Mathur, P.C. and Woods, J. (1978a)

J. Appl.Phys. 49, p.3618.

Sethi, B.R, Talwar, P.L, Sharma, O.P. and Mathur, P.C. (1978b)

Phys. Stat. Sol (a), 47, p. 699.

Sethi, B.R, Mathur, P.C. and Woods, J. (1980)

J. Appl.Phys. 50, p.352.

Shirakawa, Y. and Kukimoto, H. (1980)

Sol.St. Communications, 34, p.359.

Smith, W. (1873)

Am. J. Sci. 5, 301.

Stringfellow, G.B.and Bube, R.H. (1968)

Phys. Rev. 171, 3, p.903.

Stutius, W. (1981)

Appl.Phys. Lett. 38, 5, p.352.

Stutius, W. (1982)

Appl.Phys. Lett. 40, 3, p.246.

Suda, T. and Kurita, S. (1979)

J. Appl.Phys. 50, 1, p.483.

Suda, T. and Bube, R.H. (1981)

J. Appl.Phys. 52, 10, p.6218.

Suzuki, A. and Shionoya, S. (1971)

J. Phys. Soc. Japan, 31, p.1455, p.1462.

Swank, R.K, Aven, M. and Devine, J.Z. (1969)

J. Appl.Phys. 40, 1, p.89.

Sze, S.M. (1969)

Physics of Semicond. Devices.

(Wiley Int.Ed).

Ullman, F.G. and Dropkin, J.J. (1961)

J. Electrochem. Soc. 108, p.154.

Viktorovitch, P. and Model, G. (1980)

J. Appl.Phys. 51, 9, p.4847.

Viktorovitch, P. and Jousse, D. (1980)

J. Non.Cryst.Solids, 35 & 36, p.569.

Viktorovitch, P (1981)

J. Appl.Phys. 52, 3, p.1392.

Vincent, G, Bois, D. and Pinard, P. (1975)

J. Appl.Phys. 46, 12, p.5173.

Vincent, B. (1980)

Ph.D.Thesis, University of Durham.

Wagner, P. and Lorenz, M.R. (1966)

J. Phys. Chem.Sol. 27, p.1749.

Werkhoven, C, Fitzpatrick, B.J, Herko, S.P., Bhargava, R.N. and Dean,P.J.(1981)

Appl.Phys. Lett. 38, 7, p.540.

Wheeler, R.G. and Miklosz, J.C. (1964)

Proc.7th Int.Conf. Phys.Semicond.

Ed.M. Hulin, p.873.

Woodbury, H.H. and Aven, M. (1964)

Proc.7th Int. Conf.Phys.Semicond.,p.179.

Woodbury, H.H. and Aven, M. (1974)

Phys. Rev. B, 9, 12, p.5195.

Woods, J. (1981)

Displays, p.251.

Woods, J. and Russell, G.J. (1981)

Private communications.

Wu, Z.L, Merz, J.L, Werkhoven, C.J, Fitzpatrick, B.J. and Bhargava,R.N.(1982)

Appl.Phys. Lett. 40, 4, p.345.

Yamaguchi, M, Yamamoto, A. and Kondo, M. (1977)

J. Appl.Phys. 48, 12, p.5237.

Yamaguchi, M, and Shigematsu, T. (1978)

Jpn. J.Appl.Phys. 17, 2, p.335.

Yu, P.W. and Park, Y.S. (1973)

Appl.Phys. lett. 22, 7, p.345.